

**Structure and properties  
of  
polydiacetylene-containing  
peptide amphiphile fibres**

**Maaïke van den Heuvel**

# **Structure and properties of polydiacetylene- containing peptide amphiphile fibres**

Een wetenschappelijke proeve op het gebied van de  
Natuurwetenschappen, Wiskunde en Informatica

Proefschrift

ter verkrijging van de graad van doctor  
aan de Radboud Universiteit Nijmegen  
op gezag van de rector magnificus prof. mr. S.C.J.J. Kortmann,  
volgens besluit van het college van decanen  
in het openbaar te verdedigen op donderdag 10 februari 2011  
om 10.30 uur precies

door

Maaike van den Heuvel  
geboren op 25 juni 1983  
te Almelo

Promotor: Prof. dr. ir. Jan C.M. van Hest  
Copromotor: Dr. Dennis W.P.M. Löwik

Manuscriptcommissie:  
Prof. dr. Roeland J.M. Nolte  
Prof. dr. Jan H. van Esch (TUD)  
Dr. Alexander Kros (UL)

Paranimfen: Tu Ha Vong  
Linda J.A. Hendriks

ISBN: 978-90-9025848-5

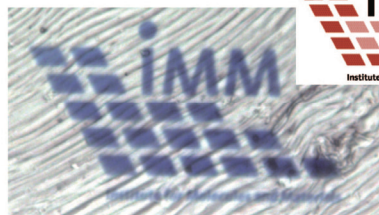
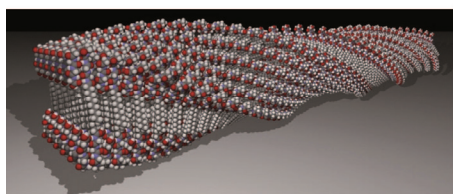
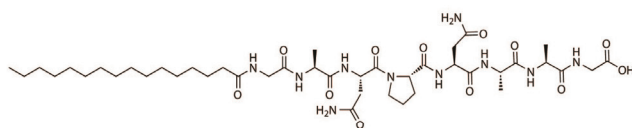
## Table of Contents

|   |     |
|---|-----|
| 1. Introduction   | 1   |
| 2. Structure elucidation of palmitoyl-GANPNAAG fibres   | 17  |
| 3. Mechanics and thermodynamics of peptide amphiphile fibres  | 39  |
| 4. Self-assembly and polymerisation of diacetylene-containing peptide amphiphiles in aqueous solution                         | 57  |
| 5. Effect of the diacetylene position on the chromatic properties of polydiacetylenes from self-assembled peptide amphiphiles | 75  |
| 6. The influence of amino acid sequence on morphology and colour of polydiacetylene-containing peptide amphiphile fibres      | 99  |
| 7. ATRP on polydiacetylene-containing peptide amphiphile fibres   | 117 |
| 8. Threading of small peptides and self-assembled fibres using ruthenium as a catalyst  | 133 |
| 9. Towards fibres of defined length   | 149 |
| 10. Patterns of diacetylene-containing peptide amphiphiles using polarisation holography                                      | 163 |
| Summary   | 173 |
| Samenvatting  | 177 |
| Dankwoord   | 181 |
| List of publications  | 183 |
| Curriculum Vitae  | 184 |



# Chapter 1

## Introduction



In this chapter, an introduction is given into the structure and function of peptide amphiphile fibres. Functional motifs such as  $\beta$ -sheets,  $\alpha$ -helices or turns can all be applied to create amphiphiles which assemble into fibrous structures. Furthermore, the introduction of a diacetylene moiety in the hydrophobic part of the amphiphiles is discussed. If strict orientational requirements are met, this moiety can be polymerised to yield a polydiacetylene. The high absorption in the visible region gives the polymer an intense colour, which is sensitive to the environment of the backbone.

## Peptide amphiphiles

In nature many materials consist of small building blocks, kept together by non-covalent interactions. The architectures assembled from these building blocks have both structural and functional properties. The cell membrane for example, self-assembled from mainly phospholipids, has a protective function, but on its surface also many functional motifs are displayed, which are involved in a variety of processes, such as transport and signalling. The functionality in the cell membrane is often introduced by proteins, frequently found in assembled superstructures. The highly defined folding of proteins combined with the large range of chemical functionalities present in amino acids makes these biopolymers important building blocks for natural materials. Quite a number of protein building blocks assemble into fibres. These superstructures have many different functions in nature. Collagen, as main constituent of the extracellular matrix keeps cells together and inside the cell structures can move over actin filaments (Figure 1). However, fibrils in nature can be harmful too. A well-known example are the amyloid fibres, associated with diseases such as Alzheimers' and diabetes II. Fibrous assemblies are, because of their versatility and intricate beauty, an inspiration to many scientists. In order to better understand formation and function of protein fibres, model systems have been developed to mimic them.

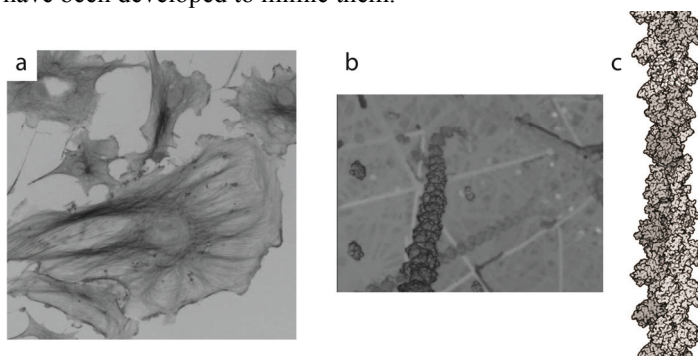


Figure 1. Actin, one of the protein fibres found in nature. a) Cells in which microtubules and actin filaments are shown. b) A schematic zoom within the cell. c) The molecular structure of one actin filament.

Peptides which self assemble into fibres have gained increasing interest over the years as a model system for protein fibres. Often they display amphiphilicity through their sequence or by the addition of a hydrophobic moiety. With their relative ease of synthesis they give the possibility of mimicking structure and function of proteins without the challenging production that traditionally accompanies these large biomolecules. Furthermore, peptide design can conveniently be varied in order to effectively explore the structure-function relationship. The peptide may be the functional part of a protein, or a motif which guides the assembly into complex superstructures. Generally, these small peptide motifs are soluble, and an additional stabilisation is needed, either to direct the peptides into their active conformation or as a driving force for assembly. Often hydrophobicity is used as a driving force.

Hydrophobic patches on misfolded proteins are the cause of the formation of amyloid fibres, and a hydrophobic ‘seam’ on an  $\alpha$ -helix guides it to form coiled coils, an ubiquitous, function-related motif in protein assembly.<sup>1</sup>

PA superstructure, function and response to stimuli such as heat, pH or salt have been extensively investigated.<sup>2-9</sup> Peptide amphiphiles can be divided into two subclasses – those consisting only of amino acids, and those in which other molecular components, accessible by synthetic methods, are used to expand the range of functionality. In all-amino acid amphiphiles, an amphiphile can consist of a stretch of hydrophobic amino acids, coupled to polar residues. However, the folding of a peptide into a secondary structure may also reveal an implicit amphiphilicity present in the molecule. Before folding, the hydrophobic and polar residues may be present in an alternating or more intricate pattern. The second subclass of PAs mainly consists of a stretch of polar amino acids to which a hydrophobic alkyl tail is coupled. The field of peptide self-assembly is extensive. Since the research described in this thesis concerns fibres of peptide amphiphiles, mainly fibrous assemblies will be discussed. The overview given here is far from complete, but aims at highlighting examples of peptide amphiphile fibres to illustrate the versatility and attractiveness of the field. Many comprehensive reviews are available which describe the subject in more detail.<sup>1-9</sup>

### All amino-acid amphiphiles

There are several possibilities to design an amphiphile from only amino acids. Of course, a stretch of hydrophobic amino acids may be coupled to a stretch of hydrophilic amino acids, as has been shown by the group of Zhang,<sup>10, 11</sup> whose peptide amphiphiles behave similarly to fatty acids. However, because of the folding into secondary structures, all-amino acid PAs may also exhibit an implicit amphiphilicity, as mentioned above. Within this class we can distinguish three different structural elements. An alternating hydrophilic-hydrophobic pattern of amino acids usually folds into a  $\beta$ -strand-like structure which assembles into  $\beta$ -sheets. A somewhat more elaborated pattern, such as hpphppp (h = hydrophobic residue, p = polar residue) yields  $\alpha$ -helical strands, two of which assemble into a coiled coil. Peptide rings can have alternating hydrophobic-polar residues, as also observed in the  $\beta$ -sheet motifs, but since their flexibility is very limited and critical for their structure, they will be described separately.

**$\beta$ -sheet structures.** Alternating hydrophobic and polar residues generally arrange themselves in a zig-zag conformation, folding into a strand which can subsequently self-assemble into a  $\beta$ -sheet. In an early example of such an alternating structure a range of dipeptide monomers was polymerised to yield an alternating (rather polydisperse) structure, which assembled into  $\beta$ -sheets.<sup>12</sup> Examples of more defined structures include the assembly of EAK16, a 16 residue containing peptide, in which (hydrophobic) alanine alternates with hydrophilic glutamic acid and lysine to form (AEAEAKAK)<sub>2</sub>.<sup>13</sup> Because of the ionic interactions between glutamic acid and lysine these peptides assembled into membranes, which were stable towards proteases and structure breaking agents such as guanidine hydrochloride or urea. Also structures which do not possess the purely alternating hydrophobic-polar motif can assemble into  $\beta$ -sheets. An example is the peptide PKhKhhEhEP,<sup>14</sup> in which the hydrophobic residues h were varied. This



peptide assembled into fibres. With biotin-functionalised peptides, it was possible to functionalise the fibres with proteins *via* the very strong biotin-avidin interaction.<sup>15</sup>

**Coiled coils.**  $\alpha$ -Helical peptides with a more elaborate pattern of hydrophobic and hydrophilic residues can yield coiled coil superstructures. These superstructures are formed *via* the interaction of hydrophobic seams which are presented on the  $\alpha$ -helical structure when the hydrophobic residues are appropriately spaced. In an  $\alpha$ -helix one turn consists of 3.6 residues. Using a pattern of hydrophobic and hydrophilic residues which has hydrophobic residues placed approximately every 3.6 residues therefore causes one side of the  $\alpha$ -helix to be hydrophobic. A hydrophobic/polar primary structure like hpphppp, in which h denotes a hydrophobic and p a polar residue, comes with its average of 3.5 residue spacing between hydrophobic residues, close to the one-turn value of 3.6 residues. The mismatch between the average of 3.5 and the turn value of 3.6 causes the hydrophobic line on the  $\alpha$ -helix to wind around the helical structure. A second  $\alpha$ -helix having the same hydrophobic ribbon on its surface can only pair with the hydrophobic residues when the helices wind around each other, yielding a coiled coil (Figure 2).<sup>16</sup> The structure of such a dimeric coiled coil can be conveniently represented with a helical wheel.

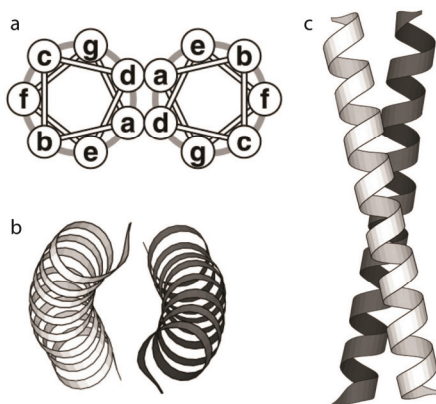


Figure 2. a) The helical wheel representation of a dimeric coiled coil. b) Top view and c) side view of a dimeric coiled coil.<sup>17</sup>

Besides a dimeric structure, also higher-order coiled coils are possible, which may combine into triangles up to hexagons, but also double triangles and other intricate patterns.<sup>18</sup> All these coiled coils and assemblies of coiled coils are based on the heptad repeat as described above, which is the most common repeat in nature. However, this seven-amino-acid repeat is not the only possible pattern which results in a hydrophobic seam on one side of an  $\alpha$ -helix. Decameric (hphpphppp) or undecameric (hpphpphppp) repeats also yield hydrophobic residues at about every 3.6 residues. The spacing of 3.33 amino acids between the hydrophobic residues in the decameric repeat codes for a more tightly coiled left-handed superhelix. On the other hand, the 3.67 residue spacing for the undecameric repeat yields an only slightly twisted right-handed helix.<sup>19, 20</sup> The decameric repeat does not occur often – due to its higher curvature it is less stable. In the assembly of coiled coils, interactions at both sides of the hydrophobic

patch play a role,<sup>21, 22</sup> and even the residues furthest away have influence on the subsequent superstructures which are formed.<sup>23</sup> This gives many possibilities to tune the assembly. With not-perfectly overlapping coiled coil structures, ‘sticky ends’ are created. With these ‘sticky ends’, the coiled coils assemble into fibres, as has been shown by the group of Woolfson.<sup>24</sup>

A well-known coiled coil sequence is the so-called leucine zipper, which can be used as supramolecular ‘glue’. This motif has been used to attach two large structures to each other, such as a virus particle to the protein GFP.<sup>25</sup> On the other hand, this ‘glue’ can also be used to create hydrogels, as shown by Tirrell *et al.*, who attached leucine zippers to both sides of PEG.<sup>26</sup> The zippers assembled into coiled coils, thereby creating a physically crosslinked network or hydrogel. However, also smaller non-covalent interactions between fibres of coiled coils can be used to create a hydrogel for tissue-engineering.<sup>27</sup>

**Peptide rings.** The group of Ghadiri investigated peptide rings designed to have a flat conformation. The rings consisted of alternating D- and L-amino acids, and self-assembled into nanotubes (Figure 3).<sup>28</sup> The assembly took place for rings containing between 8 and 12 amino acids.<sup>29</sup> Fewer residues yielded too much ring strain, and more supposedly caused too much flexibility. A similar tubular system was described by Valery *et al.*<sup>30</sup>

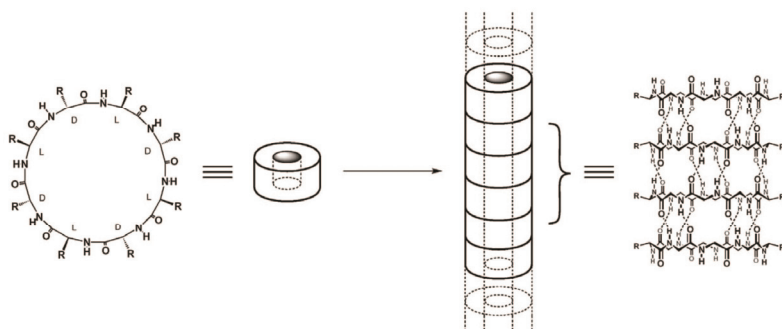


Figure 3. The peptide rings described by the group of Ghadiri.<sup>31</sup>

Even though the characteristic feature of peptide rings is that they are closed structures, other systems with limited conformational freedom may assemble into similar structures. The limited conformational freedom can originate from an equilibrium between open and folded structure where the folded structure is highly favoured. Wang *et al.*<sup>32</sup> described a peptide which folded into a  $\beta$ -turn, which served the same purpose as the rings in the above described nanotubes.

### Amphiphilic peptides with alkyl tails as hydrophobic domain

One of the first examples of fibres made from a stretch of hydrophilic amino acids coupled to a hydrophobic tail showed the coupling of two hydrophobic tails on one side and a quaternary ammonium ion on the other side of just one amino acid.<sup>33</sup> These amphiphilic structures assembled into ribbons which folded into helices and tubules. Similar amphiphiles with three amino acids instead of just one assembled into fibrous

architectures as well,<sup>34</sup> both in organic solvents and in water. The width of the three-amino acid amphiphile assemblies was approximately twice the length of the molecule. Therefore, the formation of a bilayer in which the peptides are arranged in a parallel  $\beta$ -sheet was proposed. A  $\beta$ -sheet structure of the peptides in these kind of molecules is quite common. However, the assembly in organic solvents is not. One of the few examples besides the one mentioned above is given by the group of Frauenrath,<sup>35</sup> who coupled a peptide to poly(isoprene) for solubility in organic solvents. With these self-assembled fibres the scope of the topochemical diacetylene polymerisation (see below) was investigated.<sup>36</sup> Most research however employed the solubilising properties of the hydrophilic peptide part within the amphiphile. Consequently, most of the studies on peptide amphiphiles have been performed in water. For example, the group of Stupp developed a peptide amphiphile which assembles into fibres upon acidification (Figure 4).<sup>37</sup> The assembly was driven by the hydrophobic interactions between alkyl tails; the presence of four cysteines enabled crosslinking of the structure after assembly.<sup>38</sup> A flexible linker connected this part to a solvent-exposed functional section, which could easily be varied. In one case (Figure 4) it consisted of a serine,<sup>37</sup> which bound to and directed the crystallisation of calcium phosphate, mimicking the multistage crystallisation found in bone growth.

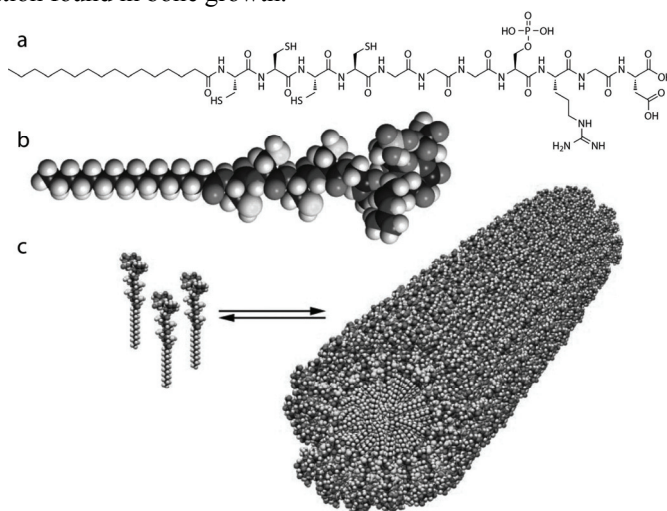


Figure 4. The peptide amphiphile fibres investigated by Stupp *et al.*<sup>37</sup>

Hydrogen bonds within the peptide headgroup generally play an essential role in the assembly of PAs. When hydrogen bond formation was impeded, for example by methylation of the NHs, fibre formation was hampered as well.<sup>39</sup> The effect was strongest closest to the hydrophobic tail. Other small structural changes may have large effects as well, as was shown in for example the dimer of PHGGG, bridged C-terminally with 1,4-diaminobutane (Figure 5). This molecule assembled into fibres, but not without the proline.<sup>40</sup> Other examples of the subtlety of peptide assembly include the increasing stabilization by extending the alkyl chain length.<sup>41, 42</sup> For example isolated small motifs (15 amino acids) based on collagen are by themselves not stable enough to

display properties that collagen has in nature. Although the typical triple helices are formed, they disassemble at a low temperature (35.6 °C). Coupling an alkyl tail to such a relatively small motif increased the stability of these triple helices. With a C<sub>6</sub> tail the melting temperature was found to be 42.2 °C, and it increased to 69.8 °C for C<sub>16</sub>.<sup>43</sup> A double tail obviously has a larger effect and increased the disassembly temperature even further (an increase of 15-20 °C for a double C<sub>12</sub> tail).<sup>44</sup>

The opposite effect is achieved by attachment of a hydrophilic moiety. Solubilisation of the supramolecular assembly as a whole was achieved by modifying peptide amphiphiles with poly(ethylene glycol) (PEG),<sup>45</sup> and attachment of this hydrophilic polymer may also lead to disassembly of the fibrous structure.<sup>46</sup> Cleaving part of the amphiphile is another factor that can cause large structural changes. It can lead to disassembly if the peptide is separated from the hydrophobic tail, which completely disrupts the balance between polar and hydrophobic forces.<sup>47</sup> On the other hand, a smaller change may be induced by cleavage of a bulky group from a place in the amphiphile important for the self-assembly. This may completely change the morphology of the assembly without causing disassembly, as was shown by Muraoka *et al.*,<sup>48</sup> who investigated a peptide amphiphile which assembled into quadruple helices. After cleavage of a nitrobenzyl group the assembly was shown to change to single fibres.

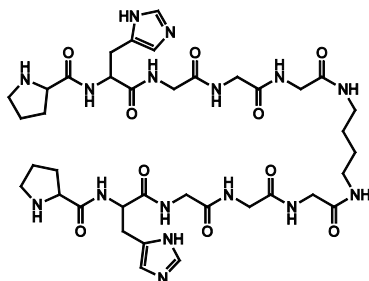


Figure 5. PHGGG, bridged C-terminally with 1,4-diaminobutane assembles into fibres in aqueous environment

Fibre formation of peptide amphiphiles is very diverse, as has already been exemplified above. The hydrophobic and polar parts do not even have to be covalently attached to each other to yield a fibrous self-assembled structure. Brizard *et al.*<sup>49</sup> designed two-step fibre assembly, in which the hydrophilic head and hydrophobic tail, held together by ionic forces, served as an amphiphile following the same rules for self-assembly as covalent amphiphiles.

### Applications of peptide amphiphiles

Peptide amphiphile fibres can be applied *in vivo* because of the biocompatibility of the peptides. Therefore, many applications of PAs are in the direction of tissue engineering. However, also the high aspect ratio has been exploited, for example in the design of molecular conductors.

**Tissue engineering.** The fibres mentioned above designed by the group of Stupp (Figure 4) have been modified for several applications.<sup>3</sup> Decoration with a metal

chelating ligand yielded fibres that could bind Gd(III) and were shown to serve as a MRI contrasting agent.<sup>50, 51</sup> Decorated with IKVAV the fibres directed neurite growth.<sup>52</sup> A different system which has the same functionality is a structure similar to the EAK peptide assembly described above.<sup>13</sup> The 16-residue peptide EAK assembled into very stable membranes, which supported neuronal growth when Glu and Lys were replaced for Arg and Asp.<sup>53</sup>

PA fibres also provide hydrogels for cell-growth. The sticky-ended coiled coil fibres developed by Woolfson *et al.* have been used to this end, and enable cell-growth in three dimensions.<sup>27</sup> Also  $\beta$ -sheet based peptide fibres were used for tissue-engineering.<sup>54, 55</sup> Because of the convenient functionalisation of  $\beta$ -sheet based fibres, a cell-recognition motif can easily be added. Fibres were for example decorated with RGD to enhance cell-adhesion, and with biotin for functionalisation with proteins *via* the very strong non-covalent biotin-avidin interaction (Figure 6).<sup>15</sup>

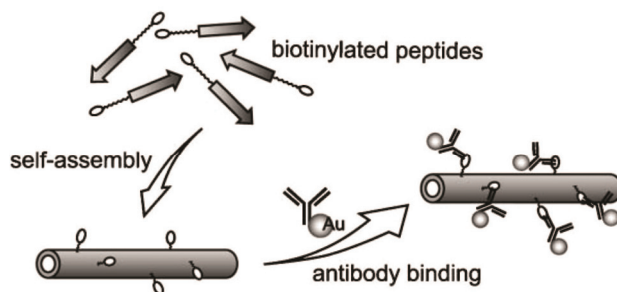


Figure 6. Biotinylated peptides may self-assemble into fibres and subsequently functionalized with antibodies *via* the biotin-avidin interaction.<sup>15</sup>

**Molecular conductors.** The long aspect ratio of self-assembled fibres has been used for design of (semi) conducting molecular wires.<sup>56</sup> As a conducting motif, several  $\pi$ -conjugated systems have been employed. The moiety capable of energy transduction can be coupled to a system which is known to self-assemble, but the  $\pi$ - $\pi$  stacking may also provide the driving force for assembly. Ghadiri *et al.*<sup>57</sup> followed the first strategy in employing the peptide rings with alternating L and D amino acids which assemble into nanotubes as described above. The most stable, eight-membered peptide ring was chosen for functionalisation with naphthalenediimine for charge transduction. Schenning *et al.*<sup>58</sup> used the second strategy and employed oligo(p-phenylenevinylene) as a  $\pi$ -conjugated moiety for both conductivity and to provide a driving force in the assembly. Two  $\beta$ -sheet forming peptides were coupled to this moiety: GANPNAAG and GAGAG. The latter sequence was also used as a molecular conductor when coupled to thiophene.<sup>59</sup>

In a completely different approach, nanotubes of FmocFF have been constructed as a scaffold to make silver nanowires (Figure 7).<sup>60</sup> Silver ions reduced in the hollow core of the nanotubes to yield high-aspect ratio silver wires after enzymatic degradation of the peptide backbone.

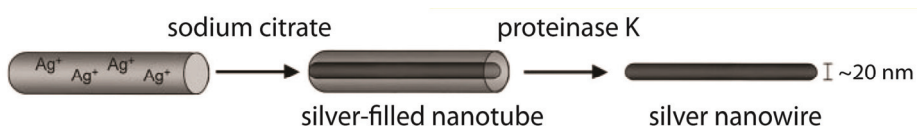


Figure 7. Hollow tubes from FmocFF are placed in an aqueous solution containing ionic silver (left). Middle: the silver is reduced using silver nitrate. Right: after enzymatic removal of the peptide shell silver nanowires are obtained.<sup>60</sup>

Other possible applications include using the hydrophobic interior of the fibres as a drug delivery system<sup>61</sup> or the use of the fibres as a guide for assembly of inorganic materials.<sup>37</sup> Furthermore, PA fibres can be employed as sensors. One possibility to use these structures as such is to include a diacetylene moiety in the hydrophobic tail of the PA. The diacetylene can be polymerised to a coloured polydiacetylene, which may change colour depending on its surroundings. Diacetylenes, their polymerisation and the chromism of the resulting colour changes are discussed in the next session.

## Diacetylenes

Polydiacetylenes (PDAs) are highly conjugated polymers with unique chromatic properties. They are synthesized *via* the topochemical polymerisation of diacetylenes which was first described in the early '70s, by the group of Wegner.<sup>62</sup> This polymerisation can only take place if the diacetylene moieties are closely packed, with a distance of 4.4 to 5.4 Å, close to the distance of 4.91 Å they have in the polymer (Figure 8).<sup>63</sup> Furthermore, the angle between the moieties is required to be between 45 and 55°, with little or no orientational freedom of the diacetylene groups. The most obvious way to constrain molecules in order to fulfil these requirements is by crystallisation. Of course not all crystals meet the criteria of diacetylene distance and angle, and even if they do in some cases the crystal disintegrates because of structural changes upon polymerisation. The larger the deviation from the 'ideal' value of distance and angle, the larger the rearrangement of the molecules with polymerisation<sup>64</sup> and the larger the volume change.<sup>65, 66</sup> Larger volume changes are only possible in a flexible system, that is able to accommodate the required structural rearrangements. Without flexibility, the polymerisation process may break down the assembly.<sup>67</sup> Self-assembled structures in which the polymerisation can take place (monolayers,<sup>68-70</sup> vesicles,<sup>71-73</sup> fibres<sup>35, 74-76</sup>) are such flexible architectures. The diacetylene moieties are mostly introduced in the alkyl chains of the amphiphiles and fulfil, if properly packed, the required positional criteria.

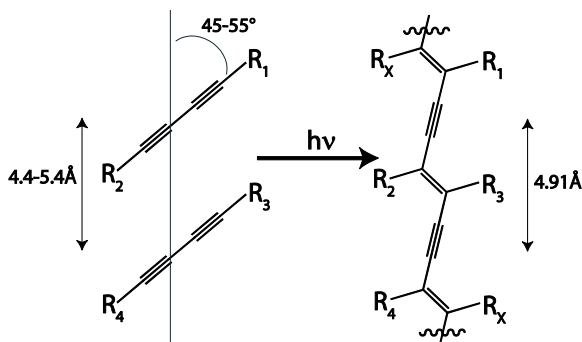


Figure 8. Polymerisation of diacetylenes to polydiacetylenes (PDAs) only occurs under strict positional conditions

### Chromism

One of the interesting properties of the highly conjugated polymers resulting from the topochemical diacetylene polymerisation is their absorption of light in the visible region, which is dependent on the PDA structure. The absorption wavelength of the backbone is caused by its 'effective conjugation length' which depends on its exact packing. The longest conjugation length – the most stable conformation of the PDA backbone – results in an absorption around 650 nm. Stress in the backbone causes a decrease of this effective conjugation length, which is accompanied by a shift of the maximum absorption wavelength to 550 or 500 nm. After dissolution of the backbone, the backbone has no well-defined maximum absorption any more, but absorbs below 400 nm. Because the absorption is in the visible region, the polymers have respectively a blue, red and yellow appearance,<sup>77-81</sup> and are therefore usually referred to as being in their 'blue', 'red' or 'yellow' state. Interestingly enough, not only colour changes, but also fluorescence can be used to probe the structural change in the polymeric backbone, since only red PDAs are fluorescent.<sup>82, 83</sup>

From the dependence of colour on the solubility – blue if in a crystal, yellow if dissolved and red somewhere in between, an as yet unresolved discussion started about the nature of the colour change. It may be caused by aggregation<sup>78, 84</sup> or by structural changes within a single chain.<sup>80, 85, 86</sup> Notwithstanding this discussion, it is generally accepted that the polymer colour is a measure of the conjugation length within the polymer backbone, as explained above. The PDA colour is influenced by the nature and spatial arrangement of the side chains, which defines the exact structure of the polymeric backbone.<sup>87</sup> Besides the nature of the colour change, also the relative stability of the blue and red state is still under discussion. Both crystals and self-assembled systems change colour from blue to red when heated and this change is usually (but not always) irreversible. The rearrangement leading to colour change may be accompanied by the transition to a better ordered structure, which is in a few cases confirmed with spectroscopy<sup>85</sup> and crystallography.<sup>88</sup> Therefore, in crystals the red state is thought to be lower in energy than the blue one.<sup>89</sup> Reduction of strain upon going from a blue to a red state in crystals may also cause the red state to be more stable. However, for self-assembled systems, where the colour change upon heating is often reversible,<sup>90-94</sup> the

situation might be slightly different. The reversibility suggests that the preferred and thus energetically favourable state may be the blue one. On the other hand, it may also be that the energy barrier between blue and red has not been overcome yet for the reversible systems, and thus upon cooling the system relaxes back into its higher energy blue state (shown schematically in Figure 9). However, not only the reversibility suggests an increase in disorder in going from blue to red. The observation of a blue colour at mild (for example room temperature, neutral pH) *versus* a red colour at harsh conditions (for example 150 °C, pH 14) indicates a more stable blue state as well. The increase in chaos may be irreversible because of entanglement of side chains rather than thermodynamic stability, thereby yielding an irreversible colour change (Figure 10).<sup>93</sup> For example, peptide amphiphile PDAs may change colour irreversibly in conditions which are denaturing for the peptide part, such as the presence of hydrogen bond breaking trifluoroacetic acid.<sup>95</sup> Also, the strain reduction in going from the blue to the red state mentioned above may not be present in self-assembled systems. Because of their larger flexibility, the strain increase may not be an important parameter during the polymerisation process.

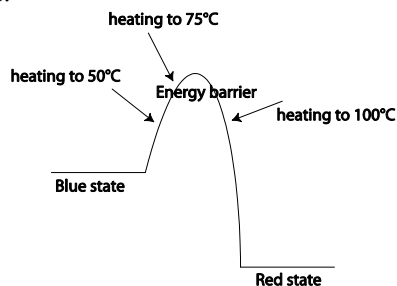


Figure 9. Crossing the energy barrier from the blue to the red state. It is unknown if the blue or the red state is higher in energy. This picture illustrates how, even if the red state is lower in energy, the PDA may exhibit reversible chromism up to a certain temperature.

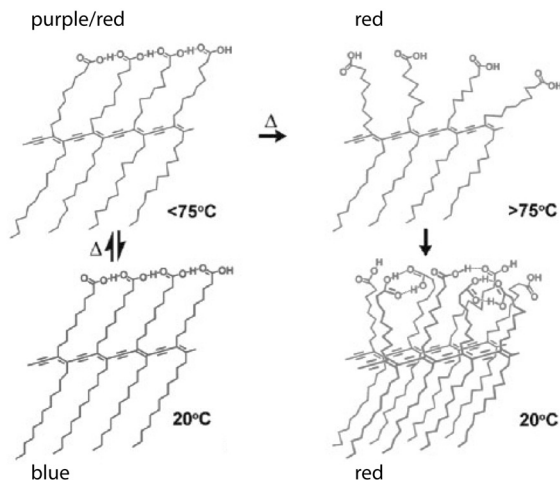


Figure 10. Side chain entanglement may lead to an irreversible colour change. The temperature above which the colour change is irreversible depends on the system (and is 75 °C for the PDA shown).<sup>93</sup>



Assemblies of diacetylene containing amphiphiles have been used for systematic studies after the effect of several molecular parameters on the polymerisability of diacetylenes and the resulting PDA colour. Extensive research has been performed on varying the headgroup both in amphiphiles and bolaamphiphiles using small organic groups,<sup>68, 72, 96-98</sup> sugars<sup>99, 100</sup> or amino-acids.<sup>101-103</sup> Cheng and Stevens<sup>103</sup> and Huo *et al.*<sup>104</sup> investigated the effect of size and charge of the headgroup on the colour of the polymer by coupling respectively one or two amino acids to 10,12-pentacosadiynoic acid, followed by polymerisation of the resulting monolayers or vesicles. In other reports variations were introduced both in the hydrophobic tail length and the position of the diacetylene moiety within the amphiphile.<sup>72, 105-108</sup>

### Applications of polydiacetylenes

Self-assembled systems have, as also discussed earlier in this chapter, been used to introduce solvent-exposed functional groups, which can be recognized by for example cells (RGD) or proteins (biotin). This functionality can be combined with the chromism of the PDAs. After locking of the self-assembled structure with the topochemical polymerisation of diacetylenes, changes in headgroup conformation can induce a shift in absorption of the polymeric backbone. The binding of a guest molecule can induce such a structural change, and thus binding of a guest (e.g. cells or proteins) may induce a colour change. Sensing with polydiacetylenes has been extensively reviewed in literature,<sup>109</sup> and is the most important PDA application. The first example of a colour change with host-guest binding was given by Charych *et al.*<sup>110, 111</sup> In a monolayer of pentacosadiynoic acid, they mixed in 2-5% sialic acid functionalized pentacosadiynoic acid. After polymerisation of this mixed diacetylene monolayer, it changed colour upon binding of the influenza virus. Other examples include detection of cells binding to RGD-functionalized PDA vesicles,<sup>73</sup> the colour change of a maleimide-functionalised polydiacetylene upon interaction with sulfur<sup>112</sup> and the binding of  $\alpha$ -cyclodextrin to amine terminated ethylene-glycol polydiacetylene.<sup>82, 83</sup> The colour change can also be caused selectively by ions. For example, when a polydiacetylene was coupled to single strand DNA, potassium induced a colour change, while the structure was insensitive towards sodium.<sup>113</sup>

Besides the sensing applications, PDAs have been employed in a few other ways. Because of the initiation of polymerisation with light, lithography may be used to selectively polymerise a sample of diacetylenes (Figure 11). In the obtained patterned surface, the more soluble monomers were removed, and other lipids could be introduced at the empty places,<sup>114</sup> yielding a selectively functionalized surface. Polymerising in steps has been shown to yield two colour images.<sup>115</sup> Furthermore, polymerised fibres are generally more stable than self-assembled fibres, and so PDA surfaces can be used as extra stable surfaces. This property was applied to cell culturing, in which cells were either grown on a monolayer displaying growth motifs,<sup>70</sup> or on a patterned surface obtained with lithography. In the latter case the effect of the design on cell growth was investigated.<sup>116</sup>

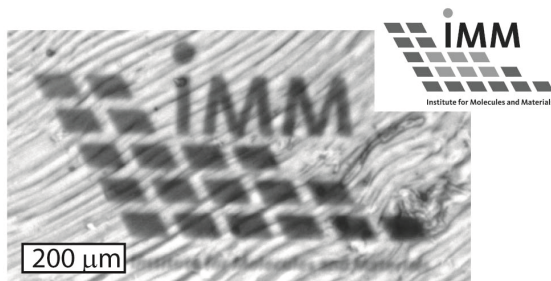


Figure 11. Lithographic patterning of diacetylenes.

## The aim and outline of the thesis

The goal envisaged at the start of this research was to study peptide amphiphile fibres to investigate their properties and possibilities for structural stabilisation. Furthermore, dimensional control of the fibre dimensions was investigated in order to make and study mesoscopic building blocks.

In chapter 2 the molecular structure of a non-polymerisable peptide amphiphile, palmitoyl-Gly-Ala-Asn-Pro-Asn-Ala-Ala-Gly-OH was studied using a range of techniques including X-ray diffraction and solid state NMR spectroscopy. The mechanical and thermal stability of this PA were investigated in chapter 3. Rheo-optics, which probes length distribution *via* rotation induced alignment, is an important measurement method in this chapter.

In chapter 4 and 5 properties of the GANPNAAG peptide functionalized with a diacetylene-containing alkyl tail are described. In chapter 4 the morphology, polymerisation properties and temperature and pH dependence of the PDA peptide amphiphiles were investigated using two similar PAs, which only differed in the length of the alkyl tail. In chapter 5 the influence of the diacetylene position on stability and colour of the resulting assemblies and polymers was evaluated while keeping the overall length of the alkyl tail constant.

In chapter 6 the diacetylene containing hydrophobic tail was kept the same and the peptide part was varied. The emphasis in this chapter was on the change in pH responsiveness when charged residues are introduced in the peptide amphiphile. We therefore started from the straight-forward  $\beta$ -sheet forming motif GAGAG, and replaced the first and last glycine with lysine and glutamic acid. Chapter 7 describes the use of one of the fibres described in chapter 6 as an initiator for atom transfer radical polymerisation to create polymeric brushes along the PDA backbone. The effect of polymer chain length on PDA colour was studied to determine if polymer crowding could be detected *via* enhanced backbone stress.

In chapter 8 a side-step to crosslinking of self-assembled systems is made. The ruthenium(II)-catalysed threading of tyrosines was explored with small molecules, yielding oligomeric species. Furthermore, it was extended to two self-assembled peptide amphiphile fibres containing tyrosine to explore the scope of the reaction. The first

system was based on a coiled-coil motif, and the second on the GAGAG sequence also employed in chapters 6 and 7.

Chapters 9 and 10 describe the alignment of the fibres also described in chapter 4, and two different methods for selective polymerisation. In chapter 9 patterning was accomplished using classic lithography, while in chapter 10 polarization holography was employed. This technique was used successfully for the first time on self-assembled fibres. It is only possible as a patterning method because of the possibility of alignment of the fibres combined with the unique difference in polymerisation rate on initiation with light parallel or perpendicular to the fibres.

## References

1. D. N. Woolfson, The design of coiled-coil structures and assemblies. In *Fibrous Proteins: Coiled-Coils, Collagen and Elastomers*, D. A. D. Parry and J. M. Squire, Eds. Elsevier: 2005; Vol. 70, pp 79-112.
2. D. W. P. M. Löwik and J. C. M. van Hest, *Chem. Soc. Rev.*, 2004, **33**, 234-245.
3. H. G. Cui, M. J. Webber and S. I. Stupp, *Biopolymers*, 2009, **94**, 1-18.
4. E. Kokkoli, A. Mardilovich, A. Wedekind, E. L. Rexeisen, A. Garg and J. A. Craig, *Soft Matter*, 2006, **2**, 1015-1024.
5. D. W. P. M. Lowik, E. H. P. Leunissen, M. van den Heuvel, M. B. Hansen and J. C. M. van Hest, *Chem. Soc. Rev.*
6. A. Aggeli, I. A. Nyrkova, M. Bell, R. Harding, L. Carrick, T. C. B. McLeish, A. N. Semenov and N. Boden, *Proc. Natl. Acad. Sci. U. S. A.*, 2001, **98**, 11857-11862.
7. S. Cavalli and A. Kros, *Adv. Mater.*, 2008, **20**, 627-631.
8. S. Cavalli, F. Albericio and A. Kros, *Chem. Soc. Rev.*, **39**, 241-263.
9. S. Cavalli, J. W. Handgraaf, E. E. Tellers, D. C. Popescu, M. Overhand, K. Kjaer, V. Vaiser, N. Sommerdijk, H. Rapaport and A. Kros, *J. Am. Chem. Soc.*, 2006, **128**, 13959-13966.
10. G. von Maltzahn, S. Vauthey, S. Santoso and S. U. Zhang, *Langmuir*, 2003, **19**, 4332-4337.
11. S. Vauthey, S. Santoso, H. Y. Gong, N. Watson and S. G. Zhang, *Proc. Natl. Acad. Sci. U. S. A.*, 2002, **99**, 5355-5360.
12. W. B. Rippon, H. H. Chen and A. G. Walton, *J. Mol. Biol.*, 1973, **75**, 369-375.
13. S. G. Zhang, T. Holmes, C. Lockshin and A. Rich, *Proc. Natl. Acad. Sci. U. S. A.*, 1993, **90**, 3334-3338.
14. S. Matsumura, S. Uemura and H. Mihara, *Chem. Eur. J.*, 2004, **10**, 2789-2794.
15. S. Matsumura, S. Uemura and H. Mihara, *Mol. BioSyst.*, 2005, **1**, 146-148.
16. F. H. C. Crick, *Acta Crystallogr.*, 1953, **6**, 689-697.
17. J. Walshaw and D. N. Woolfson, *J. Mol. Biol.*, 2001, **307**, 1427-1450.
18. E. Moutevelis and D. N. Woolfson, *J. Mol. Biol.*, 2009, **385**, 726-732.
19. M. R. Hicks, D. V. Holberton, C. Kowalczyk and D. N. Woolfson, *Fold. Des.*, 1997, **2**, 149-158.
20. A. Lupas, *Trends Biochem. Sci.*, 1996, **21**, 375-382.
21. J. Walshaw and D. N. Woolfson, *J. Struct. Biol.*, 2003, **144**, 349-361.
22. E. B. Hadley, O. D. Testa, D. N. Woolfson and S. H. Gellman, *Proc. Natl. Acad. Sci. U. S. A.*, 2008, **105**, 530-535.
23. C. Gribbon, K. J. Channon, W. J. Zhang, E. F. Banwell, E. H. C. Bromley, J. B. Chaudhuri, R. O. C. Oreffo and D. N. Woolfson, *Biochem.*, 2008, **47**, 10365-10371.
24. M. G. Ryadnov and D. N. Woolfson, *Angew. Chem., Int. Ed.*, 2003, **42**, 3021-3023.
25. I. J. Minten, L. J. A. Hendriks, R. J. M. Nolte and J. Cornelissen, *J. Am. Chem. Soc.*, 2009, **131**, 17771-17773.
26. W. A. Petka, J. L. Harden, K. P. McGrath, D. Wirtz and D. A. Tirrell, *Science*, 1998, **281**, 389-392.
27. E. F. Banwell, E. S. Abelardo, D. J. Adams, M. A. Birchall, A. Corrigan, A. M. Donald, M. Kirkland, L. C. Serpell, M. F. Butler and D. N. Woolfson, *Nat. Mater.*, 2009, **8**, 596-600.
28. M. R. Ghadiri, J. R. Granja, R. A. Milligan, D. E. McRee and N. Khazanovich, *Nature*, 1993, **366**, 324-327.
29. J. D. Hartgerink, J. R. Granja, R. A. Milligan and M. R. Ghadiri, *J. Am. Chem. Soc.*, 1996, **118**, 43-50.

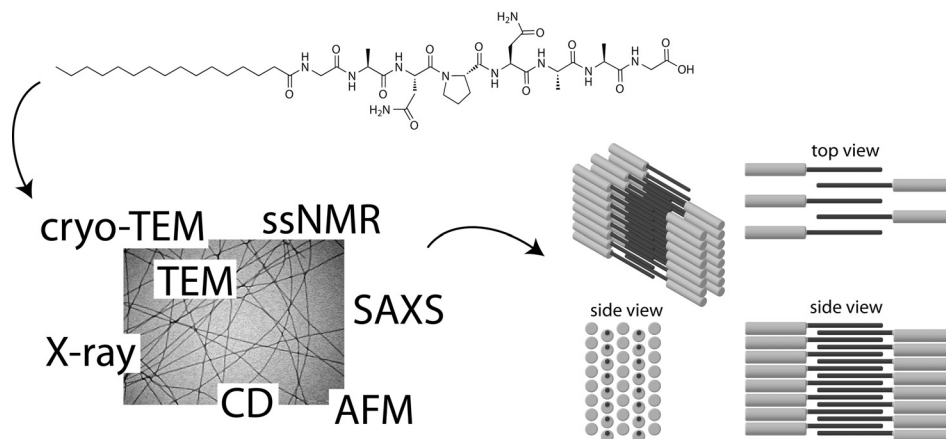
30. C. Valery, M. Paternostre, B. Robert, T. Gulik-Krzywicki, T. Narayanan, J. C. Dedieu, G. Keller, M. L. Torres, R. Cherif-Cheikh, P. Calvo and F. Artzner, *Proc. Natl. Acad. Sci. U. S. A.*, 2003, **100**, 10258-10262.
31. D. T. Bong, T. D. Clark, J. R. Granja and M. R. Ghadiri, *Angew. Chem., Int. Ed.*, 2001, **40**, 988-1011.
32. C. Wang, L. X. Huang, L. J. Wang, Y. K. Hong and Y. L. Sha, *Biopolymers*, 2007, **86**, 23-31.
33. N. Nakashima, S. Asakuma and T. Kunitake, *J. Am. Chem. Soc.*, 1985, **107**, 509-510.
34. N. Yamada, K. Ariga, M. Naito, K. Matsubara and E. Koyama, *J. Am. Chem. Soc.*, 1998, **120**, 12192-12199.
35. E. Jahnke, I. Lieberwirth, N. Severin, J. P. Rabe and H. Frauenrath, *Angew. Chem., Int. Ed.*, 2006, **45**, 5383-5386.
36. E. Jahnke, N. Severin, P. Kreutzkamp, J. P. Rabe and H. Frauenrath, *Adv. Mater.*, 2008, **20**, 409-414.
37. J. D. Hartgerink, E. Beniash and S. I. Stupp, *Science*, 2001, **294**, 1684-1688.
38. J. D. Hartgerink, E. Beniash and S. I. Stupp, *Proc. Natl. Acad. Sci. U. S. A.*, 2002, **99**, 5133-5138.
39. S. E. Paramonov, H. W. Jun and J. D. Hartgerink, *J. Am. Chem. Soc.*, 2006, **128**, 7291-7298.
40. C. Madhavaiah and S. Verma, *Chem. Comm.*, 2004, 638-639.
41. J. T. Meijer, M. Roeters, V. Viola, D. W. P. M. Löwik, G. Vriend and J. C. M. van Hest, *Langmuir*, 2007, **23**, 2058-2063.
42. D. W. P. M. Löwik, J. Garcia-Hartjes, J. T. Meijer and J. C. M. van Hest, *Langmuir*, 2005, **21**, 524-526.
43. Y. C. Yu, M. Tirrell and G. B. Fields, *J. Am. Chem. Soc.*, 1998, **120**, 9979-9987.
44. Y. C. Yu, P. Berndt, M. Tirrell and G. B. Fields, *J. Am. Chem. Soc.*, 1996, **118**, 12515-12520.
45. I. W. Hamley, M. J. Krysmann, V. Castelletto and L. Noirez, *Adv. Mater.*, 2008, **20**, 4384-4384.
46. J. T. Meijer, M. Henckens, I. J. Minten, D. W. P. M. Löwik and J. C. M. van Hest, *Soft Matter*, 2007, **3**, 1135-1137.
47. D. W. P. M. Löwik, J. T. Meijer, I. J. Minten, H. van Kalker, L. Heckenmuller, I. Schulten, K. Slieden, P. Smittenaar and J. C. M. Van Hest, *J. Pept. Sci.*, 2008, 127-133.
48. T. Muraoka, H. Cui and S. I. Stupp, *J. Am. Chem. Soc.*, 2008, **130**, 2946-2947.
49. A. Brizard, R. K. Ahmad and R. Oda, *Chem. Comm.*, 2007, 2275-2277.
50. S. R. Bull, M. O. Guler, R. E. Bras, P. N. Venkatasubramanian, S. I. Stupp and T. J. Meade, *Bioconjugate Chem.*, 2005, **16**, 1343-1348.
51. S. R. Bull, M. O. Guler, R. E. Bras, T. J. Meade and S. I. Stupp, *Nano Lett.*, 2005, **5**, 1-4.
52. G. A. Silva, C. Czeisler, K. L. Niece, E. Beniash, D. A. Harrington, J. A. Kessler and S. I. Stupp, *Science*, 2004, **303**, 1352-1355.
53. T. C. Holmes, S. de Lacalle, X. Su, G. S. Liu, A. Rich and S. G. Zhang, *Proc. Natl. Acad. Sci. U. S. A.*, 2000, **97**, 6728-6733.
54. J. M. Anderson, M. Kushwaha, A. Tambralli, S. L. Bellis, R. P. Camata and H. W. Jun, *Biomacromol.*, 2009, **10**, 2935-2944.
55. M. Zhou, A. M. Smith, A. K. Das, N. W. Hodson, R. F. Collins, R. V. Ulijn and J. E. Gough, *Biomaterials*, 2009, **30**, 2523-2530.
56. A. Jatsch, E. K. Schillinger, S. Schmid and P. Bauerle, *J. Mater. Chem.*, 2010, **20**, 3563-3578.
57. W. S. Horne, N. Ashkenasy and M. R. Ghadiri, *Chem. Eur. J.*, 2005, **11**, 1137-1144.
58. R. Matmour, I. De Cat, S. J. George, W. Adriaens, P. Leclere, P. H. H. Bomans, N. Sommerdijk, J. C. Gielen, P. C. M. Christianen, J. T. Heldens, J. C. M. van Hest, D. Lowik, S. De Feyter, E. W. Meijer and A. Schenning, *J. Am. Chem. Soc.*, 2008, **130**, 14576-14583.
59. H.-A. Klok, A. Rosler, G. Gotz, E. Mena-Osteritz and P. Bauerle, *Org. Biomol. Chem.*, 2004, **2**, 3541-3544.
60. M. Reches and E. Gazit, *Science*, 2003, **300**, 625-627.
61. M. O. Guler, R. C. Claussen and S. I. Stupp, *J. Mater. Chem.*, 2005, **15**, 4507-4512.
62. G. Wegner, *Makromol. Chem.*, 1972, **154**, 35-48.
63. D. G. Rhodes, D. A. Frankel, T. M. Kuo and D. F. O'Brien, *Langmuir*, 1994, **10**, 267-275.
64. Z. Li, F. W. Fowler and J. W. Lauher, *J. Am. Chem. Soc.*, 2009, **131**, 634-643.
65. R. H. Baughman, *J. Appl. Phys.*, 1972, **43**, 4362-4370.
66. D. W. Britt, U. G. Hofmann, D. Mobius and S. W. Hell, *Langmuir*, 2001, **17**, 3757-3765.
67. J. W. Lauher, F. W. Fowler and N. S. Goroff, *Acc. Chem. Res.*, 2008, **41**, 1215-1229.
68. B. Tiek, H. J. Graf, G. Wegner, B. Naegele, H. Ringsdorf, A. Banerjee, D. Day and J. B. Lando, *Colloid Polym. Sci.*, 1977, **255**, 521-531.
69. D. R. Day and H. Ringsdorf, *Makromol. Chem.*, 1979, **180**, 1059-1063.
70. M. A. Biesalski, A. Knaebel, R. Tu and M. Tirrell, *Biomaterials*, 2006, **27**, 1259-1269.
71. B. Hupfer, H. Ringsdorf and H. Schupp, *Chem. Phys. Lipids*, 1983, **33**, 355-374.

## Chapter 1

72. S. Okada, S. Peng, W. Spevak and D. Charych, *Acc. Chem. Res.*, 1998, **31**, 229-239.
73. M. Biesalski, R. Tu and M. V. Tirrell, *Langmuir*, 2005, **21**, 5663-5666.
74. E. Jahnke, A. S. Millerieux, N. Severin, J. P. Rabe and H. Frauenrath, *Macromol. Biosci.*, 2007, **7**, 136-143.
75. D. W. P. M. Löwik, I. O. Shklyarevskiy, L. Ruizendaal, P. C. M. Christianen, J. C. Maan and J. C. M. van Hest, *Adv. Mater.*, 2007, **19**, 1191-1195.
76. L. Hsu, G. L. Cvetanovich and S. I. Stupp, *J. Am. Chem. Soc.*, 2008, **130**, 3892-3899.
77. D. S. Johnston, S. Sanghera, M. Pons and D. Chapman, *Biochim. Biophys. Acta*, 1980, **602**, 57-69.
78. B. Tieke, G. Lieser and K. Weiss, *Thin Solid Films*, 1983, **99**, 95-102.
79. T. Kanetake, Y. Tokura, T. Koda, T. Kotaka and H. Ohnuma, *J. Phys. Soc. Jpn.*, 1985, **54**, 4014-4026.
80. K. C. Lim, A. Kapitulnik, R. Zacher and A. J. Heeger, *J. Chem. Phys.*, 1985, **82**, 516-521.
81. A. F. Drake, P. Udvarhelyi, D. J. Ando, D. Bloor, J. S. Obhi and S. Mann, *Polymer*, 1989, **30**, 1063-1068.
82. J. M. Kim, Y. B. Lee, D. H. Yang, J. S. Lee, G. S. Lee and D. J. Ahn, *J. Am. Chem. Soc.*, 2005, **127**, 17580-17581.
83. D. J. Ahn and J. M. Kim, *Acc. Chem. Res.*, 2008, **41**, 805-816.
84. S. Dei, A. Matsumoto and A. Matsumoto, *Macromol.*, 2008, **41**, 2467-2473.
85. M. Schott, *J. Phys. Chem. B*, 2006, **110**, 15864-15868.
86. K. C. Lim, A. Kapitulnik, R. Zacher and A. J. Heeger, *J. Chem. Phys.*, 1986, **84**, 1058-1059.
87. L. Adler-Abramovich and E. Gazit, *J. Pept. Sci.*, 2008, **14**, 217-223.
88. J. S. Filhol, J. Deschamps, S. G. Dutremez, B. Boury, T. Barisien, L. Legrand and M. Schott, *J. Am. Chem. Soc.*, 2009, **131**, 6976-6988.
89. Y. Lifshitz, Y. Golan, O. Konovalov and A. Berman, *Langmuir*, 2009, **25**, 4469-4477.
90. T. Kuo and D. F. O'Brien, *J. Chem. Soc., Chem. Commun.*, 1990, 839-841.
91. H. W. Beckham and M. F. Rubner, *Macromol.*, 1993, **26**, 5198-5201.
92. Z. Z. Yuan, C. W. Lee and S. H. Lee, *Angew. Chem., Int. Ed.*, 2004, **43**, 4197-4200.
93. A. Potisatituyenyong, R. Rojanathanes, G. Turncharern and M. Sukwattanasinit, *Langmuir*, 2008, **24**, 4461-4463.
94. R. W. Carpick, T. M. Mayer, D. Y. Sasaki and A. R. Burns, *Langmuir*, 2000, **16**, 4639-4647.
95. E. Jahnke, J. Weiss, S. Neuhaus, T. N. Hoheisel and H. Frauenrath, *Chem. Eur. J.*, 2009, **15**, 388-404.
96. Q. Huo, K. C. Russell and R. M. Leblanc, *Langmuir*, 1999, **15**, 3972-3980.
97. P. Deb, Z. Z. Yuan, L. Ramsey and T. W. Hanks, *Macromol.*, 2007, **40**, 3533-3537.
98. J. Yoon, Y. S. Jung and J. M. Kim, *Adv. Funct. Mater.*, 2009, **19**, 209-214.
99. M. Masuda, T. Hanada, Y. Okada, K. Yase and T. Shimizu, *Macromol.*, 2000, **33**, 9233-9238.
100. J. H. Fuhrhop, P. Schnieder, E. Boekema and W. Helfrich, *J. Am. Chem. Soc.*, 1988, **110**, 2861-2867.
101. J. Song, J. S. Cisar and C. R. Bertozzi, *J. Am. Chem. Soc.*, 2004, **126**, 8459-8465.
102. Q. Cheng, M. Yamamoto and R. C. Stevens, *Langmuir*, 2000, **16**, 5333-5342.
103. Q. Cheng and R. C. Stevens, *Langmuir*, 1998, **14**, 1974-1976.
104. Q. Huo, S. P. Wang, A. Pisseloup, D. Verma and R. M. Leblanc, *Chem. Comm.*, 1999, 1601-1602.
105. M. van den Heuvel, D. W. P. M. Löwik and J. C. M. van Hest, *Biomacromol.*, 2008, **9**, 2727-2734.
106. B. Hupfer and H. Ringsdorf, *Chem. Phys. Lipids*, 1983, **33**, 263-282.
107. Y. K. Jung, T. W. Kim, J. Kim, J. M. Kim and H. G. Park, *Adv. Funct. Mater.*, 2008, **18**, 701-708.
108. H. Tachibana, Y. Yamanaka, H. Sakai, M. Abe and M. Matsumoto, *Macromol.*, 1999, **32**, 8306-8309.
109. M. A. Reppy and B. A. Pindzola, *Chem. Comm.*, 2007, 4317-4338.
110. D. H. Charych, J. O. Nagy, W. Spevak and M. D. Bednarski, *Science*, 1993, **261**, 585-588.
111. A. Lio, A. Reichert, D. J. Ahn, J. O. Nagy, M. Salmeron and D. H. Charych, *Langmuir*, 1997, **13**, 6524-6532.
112. S. W. Lee, C. D. Kang, D. H. Yang, J. S. Lee, J. M. Kim, D. J. Ahn and S. J. Sim, *Adv. Funct. Mater.*, 2007, **17**, 2038-2044.
113. J. Lee, H. J. Kim and J. Kim, *J. Am. Chem. Soc.*, 2008, **130**, 5010-5011.
114. K. Morigaki, T. Baumgart, A. Offenhausser and W. Knoll, *Angew. Chem., Int. Ed.*, 2001, **40**, 172-174.
115. J. M. Kim, Y. B. Lee, S. K. Chae and D. J. Ahn, *Adv. Funct. Mater.*, 2006, **16**, 2103-2109.
116. A. Mata, L. Hsu, R. Capito, C. Aparicio, K. Henrikson and S. I. Stupp, *Soft Matter*, 2009, **5**, 1228-1236.

## Chapter 2

# Structure elucidation of palmitoyl-GANPNAAG fibres.



Peptide amphiphiles consisting of a hydrophobic alkyl tail coupled to the eight-amino acid GANPNAAG have been studied extensively for their fibre forming properties. However, detailed characteristics of the fibre structure, such as peptide conformation and molecular organisation are unknown to date. In this chapter a range of characterization techniques is described that have been employed to elucidate the internal structure of these fibres. Based on the results obtained by circular dichroism spectroscopy, X-ray diffraction and solid state NMR spectroscopy it was concluded that the peptide is in a stretched  $\beta$ -sheet conformation, the alkyl tails interdigitate and the hydrogen-bond direction is in the length of the fibre.

## Introduction

Peptide amphiphiles are a versatile class of building blocks with interesting self-assembly characteristics (chapter 1). In our group, a specific type of peptide amphiphile has been developed by connecting the short, eight-amino acid peptide GANPNAAG, derived from the CS protein of the malaria parasite *Plasmodium Falciparum*<sup>1</sup> to a series of hydrophobic tails.<sup>2</sup> The assembly behaviour of these peptide amphiphiles as a function of tail length has been studied in great detail. It was demonstrated that amphiphiles with a short tail (<12 carbon atoms) did not aggregate, and that the peptide part was in a random coil conformation. It is assumed the hydrophobic driving force is not large enough to induce assembly. With a long tail (>18 carbon atoms) the strong hydrophobic interactions caused the formation of random aggregates. For alkyl chains in the window between 12 and 18 carbons the driving force of the hydrophobic tail was large enough to induce assembly, which was also directed by the hydrogen bonds between the amino acids that contributed to the assembly process. Because of these directional hydrogen bonds, the amphiphiles packed into fibres which were stable at room temperature and disassembled reversibly upon heating. However, even though we knew how to make and manipulate the fibres, it was still unknown at the start of this study how the peptide amphiphiles were organised in the fibres and what kind of conformation the peptide fragment possessed after fibre assembly. In order to be able to design *de novo* this kind of self-assembled architectures, the molecular assembly and the influence of small changes in the building blocks on the final assembly have to be fully understood. In this chapter we describe detailed investigations to elucidate the molecular structure of fibres derived from the GANPNAAG peptide coupled to a saturated alkyl tail consisting of 16 carbon atoms (PA 1, Figure 1a).

## Possible models for peptide amphiphile packing

In order to obtain more insight in the structure of the peptide amphiphile fibres, first the different possibilities for packing of the peptide amphiphiles, with respect to alkyl chains and peptide head group were defined. For the alkyl part of the amphiphile two possible packings were considered, one in which the tails at one side of the bilayer do not overlap with the other side, and one in which the tails interdigitate completely (Figure 1b). Any other packing was considered unlikely, since in that case empty space is created within the fibre. For the peptide some more conformational possibilities were taken into account. It contains a proline, which, due to its restricted backbone conformation, is in general associated with turns in a protein. Furthermore, the active conformation of the peptide NPNA, the repeating unit in the CS protein of the malaria parasite *Plasmodium Falciparum* and the basis of the peptide we use, has been shown to be an antiparallel  $\beta$ -hairpin.<sup>3</sup> Hydrogen bonds stabilise the turn, and the side chains are oriented perpendicular to the plane of the turn. Although the peptide GANPNAAG is based on the NPNA motif, the hydrophobic tail introduces additional interactions and therefore the peptide could possibly fold differently from the  $\beta$ -turn observed in NPNA

crystals.<sup>3</sup> Therefore other conformations up to the extreme of a stretched peptide were considered (Figure 1c). A third important parameter of the fibre packing is the directionality of the hydrogen bonds. They may be present along the long or short axis of the fibre causing the amphiphile-amphiphile distance in that direction to be  $\sim 4.5$  Å. The side chains perpendicular to the hydrogen bonds will give rise to distances between the molecules of at least 6 Å. A similar kind of variation in orientation can be found, in case of a turn conformation, for the plane of the turn, in the length or width of the fibre. Furthermore, the hydrogen bonds may be in the plane of the turn, as for the crystals of NPNA,<sup>3</sup> or perpendicular to the turn (Figure 1d). In the latter case, turn formation is driven by hydrophobic interactions, and side chains of the amino acids are present in the turn. Finally peptide amphiphiles that adopt a turn-conformation may pack symmetrically or asymmetrically in the fibre, yielding more possible ways for assembly for the folded than for the straight peptide. In Figure 1e one of the possible asymmetric stackings for both hydrogen bond directions is given.

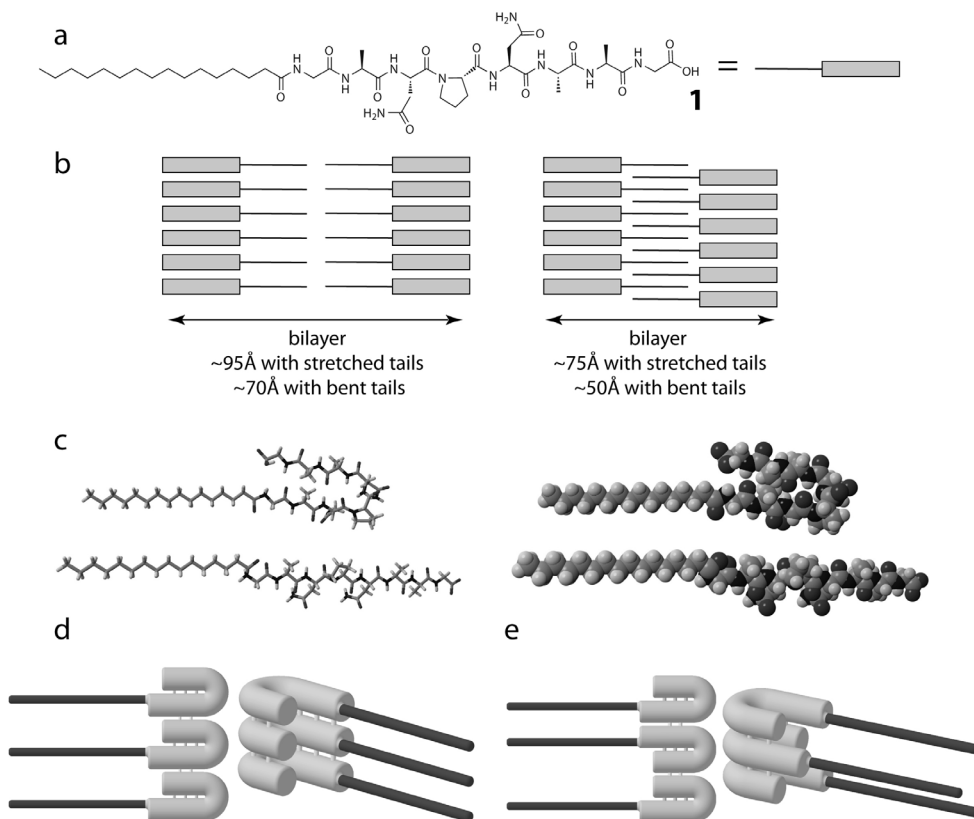


Figure 1. Important considerations with respect to fibre formation. a) Structure and schematic representation of PA 1. b) The two possible arrangements for the alkyl tail. c) Two extreme peptide conformations, shown both as a Dreiding and a CPK model. d) The hydrogen bond direction for the peptides in a turn, which can be either within (left) or perpendicular to the plane of the turn (right). The peptide amphiphiles with a turn may be d) symmetrically or e) asymmetrically stacked.



Based on these conformational parameters 12 possible models were considered (A-L), which are summarized in Table 1. In a first approximation the symmetry of the packing of the turn conformation peptides has not been considered in these models.

| <b>Model</b> | <b>Peptide</b> | <b>H-bond direction</b> |                       | <b>Alkyl tails</b> |                 |
|--------------|----------------|-------------------------|-----------------------|--------------------|-----------------|
| A            | Straight       | In length fibre         |                       | Overlapping        |                 |
| B            |                |                         |                       | Non-overlapping    |                 |
| C            |                | In width fibre          |                       | Overlapping        |                 |
| D            |                |                         |                       | Non-overlapping    |                 |
| E            | In a turn      | In length fibre         | Within the turn       | Overlapping        |                 |
| F            |                |                         |                       | Non-overlapping    |                 |
| G            |                | Perpendicular to turn   |                       | Overlapping        |                 |
| H            |                |                         |                       | Non-overlapping    |                 |
| I            |                | In width fibre          | Within the turn       | Overlapping        |                 |
| J            |                |                         |                       | Non-overlapping    |                 |
| K            |                |                         | Perpendicular to turn |                    | Overlapping     |
| L            |                |                         |                       |                    | Non-overlapping |

Table 1. A summary of the structural features of each of the considered models for molecular packing.

To determine the morphology of the assemblies and to obtain information on the width and height of the fibres, a variety of microscopy techniques were employed: transmission electron microscopy (TEM), and atomic force microscopy (AFM) were performed on dried samples and cryo-TEM on fibres in quickly-frozen solution, to elucidate the morphology in solution without the occurrence of any drying effects. The secondary structure of the peptide was investigated using circular dichroism (CD) spectroscopy, with which the most important secondary structures in proteins –  $\alpha$ -helix,  $\beta$ -sheet and random coil – can be distinguished. Furthermore, to determine repeating distances within the fibre, X-ray diffraction was used, both on dried-in samples and fibres in solution. Alternatively, nuclear magnetic resonance (NMR) was employed. Close contacts between nuclei in dried fibres were measured using solid state NMR (ssNMR) on amphiphiles labelled with NMR active nuclei such as  $^{13}\text{C}$  and  $^{15}\text{N}$ . Finally, exchange experiments were performed in which the rate of exchange of protons in the PA with protons or deuterons of the solvent was monitored with either NMR spectroscopy or mass spectrometry (MS) techniques.

## Microscopy techniques

**Dried samples.** Transmission electron microscopy (TEM) revealed micrometer long, twisted ribbons with a width of about 25 nm (Figure 2) on a carbon-coated copper grid. The same architectures were observed with atomic force microscopy (AFM) on mica (Figure 3), glass and fused silica. The fibres could be observed both in the height and in the phase mode, showing the presence of assemblies (height mode) and also the difference of material properties between the assemblies and the underlying substrate (phase mode). Typically, in the AFM pictures with mica as a substrate, assemblies of two different heights were visible (most clearly visible in the centre picture of Figure 3).

This may be due to a drying effect, or an interaction with mica. Because of the presence of similar fibres on a range of substrates, we concluded that the presence of the fibrous structures was not due to substrate effects.

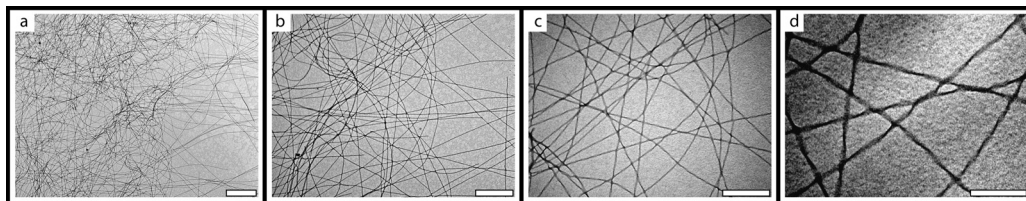


Figure 2. TEM graphs of PA 1. The succeeding images show a zoom of the same spot. The white bars represent a) 2  $\mu\text{m}$ , b) 1  $\mu\text{m}$ , c) 500 nm, d) 200 nm.

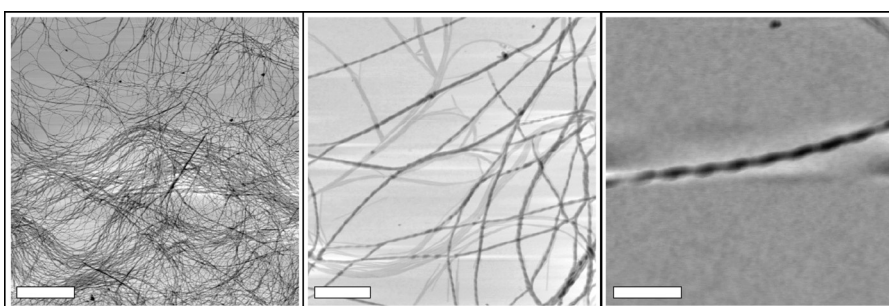


Figure 3. AFM height pictures of PA 1 on mica. The white bars represent a) 4  $\mu\text{m}$ , b) 500 nm, c) 200 nm.

**Solution samples.** The fibre formation in solution was confirmed by cryo-TEM measurements. The PAs assembled into twisted ribbons, with a width of about 25 nm (Figure 4) and an irregular twist. The relative large distribution in width of the fibres that was observed, shown in Figure 4b, is probably caused by the low contrast in the cryo-TEM measurements, due to the absence of any staining or shadowing step in the preparation of the samples.

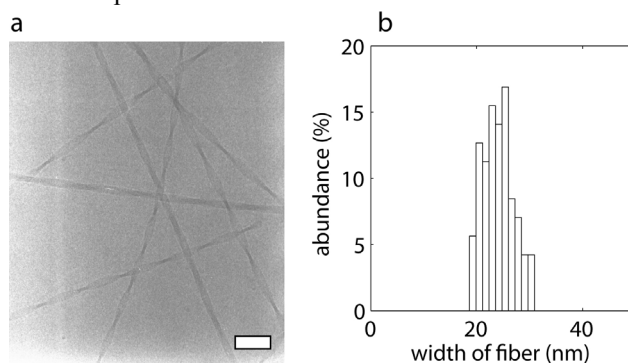


Figure 4. a) Cryo-TEM picture of PA 1. The white bar represents 100 nm. b. Width distribution of the fibres.

The morphology of the fibres depends on the molecular packing of the fibres, but the packing as shown in Figure 1 cannot be directly determined from these measurements. The observed twisted ribbon structure is indicative of fibres which consist of a bilayer with a width of 25 nm which extends in length up to micrometers. Unfortunately, the thickness of the bilayer is too small to be measured reliably with electron microscopy.

### Circular Dichroism (CD)

The conformation of the peptide moieties was probed with CD spectroscopy. As observed earlier for any GANPNAAG peptide which was modified with an alkyl tail of 14 carbons or longer, PA 1 yielded an enlarged  $\beta$ -sheet-like signal (Figure 5b). As a comparison, coupling of a short (or no) tail to the GANPNAAG peptide resulted in a random coil signal in the CD spectrum (Figure 5a).<sup>2</sup> The signal at 196 nm is higher than expected for a standard  $\beta$ -sheet signal, because of the occurrence of a linear dichroism (LD) effect, which is caused by a macroscopic orientation of the fibres in the solution resulting in an additional contribution to the CD signal.<sup>4</sup>

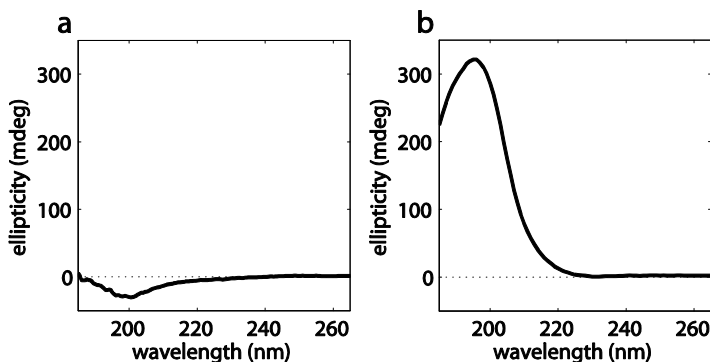


Figure 5. a) CD spectrum from GANPNAAG coupled to lauric acid ( $C_{12}$ ), yielding a random coil signal.<sup>2</sup> b) CD spectrum of PA 1.

### X-ray diffraction

To determine molecular order in the fibres we turned to X-ray diffraction. X-rays scatter on planes present in the sample. At specific angles, related to repeating planes at a defined distance, this scattering leads to positive interference which is described by Bragg's law. When instead of a crystal a powder or a dispersion of aggregates is measured an average is observed because all orientations are present in the sample. Generally, soft samples or samples in solution are more difficult to measure than crystalline samples, since these samples are less ordered. Nevertheless, soft samples such as fibres are not impossible to measure, because in fibrous systems the distances in the fibre direction are highly repetitive. When bundles of fibres are present, even the width of a single fibre can be distinguished. Both dried-in samples and fibres in solution

were measured using several set-ups. Since the fibres assemble in solution and may change structure upon external influences – like temperature and pH – we were primarily interested in the conformation of the fibre in solution. Changes in structure as a result of external influences would then be easy to measure as well. However, measuring solid samples also was of interest since first of all a much higher concentration of PAs could be obtained, giving a better signal to noise ratio, and secondly the possible structural change upon drying the samples could be investigated.

**Small Angle X-ray Scattering (SAXS).** To investigate ‘large’ features of the fibres, such as the bilayer width, small angle X-ray scattering (SAXS, at the DUBBLE beamline at the ESRF in Grenoble) was used. SAXS is commonly employed for studying structures in between 10 and 5000 Å.<sup>5,6</sup> As can be seen in Figure 1, a stretched peptide results in a fibre width of approximately 75 Å with intercalating alkyl tails and about 95 Å when the tails do not overlap. A peptide oriented in a perfect  $\beta$ -hairpin yields a bilayer width of circa 50 Å for intercalating and 70 Å for non-overlapping tails. In solution the largest observed diffraction peak corresponded with 54 Å (Table 2), suggesting intercalating tails and peptides in a turn conformation (models **E**, **G**, **J** and **L**, Table 1). At these small angles, however, not only repetitive distances but also the so-called form-factor plays an important role in the appearance of the diffraction pattern. No higher order reflections are discernible, indicating that indeed the form factor may be the cause of this peak. Furthermore, the 54 Å peak is very broad, and may therefore just depict the size of one (non-repetitive) bilayer. After drying, a much sharper peak at 73 Å was observed instead (Figure 6a), suggesting either a bent peptide with non-overlapping tails or a straight peptide with overlapping tails (models **A**, **C**, **F**, **H**, **J** and **L**). The difference in observed fibre width between solution and dried samples (54 Å and 73 Å respectively) can be accounted for by assuming a lower degree of order of solvent-exposed amino acids in the solution samples. Therefore, the very broad 54 Å peak, associated with the bilayer, may only have shown the central part of the bilayer because the rest was too flexible. On drying, the fibres get closer together and pack with several bilayers on top of each other. In this situation, all residues of the peptide are locked in a defined conformation, and the ‘real’ bilayer thickness can be observed. Amphiphiles freeze-dried from acetic acid were used as a control for the dried samples, since we anticipated that no aggregation would take place in this solvent. Unexpectedly, this solid sample also showed a peak in the X-ray measurements corresponding to a distance of 67 Å. Nevertheless, the observed peak was very broad, merely depicting a repeating distance in an unordered system. In solution and in dried samples, but not in the PAs lyophilised from acetic acid peaks were also observed at 18.5 Å and 14.6 Å. We expect these to be higher order peaks of the bilayer distance (see discussion).

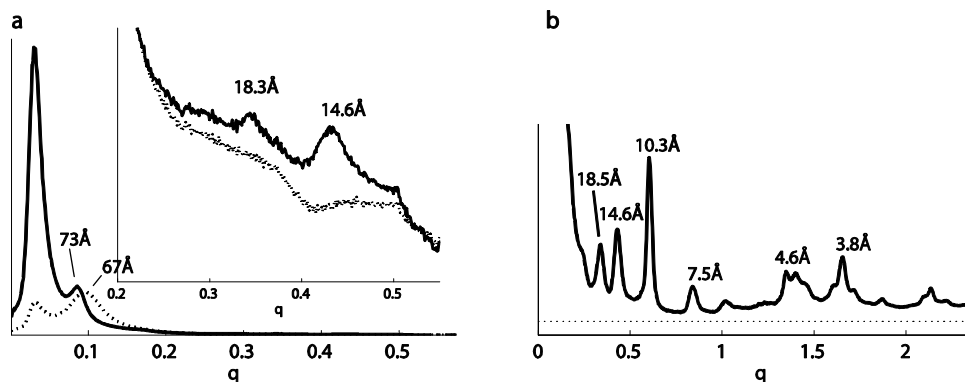


Figure 6. Two examples of X-ray spectra of PA 1. a) SAXS measured using synchrotron radiation on dried-in samples from water (solid line) and AcOH (dotted line). The inset shows an enlargement of these spectra. b) Capillary mode measurement measured using Cu  $K\alpha$  radiation of a dried-in sample.

**Capillary mode measurements.** Smaller features of the peptides were investigated in solution, measured in a capillary which was placed in a position perpendicular to the X-ray beam. In this set-up a weaker beam was used, of which the radiation was generated by Cu  $K\alpha$ . In contrast to the SAXS measurements, the wavelength could not be tuned and much longer measurement times were needed. Upon filling the capillary, the flow induced partial alignment of the fibres. Because this orientation was in the length of the capillary, perpendicular to the beam, distances in the length of the fibres could be determined. Furthermore, because of the preferred orientation, the sample did not resemble a completely randomly oriented powder, and therefore of some distances their orientation relative to each other could be determined. From these measurements, it was determined that the measured 4.7 Å, 4.5 Å and 4.3 Å distances were oriented perpendicular to the 7.5 Å, 10.3 Å, 14.6 Å and 18.5 Å distances (see below). After drying of the solution within the capillary, the sample was measured again, yielding a better resolved diffractogram (Figure 6b). The preferred orientation of the fibres in the capillary was lost upon drying. However, no structural change was induced and the circularly integrated diffractogram showed the same peak positions as the solution sample. Conservation of the structure with drying was also suggested by the microscopy techniques. An overview of observed peaks is given in Table 2. The peaks at 4.7 Å, 4.5 Å and 4.3 Å support the packing of the peptides into a  $\beta$ -sheet conformation, and should be visible both for the linear and turn conformation. Also the 3.8 Å peak is commonly observed in this type of cross  $\beta$ -sheet structures. The 7.5 Å, 10.3 Å, 14.6 Å and 18.5 Å peaks are associated with distances perpendicularly oriented to the  $\beta$  sheet, that can either be appointed to the bilayer dimension or the packing of the peptides in the non-hydrogen bonded direction of the  $\beta$ -sheet.

**Reflection mode experiments.** Samples dried in on a silicon plate were measured in reflection mode. In this orientation, the measurements did not resolve typical  $\beta$ -sheet distances. From TEM and AFM on several substrates it was deduced that the fibres were lying with their long axis parallel to the surface, which is therefore the expected orientation on silicon as well. With the long axis parallel to the surface, the repetitive

planes within that axis do not cause reflection and are therefore invisible. The absence of  $\beta$ -sheet signals suggests the  $\beta$ -sheet direction is in the length of the fibre, thus supporting models **A**, **B** and **E-H**. The peaks which were visible were in line with the other X-ray experiments (Table 2).

A summary of the results of all X-ray measurements is given in Table 2. In our opinion from these results two possible unit cells can be comprised, one of 58.8x20.6x4.7 Å and one of 73.5x10.3x4.7 Å. The first is of a model in which the peptides are in a turn conformation and asymmetrically stacked within the fibre. The 18.5 and 14.6 Å peaks however cannot be satisfactorily explained with this model, and the 73 Å peak cannot be accounted for. Therefore, we prefer the second model, with a unit cell of 73.5x10.3x4.7 Å, which corresponds to a model with a stretched peptide and interdigitating tails perpendicular to the long fibre axis (models **A** and **C**) or a model with the peptide in a turn and tails which were not overlapping (models **F**, **H**, **J** or **L**). A more extensive explanation of the results is given in the general discussion.

| q     | d    | SAXS<br>(solution) | SAXS<br>(dried-in) | Capillary<br>(solution) | Capillary<br>(dried-in) | Reflection<br>(dried-in) | Possible plane<br>(model A)     |
|-------|------|--------------------|--------------------|-------------------------|-------------------------|--------------------------|---------------------------------|
| 1.65  | 3.8  |                    |                    | x                       | x                       | x                        | combination (100 and 010)       |
| 1.40  | 4.5  |                    |                    |                         | x                       |                          | hydrogen bridge (100)           |
| 1.35  | 4.7  |                    |                    | x                       | x                       |                          | hydrogen bridge (100)           |
| 1.02  | 6.2  |                    |                    |                         | x                       | x                        |                                 |
| 0.84  | 7.5  |                    |                    |                         | x                       | x                        | perpendicular to $\beta$ -sheet |
| 0.61  | 10.3 |                    |                    |                         | x                       |                          | perpendicular to peptide (010)  |
| 0.43  | 14.6 | x                  | x                  |                         | x                       | x                        | bilayer thickness (005)         |
| 0.34  | 18.5 | x                  | x                  |                         | x                       | x                        | bilayer thickness (004)         |
| 0.17  | 36.5 |                    | x                  |                         |                         | x                        | bilayer thickness (002)         |
| 0.12  | 54.2 | x                  |                    | x                       |                         |                          | non-ordered bilayer (001)       |
| 0.095 | 66.1 |                    |                    |                         | x                       |                          | slightly ordered bilayer (001)  |
| 0.088 | 71.4 |                    |                    |                         |                         | x                        | bilayer thickness (001)         |
| 0.086 | 73   |                    | x                  |                         |                         |                          | bilayer thickness (001)         |

Table 2. Measured distances with several X-ray techniques. Dark grey means the distance could not be measured in that particular set-up, while light grey are data which were obtained very close to the beam stop and are therefore less reliable. The last column shows the interpretation of the peaks using model A.

## Solid state nuclear magnetic resonance spectroscopy (ssNMR)

As another technique to determine the packing of the amphiphiles NMR spectroscopy was employed,<sup>7-9</sup> which can elucidate the local structure of molecules. The assemblies were too large and immobile to be measured by liquid phase NMR, and therefore solid state NMR (ssNMR) on lyophilised samples was employed. Anisotropic interactions, which cause line broadening, are averaged in liquid phase NMR due to fast molecular tumbling. In ssNMR, the samples are spun very fast around the so-called magic angle (MAS, magic angle spinning) for the same reason - averaging the anisotropic interactions to increase resolution. In addition, the presence of protons (<sup>1</sup>H) shields neighbour atoms such as carbons (<sup>13</sup>C) and nitrogens (<sup>15</sup>N) *via* dipole-dipole interactions, leading to line broadening too. To eliminate this effect, a high radio frequency (RF) <sup>1</sup>H decoupling was used. Under such conditions, spectral resolution in ssNMR is increased and high-resolution measurements can be performed. One way to

elucidate the amphiphile packing in the fibre is by measuring distances between labelled positions in the molecule. The technique we employed in this study was rotational echo double resonance (REDOR).<sup>9</sup> With this method magnetisation is transferred from  $^1\text{H}$  to (in our case)  $^{15}\text{N}$  (see Figure 7 for the pulse sequence). The magnetisation on nitrogen is dephased for a period  $\tau$ , and rephased after a  $\pi$  pulse for the same period. After that, the  $^{15}\text{N}$  spectrum is recorded. During the period  $\tau$ ,  $\pi$  pulses are applied on  $^{13}\text{C}$  which cause dipole-dipole interaction effects on the  $^{15}\text{N}$  spectrum only if the  $^{13}\text{C}$  and  $^{15}\text{N}$  are close enough. The difference between the spectra with and without pulses on  $^{13}\text{C}$  is dependent on the inverse cube distance between the nitrogen and carbon atoms. Therefore, this technique measures distances reliably up to about 5 Å. To employ REDOR, we prepared amphiphiles labelled with NMR-active nuclei.  $^{13}\text{C}$  and  $^{15}\text{N}$  were incorporated at the methylgroup of the  $\text{C}_{16}$  tail (**I**), the nitrogen of the first glycine (**II**) and the carbonyl carbon of the last glycine (**III**, see Figure 8). When the peptide is folded into a perfect hairpin structure, in which hydrogen bridges are present within the molecule (models **E-F** and **I-J**), the distance between nuclei **II** and **III** is 3Å, close enough to determine with  $^{15}\text{N}$ - $^{13}\text{C}$ -REDOR NMR. Intermolecular close contacts between **I** nuclei could disclose whether the alkyl tails of the two bilayers were overlapping or not, while possible interactions between **I** and **II** or **I** and **III** might reveal to what extent the alkyl tails were overlapping.

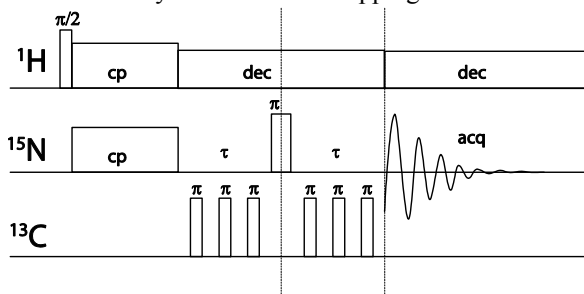


Figure 7. Pulse sequence for a REDOR experiment. The number of  $\pi$  pulses on the  $^{13}\text{C}$  channel depends on the length of  $\tau$  and the sample spinning speed. cp denotes crosspolarisation, dec decoupling and acq acquisition.

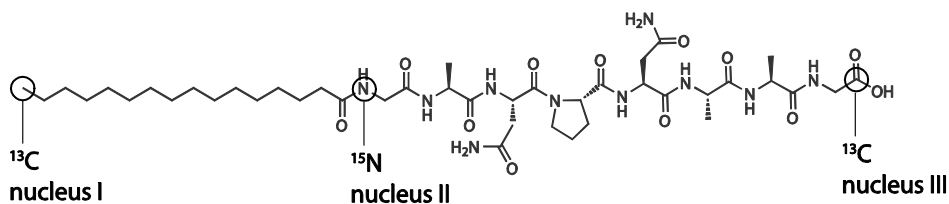


Figure 8. Isotopic labelling of the PA **1** with  $^{13}\text{C}$  and  $^{15}\text{N}$  used for ssNMR.

Carbon spectra of natural-abundance PA fibres were acquired to determine the effect of several rehydration times, one of the parameters investigated for amyloid fibres for which the exact fibre structure is extremely sensitive to the fibre preparation.<sup>8</sup> These spectra were recorded in a cross-polarisation experiment, in which magnetisation is transferred from protons to carbons and the carbon spectrum was measured. At first

sight, the spectra were similar, but since the spectra had a poor signal-to noise ratio small structural differences between the samples may not be resolved.

After the experiments on the natural abundance PAs, single-pulse  $^{15}\text{N}$  spectra were acquired of the labelled amphiphiles. These spectra showed several  $^{15}\text{N}$  resonances, whereas only one was expected since PA **1** possessed only one  $^{15}\text{N}$  label. This suggested that more than one chemical environment was present for the  $^{15}\text{N}$  atoms, which was surprising, since such was not observed in the  $^{13}\text{C}$  spectra. However, since the carbon spectra had a poor signal-to-noise ratio differences among the samples may not have been resolved, as mentioned above. One of the reasons for the difference in environment of  $^{15}\text{N}$  could be the damage of fibres due to freezing (see chapter 3). Furthermore, the fibres can be considered to exist in a kinetically trapped state, and thus an assembly of architectures may be present. Another possible explanation for the observed variety of environments could be the presence of unstructured aggregates in the solution before lyophilisation. To validate this assumption a sample was prepared in which the final annealing step (heating to 90 °C and slow cooling) was omitted, which should result in more disordered fibres and consequently yield more and broader peaks. On the other hand, a sample with an expected better defined fibre conformation was prepared by centrifugation of the sample, after which the supernatant was removed prior to lyophilisation. The removal of the liquid should remove dissolved amphiphiles, yielding a sample containing only fibres. Of course, it does not exclude the presence of large random aggregates that would still hamper the measurements. Surprisingly, the ultracentrifuged sample showed broader peaks than the sample in which the annealing step was omitted, while the opposite result was expected. Besides the broadness of the peaks, no additional spectral differences between these samples and the original one were observed. Therefore, also with these preparation methods, a variety of environments was present for the  $^{15}\text{N}$  atoms.

To examine whether the homogeneity of the fibres is affected by the pH at which they are prepared, the PA was dispersed in three different volatile buffers (pH 4, 7 and 10) and lyophilised. At pH 4, more peaks were observed than under alkaline conditions, indicating a less defined fibre (Figure 9). This was confirmed by TEM measurements and can be explained from the molecular structure of the PAs. Under acidic conditions, the free carboxylic acid ends of the peptides are protonated and the repulsive forces are reduced. Therefore, the tendency for peptide aggregation will be stronger and the assembly faster, resulting in less ordered fibres. Moreover, with decreased repulsive forces, heating to 90 °C might not be enough to disassemble the fibres, thus also yielding less ordered aggregates. However, neither for the samples prepared in alkaline conditions, nor for those prepared at low pH a single peak was observed – neither preparation method resulted in a single environment for the  $^{15}\text{N}$  atoms.



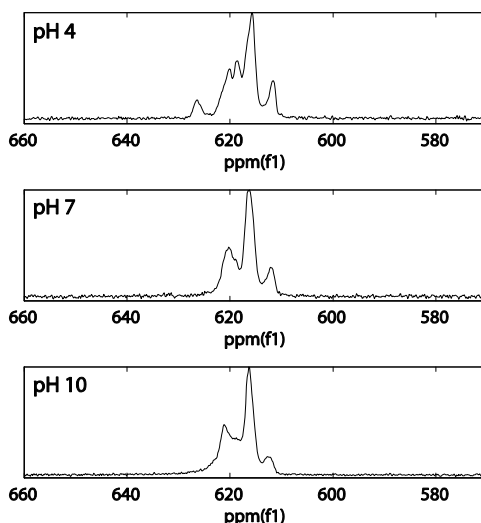


Figure 9. Nitrogen spectra of labelled  $C_{16}$ -GANPNAAG-OH, prepared at three pH values.

Despite the fact that none of the conditions that were tried resulted in a single peak  $^{15}\text{N}$  spectrum, a REDOR experiment was carried out to determine the distance between nuclei **II** and **III** within one amphiphile. To prevent intermolecular interactions from interfering, we used a 1:9 ratio of labelled amphiphile to natural abundance PA. Under these circumstances, only intramolecular interactions are expected to be visible. In the experiment, the signal intensity of an experiment with pulses on carbon was compared to an experiment where these  $\pi$  pulses were omitted, as explained above. The two obtained signals did not differ significantly, indicating that the two nuclei are far apart. Due to a small signal-to-noise ratio distances larger than 4.7 Å could not be determined, and therefore it could only be concluded that the distance between nuclei **II** and **III** was larger than 4.7 Å, and thus that the peptides cannot be in a perfect  $\beta$ -turn conformation, in which the hydrogen bonds are present within the turn.

## H/D exchange measurements

By determining the ease with which protons exchange with solvent it is possible to identify amino acids positioned at the periphery of a protein or peptide assembly.<sup>10-12</sup> Especially amide protons are amenable to such exchange in a protic solvent. The more solvent-exposed the amide protons are, the faster this exchange is. If a protein is prepared in water, it can be diluted into  $\text{D}_2\text{O}$  and exchange of protons for deuterons will take place (Figure 10). For the fibres, measuring the exchange rate could elucidate if the peptides are stretched or in a turn conformation.

**Nuclear magnetic resonance (NMR).** The most direct way to measure exchange is *via* time-dependent NMR measurements (Figure 10). The intensity of the proton peaks decrease upon exchange.

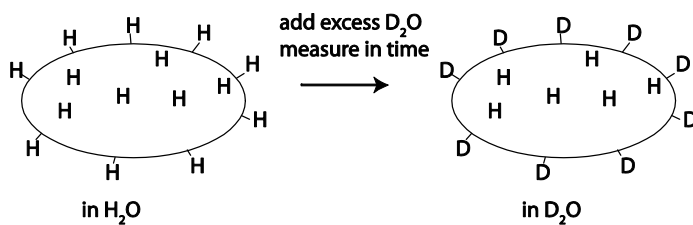


Figure 10. General strategy for measuring exchange in a protein (schematically represented by an ellipse).

Unfortunately, in the case of fibres, aqueous solutions could not be measured directly. The fibres are large and immobile, yielding a broad unresolved NMR spectrum in water (chapter 3). Furthermore, if the fibres are diluted too much, they will disassemble (see chapter 3 for the critical aggregation concentration). Therefore, we prepared fibres in  $\text{H}_2\text{O}$ , subsequently freeze-dried them, redissolved them in  $\text{D}_2\text{O}$ , and after a certain time interval, in which the exchange was allowed to take place, lyophilised them again (Figure 11, left pathway). After this second freeze-drying step, the fibres were dissolved in deuterated DMSO in which no further exchange is supposed to take place and which allows the acquisition of fully resolved  $^1\text{H}$ -NMR spectra. It was important for these measurements that the fibre structure was retained upon lyophilisation. This seemed to be a valid assumption, since with TEM fibres were found to be damaged but still present after freezing (see also chapter 3). Furthermore, X-ray diffractograms supported the conservation of the structure upon drying.

Typically, the amide peaks in the NMR spectra did not decrease upon exposing the sample to  $\text{D}_2\text{O}$ . Even when samples were used below the critical aggregation concentration, in which no fibres were expected to be present and all protons were exposed to  $\text{D}_2\text{O}$ , no exchange was observed (right pathway in Figure 11). Furthermore, preparing the fibres in  $\text{D}_2\text{O}$  – e.g. by heating the amphiphilic solution in  $\text{D}_2\text{O}$  above the temperature at which the fibres are expected to disassemble and all protons should be exposed to  $\text{D}_2\text{O}$  – did not result in the expected 100 % exchange. Only when to a (molecularly dissolved) amphiphile solution in  $\text{DMSO-d}_6$   $\text{D}_2\text{O}$  was added full exchange was observed (last step of the right pathway in Figure 11). Within minutes, all amide peaks had disappeared. Therefore, we performed the same experiment on the peptide without a hydrophobic tail, which does not assemble into fibres at all. Even with this peptide no fully exchanged spectrum was observed. Therefore, a water source might have been present at some point during the sample preparation, causing back-exchange from deuterium atoms to protons. Water may be transferred from other samples during the lyophilisation process or may be present in the deuterated DMSO itself which was used in the NMR experiments. However, even when the presence of any  $\text{H}_2\text{O}$  was thoroughly excluded by using a lyophilizer without any other samples, drying the NMR tubes and employing a fresh ampoule of dry DMSO (<50 ppm  $\text{H}_2\text{O}$ ), the same results were obtained.

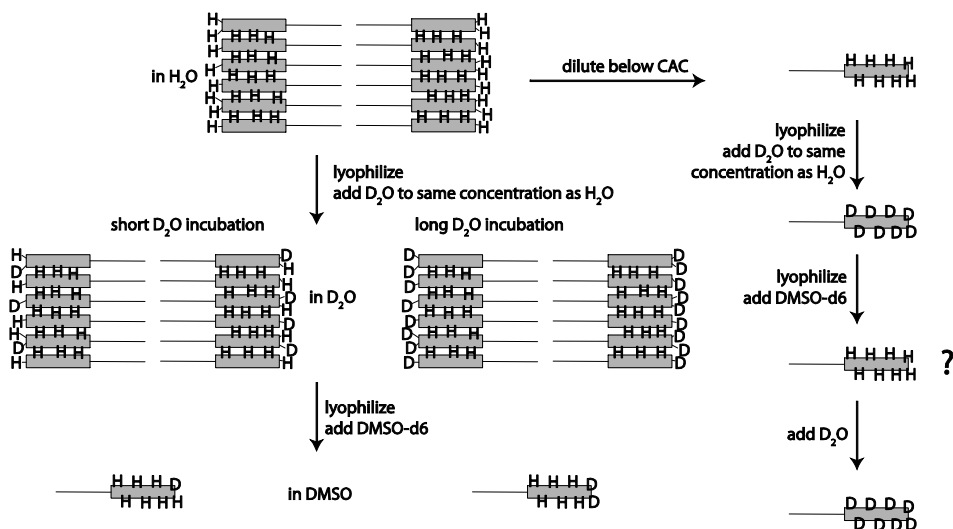


Figure 11. Two exchange strategies. Left: After lyophilisation, the fibres were resuspended in  $D_2O$ , and exchange took place for a defined period before the fibres were lyophilised once more and dissolved in DMSO for NMR measurements. Right: Dissolved amphiphiles were expected to yield full exchange after lyophilisation and incubation with  $D_2O$ , but NMR measurements in DMSO showed no exchange. Addition of  $D_2O$  to the DMSO sample yielded almost immediate exchange.

**Mass spectrometry (MS).** Because of the difficulties we encountered measuring exchange using NMR, another way of determining proton exchange was exerted, employing mass spectrometry (MA). Of the two techniques that were used – matrix assisted laser desorption/ionisation time of flight (MALDI-TOF) and electrospray-ion trap (ESI) – the first has the advantage that during the measurements no solvent is used, and thus no further exchange should take place. The advantage of the ESI measurements is the easier sample preparation. For both MS techniques samples of peptides prepared in  $D_2O$  were used and compared to samples prepared in  $H_2O$ . To ensure full exchange the previously described, non-fibre forming GANPNAAG was used, also employed in the NMR experiments: in  $H_2O$  all amide hydrogens should be protons, in  $D_2O$  they should all have exchanged for deuterons.

For the MALDI experiments, the matrix solution was prepared in  $D_2O$  for the deuterated samples and in  $H_2O$  for the controls. The samples were prepared by putting one microliter of the sample solution on the sample holder and adding one microliter of a matrix solution. Surprisingly, after drying in air no difference in mass was observed for the two solutions. When the sample holder was dried in a desiccator, some exchange was visible, but still not the expected 100 %. The most abundant peak, accounting for about 20 % of the peptide, corresponded to a species in which two protons had been exchanged. Water during the sample preparation may play a role even though a desiccator was used. However, we think it unlikely this is the only cause for the limited exchange. Similar to the NMR experiments, there may be another cause for the back-exchange or lack of exchange in the peptide.

In the ESI measurements a protic solvent was used to inject the peptide into the measurement chamber. Therefore, back-exchange was expected during injection. Indeed, no full exchange was observed for the sample prepared in deuterated water. The maximum exchange, with an abundance of about 20 %, amounted to six protons (Figure 12). The higher mass peaks present were caused by the  $^{13}\text{C}$  natural abundance isotopes of the species with the lower masses. The exchange percentages were determined using fitting of the mass spectra. Typically, these results show that less back-exchange occurred with ESI than with MALDI-TOF. Apparently the presence of water or, as mentioned above, an unknown cause preventing exchange during sample preparation for MALDI played a larger role than diffusion in the ESI experiments. To reduce the exchange further, syringe mode measurements were carried out, in which the deuterated solution was injected directly. However, also with this technique no full exchange was observed, although more protons had exchanged compared to normal injection. To determine the position of exchange, it was attempted to perform MS/MS measurements, but after realising that during the fragmentation scrambling of the deuteriums may take place,<sup>13</sup> these measurements were not further pursued.

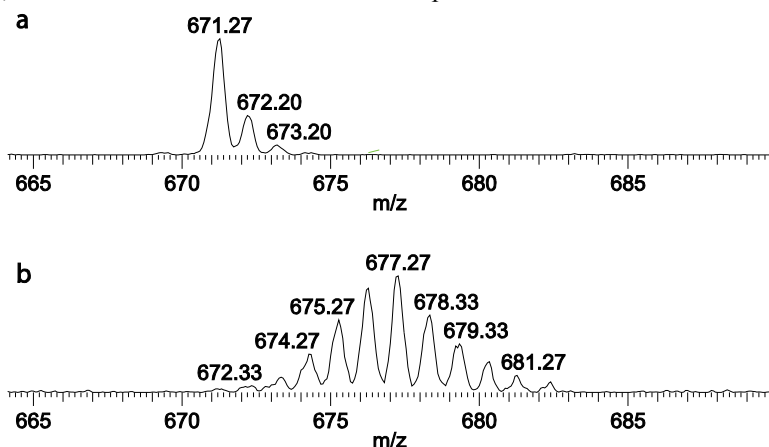


Figure 12. Exchange experiment on the GANPNAAG peptide without alkyl tail using ESI ion trap mass spectrometry. a) control experiment, no exchange, b) largest peak: nine exchanged protons

## General discussion

From electron microscopy and AFM, we conclude that the eight-amino acid peptide GANPNAAG assembles into fibrous architectures in aqueous solution when coupled to an alkyl tail of 16 carbon atoms. The observed twisted ribbons had a width of about 25 nm (determined with cryo-TEM) and were tens to hundreds of micrometers long (observed with TEM, AFM and cryo-TEM).

The possible models for the molecular packing are summarized in Figure 1, and result from differences in overlap of the alkyl tails, conformation of the peptide (stretched or in a  $\beta$ -hairpin) and direction of the hydrogen bond (width or length of fibre). If the peptides adopt a  $\beta$ -hairpin conformation, some more possibilities are considered. The hydrogen bonds may localise in the turn or form perpendicular to the

turn, and the peptides may stack symmetrically or asymmetrically in the fibre. In Table 3 the reasons to reject models are summarized. CD spectroscopy measurements confirmed the validity of a model in which the peptides are oriented in a  $\beta$ -sheet fashion (as in all of the models **A-L**).

The diffraction experiments showed a  $\beta$ -sheet packing, which agreed with the CD experiments, but contained more information. In the reflection mode experiments the typical  $\beta$ -sheet peaks at 4.3, 4.5 and 4.7 Å were not observed, while they were present in the capillary mode experiments. Distances parallel to the surface are invisible in the reflection mode experiments, and therefore the  $\beta$ -sheet direction should be parallel to the surface. In TEM and AFM the fibres were shown to lay flat on several substrates, which is therefore also the expected orientation on silicon, the substrate for X-ray reflection experiments. The flat orientation of the fibres combined with the invisible  $\beta$ -sheet direction suggests that the  $\beta$ -sheet direction is along the long axis of the fibre. This was confirmed by polymerisation experiments on similar PAs with a diacetylene moiety in the hydrophobic tail (chapter 4). Diacetylenes can only polymerise if the distance between adjoining units is approximately 4.5 Å, a distance which coincides with the hydrogen bond direction. Since we observed the polymerisation to take place in the long axis direction of the fibre, this should be the hydrogen bond direction. Therefore, models **C**, **D** and **I-L** are discarded.

From the X-ray results in solution, the bilayer width seemed to be 54 Å, which could be compatible with a model in which the peptide is in a turn conformation (models **E-L**) and the alkyl tails intercalate (leaving models **E**, **G**, **I** and **L**). To explain the 18.5 Å and 14.6 Å peaks, the peptide should then be asymmetrically stacked to yield a unit cell of dimensions 58.8x20.6x4.7 Å. However, with this unit cell the interpretation of the 18.5 Å and 14.5 Å still is unsatisfactory. Either one or the other peak does not really fit in the model. Furthermore, the ~73 Å observed in the dried samples cannot be accounted for by this model. Therefore, a unit cell of dimensions 73.5x10.3x4.7 Å is proposed, which suggests either a bent peptide with non-overlapping tails or a straight peptide with overlapping tails (models **A**, **C**, **F**, **H**, **J** and **L**). The 36.5 Å, 25 Å, 18.5 Å and 14.6 Å peaks were accounted for as higher order peaks of the bilayer (see Table 2). The shorter value of the bilayer in solution (54 Å instead of 73 Å) can be explained by assuming less order of the solvent-exposed amino acids in the solution. Therefore, the very broad 54 Å peak, associated with the bilayer, only reflects the centre part of the bilayer. On drying, the fibres get closer together and pack with several layers of the bilayer upon each other. In this situation, all residues of the peptide are locked in a defined conformation, and the 'real' bilayer thickness is visible. The higher mobility of the peptides in solvent seems more likely for a stretched (**A**, **C**) than for a bent peptide (**F**, **H**, **J**), but both are possible. Following this argument, models **B**, **D**, **E**, **G**, **I** and **K** become improbable. From the combined X-ray observations, model **A** seems the most plausible although **H** is also possible. A drawback of this interpretation of the X-ray measurements is the assumed high order in the bilayer direction. For seventh and maybe even tenth order peaks, observed in the dried samples, to show up, the system has to be highly ordered in this direction, while we expected the bilayer direction to be the least ordered.

The solid state NMR measurements excluded the models in which the peptide was folded and the  $\beta$ -sheet was present in a turn (**E**, **F**, **I** and **J**) which supports the X-ray experiments.

In conclusion, the abovementioned observations only leave models **A** and **H** as possibilities for the amphiphile packing. However, the models in which a turn conformation is combined with non-overlapping tails (models **F**, **H**, **J** and **L**) would introduce thermodynamically very unfavourable empty space into the fibre, and are thus considered less likely models. Furthermore, the increased mobility of the bilayer in solvent may be also easier accounted for in stretched peptides than for peptides in a turn conformation. For both of these reasons, model **H** is less likely, and therefore we are of the opinion that the fibres are packed according to model **A**.

| Model | Peptide   | H-bond direction |               | Alkyl tails     | Discarded because                           |                                      |
|-------|-----------|------------------|---------------|-----------------|---|--------------------------------------|
| A     | Straight  | Length           |               | Overlapping     | Bilayer                                     |                                      |
| B     |           | Width            |               | Non-overlapping |   |                                      |
| C     |           |                  |               | Overlapping     |   | Invisibility $\beta$ -sheet          |
| D     |           |                  |               | Non-overlapping |   | Invisibility $\beta$ -sheet; Bilayer |
| E     | In a turn | Length           | In turn       | Overlapping     | Bilayer; ssNMR                              |                                      |
| F     |           |                  |               | Non-overlapping |   | ssNMR; Empty space                   |
| G     |           | Perpendicular    |               | Overlapping     | Bilayer                                     |                                      |
| H     |           |                  |               | Non-overlapping |   | Empty space                          |
| I     |           | Width            | In turn       | Overlapping     | Invisibility $\beta$ -sheet; Bilayer; ssNMR |                                      |
| J     |           |                  |               |                 |   | Non-overlapping                      |
| K     |           |                  | Perpendicular |                 | Overlapping                                 | Invisibility $\beta$ -sheet; Bilayer |
| L     |           |                  |               |                 | Non-overlapping                             |                                      |

Table 3. Summary of reasons for which the different models are discarded. ‘Invisibility  $\beta$ -sheet’ refers to the absence of typical  $\beta$ -sheet distances in reflection mode X-ray experiments. The entries labelled ‘bilayer’ are discarded because of the incompatibility of the bilayer width in that model with the measured 73 Å. Solid state NMR measurements showed that the peptides were not in a perfect turn fold (‘ssNMR’) and the models labelled ‘empty space’ are less likely because of thermodynamic considerations.

## Conclusions

A schematic representation of the fibre model that fits all the acquired data (model **A**) is shown in Figure 13. PA fibres built up of **1** organise according to this model, which means that the peptides are in a stretched  $\beta$ -sheet conformation, with hydrogen bonds directed along the long axis of the fibre, and with alkyl chains that are interdigitated. These single layer fibres stack *via* both hydrophobic and hydrogen bonding interactions into fibres of 25 nm width and micrometers length which are observed with TEM and AFM.

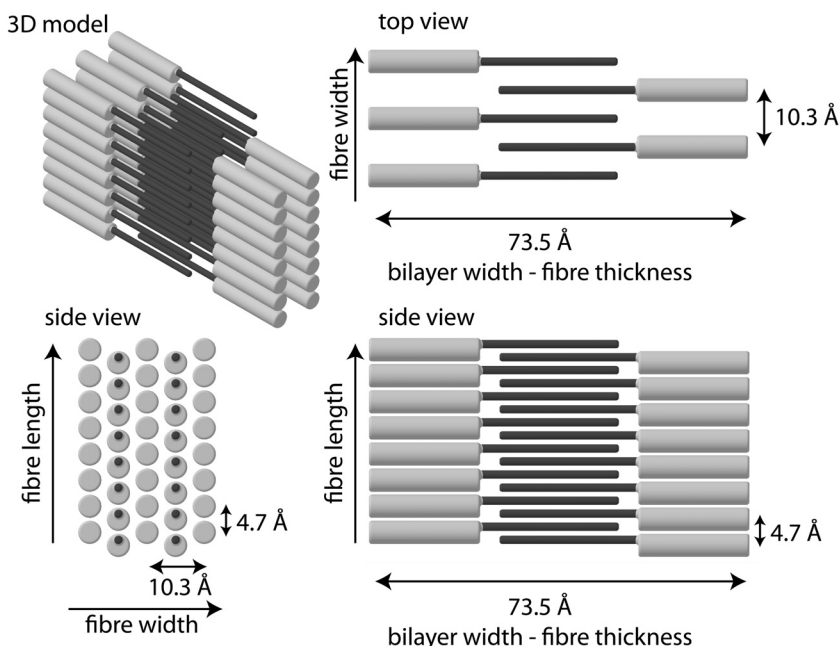


Figure 13. The model of the PA fibre which combines the observations from all performed measurements.

## Acknowledgements

For the cryo-TEM measurements we want to thank Peter Frederik from Maastricht University. For the SAXS measurements in Grenoble we want to thank Kristina Kvashnina and Wim Bras, from BM 26, and Arnold Nijhuis, Martin Feiters and Mark Damen for help with the measurements. The capillary mode measurements were performed by Loes Kroon-Batenburg from the University of Utrecht, who also helped with the interpretation. We want to thank René de Gelder and Carmen Guguta for help with the reflection mode X-ray. For the solid state NMR measurements we would like to thank Andreas Brinkmann, Ernst van Eck and Jorge Garibay. Loes Ruizendaal did most of the exchange NMR experiments, and Peter van Galen helped me with the ESI part of the exchange experiments. Furthermore, for the drawing of the 3D models we want to thank Pieter Nieuwland.

## Experimental section

**General.** All starting materials were obtained from commercial suppliers and used as received. Thin layer chromatography was performed on Kieselgel F-254 pre-coated silica plates or RP-8 F-254s. Visualization was accomplished with TDM.<sup>14</sup> Column chromatography was carried out on Merck silica gel 60 (230-400 mesh ASTM). <sup>1</sup>H-NMR spectra were recorded on a Varian Mercury, 400 MHz. DMSO-d<sub>5</sub> ( $\delta = 2.50$  ppm) was used as a solvent shift reference. Mass spectra were recorded on a JEOL AccuTOF-CS spectrometer.

**Synthesis of the amphiphiles.** The GANPNAAG peptide was prepared by standard solid-phase Fmoc protocols.<sup>15</sup> To couple the first glycine to a p-alkoxybenzy alcohol resin,<sup>16</sup> the resin was washed three times with dichloromethane and subsequently suspended in dimethylformamide (DMF). Two equivalents of the Fmoc protected glycine, 4 equivalents 1-hydroxybenzotriazole hydrate (HOBt), 2 eq diisopropylcarbodiimide (DIPCDI) and 2 eq 4-dimethylaminopyridine (DMAP) were added. The suspension was agitated overnight. The suspension was then filtered, washed and dried under vacuum, to result in a resin with a loading of 0.67 mmol Fmoc-Gly per gram.

In all subsequent couplings we used 3 equivalents of the amino acid, 3.3 equivalents DIPCDI and 3.6 equivalents HOBt in DMF. Deprotections were carried out using a 20% piperidine solution in DMF. After each coupling and deprotection a Kaiser test<sup>17</sup> was performed to check the completeness of the reactions. After removal of the final Fmoc group the peptide was functionalized on the resin employing 3 equivalents palmitic acid dissolved in dichloromethane to which 3.3 equivalents DIPCDI and 3.6 equivalents HOBt in DMF were added. The product was cleaved from the resin by treatment with trifluoroacetic acid/H<sub>2</sub>O/triisopropylsilane (95:2.5:2.5) for two hours followed by precipitation in ether or removal of the volatiles in vacuo. Column chromatography (eluent: CHCl<sub>3</sub>/MeOH/H<sub>2</sub>O 65:25:4) and subsequent lyophilization afforded pure compounds according to <sup>1</sup>H-NMR, MS and TLC.

Yield: 76%, based on Fmoc-Gly loading (0.67 mmol/g) of initial resin.

TLC: R<sub>f</sub> 0.33 (eluent: MeOH/ CHCl<sub>3</sub>/ AcOH 25:65:10).

<sup>1</sup>H-NMR [DMSO-d<sub>6</sub>]: δ 0.85 (t, CH<sub>3</sub> -alkyl chain, 3H), 1.12 (d, CH<sub>3</sub> -Ala, 3H), 1.20 (m, -CH<sub>2</sub>-alkyl chain; CH<sub>3</sub> -Ala, 30H), 1.48 (m, CH<sub>2</sub>-alkyl chain, 2H), 1.85 (m, CH<sub>2</sub> Pro, 3H), 2.18 (m, CH<sub>2</sub> Pro; α-CH<sub>2</sub>-alkyl chain, 3H), 2.40 (m, CH<sub>2</sub> Asn, 2H), 2.55 (dd, CH<sub>2</sub> Asn, 1H), 2.65 (dd, CH<sub>2</sub> Asn, 1H), 3.65 (m, α-CH<sub>2</sub> Gly; CH<sub>2</sub> Pro, 3H), 3.75 (m, CH<sub>2</sub> Pro; α-CH<sub>2</sub> Gly, 3H), 4.20 (m, CH<sub>2</sub> Pro; α-CH<sub>2</sub> Ala, 4H), 4.40 (m, α-CH<sub>2</sub> Asn, 1H), 4.73 (q, α-CH<sub>2</sub> Asn, 1H), 6.92 (s, NH<sub>2</sub> Asn, 1H), 7.10 (s, NH<sub>2</sub> Asn, 1H), 7.20 (s, NH<sub>2</sub> Asn, 1H), 7.52 (d, α-NH Ala, 1H), 7.64 (s, NH<sub>2</sub> Asn, 1H), 7.72 (d, α-NH Ala, 1H), 7.88 (two d, α-NH Asn; α-NH Ala, 2H), 7.96 (broad s, α-NH Gly, 2H), 8.27 (d, α-NH Asn, 1H), 12.45 (broad s, OH, 1H).

Maldi-TOF: Calc. for [C<sub>42</sub>H<sub>72</sub>N<sub>10</sub>O<sub>12</sub> + Na]<sup>+</sup> 931.5, found 931.2.

**Fibre preparation.** Unless stated otherwise, for preparation of the fibres, the amphiphiles were dispersed in milli-Q at the desired concentrations. The samples were heated to 50 °C for 30 min, followed by 15 min sonication at that temperature. Subsequently, the samples were heated to 90 °C and allowed to cool to room temperature.

**Transmission electron microscopy (TEM).** TEM samples were prepared by floating a carbon-coated copper grid on a peptide amphiphile solution of either 1.0 or 0.2 mg/mL for 5 min, followed by removal of residual water by blotting with a paper filter. The samples were visualized using a JEOL 1010 transmission electron microscope set on an accelerating voltage of 60 kV.

**Cryo-TEM.** Samples for the cryo-TEM (PA 1 solution of 5 mg/mL, prepared following the standard procedure described above) were prepared on carbon-coated copper grids which were treated with ozone to increase their hydrophilicity. A droplet of 3 μl was placed on the grid and excess of sample was blotted with filter paper to leave a thin film on the grid. This film was vitrified in liquid ethane and analyzed in a Philips TEM (CM 12) at -170 °C. The whole sample preparation was carried out in a controlled environment vitrification system to ensure cryofixation of the specimen from a controlled temperature and without loss of water or volatile compounds.

**Atomic Force Microscopy (AFM).** AFM measurements were performed on a DI Dimension 3100. A 5 μL sample of PA 1 with a concentration of 0.2 mg/mL, prepared following the standard procedure (see above), was placed on either a mica, a glass or a fused silica substrate and allowed to dry. The data were processed using the WSxM software package.<sup>18</sup>



**Circular dichroism (CD) spectroscopy.** Measurements were carried out at a concentration of 0.2 mg/mL using a 1 mm quartz cell. The spectra were recorded on a JASCO J-810 spectropolarimeter equipped with a Jasco PTC-423S/L Peltier type temperature control system. Spectra were measured from 265-185 nm at 100 nm/min. To measure temperature curves, a heating or cooling rate of 3°C/min was used. During the heating and cooling the CD intensity was measured at 196 nm.

### **X-ray diffraction.**

**Small Angle X-ray Scattering.** SAXS experiments were conducted on the SAXS station (BM 26.2) at the Dutch-Flemish beamline (DUBBLE) at the European Synchrotron Radiation Facility in Grenoble, France. During the experiments the ESRF was running at 170 mA, and the monochromator of the SAXS station was set at 1.24 Å. A measuring window from 10 to 200 Å was employed, using a wavelength of 0.95 Å. SAXS data of fibres with a concentration of either 10 or 20 mg/mL in 2 mm diameter capillaries were recorded with the gas multiwire 2-dimensional detector at a sample to detector distance of 1.5 m. The data were successively normalized for absorption and detector uniformity; the background scattering due to solvent and empty capillary was subtracted. Spatial calibration was performed with silver behenate,<sup>19</sup> with an estimated error margin of ± 0.5 % in the observed periodicities.

**Capillary mode.** X-ray diffraction data in the capillary mode set-up were recorded on a Mar Image Plate using Cu K $\alpha$  radiation from a BrukerAXS FR591 generator with rotating anode and Montel 200 mirrors. A 10 mg/mL solution of the amphiphile was inserted into a capillary. The samples were measured in the solution state, but were also allowed to dry under ambient conditions. The capillaries were placed in a position perpendicular to the X-ray beam and at a distance of 250 mm from the detector. Scattering of air and the capillary was subtracted by using in-house software (VIEW/EVAL).<sup>20</sup>

**Reflection mode.** X-ray powder diffraction in reflection mode was performed on dried samples using a Bruker D8 AXS Advance X-ray Diffractometer with a VÅNTEC-1 detector. The diffractometer was equipped with a Johansson type monochromator. The detector was set at an effective angular region of 2 °. The data were collected in reflection geometry using monochromatic Cu K $\alpha$  radiation, 2  $\theta$  range 0.2-60 °, stepsize 0.01 ° and counting time 10 s.

### **Solid state nuclear magnetic resonance (ssNMR) spectroscopy.**

**General.** For the ssNMR measurements, amphiphiles with three NMR active nuclei were synthesized following standard solid phase chemistry and purification as described for the unlabelled compound. The spectra were measured on a 400 MHz wide bore Varian spectrometer with a triple resonance probe (<sup>1</sup>H, <sup>13</sup>C, <sup>15</sup>N), under magic angle spinning. The magic angle was set using KBr, and adamantane was used as reference.

**Rehydration.** Fibres from unlabelled amphiphiles were prepared following the standard method with a concentration of 2 mg/mL, followed by freeze-drying and rehydration of the sample in a humid environment for 0, 1 and 3 h. <sup>13</sup>C spectra were measured using cross-polarisation and under 3.5 kHz magic angle spinning. The 90 ° pulse on protons was 2.4  $\mu$ s, the contact time 2.2 ms. Proton decoupling was performed at 75 kHz, using a TPPM sequence, with pulses of 35 ° with a length of 6.3  $\mu$ s.

**Variation of preparation method.** The <sup>15</sup>N spectra of 100 % labelled fibres prepared via several methods (a-d) were compared. a) PA 1 (2 mg/mL) was prepared following the standard method and freeze-dried. b) PA 1 (2 mg/mL) was prepared following the standard method, but omitting the heating step to 90 °C and lyophilised. c) PA 1 (2 mg/mL) was divided into six fractions which were ultracentrifuged with 50.000 rpm, applying a force of 302.000g. The pellets were combined and lyophilised d) PA 1 was prepared at a concentration of 2 mg/mL using the

standard method but using buffers with a concentration of 0.2 M instead of milli Q water as solvent (pH 4: ammonium acetate/acetic acid; pH 7: ammonium carbonate/acetic acid; pH 10: ammonium carbonate/ammonia). Nitrogen spectra were measured after lyophilisation.

$^{15}\text{N}$  spectra were obtained in a 3.2 mm sample spinner probe, under magic angle spinning of 9 kHz. The  $90^\circ$  pulse on the  $^1\text{H}$  channel was optimized *via* nutation experiments to be about 2.3  $\mu\text{s}$  (RF field strength 108 kHz). The Hartmann-Hahn condition was set for a contact time between the  $^1\text{H}$  and  $^{15}\text{N}$  of 4 ms, and the RF field strength of  $^1\text{H}$  to 60 kHz. The proton decoupling power and decoupling time were in general about 100 kHz and 5 ms respectively, the decoupling was set using TPPM with an angle of about  $17^\circ$  and a time of about 5  $\mu\text{s}$ . All these parameters were optimised for all experiments. The number of transients was between 11000 and 43000 spectra.

**REDOR experiments.** For the intramolecular close-contact measurements a solution consisting of 10 % labelled and 90 % unlabelled amphiphile (total concentration 2 mg/mL) was used to prepare the fibres following the standard method. The measurements were performed with 9 kHz magic angle spinning speed, and the pulse sequence described by Jaroniec et. al.<sup>9</sup> A cross polarisation time between  $^1\text{H}$  and  $^{15}\text{N}$  of 2 ms was used. A TPPM proton decoupling was used with an angle of  $15^\circ$  for 6.25  $\mu\text{s}$ . The  $180^\circ$  pulse on  $^{13}\text{C}$  was determined to be 12.5  $\mu\text{s}$  (RF strength of 39.9 kHz).

### Exchange experiments

**NMR.** For the exchange experiments with NMR we started from a fibre solution (0.2 mg/mL) in water prepared following the standard procedure. After freeze-drying, the fibres were redissolved in  $\text{D}_2\text{O}$  without heating or ultrasonic treatment. After a defined time, the solution was lyophilized, dissolved in DMSO and measured on a Varian Mercury 400 MHz NMR.

**MALDI-TOF.** Samples (0.2 mg/mL) were prepared in either  $\text{D}_2\text{O}$  or  $\text{H}_2\text{O}$ , and 10 mg/mL 2,5-dihydroxybenzoic acid (DHB) in either  $\text{D}_2\text{O}$  or  $\text{H}_2\text{O}$  was used as a matrix. One microliter of sample solution was pipetted onto the MALDI-TOF plate, followed by one microliter of matrix solution. Drying of the plate was done in air or in a dessicator. In the latter case, the periods during spotting of the sample in which the plate was exposed to air were kept as short as possible. The spectra were recorded on a Bruker Biflex II mass spectrometer, with a MTP 384 target ground steel plate as sample plate.

**ESI-iontrap.** For the ESI measurements the samples were prepared at a concentration of 0.2 mg/mL. 10  $\mu\text{L}$  of this solution was injected into the sample chamber in case of the injection experiments. For the syringe experiments, a continuous flow of the sample solution was injected into the sample chamber. The spectra were recorded on a Thermo Scientific LCQ Advantage Max mass spectrometer.

### References

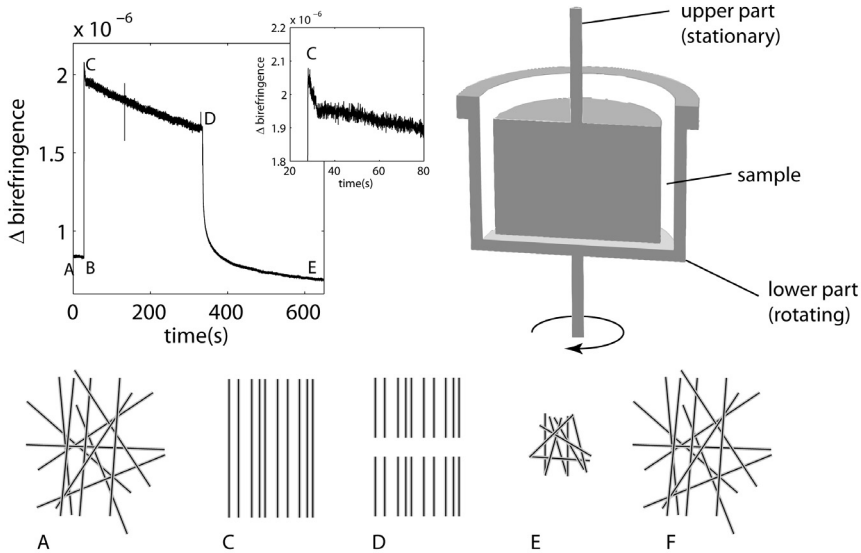
1. C. Cerami, U. Frevert, P. Sinnis, B. Takacs, P. Clavijo, M. J. Santos and V. Nussenzweig, *Cell*, 1992, **70**, 1021-1033.
2. D. W. P. M. Löwik, J. Garcia-Hartjes, J. T. Meijer and J. C. M. van Hest, *Langmuir*, 2005, **21**, 524-526.
3. A. Ghasparian, K. Moehle, A. Linden and J. A. Robinson, *Chem. Comm.*, 2006, 174-176.
4. M. Wolffs, S. J. George, Z. Tomovic, S. C. J. Meskers, A. Schenning and E. W. Meijer, *Angew. Chem., Int. Ed.*, 2007, **46**, 8203-8205.
5. M. H. J. Koch, P. Vachette and D. I. Svergun, *Q. Rev. Biophys.*, 2003, **36**, 147-227.
6. M. J. Krysmann, V. Castelletto, A. Kelarakis, I. W. Hamley, R. A. Hule and D. J. Pochan, *Biochem.*, 2008, **47**, 4597-4605.
7. T. Asakura, H. Sato, F. Moro, Y. Nakazawa and A. Aoki, *J. Am. Chem. Soc.*, 2007, **129**, 5703-5709.
8. R. Tycko, *Q. Rev. Biophys.*, 2006, **39**, 1-55.

## Chapter 2

9. C. P. Jaroniec, C. E. MacPhee, V. S. Bajaj, C. M. Dobson and R. G. Griffin, *Biophys. J.*, 2003, **84**, 154A-154A.
10. M. V. Jagannadham and R. Nagaraj, *J. Pept. Res.*, 2005, **66**, 94-100.
11. Y. Z. Zhang, Y. Paterson and H. Roder, *Protein Sci.*, 1995, **4**, 804-814.
12. X. J. Lu, P. L. Wintrode and W. K. Surewicz, *Proc. Natl. Acad. Sci. U. S. A.*, 2007, **104**, 1510-1515.
13. T. E. Wales and J. R. Engen, *Mass Spectrom. Rev.*, 2006, **25**, 158-170.
14. E. V. Arx, M. Faupel and M. Brugger, *J. Chromatogr.*, 1976, **120**, 224-228.
15. G. B. Fields and R. L. Noble, *Int. J. Pept. Protein Res.*, 1990, **35**, 161-214.
16. J. W. Van Nispen, J. P. Polderdijk and H. M. Greven, *Recl. Trav. Chim. Pays-Bas*, 1985, **104**, 99-100.
17. E. Kaiser, R. I. Colescot, C. D. Bossinge and P. I. Cook, *Anal. Biochem.*, 1970, **34**, 595-598.
18. I. Horcas, R. Fernandez, J. M. Gomez-Rodriguez, J. Colchero, J. Gomez-Herrero and A. M. Baro, *Rev. Sci. Instrum.*, 2007, **78**, 0137051-0137058.
19. T. C. Huang, H. Toraya, T. N. Blanton and Y. Wu, *J. Appl. Crystallogr.*, 1993, **26**, 180-184.
20. A. J. M. Duisenberg, L. M. J. Kroon-Batenburg and A. M. M. Schreurs, *J. Appl. Crystallogr.*, 2003, **36**, 220-229.

## Chapter 3

# Mechanics and thermodynamics of peptide amphiphile fibres.



In this chapter the mechanical and thermal stability of self-assembled fibres of palmitoyl functionalized GANPNAAG were studied. In order to study the mechanical stability shear stress and elongational forces were applied. Furthermore, solutions were frozen to see the influence of ice formation on mechanical stability, i.e. to investigate fracture as a function of freezing. The thermal stability was investigated by following the disassembly upon heating and reassembly upon cooling. The determination of the temperature dependent critical aggregation concentration allowed us to estimate the entropy and enthalpy for fibre growth. The fibres turned out to be thermodynamically very stable, but mechanically weak, a seemingly contradictory combination.

## Introduction

Amphiphiles in water assemble into architectures which are defined by the choice of the amphiphile structure, pH, temperature and additives in the solution and which can thus be tuned for a variety of applications. As was described in chapter 1, fibres are an important class of self-assembled architectures, and have been used amongst others as hydrogels for tissue-engineering,<sup>1-3</sup> as drug-delivery vehicles, as MRI contrasting agent<sup>4,5</sup> and to direct neurite growth.<sup>6</sup> To determine the possible scope of applications in which these architectures can be applied, not only structure but also dynamic behaviour is of importance. For example, in blood vessels and the extracellular matrix shear rates of  $100 \text{ s}^{-1}$  to  $8000 \text{ s}^{-1}$  are present.<sup>7</sup> An effective drug delivery cargo has to withstand these forces without breaking. In natural systems such as amyloid fibres and actin filaments, shear force has a large influence on fibre growth and fracture.<sup>7,8</sup> Furthermore, breakage of amyloid fibres is thought to play a significant role in the growth mechanism of these disease-associated fibrils.<sup>9</sup> The component in the shear force that causes the breakage of the fibres is elongational flow. This force stretches a macromolecule with a parabolic force profile in which the largest force is present in the middle of the fibre.<sup>10,11</sup> The elongational force can even be large enough to break (covalently bound) polymers such as polystyrene<sup>10</sup> and poly(ethylene glycol).<sup>11</sup> Amyloid fibres<sup>7</sup> and fibres from whey protein isolate<sup>12</sup> are also known to fracture under elongational forces. In contradistinction, mechanical disturbance is also known to accelerate fibre growth.<sup>9,13</sup> This enhanced growth rate is probably caused by the presence of more growth sites. Besides the stability to mechanical forces, also thermal stability is an important factor for self-assembled systems. Dynamic architectures may change morphology or disassemble upon heating.<sup>14</sup> The structural changes may be employed but can also hamper possible applications. In both cases thermal behaviour should be known to determine the scope of possible applications.

The eight amino acid peptide GANPNAAG coupled to palmitic acid (PA 1, Figure 1) which assembles into fibres in aqueous environment has been studied extensively in our group.<sup>15</sup> The peptide is derived from the CS protein of the malaria parasite *Plasmodium Falciparum*.<sup>16</sup> The synthesis, investigation of morphology and molecular arrangement of these PAs has been described in chapter 2. The morphology was studied with transmission electron microscopy (TEM, Figure 2) and CD spectroscopy.<sup>15</sup> The peptide amphiphiles pack in a stretched  $\beta$ -sheet structure with intercalating tails.

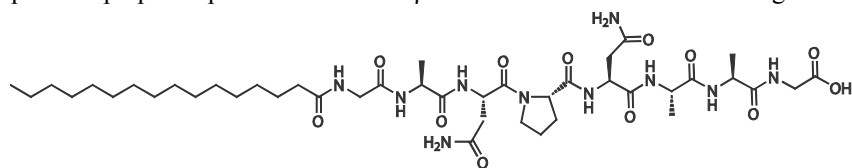


Figure 1. The structure of the peptide amphiphile studied in this chapter, PA 1.

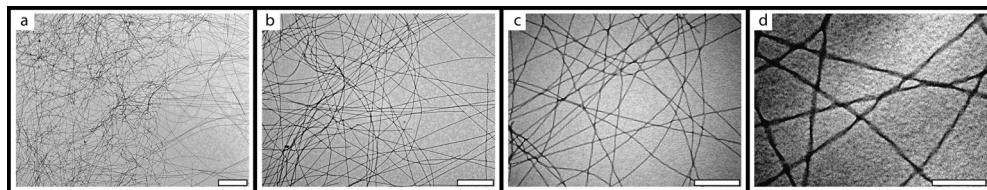


Figure 2. TEM graphs of PA 1. The succeeding images show different magnification of the same sample. The white bars represent a) 2  $\mu\text{m}$ , b) 1  $\mu\text{m}$ , c) 500 nm, d) 200 nm.

In this chapter the thermodynamic and mechanical stability of these self-assembled fibres are described. To investigate mechanical stability, properties at room temperature, such as the critical aggregation concentration, the dynamics of disassembly and the effects of shear and elongational flow, were investigated. Since lyophilisation is often applied to preserve nanostructures, the effect of freezing which is known to damage many proteins<sup>17, 18</sup> was investigated as well. Besides mechanical stability, we studied the effect of temperature on disassembly and reassembly of the fibres. Thermodynamic parameters for the assembly were determined by combining the critical aggregation concentration with the disassembly and assembly temperatures.

One of the main characterisation techniques used in this chapter is rheo-optics.<sup>19</sup> This unique technique is based on the birefringence of aligned fibre samples. A fibre containing solution is placed in a Couette cell (Figure 3) and a laser is guided through from top to bottom. In Figure 3 a typical rheo-optics experiment is shown. The birefringent signal for a solution in a cell in rest is low (Figure 3, **A** to **B**), and the fibres are randomly oriented. Upon rotation of the cell, the fibres align in the direction of flow, which results in an increase in birefringence signal if the fibres are birefringent. At the onset of rotation (**C**) the signal is higher, but it quickly comes back to a signal intensity which changes only slowly in time. This observed 'peak' is caused by the difference in time scale between convection and diffusion. Immediately after starting the rotation, the time scale of convection is smaller than that for diffusion, and therefore fibres are effectively aligned. After this initial short time, the rotational diffusion decreases the alignment and with that the birefringent signal.<sup>20</sup> A decrease in birefringence signal during rotation (between **C** and **D**) indicates fibre breakage because of elongational forces. Generally, however, the signal has a constant value in this part of the curve.<sup>7, 21</sup> After a rotation of five to fifteen minutes the rotation stops (**D**) and the fibres relax into a random orientation. For short fibres the decay back to the baseline will take less than a minute, for longer fibres it can take up to hours, especially for entangled systems. From the decay curve (between **D** and **E**) a length distribution of the fibre sample can be determined, as has been described by Rogers *et al.*<sup>21</sup> In a dynamic system in which fibre breakage (birefringent signal decrease) was observed between **C** and **D**, the fibres not only go back to random orientation, but also reassemble to their original length (between **D** and **F**).

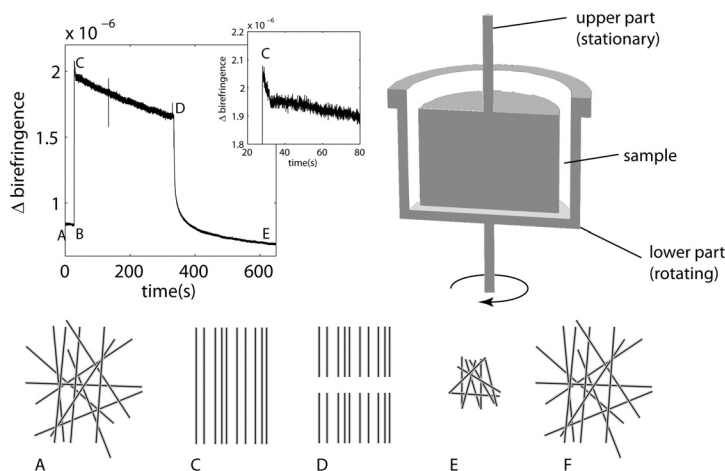


Figure 3. A typical rheo-optics experiment, in which a concentration of 100  $\mu\text{g/mL}$  of PA **1** was used. **A**) The fibres are randomly oriented. **B**) The Couette cell starts rotating and the fibres are aligned. **C**) At the beginning of the rotation a small peak (inset) is visible, due to overshoot. Between **C** and **D**) The Couette cell rotates and the fibres are breaking due to elongational forces. **D**) The rotation of the cell is stopped and the damaged fibres relax back to **E**) random orientation. **F**) The fibres regrow after damage, yielding the starting situation (**A**). The couette cell in which the measurements are performed is shown in the upper right corner.

### The critical aggregation concentration (CAC)

Like all self-assembling molecules, PA **1** is molecularly dissolved up to a concentration called the critical aggregation concentration (CAC). Above this concentration the additional amphiphiles assemble, leaving the concentration of molecularly dissolved amphiphiles constant. We have attempted to determine the CAC using surface tension measurements, isothermic titration calorimetry (ITC), rheology, fluorescence spectroscopy measurements with a fluorescent probe, circular dichroism (CD) spectroscopy and rheo-optics.

**Surface tension.** Free amphiphiles influence the surface tension of an aqueous solution, which can be probed by the shape of a droplet.<sup>22</sup> The concentration at which the droplet shape stops changing with increasing concentration is the CAC. Unfortunately, the results obtained from the surface tension measurements on PA **1** were not reproducible. This was probably due to the high temperature of the solid-to-liquid transition of the alkyl tails in the fibres. Reliable surface tension measurements are only possible if the fatty acid chains of the amphiphile are in their liquid-like phase. In fibres of PA **1** the alkyl chains are probably in their solid-like state at room temperature. Differential scanning calorimetry (DSC) measurements were performed to reveal the solid-to-liquid transition temperature of the alkyl tails. Unfortunately, no transition was visible using this technique in the temperature range measurable in aqueous solution (between 5 and 90°C) using scanning rates between 0.3 and 15 °C/min and concentrations from 0.2 to 60 mg/mL. This led us to believe the tails were in the

solid-like state over the entire temperature range. This was corroborated by the fact that it was possible to polymerise a similar PA with a diacetylene functionality in the hydrophobic tail (see chapter 4).<sup>23, 24</sup> This PA behaves very similarly to PA **1** and we therefore think the packing of the tails is comparable in both cases. The diacetylene moiety gives the possibility of polymerisation only if the alkyl tails are in an almost crystalline lattice – thereby confirming the solid-like state of the alkyl tails in these fibres.

**Isothermal titration calorimetry (ITC).** ITC is a technique mostly used to measure binding constants. The titration of a guest to a host results in binding of the guest, and the dissipated heat is monitored with ITC.<sup>25</sup> In addition, also the disassembly of a complex can be measured by ITC.<sup>26</sup> A concentrated fibre solution diluted below the CAC is expected to disassemble, and the heat generated by the disassembly process can be measured to determine the CAC. With each addition the solution becomes more concentrated, and when the CAC is reached the assemblies do not disassemble anymore. However, ITC relies on a fast disassembly of the aggregates and PA **1** disassembled very slowly, as we will see further on. Therefore, ITC was not suited to measure the CAC of these fibres either.

**Viscosity measurements.** Concentrated solutions of PA **1** are self-supporting gels. Above about 1 mg/mL PA **1** starts gelating. A change in viscosity was expected at the CAC, and therefore we measured the viscosities of a range of concentrations using rheology.<sup>27</sup> Unfortunately, the solutions were not viscous enough to measure the gel properties, especially at the lower concentrations. The difficulties in measuring rheology of the samples may be caused by the thixotropic behaviour of the fibre samples. Up to a concentration of 2 mg/mL shaking destroyed the gel properties, which did not – within the time span of a few hours – recover. Either the handling of the sample while putting it in a couette cell or the movements of the cell during the measurements could have been sufficient to affect the measurement.

**Fluorescence spectroscopy.** DPH (1,6-diphenyl-1,3,5-hexatriene) is a compound which is only fluorescent in a hydrophobic environment and is therefore often employed to determine the presence of aggregates with a hydrophobic core.<sup>28</sup> A stock solution of DPH in THF was added to each of the samples of a dilution series of the amphiphile. Next, the solution was heated in order to disassemble the aggregates. During the subsequent cooling step, fibres reformed and DPH inserted into the hydrophobic interior during the assembly process. This insertion process was observed to be more efficient than when DPH was added to a solution with preformed fibres, which could be concluded from the much higher fluorescence intensity. The low insertion efficiency in absence of a heating step may be caused by the screening of the hydrophobic interior from insertion by the peptide layer. From fluorescence measurements on a series of concentrations, a CAC of about 44 µg/mL (48 µM) was derived (Figure 4).



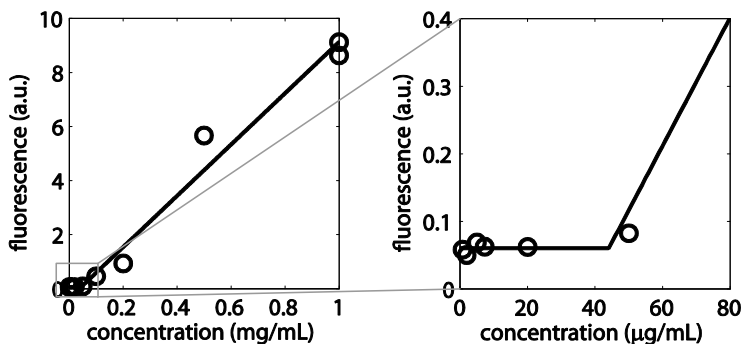


Figure 4. Determination of the CAC using DPH as a fluorescent probe. In the right picture, a part of the graph is blown up.

**Circular dichroism (CD) spectroscopy.** Because of the structural change in the peptide part of the fibres during assembly and disassembly,<sup>15</sup> also CD measurements could be used as a means to determine the CAC. A concentration range of the amphiphile in milli-Q water was measured, and the transition from a random coil to a  $\beta$ -sheet was found between 60 and 80  $\mu\text{g/mL}$  (between 65 and 90  $\mu\text{M}$ ). In presence of the fluorescent probe DPH the same result was found, validating the use of this probe in the fluorescence measurements.

**Rheo-optics.** Rheo-optics can be used to determine the presence of fibres and thus the CAC when these fibres are birefringent. However, the measurement of a concentration series is complicated with this technique. The measurement shown in Figure 3 was performed at a concentration of 100  $\mu\text{g/mL}$ . At higher concentrations the signal without shearing was large, which could be caused by the fibres being in a nematic phase. The large background signal hampered the measurements. Therefore, we diluted all samples to 25  $\mu\text{g/mL}$  (below the CAC), so that the signals could be easily compared. Because of the low dissociation rate the fibres were expected not to disassemble in the short time between dilution and measurement. Furthermore, we used low shear rates (5  $\text{s}^{-1}$ ) to prevent fibre breakage because of elongational flow. The CAC determined using this technique was about 50  $\mu\text{g/mL}$ , corroborating the CD and fluorescence measurements.

An additional benefit of rheo-optics is that it can also be used to determine the length of the fibres, *via* the speed with which the fibres relax back to random orientation (the decay curve, **D-E** in Figure 3). According to Israelachvili, the length of a one-dimensional self-assembled system in thermodynamic equilibrium increases as a function of  $\sqrt{c}$  (with  $c$  = concentration).<sup>29</sup> By measuring a concentration series, we investigated if these peptide amphiphilic fibres obey this rule. Fibres were prepared by cooling the solutions slowly over the time period of one day from 90  $^{\circ}\text{C}$  to room temperature. After that, the samples were stored at room temperature for 4 days before measuring, and 4 days later the measurements were repeated. These measurements yielded similar curves indicating negligible change had taken place in these four days. We expected this to be an indication of the fibres being in the thermodynamic minimum state. However, the predicted dependence of fibre length on concentration was not

present. When the decay curves were fitted in order to determine a length distribution, for all samples a bimodal distribution was found (Figure 5), which was independent of concentration. Therefore, either the fibres do not behave as a one-dimensional system, or they are not in their thermodynamic equilibrium. Because of the enormous aspect ratio of the fibres, indicating one growth direction is highly favoured above the other, the fibres were expected to follow the rules for one-dimensional systems. Therefore we concluded that the fibres were in a kinetically trapped state, i.e. not in thermodynamic equilibrium even though the samples were cooled slowly and left for several days. This implies a large energy barrier for rearrangement of the amphiphiles within the fibres, which is supported by the slow disassembly. Furthermore, also the variation between samples of the same concentration suggested a state other than thermodynamic equilibrium. In order to reach thermodynamic equilibrium, the samples probably would have to be cooled over a period of days or weeks, if the energetically most favourable conformation can be reached at all.

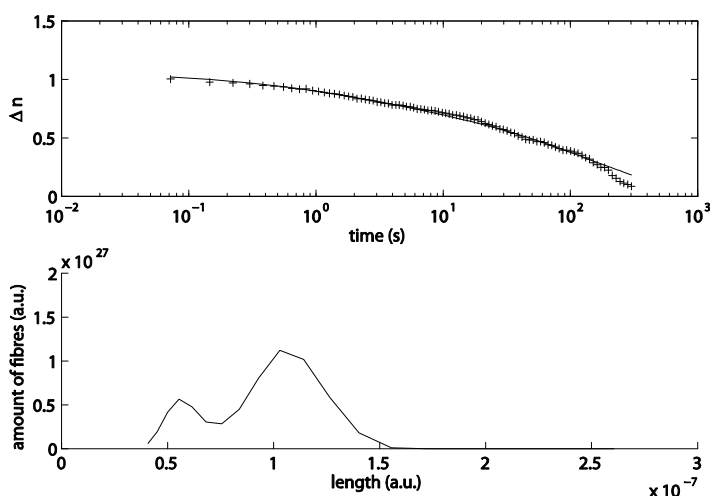


Figure 5. A decay curve (upper graph) in which the data points are shown with plusses, fitted (black line) to yield a length distribution (lower graph).

### **Dynamics of disassembly**

With rheo-optics also the dynamics of disassembly could be probed. Dilution below the CAC results in disassembly of self-assembled systems, although this can be a slow process. The CAC of fibres of PA **1** at room temperature is about 50  $\mu\text{g/mL}$  but upon dilution from 100 to 25  $\mu\text{g/mL}$  the rheo-optics signal did not disappear, showing that the disassembly of the fibres was not instantaneous. Only after 4 days to a week's time (at room temperature), no signal was left. During that period, the birefringence signal during rotation decreased, as was to be expected if fewer fibres were present. More surprising results were obtained by the decay curve, which measures the relaxation from aligned to random orientation. Directly after dilution, the decay curve

followed the expected exponential (Figure 6, black curve). Upon aging the sample, however, the decay curve started to oscillate, indicating elasticity within the sample (Figure 6, grey curve) – i.e. a varying alignment caused by components which start to randomize but rebound to a more aligned state. This elasticity could be due to a large distribution of lengths. Smaller fibres relax to random orientation and in the process ‘push’ larger ones, causing a decrease in alignment (and thus birefringent signal). However, the larger fibres may reorient, increasing it again. Such a broad distribution of fibre length may be caused by a faster disassembly rate for smaller fibres yielding a bimodal distribution with very small and very large fibres. The steepness of the decay was impossible to determine because of the oscillations. Therefore also the fibre length as a function of time could not be defined.

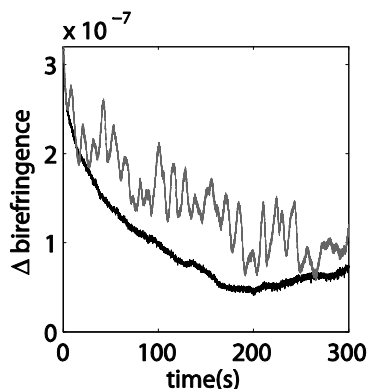


Figure 6. Decay curve for samples diluted below the CAC, directly after dilution (black curve) and after three days (grey curve).

## Mechanical properties

**Influence of shear on fibre length.** In general, the degree of alignment and thus the birefringence signal of the fibres with shearing depends on the length of the fibres (the longer the fibres, the easier they will be aligned) and on the rotation speed (the higher the speed, the more complete the alignment). In Figure 7a the birefringence signal during rotation (between C and D in Figure 3) is shown for various shear rates. The signal indicates alignment, which was higher for longer fibres and higher rotation speeds. At the lowest speed ( $2 \text{ s}^{-1}$ ) the shear force was low and therefore the fibres did not align instantaneously. The signal increased during the shearing. After a few minutes however, the maximum observed signal was reached, which did not increase any further when the shear rate was increased to  $5 \text{ s}^{-1}$ , while fibres studied by Rogers *et al.*<sup>21</sup> showed increase in signal up to  $30 \text{ s}^{-1}$ . This difference indicates that the fibres of PA 1 were much longer and therefore more easy to align than the fibres studied by Rogers *et al.* The difference in length was indeed confirmed by TEM. On the other hand, fast shearing ( $>50 \text{ s}^{-1}$ ) of PA 1 fibres resulted in a decrease in signal during the shearing process, indicating fibre breakage. This demonstrates that these fibres break easier than e.g. fibres of  $\beta$ -lactoglobulin or amyloid,<sup>7, 21</sup> which may be due to a higher fragility or to a

longer fibre length. Damage of the fibres was corroborated by the decay curves after fast shearing (steeper for smaller fibres, because of faster relaxation to random orientation – between **D** and **E** in Figure 3). Faster shear rates resulted in steeper decay curves (Figure 7b). The decay curves could be converted to fibre length, which showed a decrease in fibre length with increasing shear rates. The fit calculated for these measurements was good for the lower rates, but got worse for faster decays, probably because the curves showed oscillations between 100 and 300 s. In order to determine real fibre length and not only length in arbitrary units, the curves needed calibration. Rogers *et al.*<sup>21</sup> calibrated fibre length distribution using TEM. The fibres of self-assembled PA **1** are much longer than the fibres they investigated, but are still very thin. Because of this combination of properties – long, but very thin fibres – the length of the fibres could not be determined with TEM. At large magnification the fibres stretched over the whole visible area, but lower magnification did not resolve the very thin fibres (Figure 2). Therefore, the rheo-optics measurements could not be calibrated and only relative length distributions could be determined. Furthermore, unlike the fibres of Rogers *et al.*, fibres of PA **1** showed fast recovery. A waiting time of about 15 min after shearing yielded decay curves identical to those before fast shearing. This fast recovery hampered TEM sample preparation of the broken fibres.

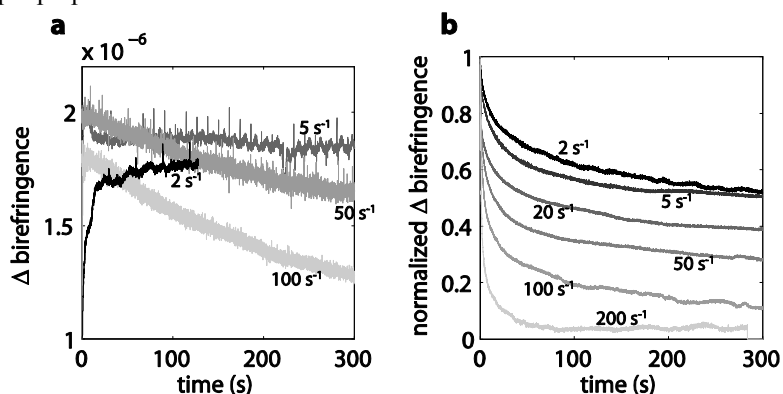


Figure 7. Effect of shear rate on fibre length. A faster shear rate is shown by a lighter colour. a) Signal decrease during rotation indicates damage of the fibre structure. b) A faster shear rate results in a steeper decay, indicating smaller fibres.

**Elongational forces.** The experiments described above revealed that shear damaged the fibres of PA **1**. As discussed in the introduction, the elongational force is the component in the shear force responsible for breaking fibres above a certain length in half. To see if we could break the fibres more than with rotation, a set-up was used in which the elongational forces were much higher than in a rotating Couette cell.<sup>12</sup> A fibre containing solution was extruded from a syringe into a capillary. At the transition point high elongational forces were present because of the difference in diameter between syringe and capillary. The fibre breakage was studied using rheo-optics and TEM. With rheo-optics the birefringent signal during shear (between **C** and **D**, Figure 3) was measured. This signal was higher with increasing alignment. Longer fibres reached the maximum alignment at lower speeds than shorter fibres, and therefore showed no or

little increase in the alignment (birefringence signal) with increasing shear rates. Measuring rheo-optics before, after 3 and after 10 passes through the capillary showed a decreasing alignment (Figure 8). This indicates shorter fibres (not aligned completely at the lower speeds). At higher shear rates the difference between the three samples was much smaller, though still the highest alignment was observed for the untreated sample, indicating the largest fibres were present in that case. The increase in alignment with faster shearing was largest for the smallest fibres (in the sample which was extruded setup ten times). Besides the signal during rotation (between **C** and **D** in Figure 3), also the decay curves (relaxation back to random orientation, between **D** and **E** in Figure 3) were steeper for the samples which had passed through the set-up more often, once more indicating the decrease in fibre length when treated with elongational forces.

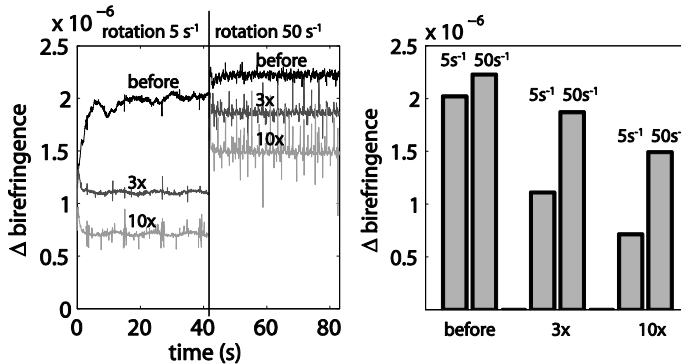


Figure 8. Birefringence during shear. Left: Samples without treatment (black, 'before'), after 3x (dark grey, '3x') and after 10x (light grey, '10x') extrusion. The birefringence was measured at two rotation speeds – 5 s<sup>-1</sup> (left) and 50 s<sup>-1</sup> (right). Right: The same results shown in a bar plot.

TEM also showed the difference between fibres before and after extrusion, although it was not possible to quantify these results. In Figure 9 the difference between the sample before (a) and after (b) applying elongational force is shown. Figure 9b was exemplary for most of the extruded fibres, but also some fibre bundles (Figure 9c) were present. These bundles may just be an accumulation of the short fibres, but might also indicate incomplete breakage or fast recovery of the fibres.

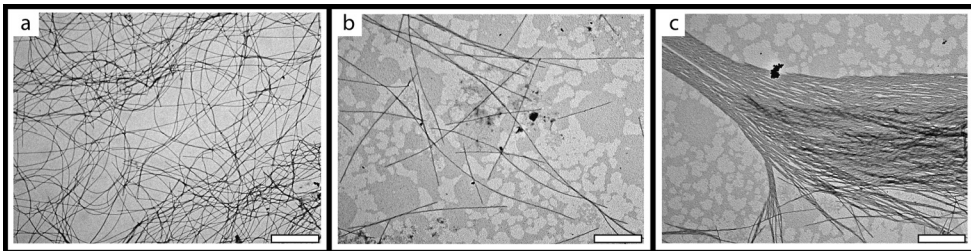


Figure 9. TEM samples of samples before and after applying elongational force. a) Before treatment long fibres are observed. b) and c) are both from the sample extruded 10x. Mainly small fibres as shown in b) but also some fibre bundles (c) which might indicate longer fibres were present. The white bars represent 1  $\mu$ m.

**Freezing.** Lyophilisation is an important step for conservation of nanostructures. Furthermore, it is well-known that protein and tissue samples may damage during the freezing process because of the formation of ice crystals.<sup>17, 18</sup> Since the fibres are fragile and break easily mechanically, freezing might also have an effect. Indeed, samples which had been frozen showed no birefringence signal at all during rotation (between **C** and **D**, Figure 3), indicating absence of fibres. In contradiction however, TEM measurements showed presence of fibres (Figure 10), even though at first sight damage was obvious. It is possible that after freezing a few long fibres and almost no shorter ones were present in the solution. Possibly this amount of fibres was too small to induce a birefringence signal. On the other hand, the high affinity of the fibres to the carbon-coated TEM grid would ensure the presence of fibres on the grids, which would lead to an overestimation of the amount and length of fibres still present.

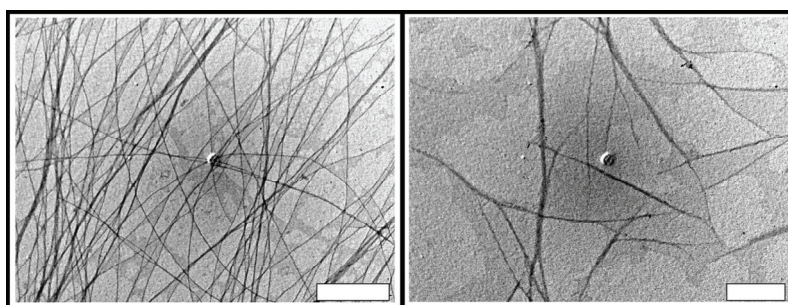


Figure 10. TEM pictures of samples of PA **1** before and after freezing. Left: before freezing. Right: after freezing. The white bar represents 1  $\mu\text{m}$  and 500 nm respectively. The circular structure in the middle of the pictures is an artefact.

Following the reformation process by continuous shearing overnight a sudden (but irreproducible) onset of the birefringence signal (indicating fibre formation) was observed. This also suggests a nucleation process with a lag time after which the fibre formation started. The irreproducibility of the lag time supported the nucleation-growth theory. However, a nucleation process would suggest the absence of fibres directly after the freezing, which is seemingly in contradiction with the TEM results. As explained above, probably after freezing only a few very long fibres were present, which only represent very limited possibilities for growth. One might even argue that fibres above a certain length cannot increase in length anymore and therefore cannot function as a growth site. Therefore, a nucleation growth mechanism for the fibres is largely in accordance with the experiments.

## **Thermal properties**

As already mentioned, the fibres disassembled upon heating. This disassembly was investigated using NMR, CD, dynamic light scattering (DLS) and fluorescence spectroscopy. Because the optical train in the rheo-optics set-up is very sensitive to temperature variations, the rheo-optical set-up does not allow for temperature control other than by room temperature conditioning.

**Nuclear magnetic resonance (NMR).** At room temperature, the fibres were too immobile to be measured with (liquid phase) NMR (Figure 11a). However, after heating above the disassembly temperature it was possible to measure the mobile non-aggregated amphiphiles (Figure 11b). During heating the signals sharpened between 54 °C and 79 °C, implying the disassembly of the fibre, while upon cooling the assembly took place between 72 °C and 65 °C. The exact transition temperatures were difficult to determine, because the peak shape changed gradually.

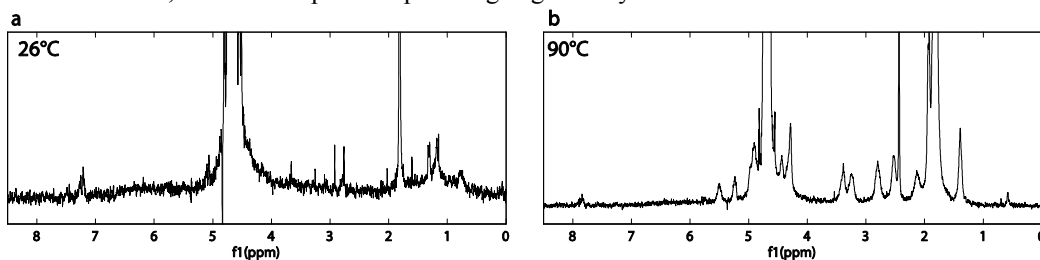


Figure 11. NMR spectra of PA 1 in D<sub>2</sub>O at a) 26 °C b) 90 °C.

**Circular dichroism (CD) spectroscopy.** With CD spectroscopy the structural transition of the peptide part of the fibres was monitored. The disassembly temperature was derived by measuring the intensity of the 196 nm peak during the heating process, and was found to be about 70 °C,<sup>15</sup> in accordance with the NMR measurements. Cooling revealed two transitions of the ellipticity signal— one around 60 °C and one around 30 °C (Figure 12). The first transition (60 °C) probably depicts the reformation of the fibres. The hysteresis between heating and cooling is most likely an undercooling effect, common in nucleation-induced processes. The second transition temperature (30 °C) was possibly associated with a molecular rearrangement of either alkyl tails or peptides.

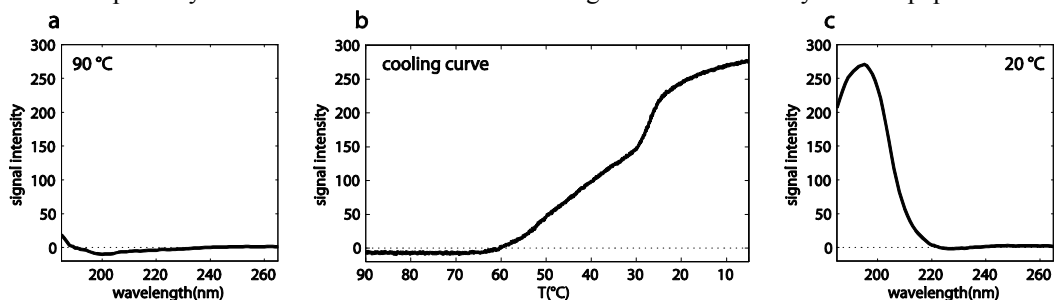


Figure 12. CD measurements of PA 1 at several temperatures. a) at 90 °C b) The signal intensity at 196 nm upon cooling c) At 20 °C.

**Dynamic light scattering (DLS).** DLS was used to measure the total scattering intensity of a fibre sample at different temperatures. Particle sizes for these samples were not determined, since for rod-like particles with an unknown size distribution this is difficult. The temperatures at which the fibres were disassembled or started to assemble were determined, i.e. the transition point from no assembly to assembly and deviation from the DLS scattering intensity from zero. These were about 75 °C and 50 °C for heating and cooling, respectively (Figure 13).

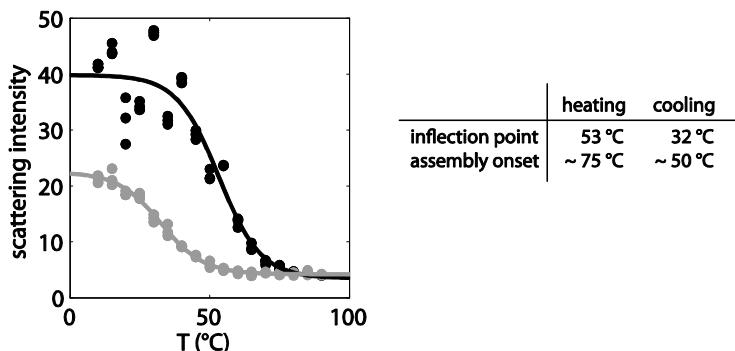


Figure 13. DLS measurements of PA 1. Black is heating, grey cooling. The circles are data points, the line is a fitted sigmoidal curve.

**Fluorescence.** DPH was employed as a fluorescent probe which only fluoresces if fibres are present.<sup>28</sup> The fluorescence intensity increased sharply around 50 °C (Figure 14), indicating a larger amount of DPH in a hydrophobic environment. This can be caused by a higher conformational freedom of the amphiphiles in the fibres or by a small change in the mobility of the alkyl tails. After this increase in fluorescence intensity, it was constant up to 70 °C where it decreased sharply, indicating disassembly of the fibres. Upon cooling, the increase in fluorescence intensity was large, but gradual. The gradual change indicates a gradual increasing presence of DPH in hydrophobic environment, which may be caused by the larger freedom of the amphiphiles in fibres at higher temperatures. However, it may also indicate that the fibre assembly was influenced by the presence of DPH. The difference in fluorescence intensity before and after heating indicated the more effective incorporation of DPH after a heating step.

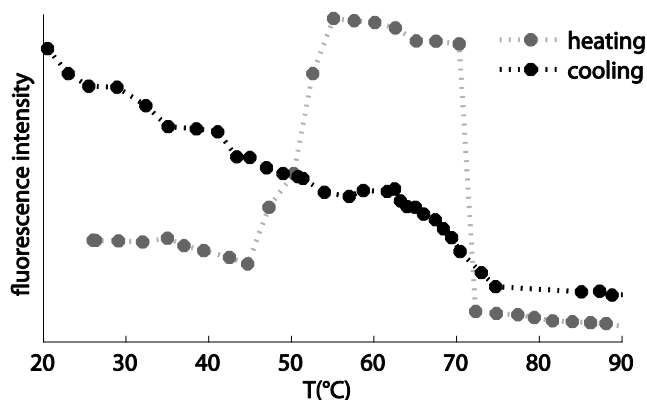


Figure 14. Fluorescence signal of DPH upon heating a fibre solution.

In summary, all measurement techniques yielded a transition temperature of about 70 °C upon heating, most probably indicating disassembly of the fibres. The reassembly temperature (upon cooling) was found to be about 50 °C. The large hysteresis between disassembly (heating) and reassembly (cooling) indicates undercooling before assembly takes place and supports a nucleation-induced assembly process.



A second, lower, transition temperature was observed in CD and fluorescence spectroscopy. A conformational change of the amphiphiles within the fibres might be the cause of this transition. A small change in either peptide packing or mobility of the alkyl tails could cause more incorporation of DPH in the hydrophobic core of the fibre or an increase in ellipticity in CD.

The different techniques yielded similar but not identical transition temperatures. This was caused by the combination of a few parameters. First of all, there are differences in what the techniques observed – an NMR signal sharpens at another assembly size than the size at which a random coil to  $\beta$ -sheet transition is observed in CD spectroscopy. Furthermore, the variation between samples may have an influence. As mentioned before, the fibres are most probably in a kinetically trapped state and thus each sample is slightly different. Moreover, the hysteresis between the disassembly and assembly temperatures indicated an undercooling of the sample before assembly took place. Therefore, also the cooling rate played a role in the determined assembly temperature. Only in the CD measurements the cooling rate was controlled, and even with that technique it was relatively fast (3 °C/min). Besides these variations because of techniques and sample preparation, also the sample concentration is important. Higher concentrations yielded higher disassembly temperatures, as is illustrated in the next paragraph.

### Thermodynamic parameters of the assembly process

In order to determine enthalpic and entropic parameters of the assembly process, the concentration dependent disassembly temperature was investigated. Kroes-Nijboer *et al.*<sup>30</sup> determined the thermodynamic parameters of the packing of  $\beta$ -lactoglobulin based fibres from the disassembly temperatures of a series of concentrations. To exclude all variations because of technique, only DLS was used, because of the possibility to do measurements over a large concentration range. Even though in gelled samples the signal could not be used to determine particle size, a large change is observed when the sample disassembles. The transition temperatures were obtained by fitting a sigmoidal curve to the data points and taking the inflection point of that curve (see Figure 13). The inflection point was used as a measure for transition, because the end of the disassembly process was more difficult to determine and yielded large errors. Especially at higher concentrations (2 and 5 mg/mL), the fits were poor, probably because the transition temperature was at the edge of the measured temperature range. The resulting concentration dependent disassembly temperature is shown in Figure 15a and the thermodynamic parameters calculated from these data in Figure 15b to d. The black lines show the fit made using the theory explained by Kroes-Nijboer *et al.* for a one-dimensional system.<sup>30</sup> The measurements showed a large spreading, but followed the trend of the theoretical curve. The total free energy  $dG/RT$  was found to be negative, indicating the higher stability of fibres *versus* amphiphiles, which gets smaller at higher temperatures. The magnitude of the free energy is only slightly lower than determined for  $\beta$ -lactoglobulin based fibres,<sup>30</sup> which are much more resistant towards mechanical stress.<sup>21</sup> Both enthalpy and entropy were negative as well, which indicated that the

assembly process was enthalpy driven. At higher temperatures the values of both  $dH$  and  $dS$  decreased (got more negative), indicating a larger enthalpy gain for assembly. However, because of the larger entropic contribution, assembly yielded overall a free energy loss.

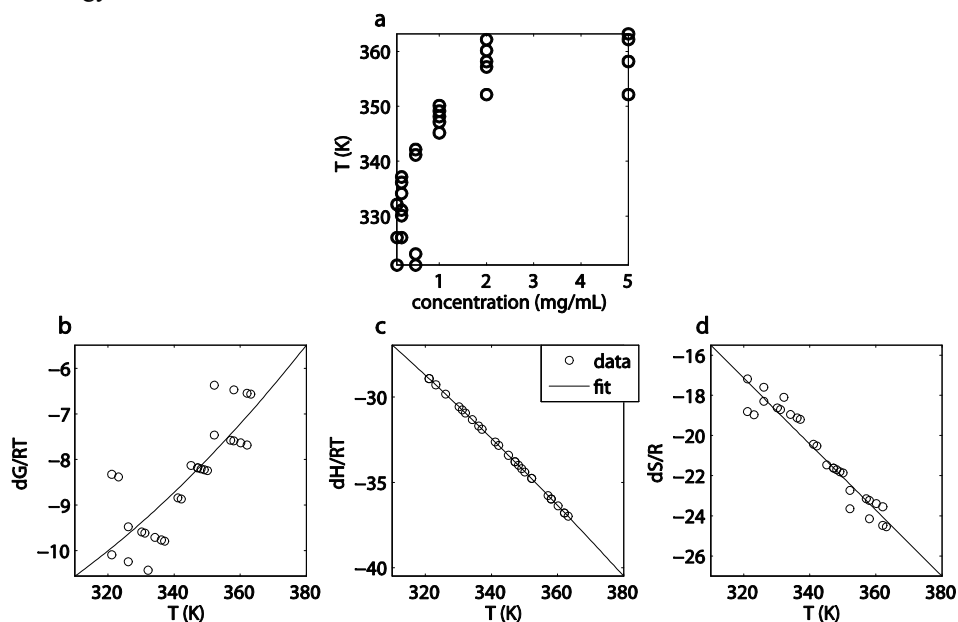


Figure 15. Thermodynamic parameters derived from DLS measurements for the assembly of PA 1. a) Disassembly temperatures as a function of concentration. Temperature dependence of b) free energy, c) enthalpy and d) entropy.

## Conclusions

For PA 1 the derived critical aggregation concentration is about 50  $\mu\text{g/mL}$  (55  $\mu\text{M}$ ). Above this concentration, PA 1 assembled into fibres in a kinetically trapped state. Dilution of a fibre containing solution below the CAC did not result in instantaneous disassembly – only after a few days the amphiphiles were completely dissolved. This slow disassembly supports a kinetically trapped architecture – if disassembly takes days already, reorganization to the thermodynamic most stable structure probably will take much longer, if the thermodynamic minimum can be reached at all. The fibres broke easily with mechanical stress, such as caused by elongational force or ice formation. On heating, the fibres disassembled at a temperature of about 70 °C and reassembly was observed at about 50 °C. The large hysteresis suggests a nucleation-induced assembly process. A second transition temperature was observed at 50 °C and 30 °C upon heating and cooling, respectively. This transition might be associated with a conformational change in the peptide or an increase in mobility of the alkyl tails. From the combination of disassembly temperature with concentration thermodynamic parameters for the fibre formation were determined. The fibres were found to be thermodynamically very stable, seemingly in contradiction with the low mechanical stability.

## Acknowledgements

We want to thank Paul Venema, Harry Baptist and Erik van der Linden for help with rheology, rheo-optics and elongational flow measurements and useful discussions. We want to thank Aurelie Brizard for help with surface tension and isothermic titration calorimetry measurements and Remco Fokink for help with the DLS set-up in Wageningen. We want to thank Ad Swolfs for help with the temperature NMR measurements, and Pieter Nieuwland for the 3D drawing of the Couette cell.

## Experimental section

**Fibre preparation.** The amphiphiles were dispersed in milli-Q, heated to 50 °C for 30 min, followed by 15 min sonication at that temperature. Subsequently, the samples were heated to 90 °C and allowed to cool to room temperature.

**Surface tension.** Surface tensions were determined by shape analysis of a pendant drop using a KRÜSS FM40 Easy Drop and were carried out in triplicate.

**Differential Scanning Calorimetry (DSC).** DSC measurements were performed on a Mettler Toledo DSC822 with concentrations of the amphiphile in milli-Q between 0.2 and 60 mg/mL using heating rates ranging from 0.3 to 15 °C/min. The samples were prepared *via* the standard procedure (see above) for concentrations ranging from 0.2 to 10 mg/mL. For higher concentrations the solution was heated up to the boiling point, which was required to dissolve the amphiphiles. While hot, the solution was put into a DSC cup in which it was allowed to cool.

**Isothermic titration calorimetry (ITC).** ITC was performed on a Microcal VPITC microcalorimeter, with a volume sample-cell and reference cell volume of 1.603 ml. Milli Q water was loaded in the cell, while the syringe was filled with PA **1** at a concentration of either 1 mg/mL, 0.5 mg/mL or 0.25 mg/mL. The solutions were degassed at 50 °C prior to measurements. The fibre solution was added in aliquots of 5 µL to the sample cell with a time between injections of 6 min for the 1 mg/mL experiment and 15 min for concentrations of 0.5 and 0.25 mg/mL.

**Rheology.** Rheology measurements were performed on samples with concentrations between 0.2 and 5 mg/mL using a Paar Physica MCR 301 rheometer with a coaxial cylinder CC17 geometry. The rotation shear rate was 2 s<sup>-1</sup> and the oscillation strain 1 %. A frequency of 1 Hz and heating and cooling rates of 1 °C/min were used.

**Rheo-optics.** Birefringence experiments were performed on a strain-controlled ARES rheometer (Rheometrics Scientific) equipped with an optical analysis module. The system has undergone development by Klein *et al.*<sup>31</sup> to increase the sensitivity, reduce the background (residual birefringence in the optical train), and give better angle measurements. All measurements were performed in Couette geometry with a static inner bob of diameter 32 mm and rotating outer cup of diameter 33.8 mm. A laser beam of wavelength 670 nm passes between the cup and bob through 20 mm of sample. In this arrangement, the apparatus was capable of measuring birefringence down to 10<sup>-8</sup> at a sampling frequency of 24 times per second. The geometry requires 12 mL of sample.

**Fluorescence spectroscopy.** Fluorescence measurements were performed on a Perkin Elmer LS-55 fluorescence spectrometer. The excitation wavelength was 362 nm, and the emission was recorded between 360 and 550 nm, while the maximum extinction at 429 nm was used to determine a change in fluorescence. The spectra were recorded at a speed of 300 nm/min. Both excitation and emission slit were set to 2.5.

**CAC measurements.** DPH (1,6-diphenyl-1,3,5-hexatriene, 1  $\mu\text{L}$  of a 10 mM solution in THF)<sup>28</sup> was added to samples of PA **1** with a volume of 1.5 mL and a concentration of 1000, 500, 200, 100, 50, 20, 10, 5, 2 and 1  $\mu\text{g}/\text{mL}$ . After addition of DPH, the sample containers were wrapped in aluminium foil to exclude light, and the fibres were prepared following the standard procedure.

**Temperature measurements.** To 1.5 mL fibre sample of 1 mg/mL PA **1**, prepared following the standard procedure, 1  $\mu\text{L}$  of 10 mM DPH was added. The sample was left in the dark for 1 h. The samples were heated from 20 to 90  $^{\circ}\text{C}$  in about 30 min using a water bath connected to the spectrometer and cooled in the same way.

**Circular dichroism (CD) spectroscopy.** The spectra were recorded on a JASCO J-810 spectropolarimeter.

**CAC measurements.** Samples with a concentration PA **1** of 1000, 800, 600, 400, 200, 100, 80, 60, 40, 20, 10, 8, 6, 4, 2 and 1  $\mu\text{g}/\text{mL}$  were prepared following the standard procedure. The CD measurements were performed from low to high concentrations, starting with a 1 cm pathlength quartz cell, and switching to 1 mm and 0.2 mm pathlength quartz cells when the high tension signal was higher than 800 during the measurements. Spectra were recorded from 265 to 185 nm, using a scanning speed of 100 nm/min.

**Temperature measurements.** The measurements were carried out at a concentration of 0.2 mg/mL prepared following the standard procedure using a 1 mm quartz cell. A heating or cooling rate of 3 $^{\circ}$  C/min was used, and the ellipticity at 196 nm was measured between 10 and 90  $^{\circ}\text{C}$

**Transmission electron microscopy (TEM).** TEM samples were prepared by floating a carbon-coated copper grid on a peptide amphiphile solution of either 1.0 or 0.2 mg/mL for 5 min, followed by removal of residual water by blotting with a paper filter. The samples were visualized using a JEOL 1010 transmission electron microscope set on an accelerating voltage of 60 kV.

**Fibril fracture using elongational flow.** For the establishment of the elongational flow field a PEEK-tube was connected to a syringe. The PEEK-tube had a diameter of 0.254 mm. The syringe (50 mL) had a diameter of 26 mm. The syringe was vertically placed in a holder in a texture analyzer (TA.XT Plus, Stable Micro Systems with a loadcell of 50 kg) that was used to empty the syringe at constant discharge, with a speed of 0.5 mm/s. In this way a flow with a strong elongational component was established at the transition area of syringe to PEEK-tube. The sample was passed through the constriction either 3 or 10 times.

**Nuclear magnetic resonance (NMR).** The temperature NMR measurements were performed on a Bruker DMX300 spectrometer. The temperature was controlled with a B-VT-2000 controller, which was calibrated with a 100% ethylene glycol sample. A sample of 6 mg/mL PA **1** in D<sub>2</sub>O was measured at 26, 54, 79 and 91  $^{\circ}\text{C}$  during heating, and at 86, 79, 72, 65 and 54  $^{\circ}\text{C}$  during cooling.

**Dynamic light scattering (DLS).** DLS measurements were performed on a Zetasizer Nano S (Malvern Instruments Ltd, England). Every 5  $^{\circ}\text{C}$  between 10 and 90  $^{\circ}\text{C}$  the sample was equilibrated for 5 min before a measurement in triplicate was performed. Every measurement consisted of 6 runs of 6 s, with a measurement position of 4.65 and a set attenuation of 7. The sample was heated and cooled for several cycles, and for each concentration at least two different samples were measured.

## References

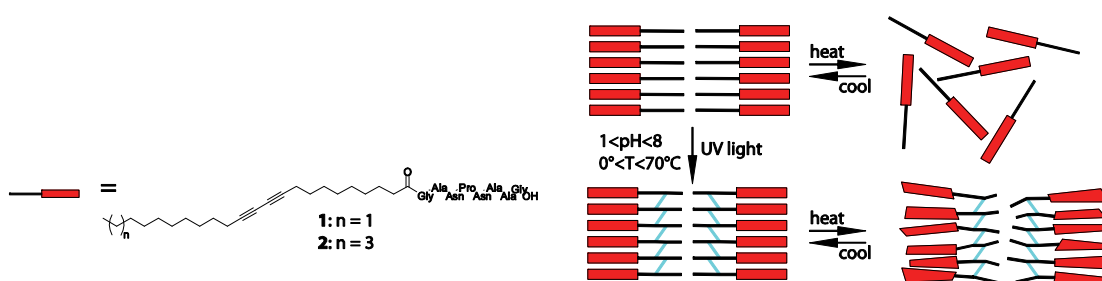
1. E. F. Banwell, E. S. Abelardo, D. J. Adams, M. A. Birchall, A. Corrigan, A. M. Donald, M. Kirkland, L. C. Serpell, M. F. Butler and D. N. Woolfson, *Nat. Mater.*, 2009, **8**, 596-600.

## Chapter 3

2. J. M. Anderson, M. Kushwaha, A. Tambralli, S. L. Bellis, R. P. Camata and H. W. Jun, *Biomacromol.*, 2009, **10**, 2935-2944.
3. M. Zhou, A. M. Smith, A. K. Das, N. W. Hodson, R. F. Collins, R. V. Ulijn and J. E. Gough, *Biomaterials*, 2009, **30**, 2523-2530.
4. S. R. Bull, M. O. Guler, R. E. Bras, P. N. Venkatasubramanian, S. I. Stupp and T. J. Meade, *Bioconjugate Chem.*, 2005, **16**, 1343-1348.
5. S. R. Bull, M. O. Guler, R. E. Bras, T. J. Meade and S. I. Stupp, *Nano Lett.*, 2005, **5**, 1-4.
6. G. A. Silva, C. Czeisler, K. L. Niece, E. Beniash, D. A. Harrington, J. A. Kessler and S. I. Stupp, *Science*, 2004, **303**, 1352-1355.
7. E. K. Hill, B. Krebs, D. G. Goodall, G. J. Howlett and D. E. Dunstan, *Biomacromol.*, 2006, **7**, 10-13.
8. H. J. Schnittler, S. W. Schneider, H. Raifer, F. Luo, P. Dieterich, I. Just and K. Aktories, *Pflugers Arch.*, 2001, **442**, 675-687.
9. J. F. Smith, T. P. J. Knowles, C. M. Dobson, C. E. MacPhee and M. E. Welland, *Proc. Natl. Acad. Sci. U. S. A.*, 2006, **103**, 15806-15811.
10. J. D. Clay and K. W. Koelling, *Polym. Eng. Sci.*, 1997, **37**, 789-800.
11. J. A. Odell and A. Keller, *J. Polym. Sci., Part B: Polym. Phys.*, 1986, **24**, 1889-1916.
12. A. Nijboer, P. Venema, H. Baptist and E. Van der Linden, *In preparation*, 2010.
13. C. Akkermans, P. Venema, S. S. Rogers, A. J. van der Goot, R. M. Boom and E. van der Linden, *Food Biophys.*, 2006, **1**, 144-150.
14. D. W. P. M. Löwik, E. H. P. Leunissen, M. van den Heuvel, M. B. Hansen and J. C. M. van Hest, *Chem. Soc. Rev.*
15. D. W. P. M. Löwik, J. Garcia-Hartjes, J. T. Meijer and J. C. M. van Hest, *Langmuir*, 2005, **21**, 524-526.
16. C. Cerami, U. Frevert, P. Sinnis, B. Takacs, P. Clavijo, M. J. Santos and V. Nussenzweig, *Cell*, 1992, **70**, 1021-1033.
17. W. Abdelwahed, G. Degobert, S. Stainmesse and H. Fessi, *Adv. Drug Delivery Rev.*, 2006, **58**, 1688-1713.
18. W. Abdelwahed, G. Degobert and H. Fessi, *Int. J. Pharm.*, 2006, **324**, 74-82.
19. C. Akkermans, A. J. Van Der Goot, P. Venema, H. Gruppen, J. M. Vereijken, E. Van Der Linden and R. M. Boom, *J. Agric. Food Chem.*, 2007, **55**, 9877-9882.
20. A. W. Chow and G. G. Fuller, *Macromol.*, 1985, **18**, 786-793.
21. S. S. Rogers, P. Venema, L. M. C. Sagis, E. van der Linden and A. M. Donald, *Macromol.*, 2005, **38**, 2948-2958.
22. S. Y. Fung, C. Keyes, J. Duhamel and P. Chen, *Biophys. J.*, 2003, **85**, 537-548.
23. D. W. P. M. Löwik, I. O. Shklyarevskiy, L. Ruizendaal, P. C. M. Christianen, J. C. Maan and J. C. M. van Hest, *Adv. Mater.*, 2007, **19**, 1191-1195.
24. M. van den Heuvel, D. W. P. M. Löwik and J. C. M. van Hest, *Biomacromol.*, 2008, **9**, 2727-2734.
25. B. Schnatwinkel, M. V. Rekharsky, R. Brodbeck, V. V. Borovkov, Y. Inoue and J. Mattay, *Tetrahedron*, 2009, **65**, 2711-2715.
26. J. Lasch and A. Hildebrand, *J. Liposome Res.*, 2002, **12**, 51-56.
27. C. Veerman, G. de Schiffart, L. M. C. Sagis and E. van der Linden, *Int. J. Biol. Macromol.*, 2003, **33**, 121-127.
28. A. Riepe, H. Beier and H. J. Gross, *FEBS Lett.*, 1999, **457**, 193-199.
29. J. Israelachvili, *Intermolecular and surface forces, 2nd edition*, Elsevier Ltd., 1991.
30. A. Kroes-Nijboer, P. Venema, J. Bouman and E. van der Linden, *Food Biophys.*, 2009, **4**, 59-63.
31. C. Klein, P. Venema, L. Sagis, D. van Dusschoten, M. Wilhelm, H. W. Spiess, E. van der Linden, S. S. Rogers and A. M. Donald, *Appl. Rheol.*, 2007, **17**.

## Chapter 4

# Self-assembly and polymerisation of diacetylene-containing peptide amphiphiles in aqueous solution.



A systematic study was performed after the fibre forming properties and polymerisation characteristics of two peptide amphiphiles containing a diacetylene functionality in the alkyl tail, comprising 23 and 25 C atoms, respectively. Despite the large structural similarity, the behaviour of the two amphiphiles was remarkably different. Although both amphiphiles formed  $\beta$ -sheet fibres in water which could be polymerised and remained very stable towards pH changes, their disassembly and reassembly temperatures and chromatic properties after polymerisation were quite dissimilar. The large difference in assembly properties and polymerisation behaviour of the two similar-looking amphiphiles is indicative of the subtlety of the assembly and disassembly processes in these fibrous architectures.

---

This work has been published in M. Van den Heuvel, D. W. P. M. Löwik and J. C. M. van Hest, *Biomacromol.*, 2008, **9**, 2727-2734.

## Introduction

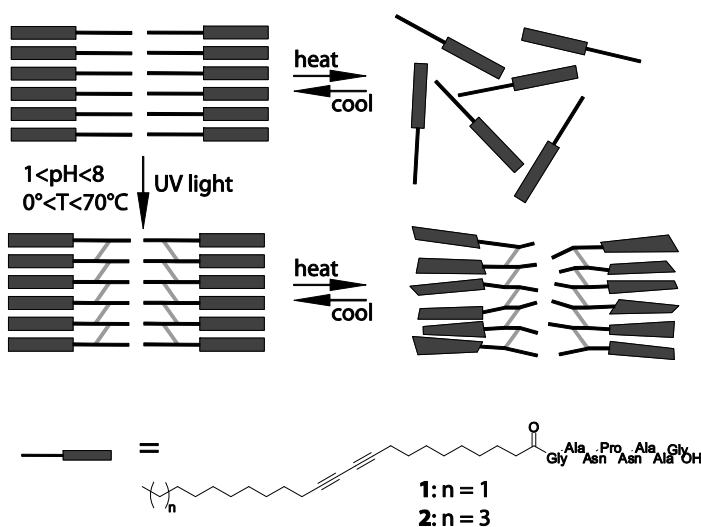
Materials that are constructed *via* a spontaneous hierarchical molecular self-assembly process have intrigued scientists for many years. Nature provides, in this respect, beautiful examples where, through extreme control over recognition and consequent directed self-assembly on a molecular level, discrete objects are constructed, such as virus capsids<sup>1</sup> or the triple helical rods found in collagen.<sup>2</sup>

Two of the main driving forces for self assembly are hydrogen bonding and hydrophobicity. It is the subtle interplay and balance between these forces that have given peptide amphiphiles much interest as molecular building blocks. Furthermore, with our present synthetic capabilities many non-covalent interactions can be introduced into molecules to construct supramolecular assemblies. The resulting architectures with a wide variety of functionality have been used for the development of a new generation of materials with a high degree of order on a nanoscopic level,<sup>3</sup> which can be applied as functional scaffolds in e.g. biomineralization<sup>4</sup> or cell proliferation processes.<sup>5</sup>

Previously, we described the modification with hydrophobic moieties of the short eight-amino-acid GANPNAAG peptide, derived from the CS protein of the malaria parasite *Plasmodium Falciparum*.<sup>6</sup> When the peptide was coupled N terminally to short alkyl tails no fibres were formed, whereas with longer tails (containing more than 15 carbons) the peptide amphiphile (PA) formed highly stable assemblies,<sup>7</sup> showing the subtlety of assembly. The driving force for the assembly stems from the hydrophobic forces within the alkyl tail, while the directionality is provided by the peptide part. The fibres disassembled reversibly when heated, and the transition temperature, measure for the stability, depended on the nature and length of the tail coupled to the peptide. Longer hydrophobic tails increased this temperature, while coupling of a hydrophilic PEG chain considerably decreased the stability of the peptide assembly.<sup>8</sup>

When an assembly process yields an interesting functional structure, one may want to covalently link it. The obtained assembly can be locked using covalent interactions such as sulphur bridges, which has been demonstrated for example by the group of Stupp.<sup>4</sup> We have chosen to covalently link the self-assembled peptide amphiphiles *via* the well-known topochemical, light-initiated radical polymerisation of diacetylenes.<sup>9, 10</sup> In order for this reaction to proceed the diacetylenes have to be positioned at a well-defined distance and angle with respect to each other. With the diacetylene units embedded in alkyl tails, as is the case for the system we study, these tails should have a highly ordered packing for the polymerisation to occur. A first example of stabilising PAs with this method was given by Frauenrath *et al.*, who polymerised assemblies of peptides modified with a hydrophobic polymer in organic solvents.<sup>11, 12</sup> Stupp *et al.* and our group have recently shown that this approach is also possible for low molecular weight PAs in an aqueous solution.<sup>13, 14</sup> Polymerisation of these assemblies yields very stable fibres of micrometer length. Since the peptide functionalized polydiacetylenes have a highly conjugated chromophoric structure, the optical properties of the polymers are indicative for the structure of the polymer backbone.<sup>15, 16</sup> Because both the peptide

and the polymer are sensitive to changes in their environment, this combination could possibly be used as a biosensor.<sup>10, 17</sup>



Scheme 1. Assembly and polymerisation of PAs **1** and **2** under various conditions. The temperature and pH values given in the scheme are obtained for **1**. The assembly of peptide **2** is even more stable towards environmental changes

From previous investigations it is known that assembly<sup>7</sup> and polymerisation<sup>18, 19</sup> properties are largely dependent on the length of the hydrophobic tails. In this systematic study we therefore compare the fibre forming properties and polymerisation characteristics of two PAs with diacetylene functional alkyl tails of different length (Scheme 1).<sup>13</sup> In order to obtain a better understanding of the sensitivity to environmental changes the temperature and pH dependence of the assembly process, the formed assemblies, the polymerisation process and the subsequent polymers were investigated.

## Self-assembly

**Synthesis of the peptide amphiphiles.** The peptides were synthesized using standard Fmoc solid phase peptide synthesis. The alkyl chain was coupled N-terminally to the peptide on the solid support. The amphiphiles were purified using column chromatography and the purity of the product was established with thin layer chromatography (TLC), NMR and mass spectroscopy (MS).

**Fibre formation.** After freeze-drying the monomer from acetic acid, fibres were prepared in an aqueous solution *via* procedure A. In this procedure, which is also shown in Figure 1a, two heating steps were applied after the addition of milli-Q to the dry amphiphile.



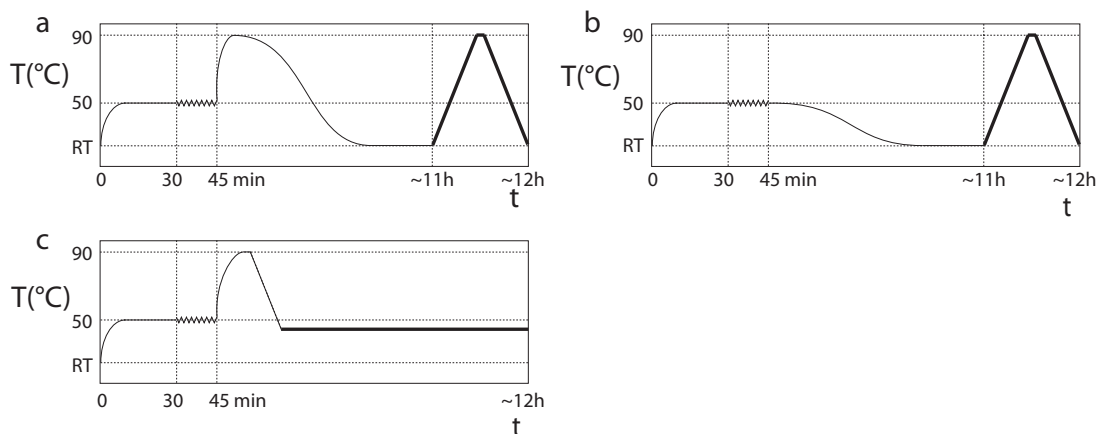


Figure 1. a) Preparation of samples *via* procedure A. b) Preparation of samples *via* procedure B, which excludes an annealing step. c) Sample preparation for overnight assembly experiments for compound **1** for one of the measured temperatures. Thin lines ‘show’ the temperature profile during sample preparation, in which the zigzag line denotes ultrasonic sound treatment. The thick line shows the temperature profile during measurements, where the heating or cooling rate was set to 3°C/min. Dotted lines are only to guide the eye

In the first heating step the large aggregates were partly dissolved by heating to 50°C and partly mechanically reduced to smaller aggregates by sonication at that temperature. The solution was subsequently heated to 90°C to ensure complete disassembly of all aggregates, after which it was allowed to cool down to room temperature. Transmission electron microscopy (TEM) revealed the formation of twisted fibres 20 nm in width and with lengths of several micrometers (Figure 2a) as was reported before by our group.<sup>7, 13</sup>

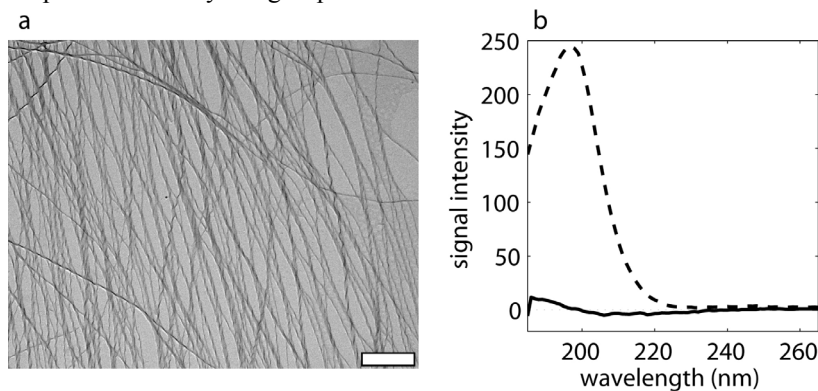


Figure 2. a) Transmission electron microscopy picture of fibres of amphiphile **2**. The white bar represents 500 nm. b) CD spectra of amphiphilic peptide **1** at room temperature (dashed line) and 90 °C (solid line). PA **2** shows similar results.

Circular dichroism (CD) spectra showed for both compounds a signal with an enhanced peak at 196 nm, indicating assembly. This intense 196 nm signal is due to macroscopic orientation in solution, resulting in a linear dichroism (LD) signal which obscures the CD signal. Wolffs *et al.*<sup>20</sup> also reported that LD can be predominantly

present in fibre-containing solutions. Heating the samples led to disassembly of the fibres, as indicated by a change from a large signal to a random coil CD spectrum (Figure 2b). The typical 196 nm signal was followed in time during heating of the sample (Figure 3a). Fibre disassembly was indicated by the decrease of the 196 nm signal starting at 55 °C for **1** and at 80 °C for **2**. Measuring the peak intensity in time was hampered by the presence of the diyne functionalities which readily polymerised when illuminated with the short wavelengths used for the CD measurements. Therefore, only a limited number of spectra could be recorded before the sample needed to be replaced.

The CD signal of the samples prepared *via* procedure A showed large hysteresis upon cooling, also observed previously by O'Brien *et al.*<sup>21</sup> Amphiphile **2** disassembled at 80 °C (Figure 3a) and started to reassemble at 50 °C (Figure 3b). The hysteresis of **1** was even larger. This amphiphile disassembled at 55 °C but did not reassemble during the CD measurement. Aging of the sample overnight at temperatures below 40 °C yielded a  $\beta$  sheet signal. Above this temperature no assembly took place. Thus, the disassembly temperature for peptide **1** in this experiment was 40 °C.

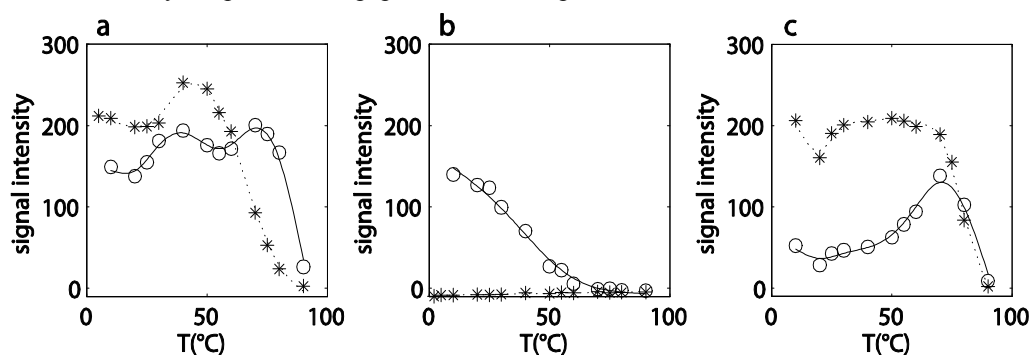


Figure 3. Mean intensity of the 196 nm CD signal during heating (a and c) or cooling (b) for amphiphiles **1** (stars) and **2** (circles). a and b: samples which were annealed at 90 °C. c: samples which were only heated to 50 °C. The lines (dashed for **1** and solid for **2**) are guides to the eye.

Fibres were also prepared using the alternative procedure B. *Via* this method, which is also shown in Figure 1b, the samples were heated to 50 °C, sonicated at that temperature, cooled down and subsequently measured during heating. The final annealing step before the start of the measurements was omitted. Using procedure B both compounds still formed  $\beta$ -sheets. Only amphiphile **1** however showed the high, LD-caused 196 nm signal. Compound **2** gave a regular  $\beta$ -sheet signal. This implies that **1** was completely disassembled during the preparation and was therefore able to form the well-defined fibres with the enhanced 196 nm signal. Heating of these samples gave a similar result (Figure 3c) as in the previously described experiment in which the sample was annealed at 90°C (Figure 3a). Amphiphile **2** showed different behaviour. It reordered during the preparation at 50 °C but only incompletely, causing a  $\beta$ -sheet signal which was much smaller. For this compound the LD caused signal increased during heating to reach a maximum at 70°C, slightly below the disassembly temperature of the fibre.

In order to be able to study fibre formation at any given temperature, procedure C was used, in which we started from a concentrated solution of the amphiphiles in TFE. In this solvent the monomers dissolved molecularly, which gave us the possibility to induce self-assembly by injection of the TFE solution in milli-Q. The conformational changes of the PA were followed in time for 2 hours using CD spectroscopy. The spectrum of amphiphile **1** gradually changed from a random coil, indicating free monomers, to a  $\beta$  sheet (Figure 4). This change took place at temperatures up to 60°C. Above this temperature no assemblies formed as indicated by the fact that the random coil signal did not change anymore.

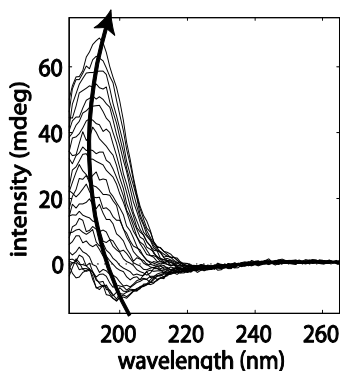


Figure 4.  $\beta$ -sheet formation of amphiphile **1** on injection from TFE in milli-Q at room temperature, followed by CD spectroscopy. The signal changed from random coil to  $\beta$  sheet in two hours time. The time course is indicated by the arrow. Spectra were recorded at a five minutes' interval.

The CD spectra of **2** showed a signal change when the TFE solution was injected at temperatures ranging from 5 °C and 60 °C (Figure 5), leading to a spectrum in between that of an  $\alpha$  helix and a  $\beta$  sheet. This is caused by the  $\alpha$ -helix forming propensities of TFE (Figure 5a) combined with the tendency of the peptides in the amphiphile to form  $\beta$  sheets. Even though the spectra did not resemble a  $\beta$ -sheet structure after the incubation between 5 °C and 35 °C (Figure 5b and c), clearly the spectrum differed from the initial random coil signal, indicating an assembly process.

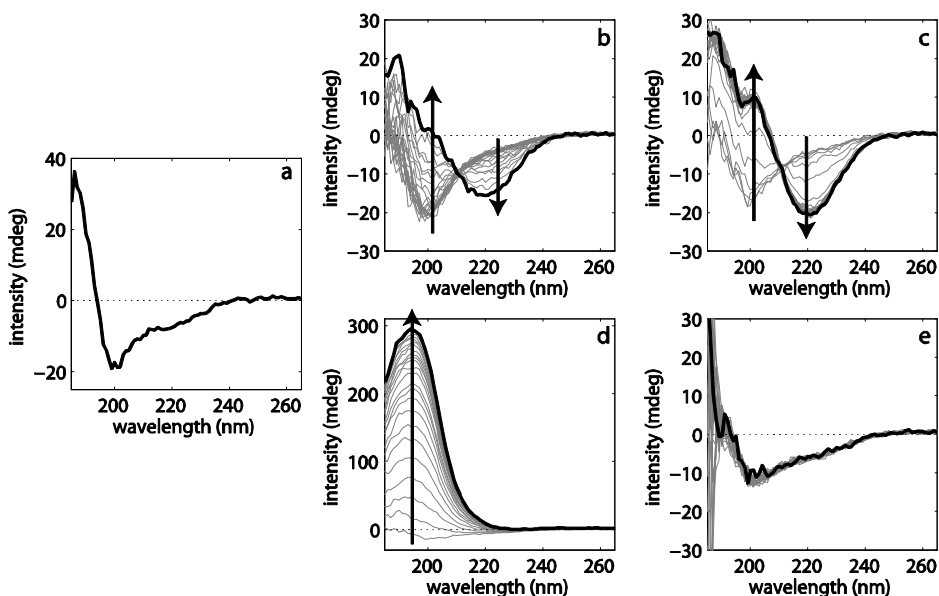


Figure 5. CD spectra of amphiphile **2**. a) In TFE, showing an alpha-helix signal, b-e) Following the change of the signal for two hours after injecting a concentrated solution in TFE into milli-Q. The grey lines show the spectra during the process, the black line the spectrum 2 hours after injection. The temperatures were set at b) 5 °C, c) 20 °C, d) 60 °C and e) 80 °C.

At 5 °C the transition did not seem to be complete within the two hours during which the sample was monitored (Figure 5b). Between 40 °C and 80 °C a  $\beta$  sheet signal was observed at the end of the experiment. For temperatures of 80 °C and higher the initial random coil signal did not change. Although the shape of the spectra could be reproduced in subsequent experiments, its intensity could not. This is probably due to the earlier mentioned linear dichroism phenomenon.

In summary, PA **2** assembled into fibres at 50 °C when cooled down from 90 °C, and disassembled at 80 °C when subsequently heated, thus showing a large hysteresis. When injected in milli-Q from a concentrated solution of TFE (procedure C) assembly was possible up to 80 °C. This maximum assembly temperature matched the disassembly temperature in the heating experiment, showing that in equilibrium, assembly is possible up to the disassembly temperature.

The assembly for **1** was so slow that it did not take place during the cooling experiment at all. However, when left overnight at temperatures up to 40 °C, the amphiphiles assembled. This sample preparation procedure is shown in Figure 1c. The disassembly temperature was 55 °C, so in principle this should be the maximum assembly temperature. However, we did not perform longer measurements to determine if the assembly would also have taken place at somewhat higher temperature on a longer timescale. Injecting from TFE led to self-assembly up to 60 °C, which coincides with the disassembly temperature measured.

## Polymerisation

**Kinetics of the diacetylene polymerisation.** The fibres were covalently linked using a light-initiated topochemical radical polymerisation of the diacetylene moieties,<sup>9</sup> resulting in intensely purple and blue coloured polymers for the C<sub>23</sub> (**p1**) and C<sub>25</sub> (**p2**) fibres, respectively. The polymerised fibres were highly insoluble in most solvents. Only in pure TFA or concentrated sulphuric acid the colour changed to yellow, indicative of a dissolved polydiacetylene. NMR spectroscopy of the polymer was therefore performed in TFA (Figure 6). The broadening of the peaks after illumination indicates the presence of polymer.

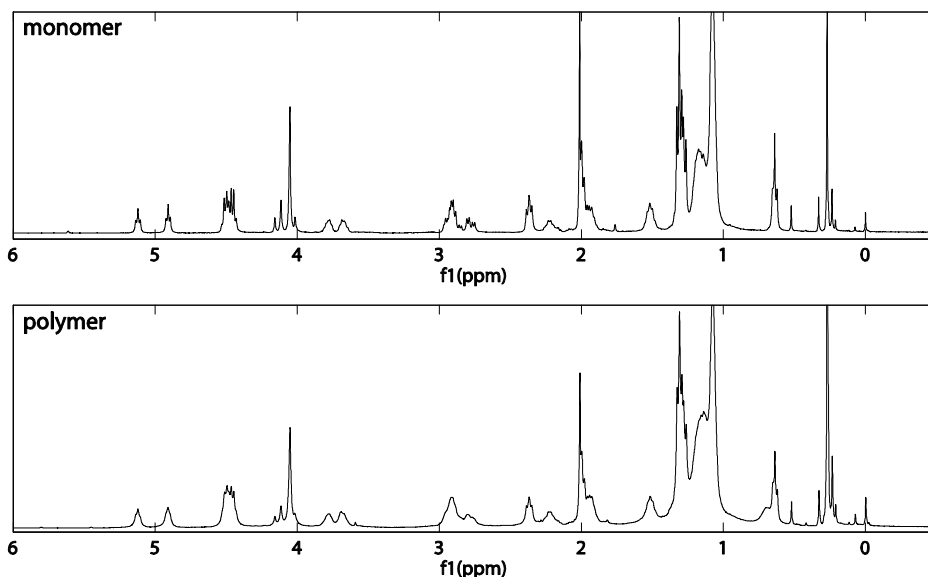


Figure 6. <sup>1</sup>H-NMR spectra of the monomer (upper) and polymer (lower) of PA 2 in TFA.

The UV absorption spectra of the polymers are shown in Figure 7a. The extinction coefficients after polymerisation are  $(6\pm 1)\cdot 10^3 \text{ cm}^{-1}\text{M}^{-1}$  and  $(18\pm 2)\cdot 10^3 \text{ cm}^{-1}\text{M}^{-1}$  for compound **p1** and **p2**, respectively. The large error in the measurements is due to the inhomogeneity of the samples. The 650 nm peak, observed for **p2** is typical for the so-called blue state of polydiacetylenes. There still is discussion about the explanation for this long-wavelength absorption. According to Giesa<sup>22</sup> and Wenz<sup>23</sup>, among others, the effective conjugation length accounts for peaks up to 550 nm; peaks appearing at higher wavelengths are caused by a solid-state effect. If this is true, inter-fibre aggregation would take place for **2** but not for **1**. However, Schott<sup>24</sup> and Beckham<sup>25</sup> claim that no solid-state aggregation is needed for the long wavelength absorption. Though the blue and red states have different structures, both are, in their view, accounted for by single chain properties.

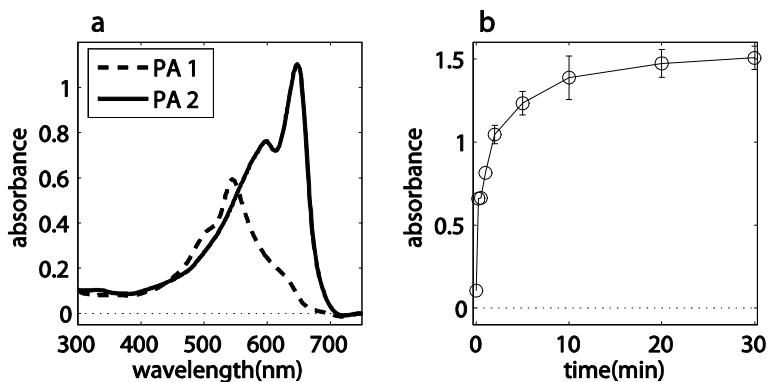


Figure 7. (a) UV absorption spectra of the polymerised assemblies of peptide PA 1 (**p1**) (dashed line) and 2 (**p2**) (solid line). (b) 650 nm absorption peak intensities of polymer **p2** during polymerisation

The increase of the 650 nm absorption peak of polymer **p2** during polymerisation is shown in fig 7b. The polymerisation occurred readily under the influence of UV light. For **2** it was found that even visible light up to 532 nm could invoke the polymerisation. As already mentioned before, polymerisation even took place during the short exposure of the light employed during CD measurements. Even though polymerisation at high wavelengths has been reported,<sup>26-29</sup> for these complex systems this phenomenon is not often observed. Since the reaction is topochemical, and hence very sensitive to the packing of the monomers, the ease of polymerisation can be considered indicative of highly ordered packing of the alkyl chains within the fibre.

After polymerisation, the polymers were visualized with atomic force microscopy (AFM) and TEM (Figure 8). These measurements confirmed that the structure of the fibres did not change upon polymerisation (compare Figure 2).

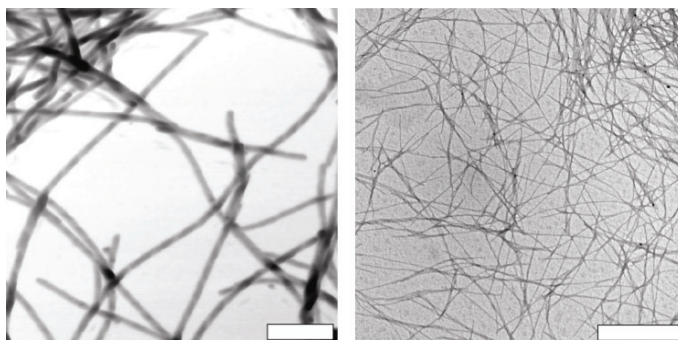


Figure 8. AFM (left) and TEM (right) pictures of **p2**. The white bar in the AFM picture represents 300nm, in the TEM picture 1  $\mu$ m.

**Temperature dependence of the polymerisation.** To obtain more insight into the fibre disassembly process, the polymerisation was performed at several temperatures. The samples were annealed at 90 °C, to ensure that all aggregates were molecularly

dissolved. The subsequent slow cooling to 0 °C allowed the amphiphiles to order into neat stacks. After this, the samples were heated to the temperatures at which they were polymerised. As expected, no polymerisation was observed when samples were irradiated at temperatures higher than the transition temperature (Figure 9a).

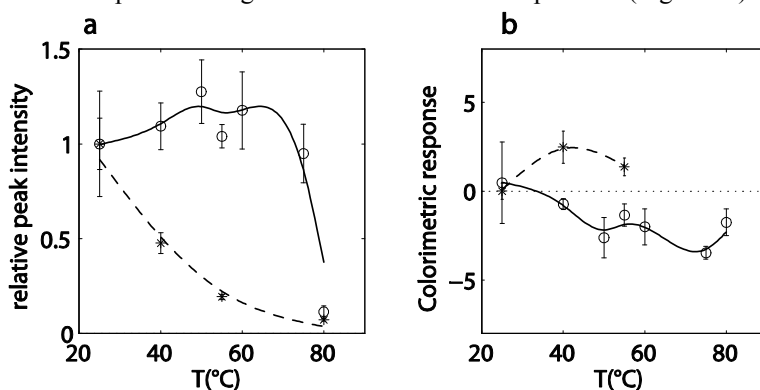


Figure 9. Polymerisation at different temperatures. Left: relative peak intensity of the most intense peak – 550 nm for amphiphile **p1** and 650nm for **p2** – in the UV spectra of **p1** (stars) and **p2** (circles) polymers. Right: colourimetric response of **p1** (stars) and **p2** (circles). The lines are included to guide the eye.

The disassembly temperatures derived in this way, estimated to be about 50 °C for **1** and 75 °C for **2**, are comparable to those determined by CD spectroscopy (55 °C and 80 °C for **1** and **2**, respectively). The slight difference may be caused by the relatively high heating rate in the CD experiments (3 °C/min) resulting in an overheating of the sample before the fibres fall apart. Polymerisations were possible up to the disassembly temperature of the fibre. Thus, the transition temperature of the alkyl chains from solid-like to gel-like – above which polymerisation is not possible<sup>26, 30-33</sup> is higher than the disassembly temperature of the fibre. This is in accordance with the fact that we did not observe a phase transition in DSC experiments. For C<sub>25</sub> diacetylene compounds transition temperatures between 40 °C and 70 °C are reported depending on the headgroup.<sup>26, 32, 34</sup> The peptide may well have a stabilizing effect which increases the solid-to-liquid transition of the lipid tails further, resulting in a phase transition temperature higher than the disassembly temperature of the fibres.

The changes in the UV absorption spectra after polymerisation at different temperatures are indicative of the change in orientation of the polydiacetylene backbone.<sup>16, 25, 33</sup> The CR (colourimetric response) was determined to quantify the difference in UV absorption between polymerisation at 25 °C (which is used as a reference) and other temperatures (Figure 9b). The CR is calculated from the ratio between characteristic peaks in the absorption spectrum to measure the colour change.<sup>10</sup> A larger value of CR indicates a bigger structural change of the polymer backbone. The formulas used to calculate the CR can be found in the experimental section.

The difference in behaviour between the amphiphiles was large. Upon polymerisation amphiphile **2** gave the same UV-absorption for each temperature up to the transition temperature, whereas the polydiacetylene absorption of **p1** decreased gradually with temperature (Figure 9a). The CR, however, was in both cases only a few

percent for polymerisations at elevated temperatures. This is in contrast to work done by Leaver *et al.*,<sup>35</sup> who observed a much larger spectral change upon irradiation at elevated temperatures. These results demonstrate that the structure of the polymer backbone of the fibres was hardly influenced when heated. The absence of structural change in the polymer backbone implies that also only minor structural changes can take place in the peptide part. The obtained results can be explained by amphiphile **1** forming fewer fibres at elevated temperature, while the number of fibres of **2** was constant up to the disassembly temperature. Beyond the disassembly temperature of the fibres no polymerisation took place and thus no CR could be determined. This points at a disassembly process which is more cooperative for **2** than for **1**.

**pH dependence of the polymerisation.** Because fibre formation was expected to be influenced by the ionisation state of the building blocks, which possess carboxylic acid C-termini, polymerisations were carried out at different pH values in the range of pH 1 to pH 13 using the appropriate buffers. We used two methods to prepare fibre solutions at the various pH values. In method 1 the fibre preparation was carried out in milli-Q, after which the pH was set. In method 2 both fibre preparation and polymerisation were carried out at the specific pH.

With method 1 the pH dependence of the assembled fibres was investigated, whereas with method 2 also the effect on the assembly process was studied. It was expected that method 1 would yield a smaller CR than method 2, because in milli-Q the fibres might pack tightly after which pH changes would have no further influence on its structure. By using method 2 the fibres might not have the opportunity to form their stable packing, resulting in a larger CR upon polymerisation. With both methods, fibres under acidic conditions formed a fluffy precipitate while at high pH the solution was mostly homogeneous. The precipitate at low pH hampered the measurement of the intensity of the solution after polymerisation, but the spectral shape could still be investigated. Changing the pH after fibre formation (method 1), did not change the colour at all for both assemblies, as evidenced by the low values (between 4 and -2) of the CR. Since the CR uses only intensity ratios, fluctuations in intensity did not hamper its determination. The absorption spectrum of polymer **p2** also did not change with pH when method 2 was employed, but for **p1** a clear pH dependence was observed. At alkaline pH, the polymerisation of **1** did not take place anymore. From these measurements we conclude that neither the fibre formation (tested with method 2) nor its backbone structure (method 1) was influenced by pH changes for amphiphile **2**, whereas fibres of amphiphile **1** are stable towards pH once formed, but their formation is hampered at alkaline pH.

## **Polymer properties**

**Temperature dependence of the diacetylene polymer.** As expected, polymerisation greatly increased the stability of the assemblies. CD spectra did not show the typical  $\beta$  sheet to random coil transition with increasing temperature which was found for the unpolymerised fibres, i.e. polymerised fibres did not fall apart upon



heating. However, in the UV spectra of the polymers a change was visible upon heating the samples. We quantified the spectral change in a colourimetric response, as described above. Upon heating the solutions above 60 °C, a fluffy precipitate formed. This precipitation was found to be irreversible, i.e. the solutions remained inhomogeneous upon cooling. As described above, the precipitate did not hamper the determination of the CR, since the CR uses only ratios of peak intensities. The CR for **p2** upon heating was at 90 °C almost twice as high as for **p1** (Figure 10). For both samples the CR returned upon cooling without any hysteresis to its original value, in contrast to other known diacetylene systems where large hystereses are observed.<sup>24, 36</sup>

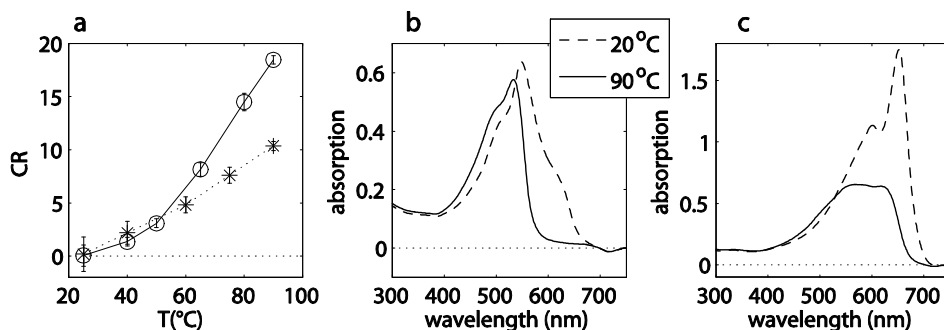


Figure 10. Temperature dependence of the colours of **p1** and **p2**. a) CR for **p1** (stars) and **p2** (circles). b and c) UV absorption spectra for b) **p1** and c) **p2** at 20 °C (dashed line) and 90 °C (solid line).

Even though the CR returned to its original value after heating the amphiphilic structures, different UV spectra of **p1** were obtained before and after heating. The spectrum of **p1** consists of one peak and two shoulders (Figure 10b). The 600 nm shoulder did not return to its original intensity after heating, indicating a change in the structure of the polymer backbone (data not shown). Because this shoulder is not accounted for in the definition of the CR it does not affect the reversibility of the CR. The change in the spectrum after heating reflects a less tight packing for amphiphile **p1** as compared to **p2**.

**pH dependence of the diacetylene polymer.** To determine the influence of pH on the polymerised fibres, they were examined in buffer solutions ranging from pH 1 to pH 13. The pH was expected not to have a large influence on the colour of the polymer, since also the polymerisation showed no sensitivity towards pH. Indeed, the change in the pH of the solution did not induce a colour change. However, as also described for the unpolymerised fibres, some change took place: a fluffy precipitate formed at low pH.

As both pH and temperature changes did not seem to affect the structure of the assemblies, we decided to vary them simultaneously to see if the combined effect would change the fibre conformation. Again, two sets of samples were prepared, using methods 1 and 2 to set the pH (see above), after which the fibres were polymerised. Heating these solutions did in both cases not lead to other results than obtained previously in milli-Q solutions.

## Discussion

Both diyne containing peptide amphiphiles are able to form stable  $\beta$  sheet fibres of micrometers length in an aqueous solution. Although the driving force for assembly stems from the hydrophobic interactions between the alkyl tails, the directionality is largely controlled by the hydrogen bond forming peptide part.<sup>7</sup> The unpolymerised fibres disassemble when heated. The transition temperature for this process is dependent on the chain length, as observed previously for saturated alkyl chains.<sup>7</sup> Upon cooling, **2** reassembles accompanied with a large hysteresis. In contradistinction, **1** only reassembles when it is allowed to stand overnight at temperatures lower than 40 °C. This large difference in behaviour is remarkable if one considers that the only difference between the two amphiphiles is the two carbons at the outer end of the alkyl chain. These are more than 10 Å away from the polydiacetylene backbone and even further from the  $\beta$  sheet forming peptide. The large observed differences in the self-assembly process indicate in our opinion its subtlety. After polymerisation of the fibres another important difference appears. Compound **p1** lacks the high-wavelength peak which is visible for **p2**. Since this peak might be associated with solid state aggregation, the two carbon difference in the chain length possibly causes fibres to have (**2**) or lack (**1**) inter-fibre aggregation.

The higher stability of amphiphile **2** as opposed to compound **1** is also observed in several of the other experiments: its formation takes place in both very acidic and very alkaline solutions, its polymerisation yields an equally intensely coloured polymer up to the melting temperature and the colour change observed upon heating the polymer is fully reversible. In contrast, fibres of compound **1** are stable towards acidic and alkaline solution, but they do not form in alkaline solution, i.e. after preparing solutions of **1** via procedure A in alkaline solutions, no polymerisation takes place. Polymerisation at elevated temperature also shows a different trend from **2**. Polymerisation is possible up to the melting temperature, but the intensity of the polymerised solution decreases with temperature, though the colour itself is similar for polymerisation at each temperature. The last important difference between **p1** and **p2** is that the colour change upon heating the polymer is not fully reversible for **p1**, where it is for **p2**. The observation that, for both amphiphilic structures, the polymerisation is possible up to the melting temperature in combination with an absence of phase transition in DSC implies that the phase transition temperature of the alkyl chains is higher than the disassembly temperature of the fibres.

As already mentioned, the self-assembled fibres of both amphiphiles showed a great stability towards pH changes. However, pH hampers the assembly formation for **1**, as opposed to **2**. For both amphiphiles, at low pH, a fluffy precipitate forms, caused by a larger tendency to aggregate. The increase in aggregation tendency is caused by the free acid groups at the C-terminus, which are protonated at low pH. This causes the repulsive forces between them to diminish, causing fibres to fold back on themselves or form inter-fibre aggregates. Since the colour of the polymer does not change, it is unlikely that the internal structure of the fibres themselves changes with pH.

## Conclusion

Functionalizing tricosadiynoic acid (**1**) or pentacosadiynoic (**2**) with the peptide sequence GANPNAAG allowed us to prepare remarkably stable nanofibres in water. Their configuration can be locked using the topochemical radical polymerisation frequently used for diacetylenes, but not often used for such small systems in an aqueous environment. From the remarkably large difference between the stability of the assemblies of these two very similar amphiphiles it can be concluded that the assembly and disassembly processes are delicate and affected by small structural features of the constituent building blocks.

## Experimental section

**General.** Proton chemical shifts are reported in ppm downfield from tetramethylsilane (TMS). Mass spectra were recorded on a JEOL AccuTOF-CS spectrometer. UV/Vis spectra were recorded on a VARIAN Cary 50 Conc spectrometer. CD spectra were recorded on a Jasco J-810 spectropolarimeter equipped with a Jasco PTC-423S/L Peltier type temperature control system. TEM images were obtained with a JEOL- JEM-1010 equipped with a CCD camera.

**Synthesis.** The GANPNAAG peptides were prepared by an earlier reported procedure,<sup>7</sup> which is described in chapter 2.

**Data for C<sub>24</sub>H<sub>41</sub>C(O)-Gly-Ala-Asn-Pro-Asn-Ala-Ala-Gly-OH:**

TLC: R<sub>f</sub> 0.18 (eluent: MeOH/ CHCl<sub>3</sub>/ AcOH 25:65:10).

<sup>1</sup>H-NMR [DMSO-d<sub>6</sub>]: δ 0.85 (t, CH<sub>3</sub> –alkyl chain, 3H), 1.12 (d, CH<sub>3</sub> -Ala, 3H), 1.20 (m, -CH<sub>2</sub>-alkyl chain; CH<sub>3</sub> –Ala, 34H), 1.48 (m, CH<sub>2</sub>-alkyl chain, 2H), 1.85 (m, CH<sub>2</sub> Pro, 3H), 2.18 (m, CH<sub>2</sub> Pro; α-CH<sub>2</sub>-alkyl tail, 3H), 2.21 (t, CH<sub>2</sub>-alkyn, 4H), 2.40 (m, CH<sub>2</sub> Asn, 2H), 2.55 (dd, CH<sub>2</sub> Asn, 1H), 2.65 (dd, CH<sub>2</sub> Asn, 1H), 3.65 (m, α-CH<sub>2</sub> Gly; CH<sub>2</sub> Pro, 3H), 3.75 (m, CH<sub>2</sub> Pro; α-CH<sub>2</sub> Gly, 3H), 4.20 (m, CH<sub>2</sub> Pro; α-CH<sub>2</sub> Ala, 4H), 4.40 (m, α-CH<sub>2</sub> Asn, 1H), 4.73 (q, α-CH<sub>2</sub> Asn, 1H), 6.92 (s, NH<sub>2</sub> Asn, 1H), 7.10 (s, NH<sub>2</sub> Asn, 1H), 7.20 (s, NH<sub>2</sub> Asn, 1H), 7.52 (d, α-NH Ala, 1H), 7.64 (s, NH<sub>2</sub> Asn, 1H), 7.72 (d, α-NH Ala, 1H), 7.88 (two d, α-NH Asn; α-NH Ala, 2H), 7.96 (broad s, α-NH Gly, 2H), 8.27 (d, α-NH Asn, 1H).

Mass spectrometry: Accu-TOF: Calc for [C<sub>51</sub>H<sub>82</sub>N<sub>10</sub>O<sub>12</sub> + Na]<sup>+</sup> 1049.601, found 1049.600.

**Data for C<sub>22</sub>H<sub>37</sub>C(O)-Gly-Ala-Asn-Pro-Asn-Ala-Ala-Gly-OH**

<sup>1</sup>H-NMR [DMSO-d<sub>6</sub>]: δ 0.85 (t, CH<sub>3</sub> –alkyl chain, 3H), 1.12 (d, CH<sub>3</sub> -Ala, 3H), 1.20 (m, -CH<sub>2</sub>-alkyl chain; CH<sub>3</sub> –Ala, 30H), 1.48 (m, CH<sub>2</sub>-alkyl chain, 2H), 1.85 (m, CH<sub>2</sub> Pro, 3H), 2.18 (m, CH<sub>2</sub> Pro; α-CH<sub>2</sub>-alkyl tail, 3H), 2.21 (t, CH<sub>2</sub>-alkyn, 4H), 2.40 (m, CH<sub>2</sub> Asn, 2H), 2.55 (dd, CH<sub>2</sub> Asn, 1H), 2.65 (dd, CH<sub>2</sub> Asn, 1H), 3.65 (m, α-CH<sub>2</sub> Gly; CH<sub>2</sub> Pro, 3H), 3.75 (m, CH<sub>2</sub> Pro; α-CH<sub>2</sub> Gly, 3H), 4.20 (m, CH<sub>2</sub> Pro; α-CH<sub>2</sub> Ala, 4H), 4.40 (m, α-CH<sub>2</sub> Asn, 1H), 4.73 (q, α-CH<sub>2</sub> Asn, 1H), 6.92 (s, NH<sub>2</sub> Asn, 1H), 7.10 (s, NH<sub>2</sub> Asn, 1H), 7.20 (s, NH<sub>2</sub> Asn, 1H), 7.52 (d, α-NH Ala, 1H), 7.64 (s, NH<sub>2</sub> Asn, 1H), 7.72 (d, α-NH Ala, 1H), 7.88 (two d, α-NH Asn; α-NH Ala, 2H), 7.96 (broad s, α-NH Gly, 2H), 8.27 (d, α-NH Asn, 1H).

Mass spectrometry: Accu-TOF: Calc for [C<sub>51</sub>H<sub>82</sub>N<sub>10</sub>O<sub>12</sub> + Na]<sup>+</sup> 1021.570, found 1021.572.

**Fibre formation.** Three procedures for fibre formation were used.

*Procedure A.* The amphiphiles were dispersed in milli-Q at concentrations of either 0.2 or 1.0 mg/mL. The samples were heated to 50 °C for 30 min, followed by 15 min sonication at that temperature. Subsequently, the samples were heated to 90 °C and allowed to cool to room temperature.

*Procedure B.* The amphiphiles were dispersed in milli-Q at concentrations of either 0.2 or 1.0 mg/mL. The samples were heated to 50 °C for 30 min, followed by 15 min sonication at that temperature, after which they were allowed to cool to room temperature.

*Procedure C.* 30 µL of a 10 mg/mL solution of the amphiphiles in trifluoroethanol (TFE) was injected in 270 µL milli-Q at room temperature.

**Polymerisations.** Polymerisations were carried out on 1 mg/mL samples in a quartz cell with a path length of 1 mm using a Bluepoint 2 UV lamp with a sample-light source distance of 15 cm.

**pH variation.** The influence of pH was investigated both on non-polymerised and polymerised samples. To obtain solutions of pH 3, 5 and 7 a citric acid-phosphate buffer was used, while for pH 9, 11 and 13 a glycine-NaOH buffer and for pH 1 a hydrochloric acid/potassium chloride buffer were applied. The pH of the solution was changed using two different methods:

*Method 1.* Samples were prepared using 270 µL milli-Q water of which the pH was set after fibre preparation using 30 µL of a 3M buffer solution.

*Method 2.* The whole sample preparation was carried out in 300µL 0.3 M buffer solution.

**Circular dichroism (CD) spectroscopy.** The measurements were carried out at a concentration of 0.2 mg/mL using a 1 mm quartz cell. The spectra were recorded on a JASCO J-810 spectropolarimeter. To measure temperature curves, a heating or cooling rate of 3 °C/min was used. Measuring the peak intensity in time was hampered by the presence of the diyne functionalities which readily polymerised when illuminated with the short wavelengths used for the CD measurements. Therefore, spectra were recorded every 10 °C (265-185 nm, 100 nm/min), and the shutter was closed (5 µm) between these measurements.

**UV-Vis spectroscopy.** The measurements were carried out at a concentration of 1.0 mg/mL using a 1 mm quartz cell. The spectra were recorded on a Varian Cary-50 spectrometer. Colour changes were quantified with the so-called colourimetric response (CR).<sup>10</sup> The CRs for amphiphile **1** and **2** (Scheme 1) were calculated as follows:

$$CR_{25} = 1 - \frac{I_{650} (I_{650}^{ref} + I_{600}^{ref})}{I_{650}^{ref} (I_{650} + I_{600})}$$
$$CR_{23} = 1 - \frac{I_{550} (I_{550}^{ref} + I_{505}^{ref})}{I_{550}^{ref} (I_{550} + I_{505})}$$

where I denotes the absorbance at the wavelength given by the subscript and I<sup>ref</sup> is the corresponding absorbance of the polymers in milli-Q at 25 °C.

**Transmission electron microscopy (TEM).** TEM samples were prepared by floating a carbon-coated copper grid on a peptide amphiphile solution of 0.2 mg/mL for 5 min, followed by removal of residual water by blotting with a paper filter. The samples were shaded with platinum in an Edwards coater model 306 by placing the grids under an angle of 45° with respect to the Pt source, and visualized using a JEOL 1010 transmission electron microscope set on an accelerating voltage of 60 kV.

**Differential Scanning Calorimetry (DSC).** DSC measurements were performed on a Mettler Toledo DSC822 with concentrations of the amphiphile in milli-Q between 0.2 and 60 mg/mL using heating rates ranging from 0.3 to 15 °C/min. The samples were prepared using procedure A as described above for concentrations ranging from 0.2 to 10 mg/mL. For higher concentrations the solutions were heated up to the boiling point, which was required to disperse the amphiphiles. While hot, the solution was put into the DSC cups where it was allowed to cool.

**Atomic Force Microscopy (AFM).** AFM measurements were performed on a DI Dimension 3100 in tapping mode. Samples were prepared using procedure A, followed by freeze-drying and the addition of milli-Q to obtain a concentration of 0.2 mg/mL. Subsequently the samples were sonicated at room temperature for 60 min. Then a 5  $\mu$ L sample was placed on a mica substrate and allowed to dry. The data were processed using the WSxM software package.<sup>37</sup>

## References

1. A. Zlotnick, *J. Mol. Recognit.*, 2005, **18**, 479-490.
2. E. Baer, A. Hiltner and H. D. Keith, *Science*, 1987, **235**, 1015-1022.
3. D. W. P. M. Löwik and J. C. M. van Hest, *Chem. Soc. Rev.*, 2004, **33**, 234-245.
4. J. D. Hartgerink, E. Beniash and S. I. Stupp, *Science*, 2001, **294**, 1684-1688.
5. G. A. Silva, C. Czeisler, K. L. Niece, E. Beniash, D. A. Harrington, J. A. Kessler and S. I. Stupp, *Science*, 2004, **303**, 1352-1355.
6. C. Cerami, U. Frevert, P. Sinnis, B. Takacs, P. Clavijo, M. J. Santos and V. Nussenzweig, *Cell*, 1992, **70**, 1021-1033.
7. D. W. P. M. Löwik, J. Garcia-Hartjes, J. T. Meijer and J. C. M. van Hest, *Langmuir*, 2005, **21**, 524-526.
8. D. W. P. M. Löwik, J. T. Meijer, I. J. Minten, H. van Kalkeren, L. Heckenmuller, I. Schulten, K. Slieden, P. Smittenaar and J. C. M. Van Hest, *J. Pept. Sci.*, 2008, 127-133.
9. G. Wegner, *Makromol. Chem.*, 1972, **154**, 35-48.
10. S. Okada, S. Peng, W. Spevak and D. Charych, *Acc. Chem. Res.*, 1998, **31**, 229-239.
11. E. Jahnke, A. S. Millerioux, N. Severin, J. P. Rabe and H. Frauenrath, *Macromol. Biosci.*, 2007, **7**, 136-143.
12. E. Jahnke, I. Lieberwirth, N. Severin, J. P. Rabe and H. Frauenrath, *Angew. Chem., Int. Ed.*, 2006, **45**, 5383-5386.
13. D. W. P. M. Löwik, I. O. Shklyarevskiy, L. Ruizendaal, P. C. M. Christianen, J. C. Maan and J. C. M. van Hest, *Adv. Mater.*, 2007, **19**, 1191-1195.
14. L. Hsu, G. L. Cvetanovich and S. I. Stupp, *J. Am. Chem. Soc.*, 2008, **130**, 3892-3899.
15. Q. Cheng, M. Yamamoto and R. C. Stevens, *Langmuir*, 2000, **16**, 5333-5342.
16. N. Mino, H. Tamura and K. Ogawa, *Langmuir*, 1992, **8**, 594-598.
17. S. K. Chae, H. Park, J. Yoon, C. H. Lee, D. J. Ahn and J. M. Kim, *Adv. Mater.*, 2007, **19**, 521-524.
18. D. R. Day and H. Ringsdorf, *Makromol. Chem.*, 1979, **180**, 1059-1063.
19. D. Day and H. Ringsdorf, *J. Polym. Sci., Part C*, 1978, **16**, 205-210.
20. M. Wolffs, S. J. George, Z. Tomovic, S. C. J. Meskers, A. Schenning and E. W. Meijer, *Angew. Chem., Int. Ed.*, 2007, **46**, 8203-8205.
21. D. F. O'Brien, T. H. Whitesides and R. T. Klingbiel, *J. Polym. Sci., Part C: Polym. Lett.*, 1981, **19**, 95-101.
22. R. Giesa and R. C. Schulz, *Polym. Int.*, 1994, **33**, 43-60.
23. G. Wenz, M. A. Muller, M. Schmidt and G. Wegner, *Macromol.*, 1984, **17**, 837-850.
24. M. Schott, *J. Phys. Chem. B*, 2006, **110**, 15864-15868.
25. H. W. Beckham and M. F. Rubner, *Macromol.*, 1993, **26**, 5198-5201.
26. D. S. Johnston, S. Sanghera, M. Pons and D. Chapman, *Biochim. Biophys. Acta*, 1980, **602**, 57-69.
27. I. T. Dorn, U. G. Hofmann, J. Peltonen and R. Tampe, *Langmuir*, 1998, **14**, 4836-4842.
28. M. Bara, M. Schott and M. Schwoerer, *Chem. Phys. Lett.*, 1990, **175**, 23-29.
29. Y. Wang, L. Li, K. Yang, L. A. Samuelson and J. Kumar, *J. Am. Chem. Soc.*, 2007, **129**, 7238-+.
30. B. Hupfer, H. Ringsdorf and H. Schupp, *Macromol. Chem. Phys.*, 1981, **182**, 247-253.
31. E. Lopez, D. F. O'Brien and T. H. Whitesides, *J. Am. Chem. Soc.*, 1982, **104**, 305-307.
32. B. A. Armitage, D. E. Bennett, H. G. Lamparski and D. F. O'Brien, Polymerization and domain formation in lipid assemblies. In *Biopolymers Liquid Crystalline Polymers Phase Emulsion*, 1996; Vol. 126, pp 53-84.
33. A. Mueller and D. F. O'Brien, *Chem. Rev.*, 2002, **102**, 727-757.
34. N. Mino, H. Tamura and K. Ogawa, *Langmuir*, 1991, **7**, 2336-2341.
35. J. Leaver, A. Alonso, A. A. Durrani and D. Chapman, *Biochim. Biophys. Acta*, 1983, **732**, 210-218.

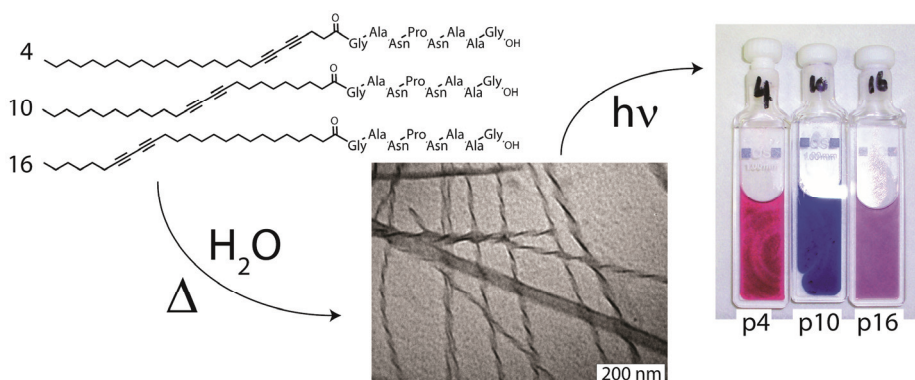
*Self-assembly and polymerisation of diacetylene-containing peptide amphiphiles in aqueous solution.*

36. K. C. Lim and A. J. Heeger, *J. Chem. Phys.*, 1985, **82**, 522-530.
37. I. Horcas, R. Fernandez, J. M. Gomez-Rodriguez, J. Colchero, J. Gomez-Herrero and A. M. Baro, *Rev. Sci. Instrum.*, 2007, **78**, 0137051-0137058.



## Chapter 5

# Effect of the diacetylene position on the chromatic properties of polydiacetylenes from self-assembled peptide amphiphiles



Three diacetylene-containing peptide amphiphiles, with exactly the same structure except for the position of the diacetylene moiety within the hydrophobic tail, were investigated on their assembly behaviour, polymerisation characteristics and chromatic properties. After polymerisation it was found that the colour and thus the conjugation length of the polydiacetylenes was dependent both on mobility and packing of the groups on both sides of the triple bonds. The polydiacetylene with the highest conjugation length and most stable structure was obtained when the diacetylenes were positioned in the middle of the hydrophobic tail. When the diacetylenes were close to the peptide, the mismatch between hydrogen bond and alkyl tail spacing resulted in a decreased conjugation length of the resulting polymer, while when positioned close to the end of the amphiphile the mobility of the terminal alkyl chains hampered the packing of the diacetylenes.

---

This work has been published in M. Van den Heuvel, D. W. P. M. Löwik and J. C. M. van Hest, *Biomacromol.*, 2010, **11**, 1676-1683



## Introduction

Polydiacetylenes are highly conjugated polymers with unique chromatic properties. They are synthesized *via* the topochemical polymerisation of diacetylenes which was first described in the early '70s, by the group of Wegner.<sup>1</sup> This polymerisation can only take place if the diacetylene moieties are closely packed, as may be the case in for example crystals, but also in self-assembled systems (including monolayers,<sup>2, 3</sup> vesicles<sup>4-6</sup> or fibres<sup>7-11</sup>) in which the diacetylene units are introduced in the alkyl chains of amphiphiles. One of the interesting properties of the resulting highly conjugated polymers is their colour, which can change under the influence of external stimuli such as heat or pH. Despite all research conducted on the blue-to-red colour change of polydiacetylenes (PDAs), the mechanism is still not completely clear. The colour change may be caused by aggregation<sup>12</sup> or by structural changes within a single chain.<sup>13, 14</sup> Furthermore, the relative stability of the two coloured states is still under debate. It is generally accepted that the polymer colour is a measure of the conjugation length within the polymer backbone and thus is influenced by the nature and spatial arrangement of the side chains.<sup>15</sup> A blue polymer has a long conjugation length, a red polymer a shorter one. Stress within the polymer backbone, caused by changes in for example temperature,<sup>11, 16-20</sup> pH,<sup>17, 19, 21-25</sup> or the binding of a guest molecule<sup>5, 26-31</sup> may induce a colour change from blue to red. Even so, for some crystals the red state is shown to have a higher order and also in other systems it is not necessarily less ordered than the blue one.<sup>13, 32-34</sup> Self-assembled systems, in contrast with crystalline materials, can more easily accommodate volume changes induced upon polymerisation, as a result of the higher flexibility. During the application of a stimulus, for which temperature is the best known,<sup>34</sup> the higher flexibility allows a gradual structural change. The 'red state' in this case is a mixture of structures, caused by disorder in the side chains of the PDA (which is impossible in crystals, due to lack of space). This disorderly state may be reversible, unless side chains are getting intertwined, in which case the system is trapped in the less ordered red state, which does not necessarily have to be higher in energy.<sup>19, 21</sup> Of course, also in self-assembled systems a transfer to a well-ordered red state is possible, but it is not the only mechanism for colour change.

Assemblies of diacetylene containing amphiphiles have been used for systematic studies after the effect of several molecular parameters on the polymerisability of diacetylenes and the resulting PDA colour. Cheng and Stevens<sup>35</sup> and Huo et al.<sup>32</sup> investigated the effect of size and charge of the headgroup on the colour of the polymer by coupling respectively one or two amino acids to 10,12-pentacosadiynoic acid, followed by polymerisation of the resulting assemblies. In other reports variations were introduced both in the hydrophobic tail length and the position of the diacetylene moiety within the amphiphile.<sup>5, 11, 28, 36, 37</sup> Tachinaba et al.<sup>37</sup> varied the position of the diacetylene in pentacosadiynoic acid and studied the polymerisation and packing properties of monolayers of these compounds.

We wondered how the polymerisation and polymer properties would change going from 2D monolayers, in which the polymerisation can proceed in both directions, to

fibres, in which the polymerisation reaction can only take place in the length direction of the fibre.<sup>9, 38</sup>

Here we present a study on the effect of the diacetylene position within the hydrophobic tail of fibre forming peptide amphiphiles (PAs), in which only the diacetylene position is varied while keeping the alkyl chain length constant. To the best of our knowledge, such a systematic study in a one-dimensional environment has not been performed before.

The peptide amphiphiles (PAs) we used in this research contain the short eight amino-acid sequence GANPNAAG, derived from the CS protein of the malaria parasite *Plasmodium Falciparum*.<sup>39</sup> Previously we have shown that when coupled to an alkyl tail or a diacetylene functionalized tail, the peptide forms fibres in aqueous solution.<sup>9, 11, 40</sup> In these compounds either no diacetylene was present or it was positioned only at the 10,12 position of the hydrophobic tail. In order to determine the effect of the position of the diacetylene on polymerisation characteristics and chromatic properties PAs with the diacetylene at the 4,6 and the 16,18 positions were synthesized (**4** and **16** respectively, Figure 1)

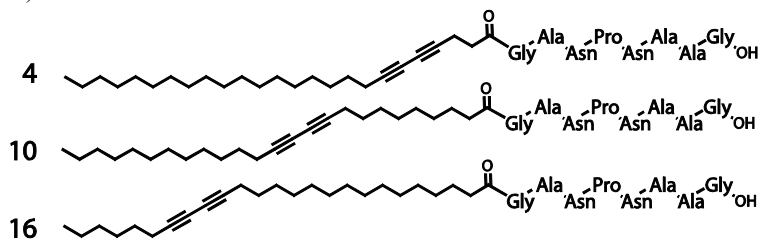
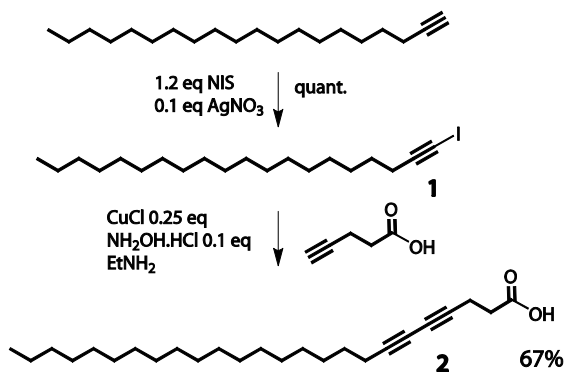


Figure 1. Structures of the three peptide amphiphiles used.

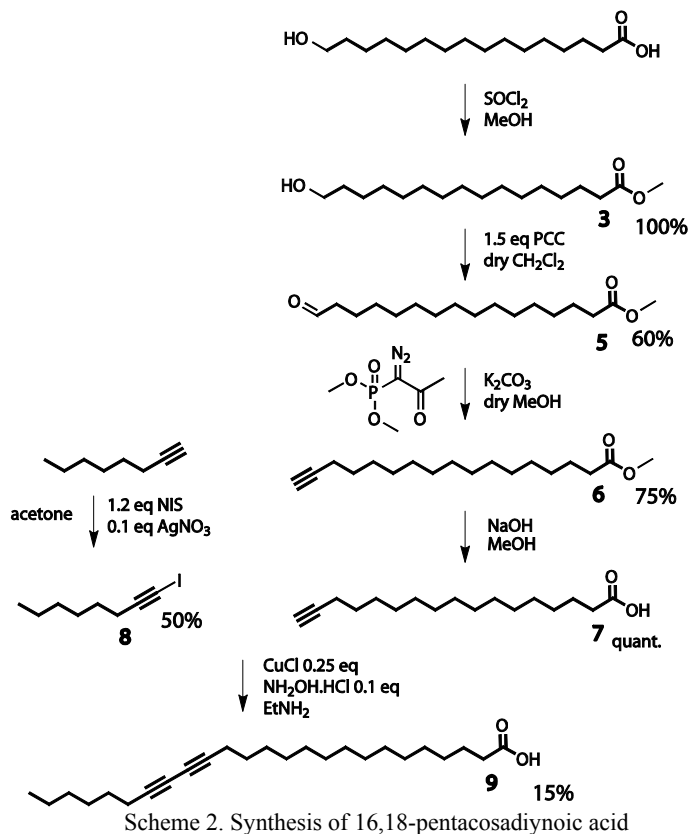
## Synthesis

To synthesize PAs with the diacetylene at the 4,6 and the 16,18 positions, the appropriate alkyl chains had to be prepared. To be able to couple the hydrophobic tails to the peptide headgroup on the solid phase, we used pentacosadiynoic acids with the diacetylene groups at different positions as building blocks. The synthesis of 4,6-pentacosadiynoic acid (**2**) started from 1-eicosyne, which was quantitatively iodated using NIS and AgNO<sub>3</sub>,<sup>41</sup> yielding **1** (Scheme 1). A copper-catalyzed Cadiot-Chodkiewicz coupling with pentynoic acid in the presence of hydroxylamine hydrochloride<sup>42</sup> yielded the pentacosadiynoic acid **2** in 67% yield after recrystallization.



Scheme 1. Synthesis of 4,6-pentacosadiynoic acid

The second diacetylene acid (**10**, 10,12-pentacosadiynoic acid) was commercially available. For 16,18-pentacosadiynoic acid (**9**) we planned to follow a similar route as for **2**, which involved coupling of octyne iodide (**8**) with heptadec-16-ynoic acid (**7**). Octyne iodide was conveniently obtained from 1-octyne using the same conditions as for the iodation of 1-eicosyne. Unfortunately several attempts to perform a substitution reaction with 15-bromopentadecanoic acid<sup>43-46</sup> failed in our hands. Therefore, another strategy was adopted to obtain the alkyne functionalized acid **7**, starting from 16-hydroxyhexadecanoic acid (Scheme 2), of which the alcohol could be oxidized to aldehyde **5** using pyridinium chlorochromate<sup>47</sup> after protection of the acid functionality (**3**). The aldehyde was converted to acetylene **6** using the Ohira-Bestmann reagent.<sup>48</sup> Since in the synthesis of 4,6-pentacosadiynoic acid (**2**) the coupling between the acetylene functionalized acid and the acetylene iodide was successful, the methyl ester was deprotected and the coupling was performed similar to the coupling for 4,6-pentacosadiynoic acid. However, the yield of this final reaction step was only 15% after column chromatography, mainly due to purification problems. Purification might be less troublesome if the ester had been coupled before deprotection.



The eight amino-acid peptide GANPNAAG was prepared on the solid phase using standard Fmoc procedures as described in Chapter 2. The hydrophobic tails were coupled to the peptide on the resin,<sup>40</sup> to yield the desired peptide amphiphiles **4**, **10** and **16** (Figure 1).

### Fibre stability

Before polymerisation, the implications of the position of the diacetylene group on the stability of the self-assembled peptide amphiphile fibres were investigated. For all three PAs it was found that fibres were able to form, as confirmed with circular dichroism (CD) spectroscopy (the appearance of a characteristic  $\beta$ -sheet signal, Figure 2) and transmission electron microscopy (TEM, Figure 3). As described previously, the CD spectra are influenced by alignment of fibres in solution which causes a linear dichroism (LD) effect that distorts the spectrum.<sup>11, 49</sup>

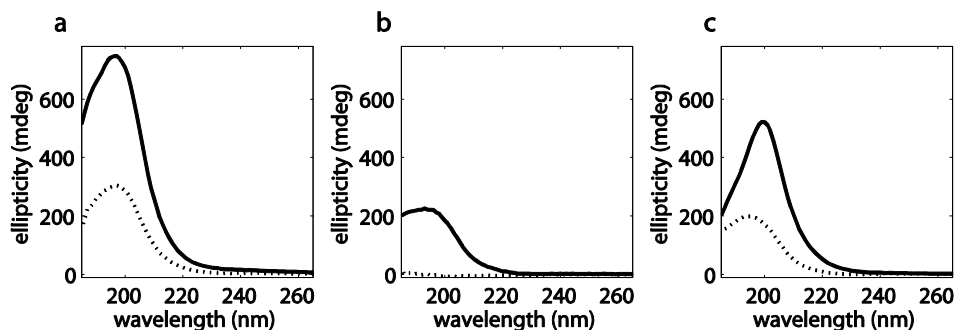


Figure 2. CD signal of a) **4**, b) **10** and c) **16** prepared in milli-Q water and measured at 20 °C (solid line) and 90 °C (dotted line)

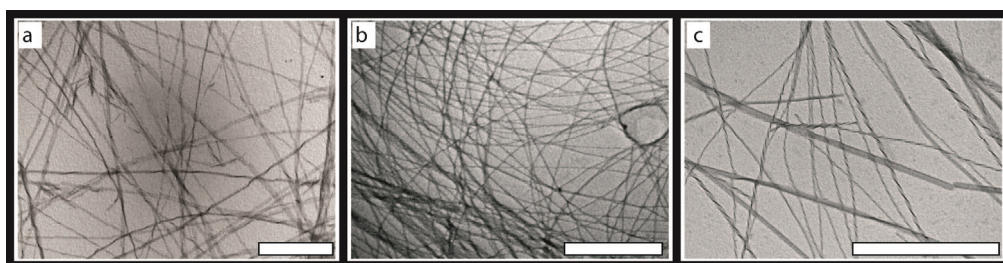


Figure 3. TEM pictures of fibres of a) **4**, b) **10** and c) **16**. The white bars represent 1  $\mu\text{m}$ .

We have shown previously with CD spectroscopy that a change from  $\beta$ -sheet to random coil is indicative for disassembly of the fibres.<sup>11, 40</sup> Preparing 0.2 mM PA solutions in milliQ using several heating and ultrasonic steps (procedure A, see experimental) yielded clear, fibre-containing solutions. Heating these samples to 90 °C caused **10** to disassemble around 80 °C. The other two PAs however did not disassemble within the temperature range measurable in aqueous solutions (Figure 2), indicating a higher stability.<sup>50</sup> To gain further insight into the assembly and disassembly properties, we decided to investigate the temperature at which the fibres assemble when the amphiphiles were injected from a good solvent (TFE) into water, yielding an aqueous 2 % TFE solution (procedure B). The amphiphiles still assembled under these conditions, with no visible difference in morphology, as confirmed with TEM. In this case, molecule **4** assembled at all tested temperatures, which is between 20 and 90 °C. Amphiphile **10** only assembled if injected into solutions of 60 °C and lower and **16** did not assemble above 80 °C (Figure 4). Fibres of **10** did not show a clear  $\beta$  sheet signal at 20 and 40 °C due to the LD effect but at 90 °C the random coil signal was clearly different from the distorted signal at 20 °C and 40 °C. The intensity of the signal is mainly caused by the LD effect and its increase with temperature indicates a better alignment because of lower viscosity and more convection in the cuvette.

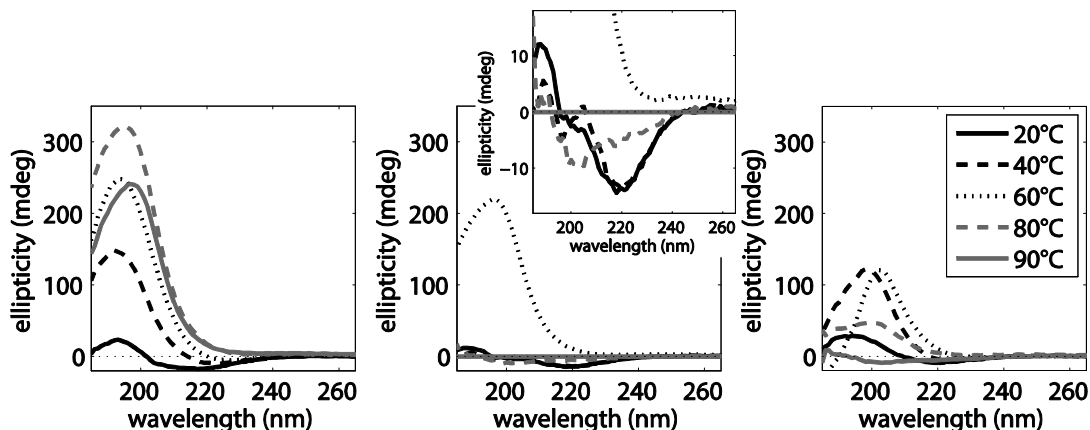


Figure 4. CD signal of a) **4**, b) **10** and c) **16** prepared in TFE, and injected in milli-Q water at several temperatures (20 to 90 °C)

From these measurements it was concluded that **4** forms the most stable fibres, followed by **16** and finally **10**. This trend correlates with the longest uninterrupted saturated alkyl tail within the amphiphile, i.e. the length from the peptide to the diacetylene functionality or from the diacetylene functionality to the end of the alkyl tail of the amphiphile. This length is 18 carbons for **4**, 14 carbons for **16** and 12 carbons for **10** (Figure 1), implying hydrophobic interactions are the main driving force for the fibres to assemble.

## Polymerisation

The polymerisability and the colour of the polymer are indicative for the packing of the diacetylenes within the amphiphile. All PAs were easily polymerised with UV light, to provide polymers **p4**, **p10** and **p16**, built up out of respectively PA **4**, **10** and **16**. The ease of polymerisation indicates a highly ordered packing of each of the alkyl chains within the fibres. The polymerisation of **10** followed similar behaviour to that of a monolayer of 10,12-pentacosadiynoic acid.<sup>37</sup> The behaviour of **4** however was completely different compared to its acid analogue, due to the stabilizing effect of the peptide. Polymerisation of a monolayer of 4,6-pentacosadiynoic acid (**2**) resulted in a yellow polymer,<sup>37</sup> indicating a dissolved polymer state and thus much disorder, while **4** yielded an ordered, stable polymer. The polymerisation, monitored by the absorption intensity, displayed an exponential behaviour for short illumination times. Extended illumination times resulted in an absorption shift to lower wavelengths and a decrease in absorption intensity (Figure 5), both of which are indications of damage (such as oxidation) to the backbone. To minimize damage of the polymer while also obtaining considerable polymerisation, an illumination time of 1 min was used.

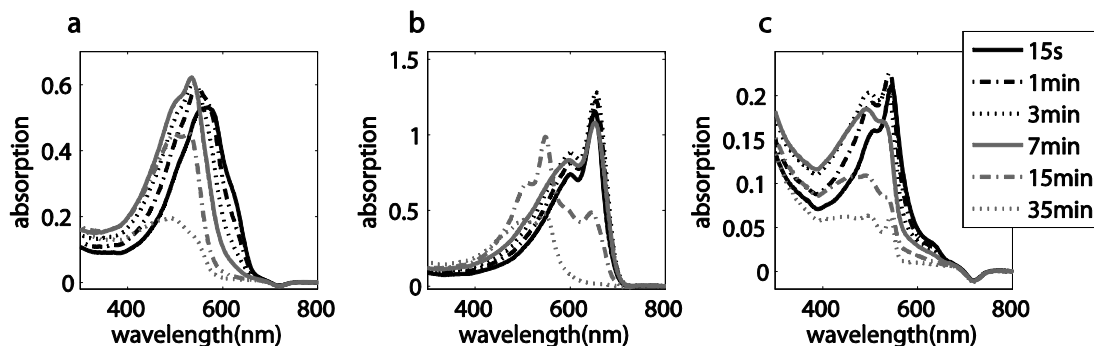


Figure 5. UV spectra of a) **p4**, b) **p10** and c) **p16** after illumination between 15s and 35min using a high-intensity UV lamp. A lighter colour depicts a longer illumination time. Note that the y-axes do not have the same scale.

The colours and absorption intensities of the three polymers after 1 min illumination showed striking differences, revealing structural variations in the packing of the polydiacetylenes (PDAs). While polymer **p10** had, with its absorption peak of maximum intensity at 650 nm, a blue appearance, **p16** was slightly pink and **p4** gave a darker pink colour (Figure 6). Moreover, the intensity of the strongest absorption peak of **p10** was the highest, followed by **p4** and finally **p16**, which indicates a reduced degree of polymerisation for **16** and to a lesser extent for **4**.

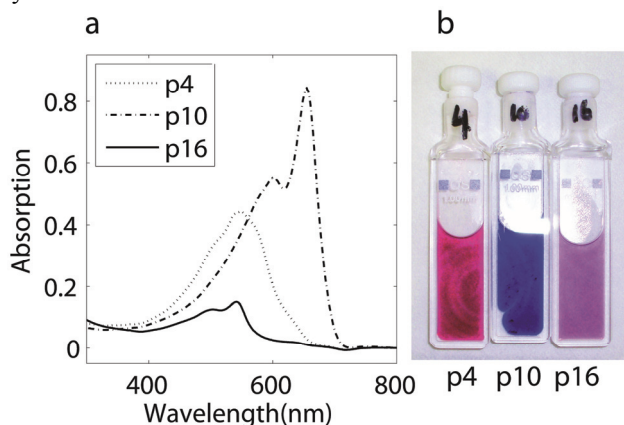


Figure 6. The colour of the three PA polymers. a) UV-Vis spectra of **p4** (dashed line), **p10** (dash-dotted line) and **p16** (solid line). b) The colour of the three polymerised samples.

As mentioned above, a colour change from blue to red can be regarded as a change from a relaxed to a stressed state, which implies that the amount of stress increases for PDA **p10** via **p4** to **p16**. The pink colour of **p4** can be explained by a slight difference in interchain distance between the peptide part (hydrogen bonds) and the alkyl tails (hydrophobic interactions). This mismatch causes the distance between the diacetylene moieties to be slightly larger than ideal, resulting in a more ‘stressed’, i.e. red, colour. For **p16**, the hydrophobic part at the end of the amphiphile was only six carbons long, and thus probably in a liquid-like state, leading to a less stabilized packing. The poorer packing of these tails partly prevented polymerisation and partly caused stress in the

backbone of the amphiphilic polymer. Polymer **p10**, with its PDA backbone well buried in the hydrophobic tail is stabilized at both sides and therefore has a blue appearance.

## Aging effects

To test if the packing of the peptide amphiphile fibres changed over time, fibres were prepared in milli-Q water and allowed to age at room temperature. At certain time intervals between 1 and 100 days, a sample was taken from the solution and polymerised after which the UV-Vis spectrum was measured. The PAs **4** and **10** polymerised to the same colour after any time period. Samples of **16**, however, polymerised to different colours and intensities over time (Figure 7). Upon aging a hypsochromic shift and increased intensity was observed. The wavelength shift implies an improved packing of the PAs within the fibres, while the higher absorption shows an increase in amount of fibres which could polymerise.

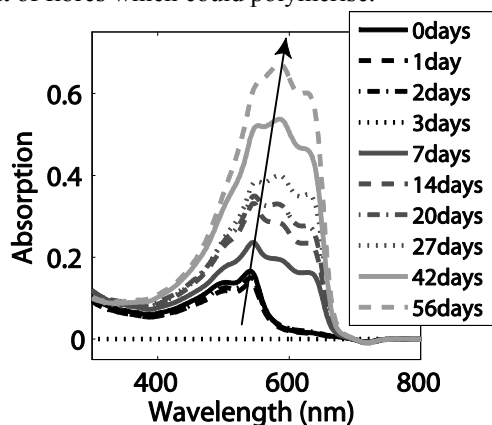


Figure 7. The absorption spectra of **p16** when polymerised after 1 to 56 days aging. The direction of the arrow shows the aging of the sample before polymerisation.

## Temperature and pH dependence

Upon heating, the side chains of PDAs gain mobility to result in a less ordered system which causes a bathochromic shift. For all three polymers the colour changed gradually to pink when heated to 90 °C in solution, showing a structural change which was largely reversible upon cooling (Figure 8). The colour of **p4** did not change much when heated, probably because it already had a distorted packing. Its spectrum at 90 °C however did not have the long-wavelength component (>600 nm) any more. PDA **p10** changed colour, but at 90 °C absorption at longer wavelengths was still visible. Polymer **p16** was most sensitive to temperature, and, like **p4**, lost the long-wavelength absorption band at 90 °C. However, the comparison between the compounds is difficult because of the differences in the starting spectra. The reversibility of the colour change was complete for **p10** and **p16**. The spectra of **p4** were very similar before and after heating.



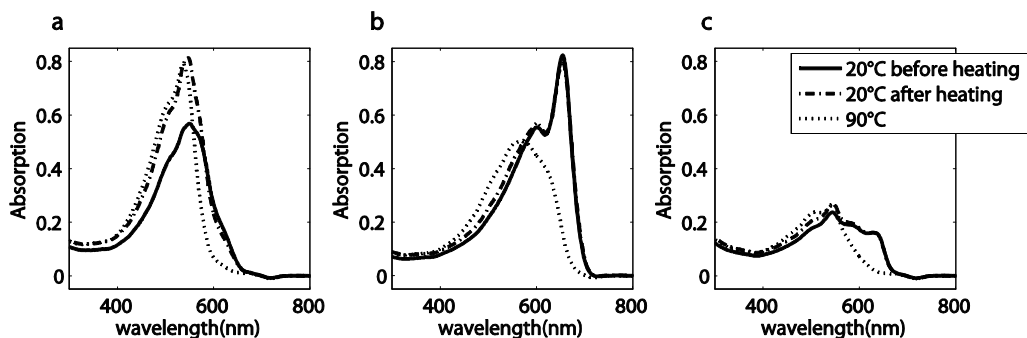


Figure 8. Reversibility of the absorption spectrum of a) **p4**, b) **p10** and c) **p16** after heating to 90 °C. The solid lines depict the colour before and the dash-dotted lines after heating, while the dotted lines show the spectrum at 90 °C.

Since the amphiphile polymers show a blue colour at ambient conditions which changes reversibly to red at *e.g.* elevated temperatures, we regard the blue state as the more and the red one as the less ordered species. To extend these measurements to a larger temperature range, we used dried samples, which were heated using a heat stage for 2 min to a temperature, and then rapidly cooled to room temperature. The resulting spots for **p10** are shown in Figure 9 ( $t = 1$  day). Spectra of these dried spots are difficult to measure, but also without the quantification some conclusions can be drawn. Up to a temperature of 100 °C the colour change is fully reversible. At 250 and 300 °C and to a lesser extent at 225 °C the polymer is degraded, i.e. the colour change is not reversible. In between 100 and 225 °C the colour change is partly reversible directly after cooling, and after a longer waiting time, the spots revert to its original colour (compare 1 and 11 days in Figure 9). We think that with heating above about 150 °C either tails or peptides are intertwined to such an extent that they prevent each other from rearranging to their most favourable packing.

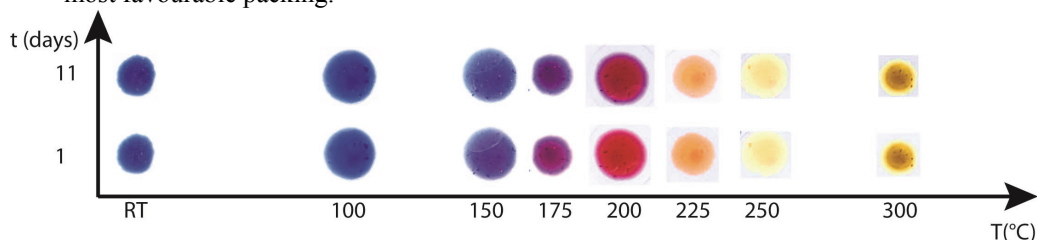


Figure 9. Colours of dried spots, heated for 1 min to a certain temperature (x-axis), and shown directly after cooling and after a waiting time of 11 days (y-axis).

Even though the position of the PDA moieties in the tail did not have a large effect on the reversibility of the colour changes after heating, it may have an effect on the pH dependence. Charych *et al.*<sup>5</sup> claimed that the pH dependence increases when the diacetylene moiety is closer to the peptide part of the amphiphile. For **p10** it was already known that it was pH insensitive.<sup>11</sup> This in fact turned out to be the case for all polymers; only when heated in 0.6 M sodium hydroxide an irreversible colour change was observed for **p16**, but not for the other polymers.

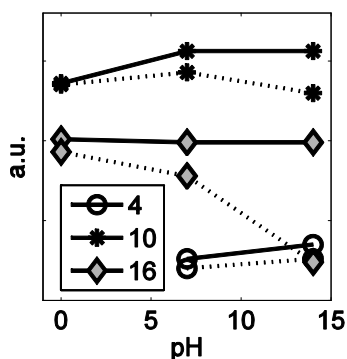


Figure 10. 'Blueness' of samples before (solid line) and after (dotted line) heating, for **p4**, **p10** and **p16** at three pH values

The change in colour upon varying the pH is shown schematically and qualitatively in Figure 10, where the absorption intensity of the longer wavelength peak (**p4**: 530 nm **p10**: 650 nm, **p16**: 630 nm) is divided by that of the shorter wavelength peak (**p4**:500 nm, **p10**: 600 nm, **p16**: 540 nm). This ratio is indicative for the colour change of the formed polymer, where a higher position depicts a bluer polymer. Since each polymer has its own unique set of wavelengths, the higher value of one compound over the other does not depict a 'bluer' colour. However, although the absolute height of the data points is qualitative, for each compound the colour change is a quantitative measure. The solid lines depict the colour before heating, indicating that none of the polymers changed colour much upon addition of acid or base. The dotted lines, after heating to 90 °C, show that only for **p16** the colour change upon heating was irreversible, as mentioned before. The insensitivity towards pH again shows the stability of the fibres once assembled and polymerised, caused not only by the hydrophobic interactions within the tail, but also by the hydrogen-bond forming head-groups.

## Mixing effects

Since closely packed diacetylenes are necessary for topochemical polymerisation, we decided to study the effect of mixing amphiphiles with different diacetylene positions on the polymerisation properties of the assemblies. For mixtures of 10,12-tricosadiynoic acid and 4,6-tricosadiynoic acid<sup>51</sup> it is known that the compounds form a 1:1 complex which polymerises due to a layered structure. However, with the much larger hydrophilic peptide headgroup and the beforementioned sensitivity to structure the mixing properties may differ. Surprisingly, all mixtures (with mixing ratios between 1:9 and 9:1) readily polymerised. Had homogeneous mixing – plausible because the tails have the same length – taken place, polymerisation should be impeded,<sup>52</sup> since in that case the diluted diacetylenes would not be close enough to allow the topochemical polymerisation to occur. Therefore, the obtained results indicate either that within the fibres domains of the separate amphiphiles are formed or that completely separated fibres are present. Since the peptide part of the used amphiphiles is the same, as is the

length of the hydrophobic tail, the formation of completely separated fibres seems improbable,<sup>53</sup> and even domain formation was unexpected.

In order to better understand this mixing behaviour we compared the UV-Vis absorption spectra of polymerised mixtures of amphiphiles on the one hand and a mixture of separately polymerised fibres on the other. Furthermore, the spectra were compared to a calculated linear combination of the pure compound spectra, which, if no interaction was present after polymerisation, should be the same as the spectra for the mixture of separately polymerised fibres.

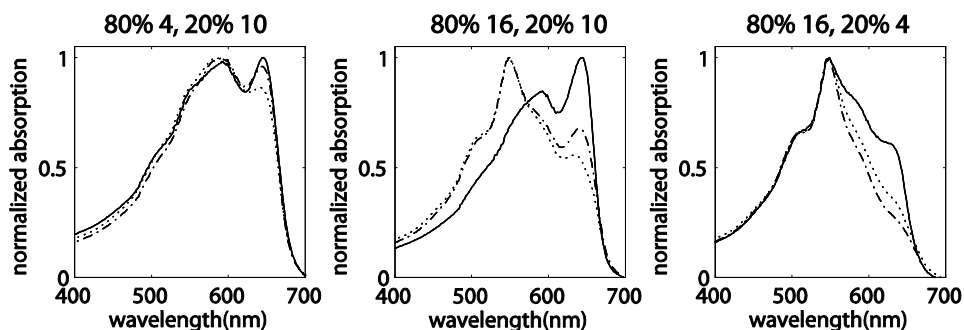


Figure 11. Spectra of polymerised mixed fibres (solid line), separately polymerised and subsequently mixed fibres (dash-dotted line) and calculated linear combinations of the pure compound spectra (dotted) of a few ratios between the amphiphiles.

Polymerisation of mixed amphiphiles (solid line Figure 11) yielded spectra with longer-wavelength absorption (with a 'bluer' colour) than mixing of separately polymerised samples (dash-dotted lines in Figure 11). This effect was most pronounced when **16** was present in the mixture (see appendix for all ratios). Mixtures of **4** with **10** only showed small deviations between polymerisation of mixed samples and mixing of separately polymerised samples, which means either that the domains within the fibres are large enough to not influence the colour or that separate fibres are formed.

The amount of mixing or separation within the amphiphilic fibres is determined by the disruption which occurs if diacetylenes of neighbouring chains are not at the same position. In a mixture of **4** and **10** (Figure 12a) or **10** and **16** (Figure 12c) the diacetylenes are close and therefore the energy penalty for mixing is large. The diacetylene moieties of **4** and **16** are further apart (Figure 12b) and therefore the energy penalty for mixing is smaller. Furthermore, the position of the disruption is of importance. In the middle of the amphiphile (a mixture of **4** and **10**, Figure 12a) the whole structure of the fibre is distorted by the mismatching of the diacetylene units, while at the edge of the amphiphile (Figure 12c) the flexibility and thus miscibility is much larger, causing **10** and **16** to partly mix or to form smaller domains. Although **10** with **16** and **4** with **16** mix better than **4** with **10** (derived from the differences in UV-Vis absorption with mixing before and after polymerisation), all combinations of peptide amphiphiles phase separate to a certain extent, enabling polymerisation.

Because the mixing effect disrupts the packing of the amphiphile, it is surprising that upon mixing the colour of the polymers gets 'bluer', while a worse packing of the

fibres was expected to result in a bathochromic shift of the PDA absorption bands. A plausible explanation is that the volume change which occurs upon polymerisation, and which was previously noted in other diacetylene polymerisations,<sup>54-56</sup> is more easily accommodated in the fibre if the polymer chains are not positioned at the same position in the alkyl tail, thus making the relaxation of the polymer backbone easier. A larger volume change during the polymerisation would result in a larger hypsochromic shift upon mixing. Since diacetylene **10** is surrounded by closely packed alkyl tails at both sides the volume change upon polymerisation is negligible.<sup>55</sup> Therefore, the mixing effect is much smaller and for large percentages of **10** the difference between polymerising mixed fibres and mixing separately polymerised fibres is small.

Surprisingly, mixing separately polymerised samples yielded, in some cases, a 'bluer' spectrum than the calculated linear combination of the pure compound spectra (dotted lines Figure 11b, and in lesser extent Figure 11a). Apparently, strands of polymerised peptide amphiphiles can influence each other in solution, even though the PDA backbone is buried well within the peptide shell. The effect is largest for a small content of **10**. Either without **10** or with a large amount of **10**, the effect decreases. For mixtures of **4** and **16** the difference between calculated and measured spectra is the smallest, indicating the least inter-fibre interactions

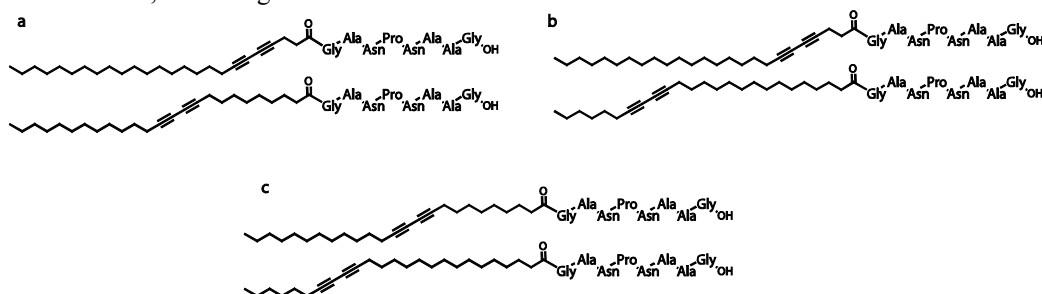


Figure 12. The three mixing possibilities. a) **4** mixed with **10**, b) **4** mixed with **16**, c) **10** mixed with **16**

## Conclusions

Three peptide amphiphiles with a diacetylene containing hydrophobic tail were prepared in which the position of the diacetylene moiety was varied while keeping the length of the tail constant. We have shown that the position of the diacetylene moiety plays an important part in the stability of the self-assembled fibre and in the colour of the derived polymer. The stability of the fibres – before polymerisation – was found to be determined by the longest uninterrupted saturated alkyl chain within the hydrophobic tail of the amphiphile, but its colour – after polymerisation – depends on how much the polydiacetylene backbone is buried within the hydrophobic part of the polymer. At the outside of the alkyl tail, the packing of the amphiphiles is hampered by the mobility of the resulting small hydrophobic tail, and therefore upon illumination a pink polymer is obtained. When the polymer backbone is situated close to the peptide headgroup, stress is induced by the difference in spacing between the peptide part and the alkyl tails. All

assemblies are very resistant to pH changes, and though the colour changes upon heating, this change is largely reversible. The reversibility of the colour change is relatively rare and is in our opinion an indication of the higher stability of the blue state as compared to the red one.

When the different PAs are mixed, polymerisation is still feasible. The amount of mixing between the amphiphiles depends on distortion of the packing, which is determined by the distance of the diacetylenes of neighbouring amphiphiles, and by the position of the distortion inside the fibre. A mixture of **4** and **10** yields very large domains, because the packing is distorted in the middle of the PA and these amphiphiles therefore have a strong tendency to phase separate, while a distortion at the edge of the amphiphile – as is the case in a mixture of **10** and **16** – is positioned in a more flexible part of the amphiphile and thus yields smaller domains.

## Acknowledgements.

We thank Dennis Waalboer for his help with the synthesis.

## Experimental section

**General.** All starting materials were obtained from commercial suppliers and used as received. Thin layer chromatography (TLC) was performed on Kieselgel F-254 pre-coated silica plates. Column chromatography was carried out on Merck silica gel 60 (230-400 mesh ASTM). <sup>1</sup>H-NMR spectra were recorded on a Varian Mercury, 400 MHz. Proton chemical shifts are reported in ppm downfield from tetramethylsilane (TMS). <sup>13</sup>C-NMR spectra were recorded on a Bruker DMX300 (75 MHz for <sup>13</sup>C). Accurate mass ESI spectra were recorded on a Jeol AccuTOF mass spectrometer. Both electron ionization (EI) and chemical ionization (CI) with methane spectra were recorded on a VG Micromass VG7070E. GC traces were recorded on a Trace GC from Interscience with a Varian VF-1701 MS column (30m, inner diameter 0.25 mm), temperature program 100 (1) [15] 300 (5).

### Synthesis

#### *1-eicosyne iodide (1)*

This procedure has been adapted from Miyawaki *et al.*<sup>41</sup> To a solution of 1-eicosyne (1.0 g, 3.6 mmol) in dry acetone (50 mL), N-iodosuccinimide (1.1 g, 4.7 mmol) and AgNO<sub>3</sub> (61 mg, 0.36 mmol) were added. After stirring the solution for three hours, heptane was added and the solution was filtered over celite. Water was added and the compound was extracted using heptane and dried over sodium sulfate to yield quantitatively an off-white solid.

<sup>1</sup>H NMR (in CDCl<sub>3</sub>): δ 2.35 (triplet, 2H), 1.50 (quartet, 2H), 1.36 (triplet, 2H), 1.26 (multiplet, 28H), 0.88 (triplet, 3H)

<sup>13</sup>C NMR (in CDCl<sub>3</sub>): δ 94.4, 31.5, 29.23, 29.21, 29.19, 29.18, 29.1, 29.0, 28.9, 28.6, 28.3, 28.0, 22.2, 20.4, 13.6, -8.2.

#### *4,6-pentacosadiynoic acid (2)*

This procedure has been adapted from Mowery and Evans.<sup>42</sup> Pentynoic acid (345 mg, 3.52 mmol) was dissolved in a solution of 1M KOH (1.8 eq, 6 mL). Methanol (10 mL), hydroxylamine hydrochloride (0.1 eq, 23 mg) and a blue solution of CuCl (0.25 eq, 82 mg) in ethylamine (10 mL 70% in H<sub>2</sub>O) were added to yield a bright yellow solution which was cooled to -78 °C. 1-

Eicosyne iodide (**1**) (1.35g, 3.35 mmol) was dissolved in 10 mL THF and added dropwise to the cooled solution, which caused a precipitate to form. The solution was allowed to warm to room temperature and stirred over night. Twice additional crystals of hydroxylamine hydrochloride were added when the solution turned blue. The solution was acidified with an aqueous solution of 10% sulfuric acid, which caused the solution to turn colourless. The solution was extracted with ether and washed with water and brine. The organic layer was dried over sodium sulfate, evaporated and recrystallized from heptane to yield 840 mg (67%) of a slightly pink solid.

TLC:  $R_f$  0.15 (eluent: heptane/ethyl acetate 4:1), using  $\text{KMnO}_4$  as a staining agent.

$^1\text{H}$  NMR (in  $\text{CDCl}_3$ ):  $\delta$  2.57 (m, 4H), 2.23 (t, 2H), 1.51 (m, 2H), 1.36 (m, 2H), 1.26 (m, 28H), 0.88 (t, 3H).

$^{13}\text{C}$  NMR (in  $\text{CDCl}_3$ ):  $\delta$  78.10, 74.01, 65.80, 64.41, 31.46, 29.23, 29.20, 29.19, 29.18, 29.14, 29.01, 28.89, 28.62, 28.38, 27.78, 22.22, 18.71, 14.45, 13.65.

Mass spectrometry: Accu-TOF: Calc for  $[\text{C}_{25}\text{H}_{42}\text{O}_2 - \text{H}]^+$  373.3165, found 373.3130

#### **methyl 16-hydroxyhexadecanoate (3)**

To a cooled ( $-10\text{ }^\circ\text{C}$ ) solution of methanol (40 mL), thionyl chloride (1.5 mL) was added dropwise. 16-hydroxyhexadecanoic acid (1.53 g, 5.62 mmol) was added, the ice-bath was removed and the solution was heated to reflux for one hour. The solvent was evaporated and the crude product was coevaporated three times with tert-butanol to yield quantitatively a white solid which was used without any further purification in the synthesis of compound **5**.

TLC:  $R_f$  0.34 (eluent: heptane: ethyl acetate 2:1), staining agent  $\text{KMnO}_4$ .

$^1\text{H}$  NMR (in  $\text{CDCl}_3$ ):  $\delta$  4.05 (t, 1H), 3.67 (s, 3H), 3.64 (t, 2H), 2.30 (t, 2H), 1.58 (m, 4H), 1.48 (m, 4H), 1.26 (m, 20H).

#### **methyl 16-oxohexadecanoate (5)**

This procedure has been adapted from Lin *et al.*<sup>47</sup> To a suspension of pyridinium chlorochromate (1.89 g, 8.8 mmol) and 1.89 g celite in 25 ml dry dichloromethane a solution of **3** (1.68 g, 5.9 mmol) in dry dichloromethane (10 mL) was added and after stirring for 2 hours, the suspension was filtered over a pad of silica which was washed with ether twice. Column chromatography (eluent: heptane/ethyl acetate 4 : 1) yielded the product as a white solid in 73% yield.

TLC:  $R_f$  0.48 (eluent: heptane/ethyl acetate 2:1), staining agent  $\text{KMnO}_4$ .

$^1\text{H}$  NMR (in  $\text{CDCl}_3$ ):  $\delta$  9.77 (t, 1H), 2.42 (dt, 2H), 2.30 (t, 2H), 1.62 (m, 4H), 1.25 (m, 20H).

$^{13}\text{C}$  NMR (in  $\text{CDCl}_3$ ):  $\delta$  202.2, 173.7, 50.8, 43.4, 33.6, 29.1, 28.9, 28.8, 28.7, 28.6, 24.4, 21.6

Mass spectrometry: Accu-TOF: Calc for  $[\text{C}_{17}\text{H}_{32}\text{O}_3 + \text{Na}]^+$  307.2249, found 307.2242.

#### **methyl heptadec-16-ynoate (6)**

This procedure has been adapted from Gung and Dickson.<sup>48</sup> Under a protective argon atmosphere, aldehyde **5** (1.1 g, 3.9 mmol) and potassium carbonate (1.1 g, 7.7 mmol) were dissolved in dry MeOH (25 mL). The Ohira-Bestmann reagent (dimethyl(1-diazo-2-oxopropyl)phosphonate, 890 mg, 4.6 mmol) was dissolved in 10 mL dry methanol and slowly added to the solution of the aldehyde. After the solution had stirred for 7 hours, diethyl ether and a 5% solution of sodium bicarbonate were added and the product was extracted with ether, dried over magnesium sulfate and the solvent was evaporated. Purification with column chromatography (eluent: heptane/ethyl acetate 19:1) gave a white solid in 68 % yield.

TLC:  $R_f$  0.32 (eluent: heptane/ethyl acetate 9:1), staining agent  $\text{KMnO}_4$ .

GC:  $R_f$  11.02 min.

$^1\text{H}$  NMR (in  $\text{CDCl}_3$ ):  $\delta$  3.67 (s, 3H), 2.30 (t, 2H), 2.18 (dt, 2H), 1.94 (t, 1H), 1.62 (q, 2H), 1.52 (q, 2H), 1.39 (m, 2H), 1.26 (m, 18H).

$^{13}\text{C}$  NMR (in  $\text{CDCl}_3$ ):  $\delta$  174.49, 84.97, 68.16, 66.00, 51.58, 29.77, 29.75, 29.65, 29.60, 29.41, 29.31, 29.26, 28.92, 28.66, 25.12, 18.55.

Mass spectrometry: EI: Calc for  $[\text{C}_{18}\text{H}_{32}\text{O}_2]^+$  280.240, found 280.239.

**heptadec-16-ynoic acid (7)**

Ester **6** (2.6 mmol, 736 mg) was dissolved in methanol (30 mL), 5 eq sodium hydroxide (aq) were added and the solution was refluxed for 2 hours. The mixture was concentrated, 1 M hydrochloric acid was added to the residue and the product was extracted with dichloromethane and dried over magnesium sulfate. Evaporation of the solvent yielded the pure product quantitatively.

TLC:  $R_f$  0.38 (eluent: heptane/ethyl acetate 2:1), staining agent  $\text{KMnO}_4$ .

$^1\text{H}$  NMR (in  $\text{CDCl}_3$ ):  $\delta$  2.35 (t, 2H), 2.18 (dt, 2H), 1.94 (t, 1H), 1.64 (q, 2H), 1.52 (q, 2H), 1.26 (m, 20H)

$^{13}\text{C}$  NMR (in  $\text{CDCl}_3$ ):  $\delta$  179.72, 84.98, 68.17, 34.15, 29.76, 29.65, 29.58, 29.39, 29.26, 29.22, 28.92, 28.66, 24.85, 18.56.

Mass spectrometry: CI: Calc for  $[\text{C}_{17}\text{H}_{31}\text{O}_2]^+$  267.2324, found 267.2326.

**1-octyne iodide (8)**

Compound **8** was synthesized similar to compound **1**, except that the octyne solution was stirred overnight. The product was purified using column chromatography (eluent: heptane) to yield a yellow oil in 45 % yield.

$^1\text{H}$  NMR (in  $\text{CDCl}_3$ ):  $\delta$  2.35 (t, 2H), 1.50 (q, 2H), 1.36 (t, 2H), 1.26 (m, 28H), 0.88 (t, 3H).

$^{13}\text{C}$  NMR (in  $\text{CDCl}_3$ ):  $\delta$  94.40, 30.80, 27.99, 22.04, 20.35, 13.56, -8.2.

Mass spectrometry: EI: Calc for  $[\text{C}_8\text{H}_{13}\text{I}]^+$  236.0062, found 236.0061.

**16,18-pentacosadiynoic acid (9)**

The synthesis was performed similar to the synthesis of **2**. After extraction with ether, the organic layer was dried over sodium sulfate, evaporated and purified by column chromatography (eluent: heptane/ethyl acetate 4:1), yielding a white solid in 15 % yield.

TLC:  $R_f$  0.32 (eluent: heptane: ethyl acetate 4:1), staining agent  $\text{KMnO}_4$ .

$^1\text{H}$  NMR (in  $\text{CDCl}_3$ ):  $\delta$  2.35 (t, 4H), 2.24 (t, 2H), 1.63 (m, 2H), 1.51 (m, 4H), 1.36 (m, 4H), 1.26 (m, 22H), 0.88 (t, 3H).

$^{13}\text{C}$  NMR (in  $\text{CDCl}_3$ ):  $\delta$  67.54, 64.77, 33.5, 30.83, 29.43, 29.12, 29.11, 29.03, 29.00, 28.96, 28.77, 28.63, 28.60, 28.38, 28.30, 28.06, 28.03, 27.89, 27.86, 24.22, 22.04, 18.74, 17.93, 13.57.

Mass spectrometry: Accu-TOF: Calc for  $[\text{C}_{25}\text{H}_{42}\text{O}_2 + \text{H}]^+$  375.3263, found 375.3255.

**4,6-pentacosadiynoic acid coupled to GANPNAAG (4)****10,12-pentacosadiynoic acid coupled to GANPNAAG (10)****16,18-pentacosadiynoic acid coupled to GANPNAAG (16)**

The GANPNAAG peptide was prepared by standard solid-phase Fmoc protocols,<sup>57</sup> as also described in chapter 2.

**Data for 4**

TLC: one spot,  $R_f$  0.25 (eluent: MeOH/  $\text{CHCl}_3$ / AcOH 25:65:4), staining agent  $\text{Cl}_2/\text{TDM}$ <sup>58</sup>

$^1\text{H}$  NMR (in  $\text{DMSO}-d_6$ ), see also Figure 13:  $\delta$  0.85 (t,  $\text{CH}_3$ -alkyl chain, 3H), 1.12 (d,  $\text{CH}_3$ -Ala, 3H), 1.20 (m,  $-\text{CH}_2$ -alkyl chain;  $\text{CH}_3$ -Ala, 34H), 1.48 (m,  $\text{CH}_2$ -alkyl chain, 2H), 1.85 (m,  $\text{CH}_2$  Pro, 3H), 2.18 (m,  $\text{CH}_2$  Pro;  $\alpha$ - $\text{CH}_2$ -alkyl tail, 3H), 2.26 (t,  $\text{CH}_2$ -alkyne, 2H), 2.35 (t,  $\text{CH}_2$ -alkyne, 2H), 2.40 (m,  $\text{CH}_2$  Asn, 2H), 2.55 (dd,  $\text{CH}_2$  Asn, 1H), 2.65 (dd,  $\text{CH}_2$  Asn, 1H), 3.65 (m,  $\alpha$ - $\text{CH}_2$  Gly;  $\text{CH}_2$  Pro, 3H), 3.75 (m,  $\text{CH}_2$  Pro;  $\alpha$ - $\text{CH}_2$  Gly, 3H), 4.20 (m,  $\text{CH}_2$  Pro;  $\alpha$ - $\text{CH}_2$  Ala, 4H), 4.40 (m,  $\alpha$ - $\text{CH}_2$  Asn, 1H), 4.73 (q,  $\alpha$ - $\text{CH}_2$  Asn, 1H), 6.92 (s,  $\text{NH}_2$  Asn, 1H), 7.10 (s,  $\text{NH}_2$  Asn, 1H), 7.20 (s,  $\text{NH}_2$  Asn, 1H), 7.52 (d,  $\alpha$ -NH Ala, 1H), 7.64 (s,  $\text{NH}_2$  Asn, 1H), 7.72 (d,  $\alpha$ -NH Ala, 1H), 7.88 (two d,  $\alpha$ -NH Asn;  $\alpha$ -NH Ala, 2H), 7.96 (broad s,  $\alpha$ -NH Gly, 2H), 8.27 (d,  $\alpha$ -NH Asn, 1H).

*Effect of the diacetylene position on the chromatic properties of polydiacetylenes from self-assembled peptide amphiphiles.*

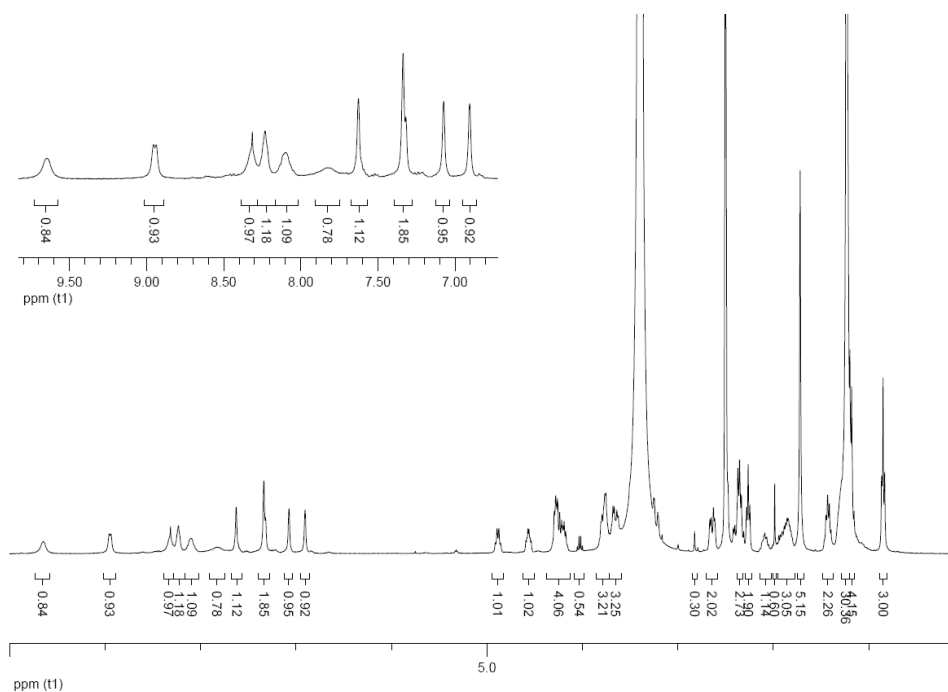


Figure 13.  $^1\text{H}$  NMR spectrum of **4**.

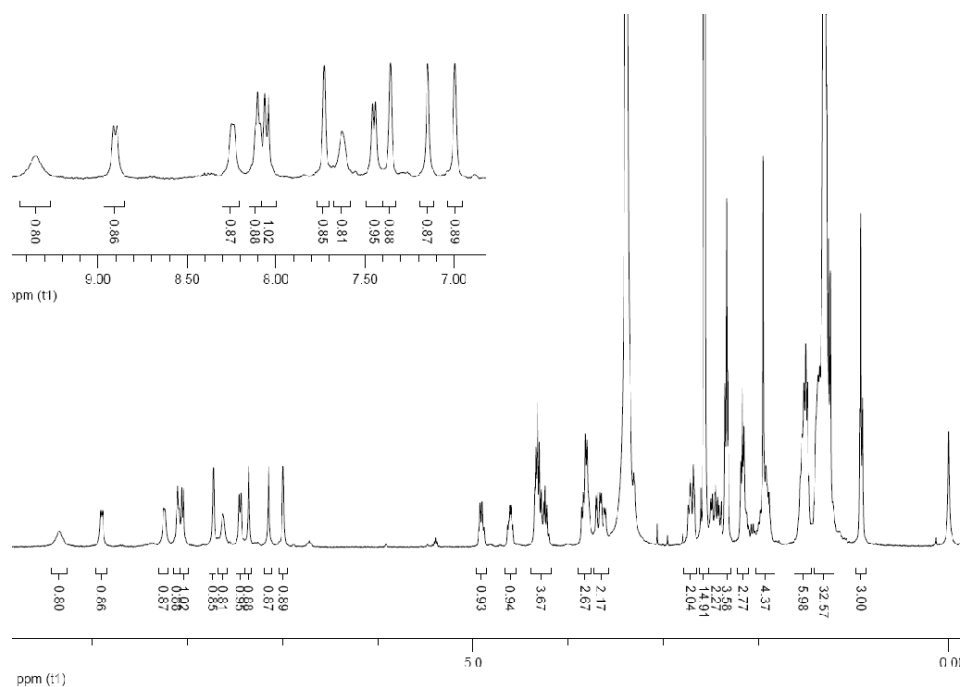
Mass spectrometry: Accu-TOF: Calc for  $[\text{C}_{51}\text{H}_{82}\text{N}_{10}\text{O}_{12}]^+$  1027.619, found 1027.623.

**Data for 10**

TLC: one spot,  $R_f$  0.25 (eluent: MeOH/  $\text{CHCl}_3$ / AcOH 25:65:4), staining agent  $\text{Cl}_2$ /TDM

$^1\text{H}$  NMR (in DMSO- $d_6$ ), see also Figure 14:  $\delta$  0.85 (t,  $\text{CH}_3$  -alkyl chain, 3H), 1.12 (d,  $\text{CH}_3$  -Ala, 3H), 1.20 (m,  $-\text{CH}_2-$  alkyl chain;  $\text{CH}_3$  -Ala, 34H), 1.48 (m,  $\text{CH}_2$ -alkyl chain, 2H), 1.85 (m,  $\text{CH}_2$  Pro, 3H), 2.18 (m,  $\text{CH}_2$  Pro;  $\alpha$ - $\text{CH}_2$ -alkyl tail, 3H), 2.21 (t,  $\text{CH}_2$ -alkyne, 4H), 2.40 (m,  $\text{CH}_2$  Asn, 2H), 2.55 (dd,  $\text{CH}_2$  Asn, 1H), 2.65 (dd,  $\text{CH}_2$  Asn, 1H), 3.65 (m,  $\alpha$ - $\text{CH}_2$  Gly;  $\text{CH}_2$  Pro, 3H), 3.75 (m,  $\text{CH}_2$  Pro;  $\alpha$ - $\text{CH}_2$  Gly, 3H), 4.20 (m,  $\text{CH}_2$  Pro;  $\alpha$ - $\text{CH}_2$  Ala, 4H), 4.40 (m,  $\alpha$ - $\text{CH}_2$  Asn, 1H), 4.73 (q,  $\alpha$ - $\text{CH}_2$  Asn, 1H), 6.92 (s,  $\text{NH}_2$  Asn, 1H), 7.10 (s,  $\text{NH}_2$  Asn, 1H), 7.20 (s,  $\text{NH}_2$  Asn, 1H), 7.52 (d,  $\alpha$ -NH Ala, 1H), 7.64 (s,  $\text{NH}_2$  Asn, 1H), 7.72 (d,  $\alpha$ -NH Ala, 1H), 7.88 (two d,  $\alpha$ -NH Asn;  $\alpha$ -NH Ala, 2H), 7.96 (broad s,  $\alpha$ -NH Gly, 2H), 8.27 (d,  $\alpha$ -NH Asn, 1H).



Figure 14.  $^1\text{H}$  NMR spectrum of **10**.

Mass spectrometry: Accu-TOF: Calc for  $[\text{C}_{51}\text{H}_{82}\text{N}_{10}\text{O}_{12} + \text{Na}]^+$  1049.601, found 1049.600.

*Data for 16*

TLC: one spot,  $R_f$  0.25 (eluent: MeOH/  $\text{CHCl}_3$ / AcOH 25:65:4), staining agent  $\text{Cl}_2$ /TDM.

$^1\text{H}$  NMR (in DMSO- $d_6$ ), see also Figure 15:  $\delta$  0.85 (t,  $\text{CH}_3$ -alkyl chain, 3H), 1.12 (d,  $\text{CH}_3$ -Ala, 3H), 1.20 (m,  $-\text{CH}_2$ -alkyl chain;  $\text{CH}_3$ -Ala, 34H), 1.48 (m,  $\text{CH}_2$ -alkyl chain, 2H), 1.85 (m,  $\text{CH}_2$  Pro, 3H), 2.18 (m,  $\text{CH}_2$  Pro;  $\alpha$ - $\text{CH}_2$ -alkyl tail, 3H), 2.21 (t,  $\text{CH}_2$ -alkyne, 4H), 2.40 (m,  $\text{CH}_2$  Asn, 2H), 2.55 (dd,  $\text{CH}_2$  Asn, 1H), 2.65 (dd,  $\text{CH}_2$  Asn, 1H), 3.65 (m,  $\alpha$ - $\text{CH}_2$  Gly;  $\text{CH}_2$  Pro, 3H), 3.75 (m,  $\text{CH}_2$  Pro;  $\alpha$ - $\text{CH}_2$  Gly, 3H), 4.20 (m,  $\text{CH}_2$  Pro;  $\alpha$ - $\text{CH}_2$  Ala, 4H), 4.40 (m,  $\alpha$ - $\text{CH}_2$  Asn, 1H), 4.73 (q,  $\alpha$ - $\text{CH}_2$  Asn, 1H), 6.92 (s,  $\text{NH}_2$  Asn, 1H), 7.10 (s,  $\text{NH}_2$  Asn, 1H), 7.20 (s,  $\text{NH}_2$  Asn, 1H), 7.52 (d,  $\alpha$ -NH Ala, 1H), 7.64 (s,  $\text{NH}_2$  Asn, 1H), 7.72 (d,  $\alpha$ -NH Ala, 1H), 7.88 (two d,  $\alpha$ -NH Asn;  $\alpha$ -NH Ala, 2H), 7.96 (broad s,  $\alpha$ -NH Gly, 2H), 8.27 (d,  $\alpha$ -NH Asn, 1H).

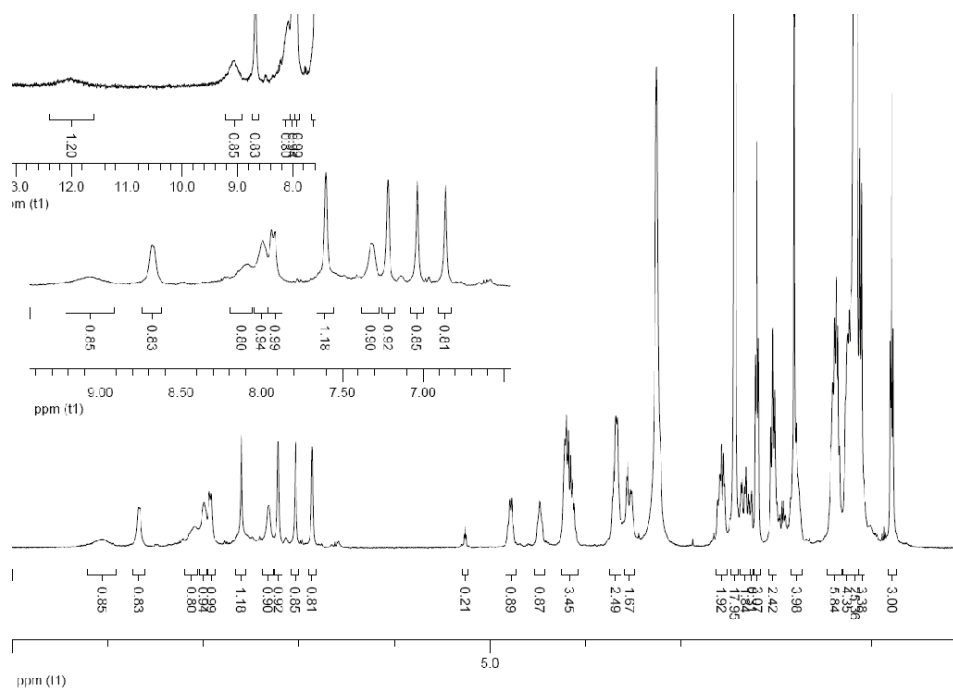


Figure 15.  $^1\text{H}$  NMR spectrum of **16**.

Mass spectrometry: Accu-TOF: Calc for  $[\text{C}_{51}\text{H}_{82}\text{N}_{10}\text{O}_{12} + \text{H}]^+$  1027.619, found 1027.625.

**Fibre formation.** Two procedures for fibre formation were used.

*Procedure A.* The amphiphiles were dispersed in milli-Q at concentrations of either 0.2 or 1.0 mg/mL. The samples were heated to 50 °C for 30 min, followed by 15 min sonication at that temperature. Subsequently, the samples were heated to 90 °C and allowed to cool to room temperature.

*Procedure B.* 30  $\mu\text{L}$  of a 10 mg/mL solution of the amphiphiles in trifluoroethanol (TFE) was injected in 270  $\mu\text{L}$  milli-Q at room temperature.

**Polymerisations.** Polymerisations were carried out on 1 mg/mL samples in a quartz cell with a path length of 1 mm using a UVASPOT 400T lamp with a sample-light source distance of 22 cm.

**Circular dichroism.** Measurements were carried out at a concentration of 0.2 mg/mL using a 1 mm quartz cell. The spectra were recorded on a JASCO J-810 spectropolarimeter. To measure temperature curves, a heating or cooling rate of 3 °C/min was used.

**UV spectroscopy.** Measurements were carried out at a concentration of 1.0 mg/mL using a 1 mm quartz cell. The spectra were recorded on a Varian Cary-50 spectrometer.

**Transmission electron microscopy.** TEM samples were prepared by floating a carbon-coated copper grid on a peptide amphiphile solution of 0.2 mg/mL for 5 min, followed by removal of residual water by blotting with a paper filter. The samples were visualized using a JEOL 1010 transmission electron microscope set on an accelerating voltage of 60 kV

## References

1. G. Wegner, *Makromol. Chem.*, 1972, **154**, 35-48.
2. B. Tieke, H. J. Graf, G. Wegner, B. Naegele, H. Ringsdorf, A. Banerjee, D. Day and J. B. Lando, *Colloid Polym. Sci.*, 1977, **255**, 521-531.
3. M. A. Biesalski, A. Knaebel, R. Tu and M. Tirrell, *Biomaterials*, 2006, **27**, 1259-1269.
4. B. Hupfer, H. Ringsdorf and H. Schupp, *Chem. Phys. Lipids*, 1983, **33**, 355-374.
5. S. Okada, S. Peng, W. Spevak and D. Charych, *Acc. Chem. Res.*, 1998, **31**, 229-239.
6. M. Biesalski, R. Tu and M. V. Tirrell, *Langmuir*, 2005, **21**, 5663-5666.
7. E. Jahnke, A. S. Millerieux, N. Severin, J. P. Rabe and H. Frauenrath, *Macromol. Biosci.*, 2007, **7**, 136-143.
8. E. Jahnke, I. Lieberwirth, N. Severin, J. P. Rabe and H. Frauenrath, *Angew. Chem., Int. Ed.*, 2006, **45**, 5383-5386.
9. D. W. P. M. Löwik, I. O. Shklyarevskiy, L. Ruizendaal, P. C. M. Christianen, J. C. Maan and J. C. M. van Hest, *Adv. Mater.*, 2007, **19**, 1191-1195.
10. L. Hsu, G. L. Cvetanovich and S. I. Stupp, *J. Am. Chem. Soc.*, 2008, **130**, 3892-3899.
11. M. van den Heuvel, D. W. P. M. Löwik and J. C. M. van Hest, *Biomacromol.*, 2008, **9**, 2727-2734.
12. G. Wenz, M. A. Muller, M. Schmidt and G. Wegner, *Macromol.*, 1984, **17**, 837-850.
13. M. Schott, *J. Phys. Chem. B*, 2006, **110**, 15864-15868.
14. K. C. Lim, A. Kapitulnik, R. Zacher and A. J. Heeger, *J. Chem. Phys.*, 1985, **82**, 516-521.
15. L. Adler-Abramovich and E. Gazit, *J. Pept. Sci.*, 2008, **14**, 217-223.
16. B. Tieke, G. Lieser and G. Wegner, *J. Polym. Sci., Part A: Polym. Chem.*, 1979, **17**, 1631-1644.
17. Q. Cheng, M. Yamamoto and R. C. Stevens, *Langmuir*, 2000, **16**, 5333-5342.
18. Z. Z. Yuan, C. W. Lee and S. H. Lee, *Angew. Chem., Int. Ed.*, 2004, **43**, 4197-4200.
19. A. Potisattiyuonyong, R. Rojanathanes, G. Turncharearn and M. Sukwattanasinitt, *Langmuir*, 2008, **24**, 4461-4463.
20. S. Wu, L. F. Niu, J. Shen, Q. J. Zhang and C. Bubeck, *Macromol.*, 2009, **42**, 362-367.
21. N. Mino, H. Tamura and K. Ogawa, *Langmuir*, 1992, **8**, 594-598.
22. W. D. Zhou, Y. L. Li and D. B. Zhu, *Chem. Asian. J.*, 2007, **2**, 222-229.
23. U. Jonas, K. Shah, S. Norvez and D. H. Charych, *J. Am. Chem. Soc.*, 1999, **121**, 4580-4588.
24. J. Song, J. S. Cisar and C. R. Bertozzi, *J. Am. Chem. Soc.*, 2004, **126**, 8459-8465.
25. J. Song, Q. Cheng, S. Kopta and R. C. Stevens, *J. Am. Chem. Soc.*, 2001, **123**, 3205-3213.
26. D. H. Charych, J. O. Nagy, W. Spevak and M. D. Bednarski, *Science*, 1993, **261**, 585-588.
27. A. Lio, A. Reichert, D. J. Ahn, J. O. Nagy, M. Salmeron and D. H. Charych, *Langmuir*, 1997, **13**, 6524-6532.
28. Y. K. Jung, T. W. Kim, J. Kim, J. M. Kim and H. G. Park, *Adv. Funct. Mater.*, 2008, **18**, 701-708.
29. J. Lee, H. J. Kim and J. Kim, *J. Am. Chem. Soc.*, 2008, **130**, 5010-5011.
30. S. W. Lee, C. D. Kang, D. H. Yang, J. S. Lee, J. M. Kim, D. J. Ahn and S. J. Sim, *Adv. Funct. Mater.*, 2007, **17**, 2038-2044.
31. B. A. Pindzola, A. T. Nguyen and M. A. Reppy, *Chem. Comm.*, 2006, 906-908.
32. Q. Huo, S. P. Wang, A. Pisseloup, D. Verma and R. M. Leblanc, *Chem. Comm.*, 1999, 1601-1602.
33. Q. Huo, K. C. Russell and R. M. Leblanc, *Langmuir*, 1999, **15**, 3972-3980.
34. J. S. Filhol, J. Deschamps, S. G. Dutremez, B. Boury, T. Barisien, L. Legrand and M. Schott, *J. Am. Chem. Soc.*, 2009, **131**, 6976-6988.
35. Q. Cheng and R. C. Stevens, *Langmuir*, 1998, **14**, 1974-1976.
36. B. Hupfer and H. Ringsdorf, *Chem. Phys. Lipids*, 1983, **33**, 263-282.
37. H. Tachibana, Y. Yamanaka, H. Sakai, M. Abe and M. Matsumoto, *Macromol.*, 1999, **32**, 8306-8309.
38. M. van den Heuvel, A. M. Prenen, J. C. Gielen, P. C. M. Christianen, D. J. Broer, D. W. P. M. Löwik and J. C. M. van Hest, *J. Am. Chem. Soc.*, 2009, **131**, 15014-15017.
39. C. Cerami, U. Frevert, P. Sinnis, B. Takacs, P. Clavijo, M. J. Santos and V. Nussenzweig, *Cell*, 1992, **70**, 1021-1033.
40. D. W. P. M. Löwik, J. Garcia-Hartjes, J. T. Meijer and J. C. M. van Hest, *Langmuir*, 2005, **21**, 524-526.
41. K. Miyawaki, R. Goto, T. Takagi and M. Shibakami, *Synlett*, 2002, 1467-1470.
42. M. D. Mowery and C. E. Evans, *Tetrahedron Lett.*, 1997, **38**, 11-14.
43. M. Schmittel and C. Vavilala, *J. Org. Chem.*, 2005, **70**, 4865-4868.

*Effect of the diacetylene position on the chromatic properties of polydiacetylenes from self-assembled peptide amphiphiles.*

44. T. Otsuki, R. F. Brooker and M. O. Funk, *Lipids*, 1986, **21**, 178-181.
45. A. Singh and J. M. Schnur, *Synth. Commun.*, 1986, **16**, 847-852.
46. F. L. M. Pattison, J. B. Stothers and R. G. Woolford, *J. Am. Chem. Soc.*, 1956, **78**, 2255-2259.
47. D. Lin, J. Y. Zhang and L. M. Sayre, *J. Org. Chem.*, 2007, **72**, 9471-9480.
48. B. W. Gung and H. Dickson, *Org. Lett.*, 2002, **4**, 2517-2519.
49. M. Wolffs, S. J. George, Z. Tomovic, S. C. J. Meskers, A. Schenning and E. W. Meijer, *Angew. Chem., Int. Ed.*, 2007, **46**, 8203-8205.
50. B. Tieke and G. Lieser, *J. Colloid Interface Sci.*, 1982, **88**, 471-486.
51. B. Tieke and G. Lieser, *J. Colloid Interface Sci.*, 1981, **83**, 230-239.
52. B. Hupfer, H. Ringsdorf and H. Schupp, *Macromol. Chem. Phys.*, 1981, **182**, 247-253.
53. A. R. Hirst, B. Q. Huang, V. Castelletto, I. W. Hamley and D. K. Smith, *Chem. Eur. J.*, 2007, **13**, 2180-2188.
54. J. W. Lauher, F. W. Fowler and N. S. Goroff, *Acc. Chem. Res.*, 2008, **41**, 1215-1229.
55. R. H. Baughman, *J. Appl. Phys.*, 1972, **43**, 4362-4370.
56. D. W. Britt, U. G. Hofmann, D. Mobius and S. W. Hell, *Langmuir*, 2001, **17**, 3757-3765.
57. G. B. Fields and R. L. Noble, *Int. J. Pept. Protein Res.*, 1990, **35**, 161-214.
58. E. V. Arx, M. Faupel and M. Brugger, *J. Chromatogr.*, 1976, **120**, 224-228.

## Appendix 1 - UV spectra for all mixing ratios.

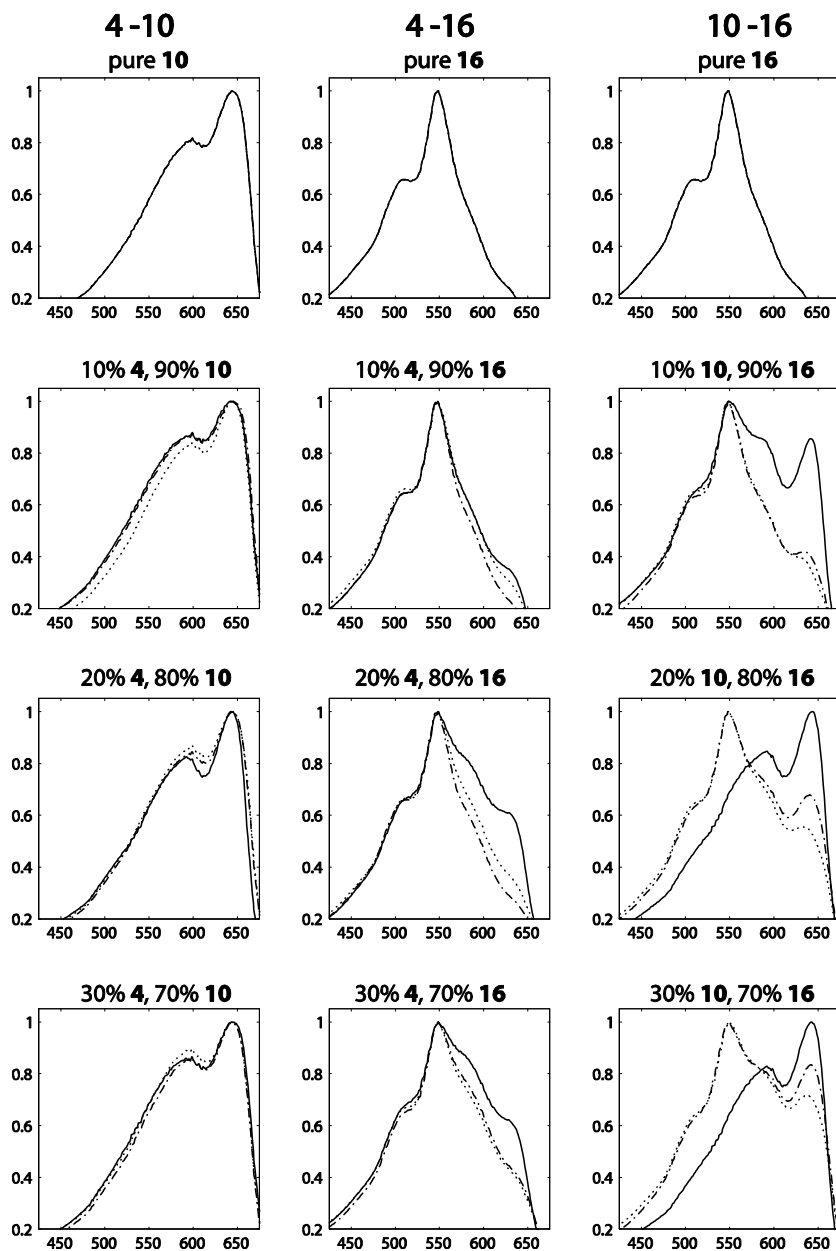


**Figure 1.** Effect of mixing before (solid line) or after (dash-dotted line) polymerisation, compared to calculated linear combinations of the pure compound spectra (dashed line). The y-axis depicts normalized intensity, the x-axis the wavelength in nm.

*Effect of the diacetylene position on the chromatic properties of polydiacetylenes from self-assembled peptide amphiphiles.*

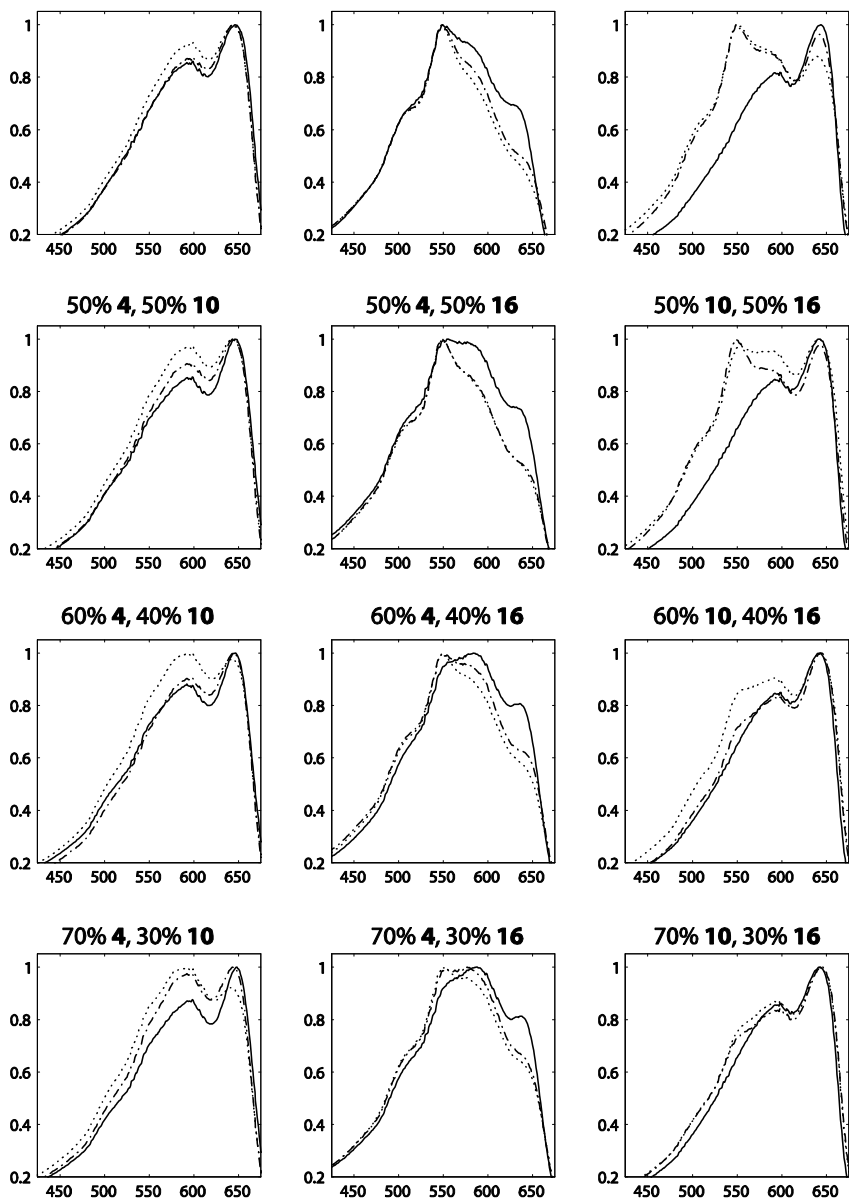


**Figure 1.** continued

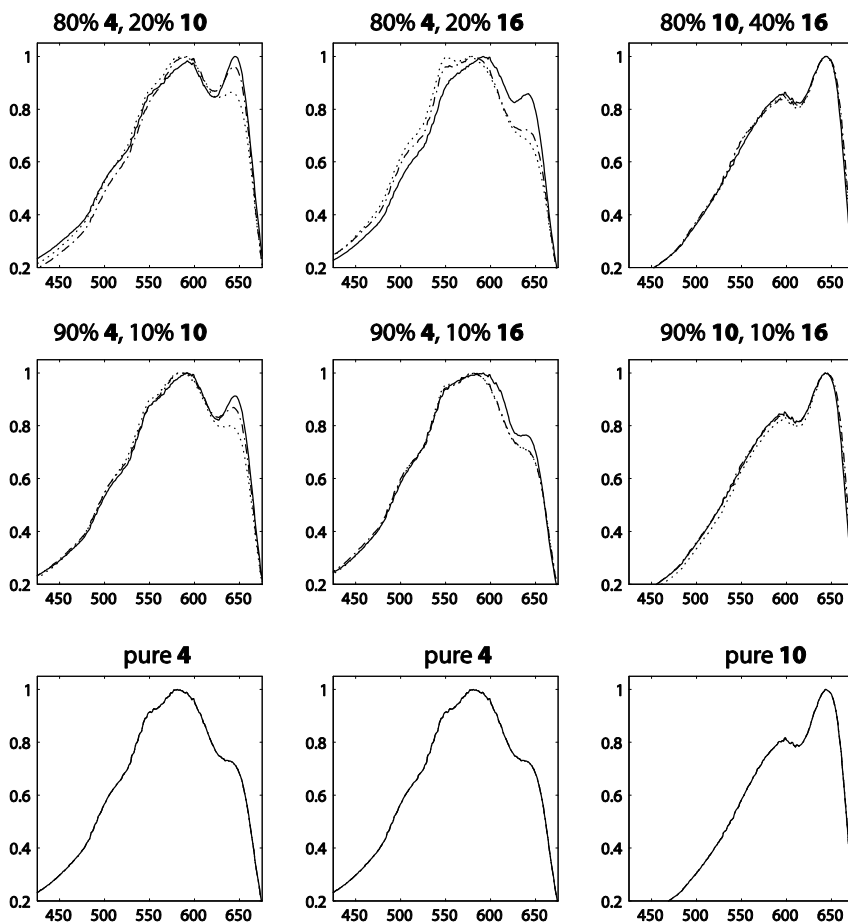
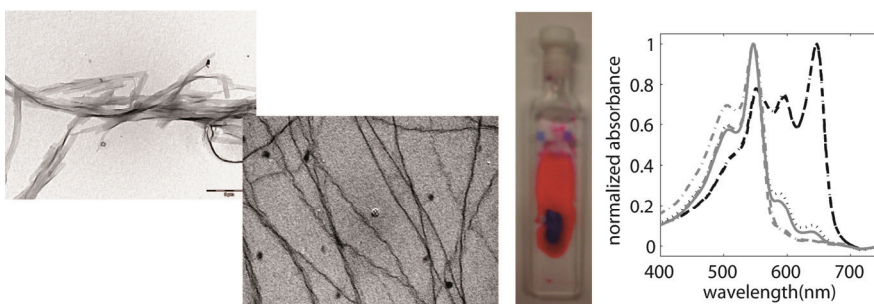


Figure 1. continued

## Chapter 6

# The influence of amino acid sequence on morphology and colour of polydiacetylene-containing peptide amphiphile fibres.



A systematic study was performed after the influence of charge and steric hindrance on the assembly of the pentameric peptide GAGAG coupled to pentacosadiynoic acid. The diacetylene containing alkyl tail provided a driving force for assembly, and allowed a light-initiated topochemical polymerisation of the diacetylene moieties. To investigate the effect of sterical hindrance and charge repulsion on the fibre structure, either the N-terminal or the C-terminal amino acid in the sequence was replaced by glutamic acid or lysine. Furthermore, amphiphiles with an amide or a free acid group at the C-terminus were investigated. Steric hindrance and charge repulsion were addressed individually by using several pH values for fibre preparation. The fibre stability was probed with circular dichroism (CD) spectroscopy, while the morphology was investigated with transmission electron microscopy (TEM). UV spectroscopy was used to probe the diacetylene packing in the hydrophobic tail, both by polymerisation behaviour and polymer properties. In general, the assembly was hindered more if the modification was close to the alkyl tail, and glutamic acid had a larger effect than lysine. The molecules with two charges yielded assemblies which showed after polymerisation a large change in absorption when the pH was changed. These fibres therefore functioned as a colour-based pH sensor. Typically, TEM and UV showed the same trends, indicating that the distorted morphology as observed with TEM gave information about the molecular packing of the peptide amphiphilic fibres, probed *via* the changes in absorption of the polydiacetylene backbone.



## Introduction

Self-assembled protein fibres are abundant in nature. They normally have an important role in biological systems, for example as actin filaments in cells but in some cases they can also be related to diseases such as Alzheimers'. In order to mimic the former and prevent the latter, fibres constructed *via* self-assembly processes have been extensively investigated. The protein building blocks that form the natural fibres are however quite complex biomolecules, and therefore smaller building blocks are often employed. Especially peptide amphiphiles (PAs) that mimic the proteins in their assembly behaviour have gained increasing interest over the years. With their relative ease of synthesis they provide a means of mimicking structure and function of proteins without the challenging production that traditionally accompanies these large biomolecules. Furthermore, insight into important structural and functional features of proteins can be obtained using these molecules, and the design can easily be varied in order to explore the structure-function relationship. The interesting structural properties combined with the relatively facile functionalisation make PA fibres attractive structures to study. A surprisingly large variety of PAs assemble into a fibre-like shape,<sup>1-8</sup> and most are designed by using hydrophobicity as the main driving force. However, also ionic forces can induce fibre formation, as was shown by Aggeli *et al.*,<sup>9</sup> who studied the assembly behaviour of two oppositely charged peptide sequences. Both peptides were in a random coil conformation in water, but yielded a  $\beta$ -sheet structure when mixed. In amphiphiles which use hydrophobicity as a driving force, the hydrophilic headgroup of the amphiphile contains structural or functional information. The combination of hydrophobic and hydrophilic moieties, their size and specific structure, determines the morphology of the assemblies, which may, for example, be used as hydrogels employed in tissue engineering.<sup>10-13</sup>

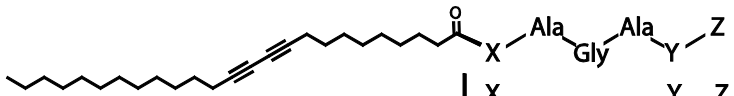
Peptide amphiphiles consisting of an alkyl tail coupled to a peptide moiety form an important class of PAs. These amphiphiles often assemble into fibre- or rod-like structures. Small changes such as in the length of the hydrophobic tail<sup>14, 15</sup> or the presence or absence of a methyl group in the hydrophilic headgroup<sup>16</sup> can have a marked effect on the morphology. The width,<sup>17</sup> helical pitch,<sup>18</sup> preferred superstructure<sup>19</sup> and other parameters can be tuned by small structural changes in the building block. In this chapter, we combine the self-assembly of these intriguing architectures with an equally interesting moiety in the hydrophobic tail of the amphiphile: a diacetylene group.

Diacetylenes can be polymerised to highly conjugated polymers with unique chromatic properties and were first described in the early '70s, by the group of Wegner.<sup>20</sup> The topochemical polymerisation can only take place if the diacetylene moieties are closely packed, as may be the case in for example crystals, but also in self-assembled systems. In the latter case, the diacetylene units are generally introduced in the alkyl chains of amphiphiles.<sup>15, 21-24</sup> One of the interesting properties of the resulting highly conjugated polymers is their chromism – their colour can change from blue to red under the influence of external stimuli such as heat,<sup>15, 25-29</sup> pH,<sup>26, 28, 30-34</sup> or the binding of

a guest molecule.<sup>35-41</sup> The colour is caused by the intense absorption of the polymeric backbone in the visible region. Generally, the blue colour is accompanied by an absorption maximum around 650 nm, while for the red colour this maximum shifts to 550 or even 500 nm. Systematic studies on assemblies of diacetylene containing amphiphiles elucidated the effect of several molecular parameters on the polymerisability of diacetylenes and the resulting PDA absorption. Both the hydrophobic tail<sup>15, 35, 38, 42, 43</sup> and the hydrophilic headgroup play an important role in packing of the molecules and thus in the properties of the fibre. Extensive research has been performed on varying the headgroup both in PDA amphiphiles and bolaamphiphiles using small organic groups,<sup>35, 44-47</sup> sugars<sup>48, 49</sup> or amino-acids.<sup>26, 33, 50</sup> Cheng and Stevens<sup>50</sup> and Huo et al.<sup>51</sup> investigated the effect of size and charge of the headgroup on the colour of the polymer. They coupled respectively one or two amino acids to 10,12-pentacosadiynoic acid, polymerised the resulting assemblies and analysed the polymer colour.

Previously, the properties of fibres made from the eight amino-acid peptide GANPNAAG coupled to a pentacosadiynoic acid were investigated in our group.<sup>15, 52</sup> It was shown that the order in the fibre was high enough to allow polymerisation. A reversible spectral shift was observed upon heating and the colour was insensitive to pH. The length of the hydrophobic tail and the diacetylene position therein were varied. The influence of the peptide sequence, however, was not investigated. GANPNAAG is a peptide with relatively much functionality, and the proline in the sequence is a known turn inducing residue which may play an essential role in the packing of the amphiphiles in the fibres. Structure determination for fibres from this amphiphile was far from trivial (chapter 2). Furthermore, small effects are known to have large effects on fibre structure (as described above) and for this peptide the changes were expected to be difficult to predict or even explain. Also the choice of the residues which would be replaced was not clear. Therefore, to investigate the influence of steric hindrance and charges on fibre morphology and polymerisation properties, we started from one of the most straightforward peptide sequences which still assembled into  $\beta$ -sheet structures – the sequence GAGAG. In the Van Hest group this silk-worm silk inspired sequence promoting  $\beta$ -sheet formation was employed before in several architectures, ranging from polymers to self-assembled systems. In the polymeric structures, the GAGAG sequence was employed to induce  $\beta$ -sheet characteristics either in the main chain of the polymer, which was constructed via protein engineering,<sup>53</sup> or in the side chain, by atom transfer radical polymerisation (ATRP) of a peptide-containing monomer.<sup>54</sup> The self-assembled structures consisted of oligo(p-phenylenevinylene) coupled to GAGAG to create self-assembling molecular electronics.<sup>55</sup> The same approach was investigated by Klok *et al.* using thiophenes as a  $\pi$ -conjugated motif.<sup>56</sup> Because of the small size of the peptide, containing residues without functionality or special characteristics, charge and steric hindrance could be systematically introduced. The starting point for the investigation was pentacosadiynoyl GAGAG, amidated at the C-terminus (GGn, structure 2, Figure 1). Either the first or the last amino acid was replaced by an ionisable residue which enabled charge to be switched ‘on’ or ‘off’ by changing the pH. Consequently, charge and steric effects could be addressed individually. For this

purpose, lysine, which is positively charged at pH values up to 10.5 and glutamic acid, only anionic at pH values higher than 4.5, were chosen. To investigate the effect of C-terminal ionisability further, the resulting five peptide sequences were not only synthesized with an amidated C-terminus but also as free acid, introducing an extra pH dependent charge. This yielded a total of ten peptide amphiphiles (Figure 1). The assembly properties, morphology, polymerisation behaviour and polymer properties of assemblies of these ten PAs were investigated. GGn, the reference compound described above, was expected to assemble most easily into a  $\beta$ -sheet structure since neither charges nor bulky residues were present. Therefore, no repulsive forces would hinder the assembly and broad fibres were expected. Furthermore, because of the absence of any pH sensitive side chains, it should assemble into the same morphology regardless of pH. The subsequent introduction of charges and steric hindrance *via* Lys and Glu was expected to disturb the assembly of the amphiphiles, yielding twisted fibres with a smaller width. Introduction of Lys or Glu closer to the alkyl tail was thought to have a larger effect on assembly. A similar effect was observed by Hartgerink *et al.* for methylation.<sup>16</sup> Furthermore, two charges should have a larger effect than just one charge, resulting in thinner fibres or molecularly dissolved amphiphiles. Besides morphology, also polymerisation and polymer properties of the diacetylene containing fibre may be influenced by the variation of the peptide sequence. Amphiphiles with the best packing for the diacetylene polymerisation were expected to have the highest wavelength absorbance. Following the reasoning above, GGn would absorb at the highest wavelength while the introduction of charges or steric hindrance would lower this absorption wavelength, an effect more pronounced if the disturbance was close to the alkyl tail. However, the exact parameters yielding the highest wavelength absorbance of the polydiacetylene backbone may be different from the parameters yielding the best packing observed with electron microscopy. In this chapter, we investigated to what extent the fibre morphology ('large' length scale organisation) shows the same trends as the polydiacetylene colour (molecular scale organisation).



|               | X   | Y   | Z               | Charges depending on pH |         |      |
|---------------|-----|-----|-----------------|-------------------------|---------|------|
|               |     |     |                 | acid                    | neutral | base |
| <b>1</b> GGo  | Gly | Gly | OH              | 0                       | -1      | -1   |
| <b>2</b> GGn  | Gly | Gly | NH <sub>2</sub> | 0                       | 0       | 0    |
| <b>3</b> GGo  | Gly | Glu | OH              | 0                       | -2      | -2   |
| <b>4</b> GEn  | Gly | Glu | NH <sub>2</sub> | 0                       | -1      | -1   |
| <b>5</b> EGo  | Glu | Gly | OH              | 0                       | -2      | -2   |
| <b>6</b> EGn  | Glu | Gly | NH <sub>2</sub> | 0                       | -1      | -1   |
| <b>7</b> GKo  | Gly | Lys | OH              | +1                      | 0       | -1   |
| <b>8</b> GKn  | Gly | Lys | NH <sub>2</sub> | +1                      | +1      | 0    |
| <b>9</b> KGo  | Lys | Gly | OH              | +1                      | 0       | -1   |
| <b>10</b> KGn | Lys | Gly | NH <sub>2</sub> | +1                      | +1      | 0    |

Figure 1. The ten PA structures investigated. The abbreviations used throughout the chapter are shown in the left column and also used for the fibres. In the right column the charges for each compound in acid, basic and neutral environment are shown. The difference in colour is only to clarify the table.

## Synthesis

All ten peptide amphiphiles (Figure 1) were synthesized on the solid phase using standard Fmoc peptide synthesis methods.<sup>57</sup> To obtain peptide amphiphiles (PAs) with a free acid terminus the synthesis was performed on a Wang resin. After cleavage from the resin, purification of the fully deprotected PAs was attempted using column chromatography. For all five compounds (GGo, GGo, EGo, GKo and KGo), purification was troublesome. Acidification by addition of a few percent acetic acid in the eluent improved purification by neutralizing the free acid group. Even for KGo this purification was possible, although the lysine side-chain is positively charged under acidic conditions. Only GKo remained problematic, but its purification difficulties were solved by using a Barlos resin in which the lysine remained Boc protected after cleavage, which allowed easy purification. The deprotection of the lysine was performed after purification using 2 M hydrochloric acid in ethyl acetate.

Using a similar strategy, GGn, EGn and GEn were synthesized on a Breipohl resin, yielding amide-terminated, deprotected species after cleavage. To facilitate purification, GKn and KGn were synthesized on a Sieber resin.<sup>58</sup> Like a Barlos resin, a Sieber resin yields fully protected peptides after cleavage, but now amidated instead of with a free C-terminus. The protected species were purified and deprotected to complete the modest library of ten PAs.

## Conformational analysis

First of all, the peptide conformation in the fibres at neutral pH was investigated using infrared (IR) and circular dichroism (CD) spectroscopy. With CD spectroscopy also the stability of the fibres was examined. Because of the high absorption of the peptide bonds in the UV region (the fingerprint region in CD for secondary structure), the samples prepared in buffer (at low and high pH) could not be investigated with CD spectroscopy.

**Infrared (IR) spectroscopy.** Since the sequence of the PAs was inspired on a well-known  $\beta$ -sheet forming peptide, a  $\beta$ -sheet signal was expected for all ten compounds. IR measurements indeed showed typical  $\beta$ -sheet structures (sharp peaks at 1540 and 1630  $\text{cm}^{-1}$ , solid line in Figure 2). From the measurements it could not be concluded if a parallel or antiparallel arrangement of the peptides in the  $\beta$ -sheets was present. Neither at 1685  $\text{cm}^{-1}$  nor at 1645  $\text{cm}^{-1}$ , positions indicative for respectively antiparallel and parallel  $\beta$ -sheets, clear peaks were visible. However, since an antiparallel arrangement would result in hydrophobic tails being exposed to the aqueous solvent a packing of the peptides into a parallel  $\beta$ -sheet was expected. Preliminary solid state NMR measurements suggested a parallel arrangement as well. In acetic acid, the PAs were not assembled into fibres (the solution could be filtrated without removing the PAs, which was not possible in water). However, the  $\beta$ -sheet arrangement was such a favourable motif that, even when prepared in acetic acid, lyophilisation of the samples resulted in formation of  $\beta$ -sheet structures (dotted line, Figure 2).

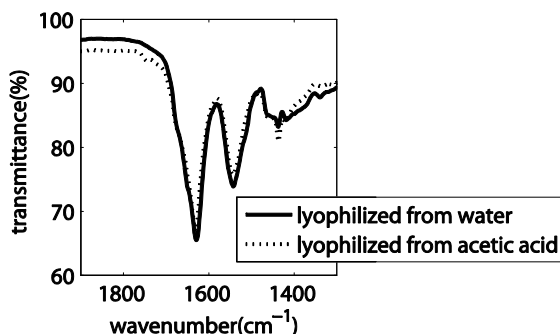


Figure 2. IR spectrum of GKn lyophilised from water (solid line) and acetic acid (dotted line).

**Circular dichroism (CD) spectroscopy.** With CD spectroscopy, the conformation of the peptide part in the fibres was monitored at different temperatures, thus revealing the stability of the assemblies. The expected  $\beta$ -sheet CD signal was obscured by a linear dichroism (LD) effect, which probes macroscopic alignment in solution and caused an increase of the CD signal. Since the fibres were in principle randomly oriented and a small deviation from exact random behaviour can be both in the vertical and the horizontal direction, the resulting ellipticity can be either positive or negative. For all but one of the PAs an ellipticity at room temperature was observed which was clearly different from a random coil conformation. The signal indicated assembly, presumably in a  $\beta$ -sheet fashion (as observed with IR spectroscopy). The only sample which did not show a clear signal was GGn, because of its low solubility.

For GEo, EGo, KGn and KGn, the large, LD enhanced signal disappeared at 90 °C and was replaced by a random coil signal, indicating complete disassembly at this temperature. On the other hand, GGo, KGo, GEN and EGn still showed a signal at 90 °C, though much smaller than at room temperature and more resembling a regular  $\beta$ -sheet signal. The signal decrease was probably caused by partial disassembly, which resulted in smaller, more mobile assemblies, causing the overall directionality and thus the LD effect to diminish. The signal of GKo disappeared upon heating, but did not come back upon cooling which may indicate precipitation or a slow nucleation process (see chapter 4). Therefore, it is unknown if the structure disassembled or precipitated.

The charges and steric hindrance present in assemblies of GEo, EGo, GKn and KGn should result in repulsive forces and may explain their lower disassembly temperatures. The same was expected for GEN and especially EGn, with their negative charge and large steric hindrance. For EGn the signal at 90 °C was indeed very small and disappeared upon heating to 95 °C. GEN gave a larger signal at 90 °C, but also in this case the PA disassembled when heated to 95 °C. This confirmed the hypothesis that the charge density and steric hindrance were responsible for the disassembly behaviour. The higher stability can be explained by the absence of much steric hindrance, which allows hydrophobic interactions to maintain fibre integrity. In case of KGo the higher observed stability was also expected, since this assembly did not have a net charge. A similar result was expected for GKo, but no signal was present.

## Fibre morphology

To compare not only the various PAs at neutral pH but also to investigate the difference in assembly at different pH values, fibres were prepared in glycine buffer of pH 2, in water and in glycine buffer of pH 12. The pH of a number of the samples was checked after preparation and samples prepared in water showed a value close to neutral (pH = 7).

**GGn.** Typically, even though no pH sensitive moieties were present in the reference PA GGn, in the pH range studied a large variation in fibre morphology was observed. At low and neutral pH broad, short ribbons were observed (Figure 3a and b), although in water also a few twisted fibres were detected. In contrast, at high pH much thinner, twisted fibres were present (Figure 3c), suggesting destabilisation of the assemblies. The cause of this destabilisation is unknown, but it is probably related to the ions in the solution. Glycine buffers were used for preparation of the fibres at low and high pH. Under basic conditions, glycine may interact with the amphiphiles in the fibres, yielding a shell of glycines around the fibres, introducing steric hindrance and thus causing the formation of thinner, twisted fibres. Even though the exact cause has not been elucidated, it influenced a peptide without pH sensitive side chains and is thus a factor to take into account in all assemblies.

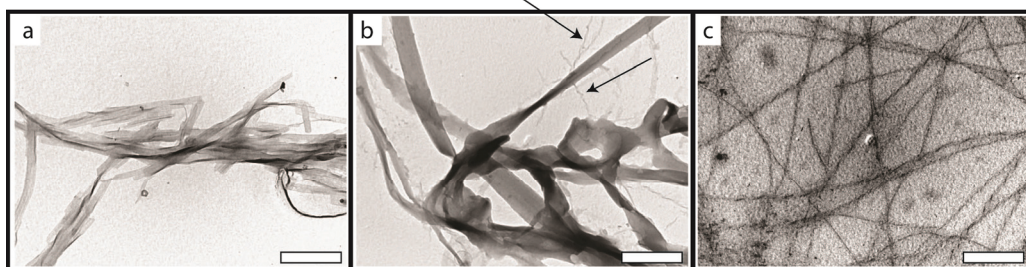


Figure 3. TEM of GGn. Assemblies prepared a) at pH 2, b) in milli Q (the arrows point to a few of the thin fibres present) c) at pH 12. The white bars represent 500 nm.

**Introduction of charges and steric hindrance.** When the first or last amino acid of GGn was replaced for either a glutamic acid or a lysine, yielding GEn, EGn, GKn and KGn, depending on the pH charge repulsion and/or steric hindrance were introduced in the structure. At neutral pH, both glutamic acid and lysine are charged, and consequently all four structures (GEn, EGn, GKn and KGn) suffered from both sterical hindrance and the charge repulsion between the amphiphiles. Because of these destabilising effects, these four modified PAs assembled into thinner and more twisted fibres compared to GGn. Because the lysine side chain is uncharged at high pH, GGn, GKn and KGn were expected to assemble into broader architectures than GEn and EGn. However, all assemblies had a thin and twisted morphology and therefore no large structural differences between the fibres in a basic environment were present. This showed the relatively large effect of the destabilisation in base, mentioned above for GGn. The charge on GEn and EGn increased with pH, and consequently the fibres became thinner and more twisted. At high pH also fewer fibres were present because of

increased solubility. At low pH GEn and EGn formed smaller and more twisted assemblies than GGn, while because of the absence of charges similar assemblies were expected. GKn also showed thinner fibres than GGn. Surprisingly, for KGn fibres of the same width as for GGn were observed, although they were longer, suggesting charge screening when the charge was close to the alkyl tail. In GKn and KGn only minor changes were observed with pH changes. These results suggest that the incorporation of lysine had a smaller effect than glutamic acid, and that steric hindrance played a larger role than charge repulsion.

**'Inside' versus 'outside' functionalisation.** When EGn was compared with GEn and KGn with GKn, thus 'inside' with 'outside' modification, a larger destabilisation was expected for modifications closer to the alkyl tail. Indeed, EGn showed a less defined fibre morphology than GEn. This effect was more pronounced when the charge was increased, i.e. at higher pH. However, when the morphologies of GKn and KGn were compared at different pH, surprising observations were made. Under acidic conditions, GKn assembled into thinner, longer fibres than KGn. Furthermore in water and basic solution no large differences between the GKn and KGn assemblies were observed. This result was the opposite effect as found for GEn *versus* EGn, where functionalisation close to the alkyl tail hampered fibre assembly. A possible explanation could be a more effective charge screening in KGn when compared to GKn, but it also suggests the easier accommodation of lysine compared to glutamic acid in the fibre assembly, since the lysine has a smaller effect when incorporated close to the alkyl tail. Close to the alkyl tail steric hindrance seems to have a larger influence on the morphology than charges, since the charges are more effectively screened, while far from the alkyl tail the (solvent-exposed) charges play a larger role.

**Acid versus amide C-terminus.** Introducing an acid group instead of an amide at the C-terminus of the peptide introduced a second ionisable group in the amphiphiles. GGo proved to be under acid and neutral conditions only moderately soluble, which was also observed for GGn. However, the fibres that formed were thinner and longer for GGo than for GGn. Under acidic conditions, neither of these two PAs were charged (Figure 1) and therefore they were expected to have the same morphology. Apparently the acid group, even at low pH, had a slightly larger charge density than the amide group causing the fibres to be thinner. In neutral conditions the same effect was observed, in accordance with the larger charges present in GGo. At high pH both PAs suffered from the destabilisation described above. However, the influence on the morphology was different. GGo showed sheets with a less defined structure instead of the thin twisted fibres of GGn at high pH (Figure 4, compare Figure 3c). The same difference was observed for EGo *versus* EGn.

The larger amount of charges in the glutamic acid functionalised PAs (Figure 1) increased the solubility, i.e. the driving force for assembly was decreased. GEo dissolved at high pH, not assembling into fibres at all because of the large charge repulsion. At low pH, four of the five acid-terminated PAs precipitated. Only GKo, in which the absence of repulsion by the acid group was compensated by the positive charge of the lysine yielded a solution of fibres rather than precipitate. The lysine of

KGo was expected to have the same effect. However, this amphiphile precipitated, confirming the buried character of the lysine charge close to the alkyl tail.

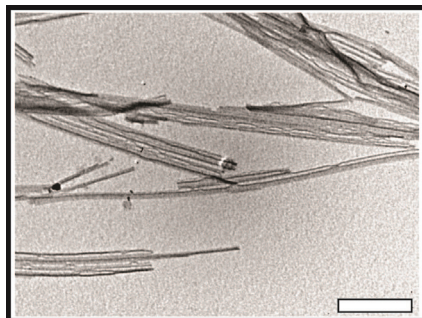


Figure 4. Fibres of GGo prepared at pH 12. The white bar represents 500 nm.

In summary, PA assemblies had a different morphology when prepared at different pH values. Charges and steric hindrance had a larger effect closer to the alkyl tail. Surprisingly, the side chain of lysine seemed to be more easily accommodated within the fibres than that of glutamic acid, causing a smaller change in morphology.

## **Polymerisability**

The diacetylene containing alkyl tail was expected to be in an almost crystalline packing, which would allow polymerisation of the diacetylene moieties. The colour of the resulting polydiacetylene could subsequently be used as an indicator for the backbone conformation, which is dependent on the peptide headgroup conformation and *via* that on the environment of the fibre.

**GGn.** GGn did not dissolve well in water. The PAs were mostly present in random aggregates. However, the part which assembled in a regular structure formed fibres (see TEM images) and IR spectroscopy showed the expected  $\beta$ -sheet conformation. Upon illumination, the colour of the white aggregates changed to blue, yielding blue suspended particles in an otherwise colourless solution. Because of the insolubility of the GGn assemblies the absorbance of the polymer could not be measured with UV spectroscopy, and we had to restrict ourselves to the observed colour changes. Preparation of fibres at low or neutral pH yielded blue polymer after illumination, while after preparation at high pH the PA fibres polymerised to a slightly purpler colour. Upon heating the solution at neutral pH the polydiacetylene packing (monitored *via* the colour) changed, but the pink colour returned almost completely to the original blue, suggesting the reversibility of the structural change of the polydiacetylenes.

**Introduction of charges and sterical hindrance.** Replacing the first or last amino acid of the sequence by the pH sensitive lysine or glutamic acid yielded fibres which polymerised to different colours, which indicated a difference in diacetylene packing. This is in marked contrast with the PA system described in chapters 4 and 5, where a GANPNAAG peptide coupled to the same hydrophobic tail resulted in polymerised fibres which had the same colour regardless of the conditions. Apparently the peptide



played an important role in the conformational freedom of the diacetylene moieties. For GEn and EEn the solution prepared at low pH yielded the same result as GEn, a coloured precipitate was observed, which could not be quantified. For GEn, neutral and basic conditions yielded comparable spectra, while EEn hardly polymerised at pH 12, showing a large difference in structure or solubility between preparations at neutral and high pH for this specific sequence.

**'Inside' versus 'outside' functionalisation.** GEn fibres polymerised under neutral conditions absorbed longer wavelength light than EEn (Figure 5, left), indicating a better packing of the diacetylenes. Furthermore, GEn yielded a more intense absorption, indicating the presence of more polymer, which also suggests less disturbance of the assembly. The difference between GEn and EEn can be explained from the higher charge repulsion and steric hindrance of the latter because of the position of the glutamic acid in the amphiphile. This is supported by the stronger pH dependence of EEn. In a similar fashion, GKEn appeared bluer (had an absorption at longer wavelength) than KEn, because the repulsive charges were located further away from the colour-determining diacetylene backbone. However, because of solvent-exposed charges in GKEn, the amount of assemblies and thus the intensity of the PDA absorption was slightly lower. The glutamic acid residues disturbed the diacetylene packing more than lysines, as shown by the smaller amount (lower absorption intensity) of polymer present for the glutamic acid containing species.

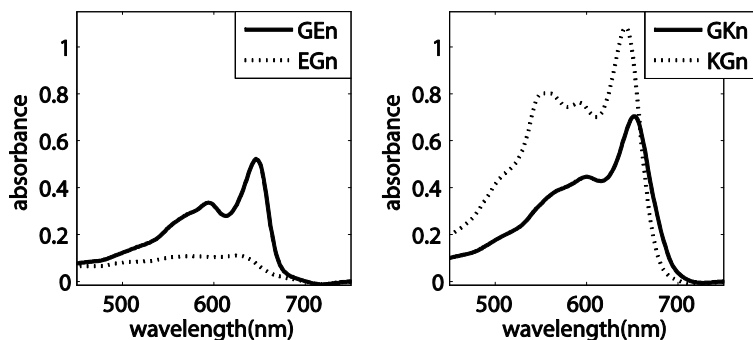


Figure 5. UV spectra of polymerised GEn, EEn, GKEn and KEn, self-assembled under neutral conditions.

**Acid versus amide C-terminus.** Additional charges were introduced by using a free acid instead of an amide C-terminus. Especially at high pH the differences between amide and acid were apparent – three of the five compounds with a free acid C-terminus (GEO, EGO and GKO) did not polymerise when prepared in base. For GEO and EGO this was expected because of the double negative charge at high pH, which increased the solubility. Quite remarkably however, also GKO did not yield a coloured solution after illumination. This peptide was expected to polymerise in base, since its charge was the same as for GGO, which polymerised under these conditions. Furthermore, the steric hindrance of the lysine was expected not to be problematic, especially since the more sterically hindered KGO did polymerise.

## **Polymer properties**

The diacetylene polymerisation yielded a covalently linked fibre, with increased stability compared to the dynamic non-polymerised fibres. Conditions which would cause disassembly of the fibre before polymerisation can after polymerisation only induce stress in the backbone, which has been shown to result in a colour change (chapter 4).<sup>15</sup> To explore the colour change of the polymerised fibres upon changing the pH, a solution of hydrochloric acid or sodium hydroxide was added to the fibres. GGo, GGn and GKn did not change colour, indicating that once the fibres were polymerised, their structure was not easily disrupted. For GGo and GGn this was in accordance with the polymerisability. Regardless of pH during fibre preparation the colour after polymerisation was similar, showing the pH independence of the alkyl chain conformation in the fibres. On the other hand, GKn showed large differences in absorption spectrum when polymerised at different pH, indicating a diacetylene packing dependent on pH. Therefore, the absence of a colour change after polymerisation was unexpected. Three other compounds (GEn, KGo and KGn) showed a small spectral shift upon pH variation after polymerisation, in accordance with the difference of the colour upon polymerisation at different pH. The last four compounds, GGo, EGo, EGn and GKo had a rather large spectral shift with increasing pH. For GGo the diffusion of a sodium hydroxide solution could even be followed by the colour change (Figure 6). Upon shaking the colour became homogeneously pink. The large colour change was expected, since addition of base before polymerisation prevented these four PAs (GGo, EGo, EGn and GKo) from assembling. The most substantial colour change was observed for GGo, followed by EGo and EGn. The colour change of GKo was the smallest in this series.



Figure 6. Colour change from blue to pink when sodium hydroxide was added to a solution of GGo polymers.

The colour change of fibres polymerised in milli-Q was studied in more detail over a range of pH values between 1 and 14. In Figure 7 the corresponding UV-Vis spectra are shown for GGo, EGn and KGn which showed respectively a very large, a large and no change in absorption spectrum upon pH variation. In order to quantify the colour change, the ratio between the higher-wavelength and lower-wavelength peak was used. In case of GGo (Figure 7a) these were the peaks at 650 nm and 550 nm. For each compound the peaks chosen as ‘higher’ and ‘lower’ wavelength peaks were at a slightly different position, and therefore the absolute value of the ratio and the sharpness of an eventual colour transition could not be compared between compounds. The peak ratio was plotted against the pH. For the four compounds which showed a large colour change upon addition of a base (GGo, EGo, GKo and EGn), this yielded a colour

transition (Figure 7d for G<sub>Eo</sub> and E<sub>Go</sub>). G<sub>Eo</sub> changed colour at a pH of approximately 7.5, E<sub>Go</sub> followed at pH 9 and E<sub>Gn</sub> at 12. G<sub>Ko</sub> only changed colour if the pH was raised to 13.5 or higher using NaOH. These pH values followed the same trend as the magnitude of the spectral shift, i.e. the compounds which showed the largest colour change (G<sub>Eo</sub>), had their transition point at the lowest pH value. This indicated that either two negative charges in close proximity (G<sub>Eo</sub>) or a charge in a susceptible location, i.e. close to the alkyl tail (E<sub>Go</sub> and E<sub>Gn</sub>) were required for a large colour change. The second charge in E<sub>Go</sub> did not have a large effect, probably because the charges were too far apart to have a cumulative effect. G<sub>Ko</sub> was least responsive but because of its small amount of charges, the effect was still surprisingly large.

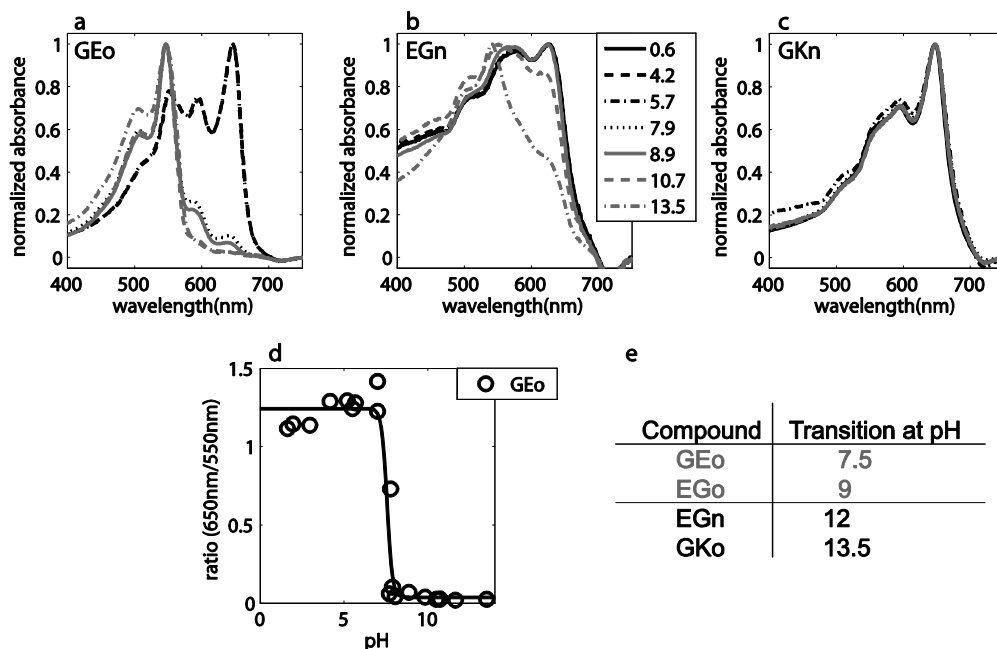


Figure 7. Variations in absorption upon changing pH. Spectra of a) G<sub>Eo</sub>, b) E<sub>Gn</sub>, c) G<sub>Kn</sub>. Dark lines indicate low, light lines high pH. d) The ratio of the high-wavelength to the low-wavelength peak for G<sub>Eo</sub>. The sigmoidal line is only to guide the eye. e) The transition pH of the four compounds with a large colour change.

## Discussion and conclusions

The effects of steric hindrance and charge repulsion on morphology and molecular packing of peptide amphiphile fibres were investigated. To this end a series of PAs was synthesized based on the pentameric GAGAG, N-terminally functionalised with a diacetylene-containing hydrophobic tail. Either the first or the last glycine in GAGAG was substituted for either lysine or glutamic acid and the C-terminus consisted of a free acid or an amide. In order to separately investigate charge repulsion and steric hindrance, the assemblies were studied at various pH values. The stability (disassembly

of the assemblies, monitored by CD), showed that the small change of replacing one amino acid or even placing it in a different position within a pentameric peptide has a large influence on the properties. A larger charge resulted in a lower disassembly temperature.

All ten peptide amphiphiles assembled into fibrous structures in aqueous solution. The morphology of the fibres showed striking differences as a result of the differences in packing. At the pH values for which the side chains are charged, both for lysine and glutamic acid charge repulsion between the amphiphiles caused a smaller, more twisted assembly. However, when uncharged, Glu was found to disturb the packing more than Lys – there were large differences between the morphologies of assemblies of GAGAE and EAGAG, while the morphological differences between GAGAK and KAGAG were negligible.

The diacetylene functionality in the hydrophobic tail of the peptide provided the opportunity to polymerise the assemblies, yielding highly coloured polymers. Their colour and responsiveness to external stimuli provided information about the molecular packing of the amphiphiles within the fibres. Overall the same trend was observed for the diacetylene packing and morphology. Apparently, the distortion of morphology (observed with TEM) correlates with changes in diacetylene packing at a molecular scale (probed by UV spectroscopy). For example in GGn the morphology changed from broad ribbons at low and neutral pH to small, twisted fibres at high pH, while the colour changed from blue when polymerised at low or neutral pH to purple when prepared at high pH. Furthermore, both morphology and colour after polymerisation of GEn and EGn indicated a worse packing for EGn, which yielded a less intense absorption, a lower wavelength maximum absorption and a more distorted morphology. However, there is an important difference between morphology observed with TEM and the diacetylene packing as observed with UV-Vis spectroscopy. The morphology is mainly determined by the outside of the fibre, while the diacetylene packing is sensitive to the changes closer to the hydrophobic tail. With TEM, broader assemblies were observed for KGn than for GKn, suggesting a better packing of the former. On the other hand, GKn had a higher wavelength absorbance than KGn, which suggested a better packing of the diacetylenes for GKn. This typical difference between effect of peripheral and internal functionalisation was only visible in the difference between KGn and GKn. The other amphiphiles showed the same trend both in morphology and colour.

When the pH of the solutions was changed after polymerisation, only peptides with multiple charges or a charge close to the alkyl tail induced a structural change in the head group large enough to also cause stress in the backbone of the polydiacetylene. The magnitude of the colour change followed the amount of charges. A large change, with a colour transition at low pH, was observed for GEo, in which the charge effect is cumulative, followed by EGo and EGn. Also GKo showed a colour transition, although only at high pH. The relatively high pH responsiveness of this PA was unexpected, but was also observed in morphological analysis (TEM) and stability (CD spectroscopy).

To conclude, the peptide amphiphile assembly is controlled by a subtle interplay between hydrophobic forces, hydrogen bonds, charge interactions and steric hindrance. Notwithstanding the complexity of the fibre formation, a few rather simple rules are

formulated which are generally complied. Firstly, without sterical hindrance or charge repulsion, these PAs assemble into broad fibres, with an almost perfect diacetylene packing. Secondly, a disturbance close to the alkyl tail has a larger effect than one further away from the alkyl tail. Thirdly, glutamic acid causes a larger disturbance than lysine, and fourthly, to have a cooperative effect of charges, they need to be close to each other.

## Acknowledgements

We thank Nicole van Gijzel, who did most of the synthesis and a considerable number of the TEM, CD and UV experiments.

## Experimental section

**General.** All starting materials were obtained from commercial suppliers and used as received. Thin layer chromatography (TLC) was performed on Kieselgel F-254 pre-coated silica plates or RP-8 F-254s. Visualization was accomplished with TDM.<sup>59</sup> Column chromatography was carried out on Merck silica gel 60 (230-400 mesh ASTM). <sup>1</sup>H-NMR spectra were recorded on a Varian Mercury, 400 MHz. DMSO-d<sub>5</sub> ( $\delta = 2.5$ ) was used as a shift reference. Mass spectra were recorded on a JEOL AccuTOF-CS spectrometer.

**Synthesis of the amphiphiles.** The ten peptides were prepared by standard solid-phase Fmoc protocols.<sup>57</sup> For GGo, GGo, EGo and KGo a Wang resin was used, for GKo a Barlos resin, GGn, GEn and EGn were synthesized on a Breipohl resin and GKn and KGn on a Sieber resin.

**Coupling of the first amino-acid to a Wang resin.**<sup>60</sup> To couple the first amino acid, the resin was washed three times with dichloromethane and subsequently suspended in dimethylformamide (DMF). Two equivalents of the Fmoc protected amino acid, 4 equivalents 1-hydroxybenzotriazole hydrate (HOBT), 2 eq diisopropylcarbodiimide (DIPCDI) and 2 eq 4-dimethylaminopyridine were added. The suspension was agitated overnight. The suspension was then filtered, washed and dried under vacuum.

**Coupling of the first amino acid to a Sieber<sup>58</sup> or Breipohl resin.** The resin was swollen for 20 min in DMF. The Fmoc group on the resin was removed using 20 % piperidine in DMF. After that, the first amino acid was coupled using a normal peptide coupling.

**Coupling of the first amino acid to a Barlos resin.** To the resin in dry dichloromethane, 2.5 eq DIPEA and 2 eq Fmoc-Lys(Boc)-OH, dissolved in dry dichloromethane, were added. The solution was agitated 30 min, after which 5 mL MeOH and another 2.5 eq DIPEA were added to the mixture and the solution was agitated for another 15 min.

**Coupling of subsequent amino acids.** In all subsequent couplings 3 equivalents of the amino acid, 3.3 equivalents DIPCDI and 3.6 equivalents HOBT in DMF were used. Deprotections were carried out using 20 % piperidine in DMF. After each coupling and deprotection a Kaiser test<sup>61</sup> was performed to check the completeness of the reactions. After removal of the final Fmoc group the peptides were acylated on the resin employing 3 equivalents of the appropriate diacetylene carboxylic acid dissolved in dichloromethane to which 3.3 equivalents DIPCDI and 3.6 equivalents HOBT in DMF were added.

**Cleavage from a Wang and Breipohl resin.** The peptides GGo, GGo, EGo, KGo, GGn, GEn and EGn were cleaved from the resin by treatment with trifluoroacetic

acid/H<sub>2</sub>O/triisopropylsilane (95:2.5:2.5) for two hours, followed by precipitation in ether or by removal of the volatiles in vacuo. Column chromatography (eluent: CHCl<sub>3</sub>/MeOH/H<sub>2</sub>O 65:25:4) and subsequent lyophilization afforded pure compounds according to <sup>1</sup>H-NMR, MS and TLC.

**Cleavage from a Sieber resin.** The peptides GK<sub>n</sub> and KG<sub>n</sub> were cleaved from the resin using 2 % TFA in dichloromethane for 1.5 hours, followed by precipitation in ether or by removal of the volatiles in vacuo. Column chromatography (eluent: CHCl<sub>3</sub>/MeOH/H<sub>2</sub>O 65:25:4) and subsequent lyophilization afforded pure compounds that were deprotected by treatment with 2 M hydrochloric acid in ethyl acetate for 30 min. Subsequent evaporation, coevaporation with tert-butanol and lyophilization from acetic acid yielded pure compounds according to <sup>1</sup>H-NMR, MS and TLC.

**Cleavage from a Barlos resin.** The peptide GK<sub>o</sub> was cleaved from the resin using a 3:1:1 mixture of dichloromethane, TFE and acetic acid. The protected product was purified using column chromatography (eluent: CHCl<sub>3</sub>/MeOH/AcOH 65:25:4) and the protecting group was removed by treatment with 2M HCl in ethyl acetate for 30 min at room temperature. The solvent was evaporated and coevaporated with tert-butanol. Lyophilization from acetic acid yielded pure compound according to <sup>1</sup>H-NMR, MS and TLC.

### Analysis

#### **C<sub>24</sub>H<sub>41</sub>C(O)-Gly-Ala-Gly-Ala-Gly-OH (GGo):**

TLC: R<sub>f</sub> 0.33 (eluent: MeOH/ CHCl<sub>3</sub>/ H<sub>2</sub>O (25:65:4)).

<sup>1</sup>H-NMR [DMSO-d<sub>6</sub>]: δ 0.85 (t, 3H), 1.24 (m, 32H), 1.44 (m, 6H), 2.11 (t, 2H), 2.27 (t, 4H), 3.5 (m, 6H), 4.23 (m, 2H), 7.41 (s, 1H), 8.25 (d, 1H), 8.35 (m, 2H), 8.49 (t, 1H).

Mass spectrometry: Calc for [C<sub>37</sub>H<sub>61</sub>N<sub>5</sub>O<sub>7</sub> + Na]<sup>+</sup> 710.4469, found 710.4479.

#### **C<sub>24</sub>H<sub>41</sub>C(O)-Gly-Ala-Gly-Ala-Gly-NH<sub>2</sub> (GGn):**

TLC: R<sub>f</sub> 0.50 (eluent: MeOH/ CHCl<sub>3</sub>/ H<sub>2</sub>O (25:65:4)).

<sup>1</sup>H-NMR [DMSO-d<sub>6</sub>]: δ 0.85 (t, 3H), 1.29 (m, 32H), 1.44 (m, 6H), 2.10 (t, 2H), 2.27 (t, 4H), 3.61 (m, 6H), 4.22 (dt, 2H), 7.06 (s, 1H), 7.16 (s, 1H), 7.99 (t, 2H), 8.09 (t, 2H), 8.20 (t, 1H).

Mass spectrometry: Calc for [C<sub>37</sub>H<sub>62</sub>N<sub>6</sub>O<sub>6</sub> + Na]<sup>+</sup> 709.4629, found 709.4615.

#### **C<sub>24</sub>H<sub>41</sub>C(O)-Gly-Ala-Gly-Ala-Glu-OH (GEO):**

TLC: R<sub>f</sub> 0.12 (eluent: MeOH/ CHCl<sub>3</sub>/ H<sub>2</sub>O (25:65:4)).

<sup>1</sup>H-NMR [DMSO-d<sub>6</sub>]: δ 0.85 (t, 3H), 1.24 (m, 32H), 1.44 (m, 6H), 1.66 (m, 1H), 1.84 (m, 1H), 2.10 (t, 2H), 2.16 (t, 2H), 2.27 (t, 4H), 3.68 (m, 4H), 4.00 (m, 1H), 4.24 (m, 2H), 7.75 (d, 1H), 8.01 (d, 1H), 8.33 (m, 3H).

Mass spectrometry: Calc for [C<sub>40</sub>H<sub>65</sub>N<sub>5</sub>O<sub>9</sub> + H]<sup>+</sup> 760.4861, found 760.4866.

#### **C<sub>24</sub>H<sub>41</sub>C(O)-Gly-Ala-Gly-Ala-Glu-NH<sub>2</sub> (GEn):**

TLC: R<sub>f</sub> 0.20 (eluent: MeOH/ CHCl<sub>3</sub>/ H<sub>2</sub>O (25:65:4)).

<sup>1</sup>H-NMR [DMSO-d<sub>6</sub>]: δ 0.85 (t, 3H), 1.24 (m, 32H), 1.44 (m, 6H), 1.80 (m, 2H), 2.10 (t, 4H), 2.27 (t, 4H), 3.69 (m, 4H), 3.90 (m, 1H), 4.11 (m, 1H), 4.22 (m, 1H), 6.90 (s, 1H), 6.95 (s, 1H), 8.02 (d, 1H), 8.18 (t, 1H), 9.02 (s, 1H), 0.88 (s, 1H), 9.55 (s, 1H).

Mass spectrometry: Calc for [C<sub>40</sub>H<sub>66</sub>N<sub>6</sub>O<sub>8</sub> + Na]<sup>+</sup> 781.4840, found 781.4842.

#### **C<sub>24</sub>H<sub>41</sub>C(O)-Glu-Ala-Gly-Ala-Gly-OH (EGo):**

TLC: R<sub>f</sub> 0.56 (eluent: MeOH/ CHCl<sub>3</sub>/ H<sub>2</sub>O (25:65:4)).

<sup>1</sup>H-NMR [DMSO-d<sub>6</sub>]: δ 0.85, 1.24, 1.44, 1.72, 1.86, 2.01, 2.10, 2.19, 2.27, 2.33, 2.64, 2.84, 3.03, 3.17, 3.51, 3.61, 3.67, 5.24, 6.69, 7.10, 7.16, 7.50, 7.69, 8.00, 8.10, 8.22, 9.4.

Mass spectrometry: Calc for [C<sub>40</sub>H<sub>65</sub>N<sub>5</sub>O<sub>9</sub> + Na]<sup>+</sup> 782.4680, found 782.4665.

#### **C<sub>24</sub>H<sub>41</sub>C(O)-Glu-Ala-Gly-Ala-Gly-NH<sub>2</sub> (EGn):**

TLC: R<sub>f</sub> 0.14 (eluent: MeOH/ CHCl<sub>3</sub>/ H<sub>2</sub>O (25:65:4)).

$^1\text{H-NMR}$  [DMSO- $d_6$ ]:  $\delta$  0.85 (t, 3H), 1.24 (m, 32H), 1.44 (m, 6H), 1.75 (m, 1H), 1.83 (m, 1H), 2.09 (m, 4H), 2.66 (t, 4H), 3.65 (m, 4H), 3.80 (m, 1H), 4.22 (m, 2H), 7.00 (s, 1H), 7.23 (s, 1H), 8.05 (d, 1H), 8.12 (d, 1H), 8.16 (d, 1H), 8.53 (s, 1H).

Mass spectrometry: Calc for  $[\text{C}_{40}\text{H}_{66}\text{N}_6\text{O}_8 + \text{Na}]^+$  781.4840, found 781.4831.

**$\text{C}_{24}\text{H}_{41}\text{C}(\text{O})\text{-Gly-Ala-Gly-Ala-Lys-OH}$  (GKo):**

TLC:  $R_f$  0.79 (eluent: MeOH/  $\text{CHCl}_3$ /  $\text{H}_2\text{O}$  (25:65:4)).

$^1\text{H-NMR}$  [DMSO- $d_6$ ]:  $\delta$  0.85 (t, 3H), 1.24 (m, 34H), 1.44 (m, 9H), 1.69 (m, 1H), 2.11 (t, 2H), 2.27 (t, 4H), 2.75 (t, 2H), 3.70 (m, 3H), 4.02 (q, 1H), 4.13 (m, 1H), 4.22 (m, 2H), 7.77 (s, 2H), 7.88 (d, 1H), 8.02 (t, 1H), 8.11 (d, 1H), 8.13 (d, 1H), 8.21 (t, 1H).

Mass spectrometry: Calc for  $[\text{C}_{41}\text{H}_{70}\text{N}_6\text{O}_7 + \text{H}]^+$  759.5384, found 759.5360.

**$\text{C}_{24}\text{H}_{41}\text{C}(\text{O})\text{-Gly-Ala-Gly-Ala-Lys-NH}_2$  (GKn):**

TLC:  $R_f$  0.34 (eluent: MeOH/  $\text{CHCl}_3$ /  $\text{H}_2\text{O}$  (25:65:4)).

$^1\text{H-NMR}$  [DMSO- $d_6$ ]:  $\delta$  0.85 (t, 3H), 1.24 (m, 34H), 1.44 (m, 9H), 1.69 (m, 1H), 2.11 (t, 2H), 2.27 (t, 4H), 2.75 (t, 2H), 3.70 (m, 3H), 4.02 (q, 1H), 4.13 (m, 1H), 4.22 (m, 2H), 7.03 (s, 1H), 7.17 (s, 1H), 7.71 (s, 2H), 7.83 (d, 1H), 8.03 (t, 1H), 8.15 (d, 1H), 8.27 (t, 1H).

Mass spectrometry: Calc for  $[\text{C}_{41}\text{H}_{71}\text{N}_7\text{O}_6 + \text{H}]^+$  758.5544, found 758.5522.

**$\text{C}_{24}\text{H}_{41}\text{C}(\text{O})\text{-Lys-Ala-Gly-Ala-Gly-OH}$  (KGk):**

TLC:  $R_f$  0.55 (eluent: MeOH/  $\text{CHCl}_3$ /  $\text{H}_2\text{O}$  (25:65:4)).

$^1\text{H-NMR}$  [DMSO- $d_6$ ]:  $\delta$  0.85 (t, 3H), 1.24 (m, 34H), 1.44 (m, 9H), 1.64 (m, 1H), 2.10 (t, 2H), 2.27 (t, 4H), 2.74 (t, 2H), 3.66 (m, 1H), 3.82 (m, 1H), 4.25 (m, 3H), 6.64 (s, 1H), 7.20 (s, 1H), 7.40 (s, 1H), 7.82 (s, 1H), 7.95 (d, 1H), 8.22 (d, 1H), 8.30 (d, 1H).

Mass spectrometry: Calc for  $[\text{C}_{41}\text{H}_{70}\text{N}_6\text{O}_7 + \text{H}]^+$  759.5384, found 759.5378.

**$\text{C}_{24}\text{H}_{41}\text{C}(\text{O})\text{-Lys-Ala-Gly-Ala-Gly-NH}_2$  (KGn):**

TLC:  $R_f$  0.45 (eluent: MeOH/  $\text{CHCl}_3$ /  $\text{H}_2\text{O}$  (25:65:4)).

$^1\text{H-NMR}$  [DMSO- $d_6$ ]:  $\delta$  0.85 (t, 3H), 1.24 (m, 34H), 1.44 (m, 9H), 1.64 (m, 1H), 2.10 (t, 2H), 2.27 (t, 4H), 2.74 (t, 2H), 3.70 (m, 4H), 4.24 (m, 3H), 7.07 (s, 1H), 7.18 (s, 1H), 7.73 (s, 2H), 7.92 (d, 1H), 8.05 (d, 1H), 8.08 (d, 1H), 8.14 (q, 2H).

Mass spectrometry: Calc for  $[\text{C}_{41}\text{H}_{71}\text{N}_7\text{O}_6 + \text{H}]^+$  758.5544, found 758.5515.

**Fibre preparation.** The amphiphiles were dispersed in milli-Q or in glycine buffer (0.1 M, pH 2 or pH 12), at concentrations of either 0.2 or 1.0 mM. The samples were heated to 50 °C for 30 min, followed by 15 min sonication at that temperature. Subsequently, the samples were heated to 90 °C and allowed to cool to room temperature. Polymerisations were carried out on 1 mM samples in a 15 mL glass vial using a UVASPOT 400T lamp with a sample-light source distance of 22 cm.

**pH variation.** The pH of polymerised samples was varied by addition of 30  $\mu\text{L}$  NaOH (6.25 M) or 30  $\mu\text{L}$  HCl (6.25 M) to 300  $\mu\text{L}$  polymer sample.

**pH variation with buffers.** The pH of polymerised samples was varied using buffers (0.1 M) of pH values between 1 and 13. Glycine buffers (with a salt concentration of 0.1 M) were used for pH values between 1.6 and 3.0 and between 8.9 and 11.6. Potassiumphthalate buffers were used between pH 4.2 and 5.7, a PBS buffer for pH 7.8, citric acid, borax and phosphate buffers for pH 8. For low and high pH hydrochloric acid or sodium hydroxide was added to a concentration of 0.6 M.

**Transmission electron microscopy (TEM).** TEM samples were prepared by floating a carbon-coated copper grid on a peptide amphiphile solution of 0.2 mg/mL for 5 min, followed by removal of residual water by blotting with a paper filter. The samples were visualized using a JEOL 1010 transmission electron microscope set on an accelerating voltage of 60 kV.

**Circular dichroism (CD) spectroscopy.** CD spectra were recorded on a Jasco J-810 spectropolarimeter equipped with a Jasco PTC-423S/L Peltier type temperature control system.

The measurements were carried out at a concentration of 0.2 mM using a 1 mm quartz cell. To measure temperature curves, a heating or cooling rate of 3 °C/min was used. Because the diyne functionalities readily polymerised when illuminated with the short wavelengths used for the CD measurements, only every 10 °C spectra were recorded (265-185 nm, 100 nm/min), and the shutter was closed (5 µm) between these measurements.

**Infrared (IR) spectroscopy.** Solutions of fibrils in water or disassembled amphiphiles in acetic acid were lyophilized and the dry samples were compressed on an ATR crystal with a pressure of 5 N. The spectra were recorded on a Thermo Mattson IR300 spectrometer, fitted with a Harrick ATR unit, accumulating 64 scans per spectrum.

**UV-Vis spectroscopy.** UV-Vis spectra were recorded on a VARIAN Cary 50 Conc spectrometer. Measurements were carried out at a concentration of 1.0 mM using a 1 mm quartz cell. The spectra were recorded on a Varian Cary-50 spectrometer, equipped with a water bath to enable temperature changes.

## References

1. S. Matsumura, S. Uemura and H. Mihara, *Chem. Eur. J.*, 2004, **10**, 2789-2794.
2. M. G. Ryadnov and D. N. Woolfson, *Angew. Chem., Int. Ed.*, 2003, **42**, 3021-3023.
3. M. R. Ghadiri, J. R. Granja, R. A. Milligan, D. E. McRee and N. Khazanovich, *Nature*, 1993, **366**, 324-327.
4. C. Wang, L. X. Huang, L. J. Wang, Y. K. Hong and Y. L. Sha, *Biopolymers*, 2007, **86**, 23-31.
5. Y. Kikkawa, E. Koyama, S. Tsuzuki, K. Fujiwara, K. Miyake, H. Tokuhisa and M. Kanetsato, *Chem. Comm.*, 2007, 1343-1345.
6. J. D. Hartgerink, E. Beniash and S. I. Stupp, *Science*, 2001, **294**, 1684-1688.
7. A. Brizard, R. K. Ahmad and R. Oda, *Chem. Comm.*, 2007, 2275-2277.
8. S. R. Diegelmann, J. M. Gorham and J. D. Tovar, *J. Am. Chem. Soc.*, 2008, **130**, 13840-13841.
9. A. Aggeli, M. Bell, N. Boden, L. M. Carrick and A. E. Strong, *Angew. Chem., Int. Ed.*, 2003, **42**, 5603-5606.
10. L. Haines-Butterick, K. Rajagopal, M. Branco, D. Salick, R. Rughani, M. Pilarz, M. S. Lamm, D. J. Pochan and J. P. Schneider, *Proc. Natl. Acad. Sci. U. S. A.*, 2007, **104**, 7791-7796.
11. E. F. Banwell, E. S. Abelardo, D. J. Adams, M. A. Birchall, A. Corrigan, A. M. Donald, M. Kirkland, L. C. Serpell, M. F. Butler and D. N. Woolfson, *Nat. Mater.*, 2009, **8**, 596-600.
12. J. M. Anderson, M. Kushwaha, A. Tambralli, S. L. Bellis, R. P. Camata and H. W. Jun, *Biomacromol.*, 2009, **10**, 2935-2944.
13. M. Zhou, A. M. Smith, A. K. Das, N. W. Hodson, R. F. Collins, R. V. Ulijn and J. E. Gough, *Biomaterials*, 2009, **30**, 2523-2530.
14. D. W. P. M. Löwik, J. Garcia-Hartjes, J. T. Meijer and J. C. M. van Hest, *Langmuir*, 2005, **21**, 524-526.
15. M. van den Heuvel, D. W. P. M. Löwik and J. C. M. van Hest, *Biomacromol.*, 2008, **9**, 2727-2734.
16. S. E. Paramonov, H. W. Jun and J. D. Hartgerink, *J. Am. Chem. Soc.*, 2006, **128**, 7291-7298.
17. H. Xu, J. Wang, S. Y. Han, J. Q. Wang, D. Y. Yu, H. Y. Zhang, D. H. Xia, X. B. Zhao, T. A. Waigh and J. R. Lu, *Langmuir*, 2009, **25**, 4115-4123.
18. L. C. Palmer and S. I. Stupp, *Acc. Chem. Res.*, 2008, **41**, 1674-1684.
19. K. Channon and C. E. MacPhee, *Soft Matter*, 2008, **4**, 647-652.
20. G. Wegner, *Makromol. Chem.*, 1972, **154**, 35-48.
21. E. Jahnke, A. S. Millerioux, N. Severin, J. P. Rabe and H. Frauenrath, *Macromol. Biosci.*, 2007, **7**, 136-143.
22. E. Jahnke, I. Lieberwirth, N. Severin, J. P. Rabe and H. Frauenrath, *Angew. Chem., Int. Ed.*, 2006, **45**, 5383-5386.
23. D. W. P. M. Löwik, I. O. Shklyarevskiy, L. Ruizendaal, P. C. M. Christianen, J. C. Maan and J. C. M. van Hest, *Adv. Mater.*, 2007, **19**, 1191-1195.
24. L. Hsu, G. L. Cvetanovich and S. I. Stupp, *J. Am. Chem. Soc.*, 2008, **130**, 3892-3899.
25. B. Tieke, G. Lieser and G. Wegner, *J. Polym. Sci., Part A: Polym. Chem.*, 1979, **17**, 1631-1644.

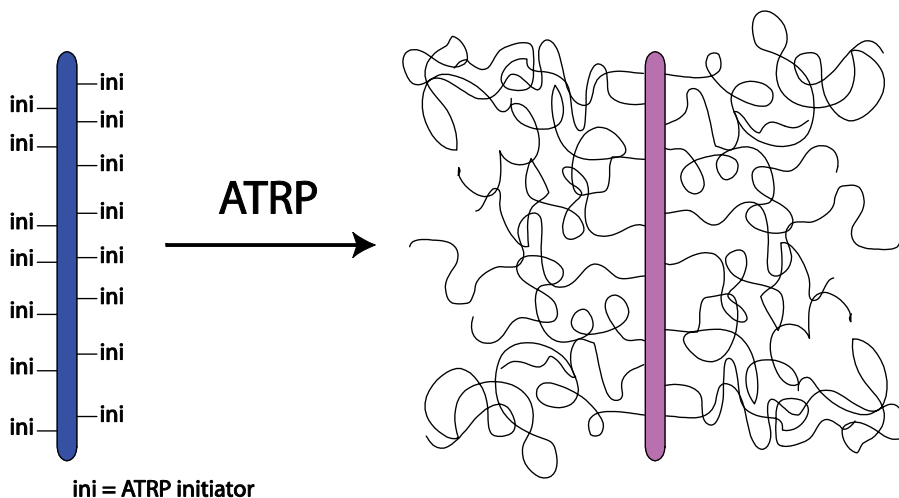


## Chapter 6

26. Q. Cheng, M. Yamamoto and R. C. Stevens, *Langmuir*, 2000, **16**, 5333-5342.
27. Z. Z. Yuan, C. W. Lee and S. H. Lee, *Angew. Chem., Int. Ed.*, 2004, **43**, 4197-4200.
28. A. Potisattiyueng, R. Rojanathanes, G. Turncharern and M. Sukwattanasitt, *Langmuir*, 2008, **24**, 4461-4463.
29. S. Wu, L. F. Niu, J. Shen, Q. J. Zhang and C. Bubeck, *Macromol.*, 2009, **42**, 362-367.
30. N. Mino, H. Tamura and K. Ogawa, *Langmuir*, 1992, **8**, 594-598.
31. W. D. Zhou, Y. L. Li and D. B. Zhu, *Chem. Asian. J.*, 2007, **2**, 222-229.
32. U. Jonas, K. Shah, S. Norvez and D. H. Charych, *J. Am. Chem. Soc.*, 1999, **121**, 4580-4588.
33. J. Song, J. S. Cisar and C. R. Bertozzi, *J. Am. Chem. Soc.*, 2004, **126**, 8459-8465.
34. J. Song, Q. Cheng, S. Kopta and R. C. Stevens, *J. Am. Chem. Soc.*, 2001, **123**, 3205-3213.
35. S. Okada, S. Peng, W. Spevak and D. Charych, *Acc. Chem. Res.*, 1998, **31**, 229-239.
36. D. H. Charych, J. O. Nagy, W. Spevak and M. D. Bednarski, *Science*, 1993, **261**, 585-588.
37. A. Lio, A. Reichert, D. J. Ahn, J. O. Nagy, M. Salmeron and D. H. Charych, *Langmuir*, 1997, **13**, 6524-6532.
38. Y. K. Jung, T. W. Kim, J. Kim, J. M. Kim and H. G. Park, *Adv. Funct. Mater.*, 2008, **18**, 701-708.
39. J. Lee, H. J. Kim and J. Kim, *J. Am. Chem. Soc.*, 2008, **130**, 5010-5011.
40. S. W. Lee, C. D. Kang, D. H. Yang, J. S. Lee, J. M. Kim, D. J. Ahn and S. J. Sim, *Adv. Funct. Mater.*, 2007, **17**, 2038-2044.
41. B. A. Pindzola, A. T. Nguyen and M. A. Reppy, *Chem. Comm.*, 2006, 906-908.
42. B. Hupfer and H. Ringsdorf, *Chem. Phys. Lipids*, 1983, **33**, 263-282.
43. H. Tachibana, Y. Yamanaka, H. Sakai, M. Abe and M. Matsumoto, *Macromol.*, 1999, **32**, 8306-8309.
44. Q. Huo, K. C. Russell and R. M. Leblanc, *Langmuir*, 1999, **15**, 3972-3980.
45. P. Deb, Z. Z. Yuan, L. Ramsey and T. W. Hanks, *Macromol.*, 2007, **40**, 3533-3537.
46. B. Tieke, H. J. Graf, G. Wegner, B. Naegele, H. Ringsdorf, A. Banerjee, D. Day and J. B. Lando, *Colloid Polym. Sci.*, 1977, **255**, 521-531.
47. J. Yoon, Y. S. Jung and J. M. Kim, *Adv. Funct. Mater.*, 2009, **19**, 209-214.
48. M. Masuda, T. Hanada, Y. Okada, K. Yase and T. Shimizu, *Macromol.*, 2000, **33**, 9233-9238.
49. J. H. Fuhrhop, P. Schnieder, E. Boekema and W. Helfrich, *J. Am. Chem. Soc.*, 1988, **110**, 2861-2867.
50. Q. Cheng and R. C. Stevens, *Langmuir*, 1998, **14**, 1974-1976.
51. Q. Huo, S. P. Wang, A. Pisseloup, D. Verma and R. M. Leblanc, *Chem. Comm.*, 1999, 1601-1602.
52. M. van den Heuvel, D. W. P. M. Löwik and J. C. M. van Hest, *Biomacromol.*, 2010, **11**, 1676-1683.
53. J. M. Smeenk, M. B. J. Otten, J. Thies, D. A. Tirrell, H. G. Stunnenberg and J. C. M. van Hest, *Angew. Chem., Int. Ed.*, 2005, **44**, 1968-1971.
54. L. Ayres, *From structural proteins to synthetic polymers*, 2005, Thesis Radboud University Nijmegen
55. R. Matmour, I. De Cat, S. J. George, W. Adriaens, P. Leclere, P. H. H. Bomans, N. Sommerdijk, J. C. Gielen, P. C. M. Christianen, J. T. Heldens, J. C. M. van Hest, D. Löwik, S. De Feyter, E. W. Meijer and A. Schenning, *J. Am. Chem. Soc.*, 2008, **130**, 14576-14583.
56. H.-A. Klok, A. Rosler, G. Gotz, E. Mena-Osteritz and P. Bauerle, *Org. Biomol. Chem.*, 2004, **2**, 3541-3544.
57. G. B. Fields and R. L. Noble, *Int. J. Pept. Protein Res.*, 1990, **35**, 161-214.
58. P. Sieber, *Tetrahedron Lett.*, 1987, **28**, 6147-6150.
59. E. V. Arx, M. Faupel and M. Brugger, *J. Chromatogr.*, 1976, **120**, 224-228.
60. J. W. Van Nispen, J. P. Polderdijk and H. M. Greven, *Recl. Trav. Chim. Pays-Bas*, 1985, **104**, 99-100.
61. E. Kaiser, R. I. Colescot, C. D. Bossing and P. I. Cook, *Anal. Biochem.*, 1970, **34**, 595-598.

## Chapter 7

# ATRP on polydiacetylene-containing peptide amphiphile fibres



Peptide amphiphiles composed of a pentapeptide GAGAE head group and a pentacosadiynoic acid tail were functionalised with an initiator for atom transfer radical polymerization (ATRP). Fibres formed from these peptide amphiphiles were stabilised *via* the topochemical polymerisation of diacetylenes and employed as a macro-initiator for ATRP. A number of monomers, varying in hydrophilic character, were used to investigate the controlled radical polymerization from these fibres, which was performed under relatively dilute conditions in water. Since the spectral properties of the polydiacetylene (PDA) backbone were sensitive to environmental changes, it was investigated whether a shift in the UV-Vis spectrum of PDA could be used as an indication for the progress of polymerisation. Spectral changes could indeed be observed. The largest shift was detected when hydroxy propyl methacrylate (HPMA), the most hydrophobic monomer, was polymerised, and the smallest shift was observed for the hydrophilic oligo ethylene methacrylate (OEGMA) monomers. In the former case the appearance of the fibre changed from blue to pink, in the latter from blue to purple. Electron microscopy and NMR spectroscopy confirmed polymer growth with the fibres as macro-initiator. The resulting conjugates possessed properties both from the polydiacetylene fibrous scaffold and the grafted polymers.

## Introduction

In chapter 6 we described the assembly and polymerisation of pentameric peptides based on the XAGAX sequence, which were N-terminally coupled to pentacosadiynoic acid and which were employed to construct peptide amphiphile (PA) fibres. The high level of order of the alkyl tails made it possible to conduct a topochemical polymerisation of the diacetylenes. The resulting polydiacetylene (PDA) backbone of the fibres was highly conjugated and absorbed visible light, resulting in an intensely coloured polymer. The exact conformation of the backbone determined the absorption spectrum of the polymeric fibres and depended on the environment of the backbone. A change in conformation of the peptides was accompanied by a colour change of the polymer. The PA based PDAs described in chapter 6 were tested for temperature and pH dependent chromism. The most sensitive of the investigated PAs was pentacosadiynoyl GAGAE, in which a glutamic acid was introduced at the periphery of the assemblies and the C-terminus of the amphiphiles was a free acid (PA **1**, Figure 1). The high pH responsiveness was probably caused by the large amount of charges in this PA – at neutral pH both acid groups are negatively charged. Because of the high sensitivity in fibre morphology and polydiacetylene absorption to pH, the responsiveness to other stimuli was anticipated to be large as well.

Besides temperature and pH, sterical hindrance is known to be able to induce a colour change, a principle widely used in PDA sensors<sup>1</sup> (see also chapter 1). We wondered if also the progress of a polymerisation reaction which induces sterical hindrance could be monitored *via* the colour of polydiacetylenes. In this approach, the fibres would function as a macro-initiator. We chose atom transfer radical polymerisation (ATRP) as a polymerisation method from these fibres. There are several controlled polymerisation reactions such as nitroxide mediated polymerisation,<sup>2</sup> reversible addition fragmentation transfer (RAFT)<sup>3</sup> and atom transfer radical polymerisation (ATRP)<sup>4</sup> have been developed. Of these, ATRP has been extensively studied, is easy to use and has a high tolerance to functional groups, allowing polymerisation in presence of esters, alcohols, amines, cyanides and even free acid groups.<sup>5</sup> Furthermore, the incorporation of initiators on a variety of molecules is easy. Because of these features, ATRP has been used to create materials using natural building blocks. It has for example been employed to polymerise peptide-containing methacrylate monomers to produce polymers with peptide side chain functionality.<sup>6-9</sup> Furthermore, also peptides and even protein based initiators have been used in ATRP.<sup>10-15</sup> In an elegant example, the group of Biesalski,<sup>16, 17</sup> used nanotubes assembled from peptide rings designed by Ghadiri *et al.*<sup>18</sup> as ATRP initiator. The peptide rings consisted of alternating D- and L-amino acids that assembled into tubes. An initiator moiety was coupled to one of these cyclic peptides, and after assembly a polymerisation with NIPAM as monomer was initiated on the tubes. During the polymerisation process, however, steric hindrance introduced by the growing polymer caused the nanotubes to break up.<sup>16</sup>

In this chapter the chromism of PDA fibres is combined with ATRP. The covalently stabilised PA assemblies are used as a macro-initiator for the polymerisation.

This research is fundamentally different from the work of Biesalski *et al.* in that the architecture used as a macro-initiator is crosslinked and therefore not dynamic any more. The polymerisation with the self-assembled nanotubes revealed considerable forces are introduced by the polymerisation reaction. Since the assembly we employed was covalently stabilised, these forces were not expected to result in fibre disassembly as was the case for the nanotubes. However, as mentioned above, the PDA backbone is sensitive to stress and therefore the growing polymers were expected to induce a colour change. This effect was investigated with a range of monomers, from hydrophobic (2-hydroxy propyl methacrylate, HPMA, monomer **3**, Figure 1) to hydrophilic (oligo(ethylene glycol) methylester methacrylate (OEGMA)), which were grafted on the fibres. The effect of the polymers on the fibres was expected to differ with their polarity – the less hydrophilic monomers may cause precipitation, while attachment of a more hydrophilic polymer may increase solubility of the only scarcely soluble PDA fibres. In addition to their hydrophilicity, the PEG-resembling monomers display lower critical solution temperature (LCST) behaviour in water upon polymerisation. Below the transition temperature the polymers are soluble, while at higher temperatures they precipitate. This temperature sensitive phase transition was also investigated for its effect on the conformation of the PDA backbone.

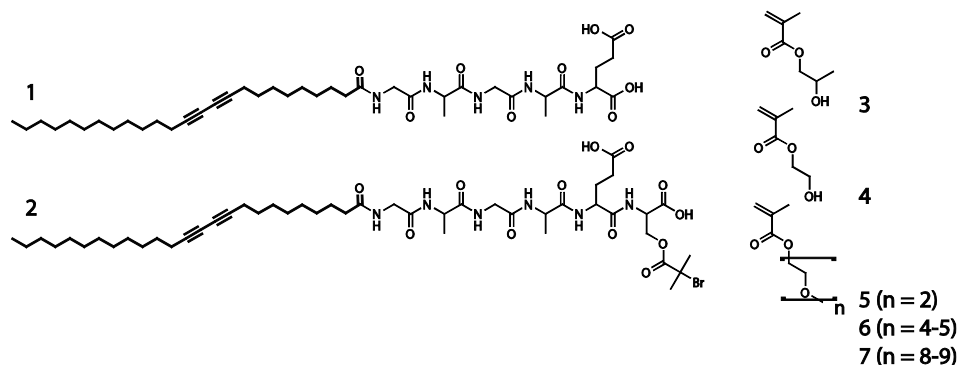


Figure 1. The molecular structures of the two peptide amphiphiles and the monomers used in this study. PA **1** (without) and PA **2** (with) ATRP initiator, and the monomers ranging from hydrophobic (**3**) to hydrophilic (**7**)

## Peptide amphiphile fibres

As already mentioned in the introduction, the most pH responsive peptide amphiphile (PA) described in chapter 6 was pentacosadiynoyl GAGAE (PA **1**, Figure 1) Therefore, we started with this sequence to investigate whether initiation of ATRP from peptide amphiphile fibres was possible and would influence the packing of the polydiacetylene fibre backbone. In order to introduce an initiator functionality at the exterior of the fibres, peptide amphiphile **2** was mixed in with PA **1**. PA **2** contained an additional serine C-terminally, which was functionalised with a 2-bromoisobutyryl bromide initiator moiety. Mixing of the two amphiphiles enabled us to tune the initiator

density on the fibre surface. Because of structural similarity, the two amphiphiles were expected to mix well.<sup>19</sup>

**Synthesis.** The peptide amphiphiles were synthesized on the solid phase as has been described in chapter 6 for PA **1**. This methodology was adapted to introduce an initiator moiety on a serine residue employing the solid phase strategy described by Ayres *et al.*,<sup>20</sup> yielding PA **2**. In short, a Wang resin was provided with a trityl protected serine, after which all other amino acids and the hydrophobic tail were coupled with standard Fmoc-based solid phase peptide synthesis as described for PA **1**. Before cleavage from the resin, the serine side chain was deprotected under mildly acidic conditions, which did not cleave the peptide from the resin. The initiator functionality was attached by addition of 2-bromoisobutyric acid, DIPEA, DMAP and DPCDI as a coupling agent, yielding PA **2** after cleavage from the resin using strongly acidic conditions.

**Fibre formation.** In order to confirm whether the PAs assembled into fibres, transmission electron microscopy (TEM) and circular dichroism (CD) spectroscopy measurements were performed on aqueous solutions of **1**, **2** and a mixture with a 2:1 ratio of PA **1** and PA **2**. All fibres displayed a morphology similar to that of PA **1** (Figure 2). The fibre formation was corroborated by CD spectroscopy, which showed the expected  $\beta$ -sheet signal. Furthermore, for all three samples a  $\beta$ -sheet to random coil transition was observed upon heating to 90 °C, as can be expected for this type of PA assemblies (see chapter 6).

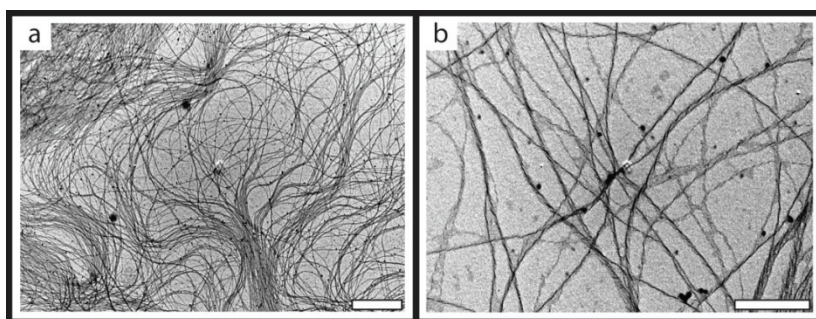


Figure 2. TEM pictures typical for the fibres of PA **1**, PA **2** and their 2:1 mixture. Here PA **1** is shown. The white bars represent a) 2  $\mu$ m, b) 500 nm.

**Diacetylene polymerisation.** The almost crystalline packing of the diacetylene moieties within the hydrophobic tail of the amphiphile allowed these PA fibres to be polymerised using UV light to yield species strongly absorbing in the visible region (see chapter 6). Polymers of PA **1**, PA **2** and their 2:1 mixture (the macro-initiator) yielded slightly different absorption spectra (Figure 3) but all had a blue appearance. Upon heating the maximum absorption wavelength shifted to lower wavelengths, resulting in pink solutions for all three PDAs. The absorption shifted back to blue upon cooling, although the final spectrum contained more short wavelength components than before heating (Figure 4).

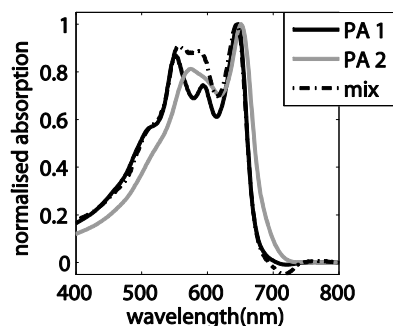


Figure 3. Difference in UV spectra between polymerised fibres of PA 1, PA 2 and the 2:1 mix of these compounds. All three polymers have a blue appearance, although the spectra are not exactly the same.

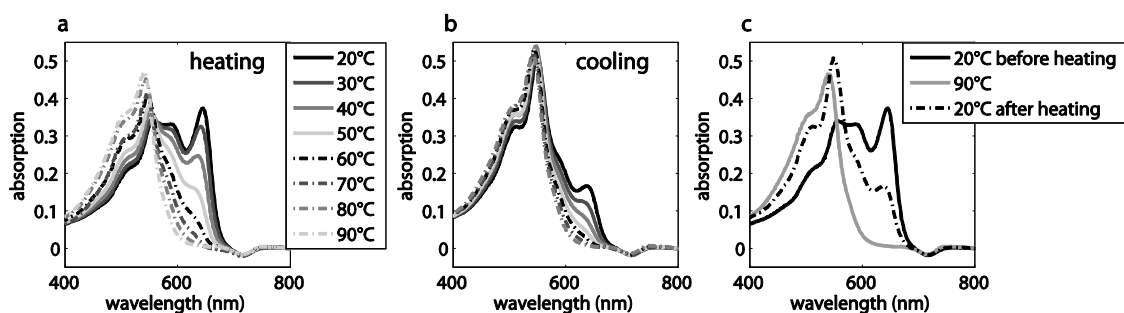


Figure 4. Temperature dependence of UV spectra of the macro-initiator. a) Heating, b) cooling, c) the low and high temperature spectra.

### ATRP conditions explored.

In this study, we intend to exploit the sensitivity of the PDA backbone in PA fibres as a sensor for the grafting of monomers during an ATRP polymerisation. Therefore, in order to ascertain any colour change can be ascribed to the grafting process, reaction conditions and reagents used in ATRP had to be found that did not influence the colour of the PDA fibres.

**Solvent.** Although ATRP is possible in water, it is not trivial and often difficult to reproduce because of high reaction rates.<sup>21-23</sup> Therefore, the possibility of using other solvents was explored. After the topochemical diacetylene polymerisation with UV-light in water, the samples were either diluted in several solvents, or lyophilized and subsequently redissolved in a range of solvents. In both cases, all tested solvents caused the fibres to change colour. Furthermore, after lyophilisation it was not possible to redissolve the PDA fibres. Therefore, all ATRP reactions had to be performed in water.

**Deoxygenation.** Freeze-pump-thawing is a common method for the deoxygenation required for an ATRP reaction. However, freezing the PA fibres is known to damage them (see chapter 3), which was observed also for the macro-initiator fibres, reflected in a colour change of the fibres from blue to purple upon freezing. Therefore, as an alternative method for freeze-pump-thawing, the sample was made oxygen-free by

employing cycles of purging with argon atmosphere and subsequent degassing under vacuum, which did not induce a colour change in the fibres.

**Quenching.** ATRP reactions are frequently quenched by addition of EDTA, which forms a complex with the copper catalyst. However, upon pouring a solution of fibres in an EDTA containing solution, the fibres turned bright pink. Therefore, the ATRP reaction was quenched by bubbling air through the reaction mixture instead.

**Presence of reagents.** ATRP polymerisations are generally performed in a time span from an hour to a day. In order to investigate the effect of the reagents used in ATRP on the colour of the fibres, the fibre colour was monitored over a long period in presence of monomer, copper(I) and bipyridine (bpy). Neither in presence of 2-hydroxy propyl methacrylate (HPMA, monomer **3**, Figure 1) nor for 2-hydroxy ethyl methacrylate (HEMA, monomer **4**, Figure 1) did the colour of the polydiacetylene fibres without initiator change within a few days. Furthermore, performing an ATRP reaction with Ebib as an initiator in presence of fibres had no influence on the fibre colour in the time span of a few days. Only after three weeks, far longer than the time required for the polymerisation, a colour change from blue to pink was observed for HPMA and from blue to purple for HEMA. Therefore, colour change during a polymerisation reaction observed within a few hours time can only be caused by the attachment of monomers to the fibres.

**Concentration.** Gelation of fibres of PA **1** and **2** starts at a concentration of about 1 mM. Because gelation hampers reactions by limiting diffusion, all ATRP reactions on fibres were performed at a total PA concentration of 0.4 mM. These PA fibres also coagulated in solution upon small triggers which were not always obvious or easy to control. The occurrence of this apparent uncontrollable coagulation concealed part of the initiator functionality, hampering the reaction. However, also analysis of the fibres was impossible because of the inhomogeneity and insolubility. The fibre concentration was therefore also kept low in order to avoid these problems.

In summary, ATRP preferably had to be performed in water, at concentrations of 0.4 mM PA. The ratio PA **1**: PA **2** was set to 2:1, yielding an initiator concentration of 0.13 mM. Reaction mixtures were deoxygenated using cycles of alternating argon atmosphere and vacuum and the reaction was quenched by bubbling with air. Furthermore, since fibres changed colour after about three weeks, not only the colour change but also the time scale of this colour change had to be carefully investigated. The concentrations and ratios of the different reagents used in this study are listed and compared to commonly reported values in literature in Table 1.

| <b>Variable</b>         | <b>This study<sup>a</sup></b> | <b>Literature<sup>b</sup></b> | <b>Comparison</b> |
|-------------------------|-------------------------------|-------------------------------|-------------------|
| <b>Concentration PA</b> | <b>0.4 mM</b>                 |                               |                   |
| initiator               | 0.13 mM                       | 20-100 mM                     | 150-750x lower    |
| catalyst                | 0.13 mM                       | 20-100 mM                     | 150-750x lower    |
| monomer                 | 260 mM                        | 1-4 M                         | 4-15x lower       |
| <b>Ratio</b>            |                               |                               |                   |
| initiator:catalyst      | 1:1                           | 1:1                           | identical         |
| initiator:monomer       | 1:2000                        | 1:30 - 1:50                   | 40-70x lower      |

Table 1. Differences between the conditions <sup>a</sup> used in this study and <sup>b</sup> as reported in literature.<sup>4, 15, 24-26</sup> The last column compares these parameters.

## ATRP with a small initiator

Because the reaction conditions which are compatible with the fibres are unusual (see above), the polymerisation reaction was first performed with a small initiator. The initiator Ebib (ethyl 2-bromoisobutyrate) was chosen because of its structural similarity to the initiator moiety on the fibres, and because it has been extensively studied.

**HPMA (3) and HEMA (4).** Polymerisations of HPMA and HEMA in water using the conditions suitable for the fibres (Table 1) yielded a precipitate. Even after removal of water the polymers (**p3** and **p4**) remained insoluble in a range of solvents such as methanol, DMSO, chloroform, water, TFA, NMP and THF. The same was observed by Robinson *et al.*,<sup>25</sup> who suggested either an transesterification of the side chain or a chain transfer to be responsible for crosslinking of pHEMA, a polymer usually soluble in methanol. The insolubility of the reaction product hampered the analysis, but the occurrence of polymerisation was supported by the absence of precipitate if one of the reaction components was left out. Because of the insolubility of the reaction products, we decided to also use more hydrophilic monomers, which are known to yield soluble polymers in water.

**OEGMA<sub>4-5</sub> (6) and OEGMA<sub>8-9</sub> (7).** Polymerisations of the OEGMA monomers with Ebib was followed by monitoring the decrease in monomer intensity in NMR, relative to an internal standard (DMF). The polymerisations generally slowed down after 20 to 30 min, reaching a conversion ranging from 13 to 74 % (average 30 %). This conversion (30 %) amounts to an average of 700 monomers per initiator moiety, yielding a polymer molecular weight average ( $M_n$ ) of about 210 kDa for **p6** and 330 kDa for **p7**. Nevertheless, this approximate value may be an underestimation, since the first sample (**t0**) had to be taken after addition of all reagents. The reaction is very fast and therefore in the few moments before the sample was taken a considerable polymer growth could have taken place. The kinetics (Figure 5) did not resemble that of a living polymerisation, which was reflected in a relatively high polydispersity (about 2) of the polymers. The very low concentration of initiator and catalyst probably caused oxidation of the catalyst, which is supported by an increase in conversion after addition of an amount of fresh catalyst. Furthermore, ATRP in water proceeds with a relatively large amount of radicals, which amounted to a higher polymerisation velocity, a higher termination rate and thus a higher polydispersity. Also the polymer growth in itself may hamper the reaction because the initiator could be 'hiding' in the polymer.



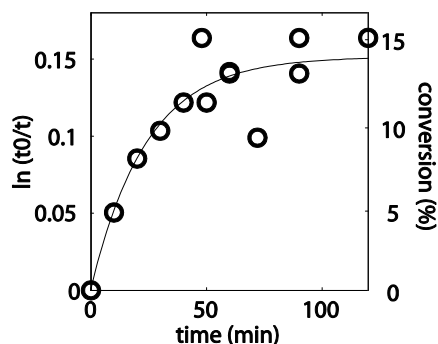


Figure 5. Kinetics for polymerisation of OEGMA<sub>8,9</sub> in water with 0.13 mM Ebib as an initiator. The line is an exponential curve to guide the eye.

In conclusion, although the ATRP reactions were not very controlled, polymerisation occurred for all monomers under the conditions we examined which were supposed to be compatible with our PDA fibres. Polymers of **3** and **4** were found to give an insoluble product.

### ATRP on fibres

Having established that the reaction conditions compatible with the fibres were suitable for ATRP using Ebib as initiator, we moved to the polymerisation from fibres using monomers **3-7** (Figure 1).

**HPMA (3) and HEMA (4).** After addition of all reagents (as listed in Table 1), within a few minutes precipitation was visible and the colour of the fibres changed from blue to purple for both monomers. During the remaining reaction time (about 1 h) the colour of the pHEMA-fibre conjugate changed further to a pinkish purple (Figure 6), while the grafting of pHPMA gave the fibres a bright pink colour. The formation of precipitate hampered monitoring of the spectral change with UV absorption spectroscopy. Therefore reflection spectroscopy was employed to quantify the spectral properties of the fibres, which showed a gradual colour change in the time span of 2 h. When one of the reagents was omitted (i.e. initiator, catalyst or monomer), the colour of the solution did not change within the time scale of the reaction (see above). Therefore, the fast colour change was attributed to the formation of a polymer that induced a conformational change in the PDA backbone of the fibres, probably due to steric crowding. A further indication that polymerisation had taken place was that the mass of the residue after lyophilisation (which removed both solvents and monomers) was larger than that of the fibres from which the reaction had started. However, in addition to a colour change of the fibres, also a white precipitate had formed in the reaction mixture, which could be indicative of polymer not covalently attached to the fibre. This could be due to the presence of molecularly dissolved PA, inherently present in solutions of self-assembled systems in a concentration equal to the critical aggregation concentration (see chapter 3). Another explanation could be that the topochemical diacetylene polymerisation did not go to completion. Nevertheless, the detached polymers cannot be

responsible for the colour change of the fibres, because as mentioned earlier when polymerisation was initiated with Ebib in presence of fibres, no such colour change took place within the time frame of the ATRP. Therefore, we concluded that polymerisation of HPMA and HEMA using the PDA fibres as initiator was successful. Unfortunately, because of the poor solubility, the products of the reaction could not be well characterised.

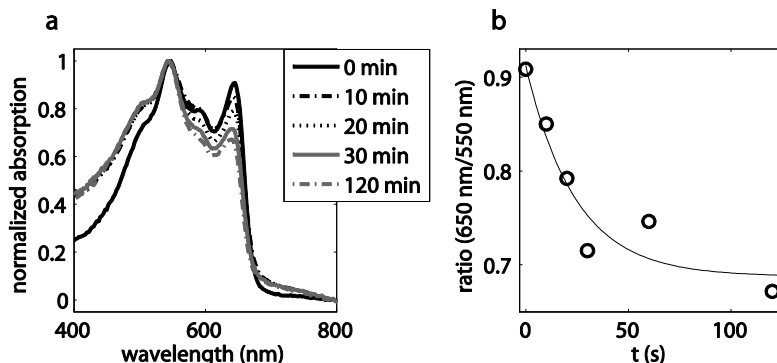


Figure 6. ATRP of HPMA on mixed fibres, monitored with reflection UV spectroscopy. a) UV-Vis spectra, b) 650nm/550nm peak ratio. The dotted line is an exponential curve to guide the eye.

**OEGMA<sub>2</sub> (5).** The polymers of the OEGMA family are more hydrophilic than HPMA and HEMA, which may increase the conjugate solubility and ease its analysis. An interesting additional property of the polymers of the PEG-like monomers is their lower critical solution temperature (LCST) behaviour. Below the transition temperature, the polymers are soluble, while at higher temperatures they precipitate. For polymers of monomers **5** (OEGMA<sub>2</sub>), **6** (OEGMA<sub>4-5</sub>) and **7** (OEGMA<sub>8-9</sub>), the transition temperatures are approximately 26, 64 and 90 °C.<sup>22</sup> The exact transition temperature depends not only on the nature of the monomer, but slightly varies with polymer length, concentration, presence of ions etc.<sup>22, 27</sup>

Upon addition of the copper catalyst and monomer **5** to the fibres, immediately a colour change from blue to purple was observed, accompanied by the formation of a precipitate, resulting in a coloured precipitate in an otherwise colourless solution. After the initial colour change no further spectral variation was observed. Slight heating turned the solution on top of the precipitated fibres turbid, showing the LCST slightly above room temperature characteristic for OEGMA<sub>2</sub> polymers. Since the solution was colourless, these polymers could not be attached to the PDA fibres, but were ‘free’ polymers, a phenomenon which was also observed with grafting using HEMA and HPMA as monomers.

**OEGMA<sub>4-5</sub> (6) and OEGMA<sub>8-9</sub> (7).** For HPMA, HEMA and OEGMA<sub>2</sub> molecularly dissolved initiator (PA **2**) was present, resulting in polymers not attached to the fibres. Therefore, prior to ATRP with monomers **6** and **7**, the fibres were dialyzed to remove any not covalently attached PA **2**. After addition of all reagents (see Table 1) the colour of the fibres changed within minutes from blue to purple, as was also observed for polymerisation with the other monomers. During the rest of the reaction time the colour did not change any further. This resembled the polymerisation with OEGMA<sub>2</sub>. During

the reaction, the fibres stayed in solution, in contrast with polymerisations of monomers **3-5**. The larger hydrophilicity of monomers **6** and **7** may have prevented the fibres from complete precipitation, although the solutions were not homogeneous.

The reaction progress was monitored using  $^1\text{H-NMR}$  spectroscopy; the decrease of the vinyl monomer peaks was compared to DMF as an internal standard. Similarly to the polymerisations with Ebib, after 20 to 30 min the reaction stopped, at conversions of roughly 30-40% (Figure 7), although as already discussed before, the actual conversion may be higher because the conversion at the first time point may already have been considerable. Likewise, when new Cu(I) was added to the reaction, the polymerisation resumed, although again only for a limited time. These results suggested the oxidation of the catalyst, as has been pointed out before. Therefore higher conversions may be obtained by starting with more catalyst or by using a catalyst which is constantly regenerated *in situ*. The latter can be realized using ARGET, a method similar to ATRP, which can be applied with a smaller amount of copper in presence of air.<sup>28</sup>

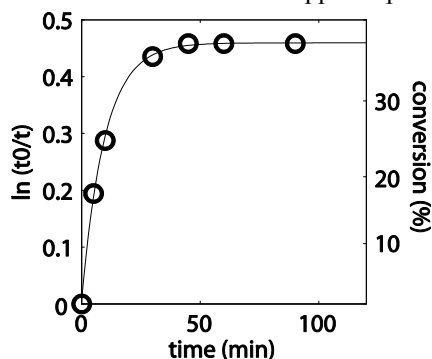


Figure 7. Kinetics of polymerisation of OEGMA<sub>8,9</sub>, with the mixed fibres as initiator. The line is an exponential curve to guide the eye.

To confirm the polymers were covalently attached to the fibres, after polymerisation the reaction mixture was dialyzed again. Had the polymerisation taken place free in solution, the polymers were expected to be removed upon dialysis. Although a membrane with 300 kDa cut-off was employed, the polymers with a calculated average weight of 330 kDa were still expected to diffuse through the membrane, since polymers are known to pass membranes with a cut-off made for proteins of much smaller molecular weight. After the dialysis step, the polymer signal in NMR had not changed, showing that indeed polymerisation with fibres as macro-initiator had taken place. Because of the size of the fibres, no other analyses to assess the length of the polymer were performed.

### Fibre-polymer conjugate properties.

The fibre-polymer hybrids were studied with electron microscopy (for **p3**, **p4**, **p6** and **p7**) and with UV spectroscopy for the soluble conjugates (**p6** and **p7**). TEM revealed the presence of fibres in all samples. At longer reaction times denser layers of

material were present that were difficult to visualise. Therefore, it was unclear what this material represented, indicating the limitations of TEM. A further disadvantage of TEM was that only part of the sample was imaged. The samples were prepared by floating a grid on a drop of reaction mixture, and therefore only that part of the mixture which adhered to the grid was visible. It is unlikely that the large, precipitated products would be present on the grids and if they were, they probably formed a layer too dense to visualise with transmission electron microscopy methods. Therefore, scanning electron microscopy (SEM) was employed to analyse the reaction mixture of **p3** after lyophilisation revealing a large change in morphology between start and end of polymerisation (Figure 8). This change probably reflects the difference between fibre and fibre conjugated with polymer, although we cannot exclude that it is due to the precipitation during the reaction.

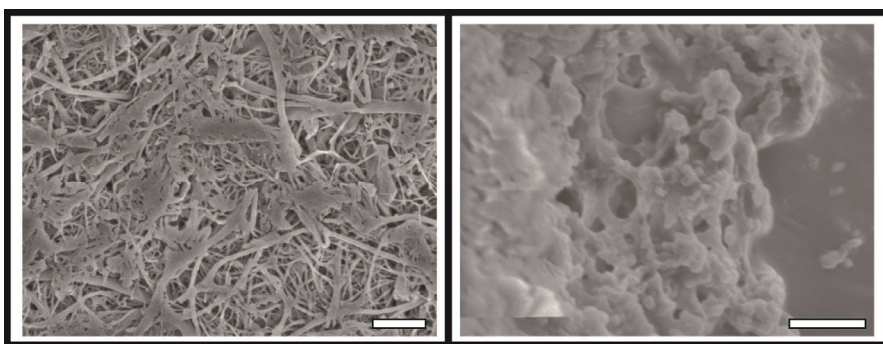


Figure 8. SEM pictures of HPMA grafted PA fibres. At the a) start ( $t = 0$ ), and the b) end ( $t = 1$  day) of the polymerisation. The white bars represent  $1 \mu\text{m}$ .

The soluble grafted fibres with **p6** and **p7** were analysed with UV spectroscopy as well. Because the PDA showed a temperature dependent spectral shift and polyOEGMAs were chosen for their LCST behaviour, the temperature dependence of the UV-Vis absorption was investigated. The purple reaction products changed colour upon heating to bright pink (Figure 9a), as was also observed for the fibre on which no ATRP had been performed (Figure 4a). In contrast to ungrafted fibres, the hybrids precipitated after heating above  $67 \text{ }^\circ\text{C}$  and  $93 \text{ }^\circ\text{C}$  for **p6** and **p7**, respectively, impeding the UV-Vis spectral measurements. The precipitation was reversible and indicated LCST behaviour, at values similar to those reported in literature.<sup>22</sup> The turbidity was analysed using the UV-Vis spectroscopy signal at  $800 \text{ nm}$ , which is mainly caused by scattering. This signal was used to determine the transition temperature (Figure 9b for **p6**). From these measurements we concluded that the conjugates exhibited the behaviour of both components – the colour change of the fibres and the LCST from the poly-OEGMA – which seemed largely independent.

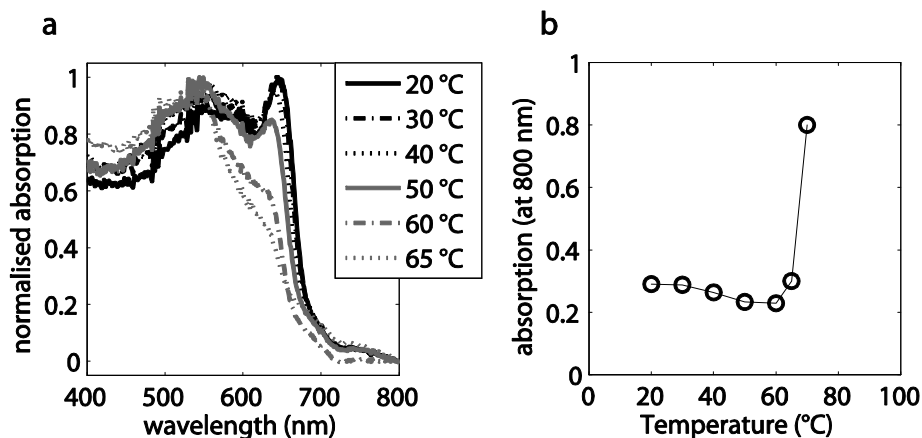


Figure 9. Temperature dependence of fibres grafted with OEGMA<sub>4.5</sub>. a) Colour change up to the temperature at which the fibres precipitated. b) The absorption at 800 nm.

## Conclusions

We have successfully prepared polydiacetylene containing fibres which could be employed as an initiator in an ATRP reaction. The optical properties of the macro-initiator were dependent on the polymerisation reaction. The macro-initiator fibres were successfully used in ATRP reactions with a range of monomers. Typically, grafting hydrophobic monomers induced a larger spectral shift than grafting hydrophilic monomers: HPMA yielded a bright pink conjugate and HEMA a pinkish purple product, while grafting the increasingly hydrophilic PEG-like polymers caused an immediate colour change from blue to purple that did not change any further during the course of the reaction. The resulting conjugates combined properties of the polydiacetylene fibre and the attached polymer, changing colour when heated whilst exhibiting LCST behaviour.

## Acknowledgements

I want to thank Nearchos Tsihchlis i Spithas who performed most of the work described in this chapter and René Brinkhuis for the daily guidance of Nearchos while I was in Bristol, UK.

## Experimental section

**General.** All starting materials were obtained from commercial suppliers and used as received. Thin layer chromatography was performed on Kieselgel F-254 pre-coated silica plates or RP-8 F-254s. Visualization was accomplished with TDM and chlorine gas<sup>29</sup> or by an aqueous 0.1 M potassium permanganate solution. Column chromatography was carried out on Merck silica gel 60 (230-400 mesh ASTM). <sup>1</sup>H-NMR spectra were recorded on a Varian Mercury, 400 MHz.

As a solvent shift reference DMSO-d<sub>5</sub> ( $\delta = 2.50$  ppm) was used. Mass spectra were recorded on a JEOL AccuTOF-CS spectrometer. GPC spectra were recorded on a Shimadzu LC-10AD chromatograph, with an RID10A refractogram and an SPD-10AV UV-Vis detector at 30 °C with THF as a solvent at a flowrate of 1 mL/min, with polystyrene calibration.

**Synthesis.** PA **1** was synthesized as described in chapter 6. The synthesis of PA **2** started similarly with 1 g Wang resin (0.6 mmol/g), swollen in DMF. Fmoc-Ser(Trt)-OH (1.0 g, 1.8 mmol, 3 eq) was dissolved in DCM, to which a solution of HOBt (3.6 eq, 6.5 mL 1M in DMF) and DIPCDI (3.3 eq, 5.9 mL 1M in DMF) was added, after which the mixture was added to the swollen resin. Overnight reaction gave an Fmoc-Ser(Trt) functionalized resin of 0.51 mmol/g (86%, detected with UV absorption spectroscopy<sup>30</sup>). The subsequent attachment and deprotection of Fmoc protected amino acids and pentacosadiynoic acid was performed analogous to the synthesis of PA **1**. After coupling of pentacosadiynoic acid, the serine was deprotected with 20 mL 3% TFA and 5% TIS in DCM (5 min), followed by rinsing with DCM, and addition of another 20 mL 3% TFA and 5% TIS in DCM, (20 min). After washing the resin (DCM, DMF and DCM), DMAP (6 eq, 660 mg, 5.4 mmol), DIPCDI (6 eq, 836  $\mu$ L, 5.4 mmol) and DIPEA (6 eq, 918  $\mu$ L, 5.4 mmol) were added to the resin which was suspended in DCM, after which 2-bromo isobutyric acid (900 mg, 6 eq, dissolved in 10 mL DCM) was added, and the mixture was shaken overnight. The resin was washed (DCM, DMF and MeOH) and left to dry. The product was cleaved from the resin with 10 mL TFA:TIS:water (95:2.5:2.5, 2h). The product was precipitated in diethyl ether, and separated from the solvent through centrifugation. After drying, PA **1** was lyophilized from acetic acid to yield 225 mg of a white solid. Column chromatography (eluent: CHCl<sub>3</sub>:MeOH:water 65:25:4) afforded 158 mg (0.16 mmol, 31%) of a white solid.

**PA 1 (C<sub>24</sub>H<sub>41</sub>C(O)-Gly-Ala-Gly-Ala-Glu-OH):**

TLC: R<sub>f</sub> 0.12 (eluent: MeOH/ CHCl<sub>3</sub>/ H<sub>2</sub>O (25:65:4).

<sup>1</sup>H-NMR [DMSO-d<sub>6</sub>]:  $\delta$  0.85 (t, 3H), 1.24 (m, 32H), 1.44 (m, 6H), 1.66 (m, 1H), 1.84 (m, 1H), 2.10 (t, 2H), 2.16 (t, 2H), 2.27 (t, 4H), 3.68 (m, 4H), 4.00 (m, 1H), 4.24 (m, 2H), 7.75 (d, 1H), 8.01 (d, 1H), 8.33 (m, 3H).

Mass spectrometry: Calc for [C<sub>40</sub>H<sub>65</sub>N<sub>5</sub>O<sub>9</sub> + H]<sup>+</sup> 760.4861, found 760.4866.

**PA 2 (C<sub>24</sub>H<sub>41</sub>C(O)-Gly-Ala-Gly-Ala-Glu-Ser(C(O)C(CH<sub>3</sub>)<sub>2</sub>Br)-OH):**

TLC: R<sub>f</sub> 0.20 (eluent: MeOH/ CHCl<sub>3</sub>/ H<sub>2</sub>O (25:65:4).

<sup>1</sup>H-NMR [DMSO-d<sub>6</sub>]:  $\delta$  0.85 (t, 3H), 1.1-1.3 (m, 32H), 1.4-1.5 (m, 6H), 1.8-1.85 (m, 8H), 2.10 (t, 2H), 2.18 (m, 2H), 2.27 (t, 4H), 3.65-3.75 (m, 4H), 4.05-4.15 (m, 3H), 4.20-4.32 (m, 2H), 4.53 (d, 1H), 7.54 (s, 1H), 7.88 (d, 1H), 8.04 (d, 1H), 8.26 (s, 1H), 8.52 (s, 2H).

Mass spectrometry: Calc for [C<sub>47</sub>H<sub>75</sub>BrN<sub>6</sub>O<sub>12</sub> + H]<sup>+</sup> 995.4705, found 995.4744.

**Fibre preparation.** The amphiphiles were dispersed in milli-Q at concentrations of either 0.2 or 1.0 mg/mL. The samples were heated to 50 °C for 30 min, followed by 15 min sonication at that temperature. Subsequently, the samples were heated to 90 °C and allowed to cool to room temperature.

**PDA polymerisation.** Polymerisations were carried out on 1 mg/mL samples in a 15 mL glass vial (containing approximately 10 mL fibre solution), which was open and illuminated from above using either a UVASPOT 400T lamp with a sample-light source distance of 22 cm for 1 min, or a Bluepoint 2 UV lamp with a lamp-sample distance of 10 cm for 999 s. These two conditions gave the same UV spectrum.

**Circular dichroism spectroscopy.** Measurements were carried out on fibres prepared following the standard procedure (see above) at a concentration of 0.2 mg/mL using a 1 mm quartz cell. The spectra were recorded on a JASCO J-810 spectropolarimeter. To obtain temperature curves, a heating or cooling rate of 3 °C/min was used. Measuring the peak intensity in time was hampered by the presence of the diyne functionalities which readily polymerised when illuminated with the short wavelengths used for the CD measurements. Therefore, spectra

were recorded every 10 °C (265-185 nm, 100 nm/min), and the shutter was closed (5 µm) between these measurements.

**UV spectroscopy.** *Absorption:* Measurements were carried out at a concentration of 1.0 mg/mL using a 1 mm quartz cell. The spectra were recorded on a Varian Cary-50 spectrometer.

*Reflection:* Samples taken during the polymerisation were transferred to a 1 mm quartz cell and the spectra were recorded on a Perkin-Elmer Lambda 35 UV/Vis spectrometer.

**Transmission electron microscopy.** TEM samples were prepared by floating a carbon-coated copper grid on a peptide amphiphile solution of 0.2 mg/mL for 5 min, followed by removal of residual water by blotting with a paper filter. The samples were visualized using a JEOL 1010 transmission electron microscope set on an accelerating voltage of 60 kV.

**Scanning electron microscopy.** SEM samples were prepared by attaching a lyophilised fibre sample to a SEM sample holder using double-sided carbon tape. The samples were coated with 1.5 nm of platinum using a Cressington 208HR sputter coater, and visualized using a JEOL 6330 Cryo FESEM.

### ATRP

All ATRP reactions were performed under Argon using standard Schlenk conditions. Solvents were deoxygenated with roughly 10 cycles alternating between vacuum and argon.

**Removal of stabilisers.** Stabilisers in HPMA and HEMA (monomers **3** and **4**) were removed by distillation of the monomers, which were subsequently stored under argon at -20 °C prior to use. Stabilisers in the OEGMA monomers (**5**, **6** and **7**) were removed by column chromatography on neutral Al<sub>2</sub>O<sub>3</sub> after which the monomers were used immediately.

**Preparation catalyst solution.** For HPMA (**3**), HEMA (**4**) and OEGMA<sub>2</sub> (**5**): Under argon atmosphere, CuBr (1.44 mg, 0.01 mmol, 1eq) was mixed with 2,2'-bipyridine (bpy, 3.28 mg, 0.021 mmol, 2.1 eq) in 5 mL deoxygenated milli Q water. The solution was left stirring for 30 min to ensure formation of the catalyst complex (Cu(bpy)<sub>2</sub>).

For OEGMA<sub>4,5</sub> (**6**) and OEGMA<sub>8,9</sub> (**7**): CuCl (1 eq, 10 mg, 0.1 mmol) was mixed with 2,2'-bipyridine (bpy, 32 mg, 0.21 mmol, 2.1 eq) in 4 mL deoxygenated deuterium oxide. The solution was left stirring for 30 min to ensure formation of the catalyst complex (Cu(bpy)<sub>2</sub>).

#### ATRP with monomers **3**, **4** and **5**.

**Preparation of the initiator solutions.** *Ebib:* Ethyl 2-bromoisobutyrate (0.067 mmol, 9.8 µL) was dissolved in 10 mL milli Q and deoxygenated.

*Fibres:* PA **1** (5.1 mg, 6.6 µmol) and PA **2** (3.3 mg, 3.3 µmol) were mixed and dissolved in 10 mL milliQ. Fibres were prepared and polymerised following the standard procedures.

**Polymerisation.** Monomer (2000 eq, 1.32 mmol, (190 mg for **3**, 172 mg for **4**, 190 mg for **5**) corresponding to 264 mM in the reaction mixture) and initiator stock solution (0.67 µmol, (2 mL of the fibres or 100 µL *Ebib* stock solution), corresponding to 0.13 mM in the reaction mixture) were dissolved in milli Q to a volume of 4.6 mL, after which the mixture was deoxygenated. Catalyst solution (0.8 µmol, 0.4 mL, corresponding to 0.16 mM) was added and the reaction mixture was stirred overnight.

#### ATRP with monomers **6** and **7**.

**Preparation of the initiator solutions.** *Ebib:* Ethyl 2-bromoisobutyrate (0.077 mmol, 11.3 µL) was dissolved in 2 mL D<sub>2</sub>O and deoxygenated.

*Fibres:* PA **1** (5.1 mg, 6.6 µmol) and PA **2** (3.3 mg, 3.3 µmol) were mixed and dissolved in 10 mL milli-Q. Fibres were prepared and polymerised following the above mentioned procedures. 2 mL

of such fibre solution was dialyzed using a membrane with a molecular weight cut-off (MWCO) of 10-12 kDa (3x 3h against 500 mL milli Q water followed by 3 x 3h against 30 mL D<sub>2</sub>O).

**Polymerisation.** Monomer (2000 eq, 1.32 mmol, (396 mg for **6** and 627 mg for **7**) corresponding to 264 mM in the reaction mixture), initiator stock solution (0.67 μmol, (2 mL of the fibres or 17 μL Ebib) corresponding to 0.13 mM in the reaction mixture) and DMF (150 μL, 2 mmol) were dissolved in milli Q water to a volume of 5.0 mL, after which the mixture was deoxygenated. Catalyst solution (0.7 μmol, 29 μL, corresponding to 0.14 mM) was added and the reaction mixture was stirred. NMR samples of 0.5 mL were taken at regular intervals.

**Analysis.** *Ebib*: During the reaction, 0.5 mL samples were taken and analysed with NMR, by comparing the vinyl monomer signals (at 6.0 and 5.6 ppm) with the DMF aldehyde signal (at 7.8 ppm). With GPC  $M_w/M_n$  of the product was determined to be 2.

*Fibres*: During the reaction, 0.5 mL samples were taken and analysed with NMR as described above. After NMR and UV-Vis spectroscopy measurements, the reaction mixture was dialyzed with a 300 kDa membrane (3x3h against 500 mL water, followed by 3x3 h against 30 mL D<sub>2</sub>O) to remove any polymer not attached to the fibre. After dialysis, the conjugate was analysed with NMR spectroscopy.

## References

1. M. A. Reppy and B. A. Pindzola, *Chem. Comm.*, 2007, 4317-4338.
2. C. J. Hawker, A. W. Bosman and E. Harth, *Chem. Rev.*, 2001, **101**, 3661-3688.
3. J. Chiefari, Y. K. Chong, F. Ercole, J. Krstina, J. Jeffery, T. P. T. Le, R. T. A. Mayadunne, G. F. Meijs, C. L. Moad, G. Moad, E. Rizzardo and S. H. Thang, *Macromol.*, 1998, **31**, 5559-5562.
4. X. S. Wang and S. P. Armes, *Macromol.*, 2000, **33**, 6640-6647.
5. K. Matyjaszewski and J. H. Xia, *Chem. Rev.*, 2001, **101**, 2921-2990.
6. L. Ayres, G. M. Grotenbreg, G. A. van der Marel, H. S. Overkleeft, M. Overhand and J. C. M. van Hest, *Macromol. Rapid Commun.*, 2005, **26**, 1336-1340.
7. L. Ayres, *From structural proteins to synthetic polymers*, 2005, Thesis Radboud University Nijmegen
8. L. Ayres, K. Koch, P. Adams and J. C. M. van Hest, *Macromol.*, 2005, **38**, 1699-1704.
9. L. Ayres, M. R. J. Vos, P. Adams, I. O. Shklyarevskiy and J. C. M. van Hest, *Macromol.*, 2003, **36**, 5967-5973.
10. M. G. J. ten Cate, H. Rettig, K. Bernhardt and H. G. Börner, *Macromol.*, 2005, **38**, 10643-10649.
11. H. Rettig, E. Krause and H. G. Börner, *Macromol. Rapid Commun.*, 2004, **25**, 1251-1256.
12. Y. Mei, K. L. Beers, H. C. M. Byrd, D. L. Vanderhart and N. R. Washburn, *J. Am. Chem. Soc.*, 2004, **126**, 3472-3476.
13. S. Venkataraman and K. L. Wooley, *Macromol.*, 2006, **39**, 9661-9664.
14. D. Bontempo and H. D. Maynard, *J. Am. Chem. Soc.*, 2005, **127**, 6508-6509.
15. W. P. Gao, W. G. Liu, J. A. Mackay, M. R. Zalutsky, E. J. Toone and A. Chilkoti, *Proc. Natl. Acad. Sci. U. S. A.*, 2009, **106**, 15231-15236.
16. J. Couet and M. Biesalski, *Macromol.*, 2006, **39**, 7258-7268.
17. J. Couet, J. D. Jeyaprakash, S. Samuel, A. Kopyshv, S. Santer and M. Biesalski, *Angew. Chem., Int. Ed.*, 2005, **44**, 3297-3301.
18. M. R. Ghadiri, J. R. Granja, R. A. Milligan, D. E. McRee and N. Khazanovich, *Nature*, 1993, **366**, 324-327.
19. M. van den Heuvel, D. W. P. M. Löwik and J. C. M. van Hest, *Biomacromol.*, 2010, **11**, 1676-1683.
20. L. Ayres, P. Hans, J. Adams, D. Löwik and J. C. M. van Hest, *J. Polym. Sci., Part A: Polym. Chem.*, 2005, **43**, 6355-6366.
21. D. M. Haddleton, S. Perrier and S. A. F. Bon, *Macromol.*, 2000, **33**, 8246-8251.
22. J. F. Lutz, *J. Polym. Sci., Part A: Polym. Chem.*, 2008, **46**, 3459-3470.
23. G. Coullerez, A. Carlmark, E. Malmstrom and M. Jonsson, *J. Phys. Chem. A*, 2004, **108**, 7129-7131.
24. D. M. Jones and W. T. S. Huck, *Adv. Mater.*, 2001, **13**, 1256-1259.

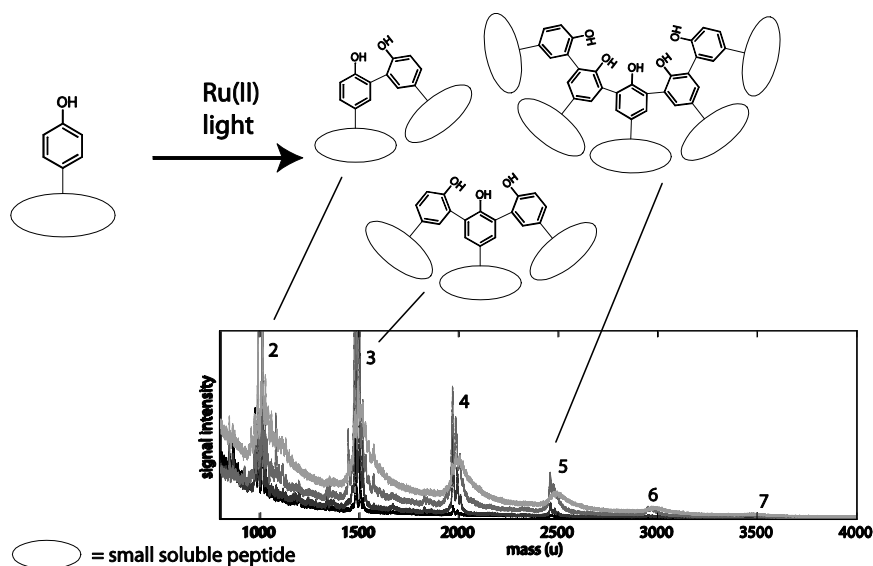


## Chapter 7

25. K. L. Robinson, M. A. Khan, M. V. D. Banez, X. S. Wang and S. P. Armes, *Macromol.*, 2001, **34**, 3155-3158.
26. X. S. Wang, S. F. Lascelles, R. A. Jackson and S. P. Armes, *Chem. Comm.*, 1999, 1817-1818.
27. S. Han, M. Hagiwara and T. Ishizone, *Macromol.*, 2003, **36**, 8312-8319.
28. K. Matyjaszewski, H. C. Dong, W. Jakubowski, J. Pietrasik and A. Kusumo, *Langmuir*, 2007, **23**, 4528-4531.
29. E. V. Arx, M. Faupel and M. Brugger, *J. Chromatogr.*, 1976, **120**, 224-228.
30. Novabiochem catalog 2000, p. p4

## Chapter 8

# Threading of small peptides and self-assembled fibres using ruthenium as a catalyst.



The highly elastic protein resilin contains many tyrosine crosslinks, which give this structural protein its characteristic mechanical properties. In order to mimic its elasticity with self-assembled fibres, a light-initiated, ruthenium-catalysed crosslinking method was employed. We applied this versatile coupling reaction on tyrosine containing, small, soluble peptides and showed the formation of tyrosine oligomers, leading us to use the term threading rather than crosslinking. When the reaction was performed on self-assembled peptide amphiphile fibres, the threading was limited and only a small amount of dimers was observed.

## Introduction

Resilin is an elastic protein, present in many arthropods.<sup>1</sup> It plays an important role in the jumping ability of the flea, the vocalisation of cicades and moths and the flight system of the dragon fly (amongst others).<sup>2</sup> As in other elastic proteins, such as elastin and silk, the protein consists of many repeats of the same motif,<sup>2, 3</sup> and has a high glycine content, which is probably responsible for its high flexibility. However, the exact mechanism for elasticity may be different for elastin and resilin. In elastin the hydrophobic interactions between strands of the basic repeat sequence (VPGVG or a similar motif) are supposed to play a role,<sup>3</sup> but resilin is found to have much more hydrophilic repeats (AQTPSSQYGAP in the african malaria musquit<sup>3</sup> and GGRPSDSYGAPGGGN in *D. Melanogaster*<sup>2, 4</sup>).<sup>5</sup> In resilin, almost no chain-chain interactions are present between the protein chains. Their movement is only limited by the covalent tyrosine bridges between protein chains which are probably also the cause of the observed elasticity.<sup>6</sup> Besides elasticity, the crosslinking also causes a high temperature stability; resilin is temperature stable up to at least 125 °C,<sup>1</sup> while heating causes decrease of the elastic properties in elastin. Although the biosynthesis of resilin has never been clarified,<sup>6</sup> the coupling reaction is probably catalysed by peroxidases,<sup>6-9</sup> which are known to catalyse tyrosine crosslinking *in vitro*,<sup>9, 10</sup> and are shown to be present in cells which produce resilin.<sup>8</sup> A proposed mechanism of tyrosine crosslinking is depicted in Figure 1.<sup>9, 11</sup>

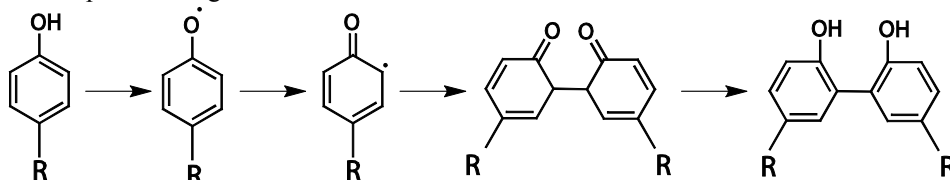


Figure 1. Proposed crosslinking mechanism for tyrosine catalysed by peroxidases.

The products from crosslinking in resilin are both di- and trityrosine,<sup>12</sup> and for other proteins even larger oligomers have been observed for coupling *in vitro*.<sup>13-15</sup> In synthetic systems, the coupling reaction of tyrosine can also be performed using more accessible catalysts than enzymes such as for example ruthenium(II), in presence of a radical initiator.<sup>16</sup> The proposed mechanism for this reaction (Figure 2) is similar as described for the enzyme catalysed reaction described above.<sup>16</sup> Light activates ruthenium(II), of which one electron is subsequently transferred to ammonium persulfate. The resulting ruthenium(III) oxidizes tyrosine, after which a nearby tyrosine (though this can also be a sulfur or amine group) can attack the radical, thereby coupling the two residues. However, the reaction is shown to still work if both hydrogens *ortho* to the tyrosine alcohol are iodated, indicating an incomplete understanding of the reaction.<sup>17</sup>

The crosslinking process is very fast and has been employed to covalently link protein-complexes in order to investigate protein-protein interactions.<sup>18</sup> The same principle was used for crosslinking a receptor with its ligand – the molecules were in close proximity and could therefore selectively be crosslinked.<sup>17</sup> Furthermore, this light-

initiated crosslinking has also been utilized to produce functional elastic materials. Crosslinking of pro-resilin (not-crosslinked resilin) using ruthenium as a catalyst yielded a material with similar properties as natural resilin.<sup>2, 4</sup> Moreover, not only pro-resilin could be used to create very elastic material upon crosslinking of the tyrosine moieties; elastic constructs were also observed by coupling of tyrosine residues in fibrinogen.<sup>19</sup> This protein consists of three polypeptide chains, of which two are rich in tyrosine ( $\beta$ -chain 4.9 %,  $\gamma$ -chain 5.6 % and  $\alpha$ -chain 0.6 %). All three chains were incorporated in the high-molecular weight product. In another approach, hydrogels were reinforced by crosslinking the individual strands.<sup>20</sup>

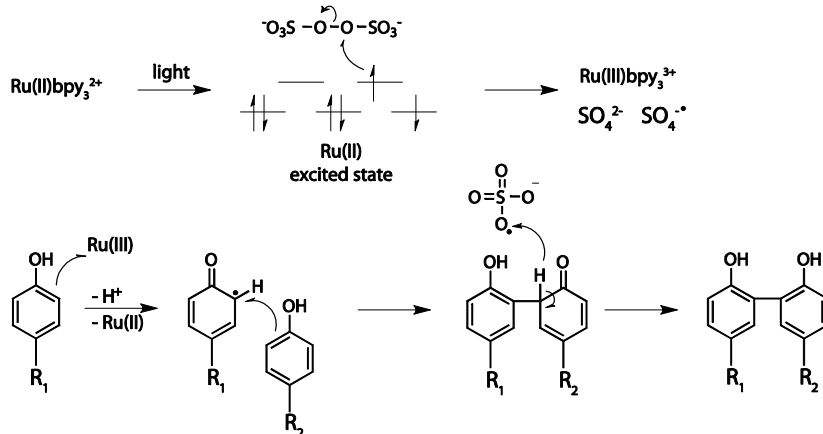


Figure 2. Crosslinking reaction of tyrosines, catalysed with ruthenium(II), ammonium persulfate and light.

Surprisingly, for all these examples, only dityrosine coupling and no larger oligomer crosslinking (threading) was observed. Moreover, ruthenium-catalyzed crosslinking has not been used yet on smaller peptides or to stabilise self-assembled systems. In this chapter we want to use the ruthenium-based tyrosine crosslinking to construct a resilin-mimetic material out of a self-assembled system, to make materials with the best of both worlds – the dynamics and the synthetic functionality accessible *via* the supramolecular building blocks and the elastic properties of the crosslinked resilin. These materials may exhibit a tunable viscosity and morphology. To investigate the scope of the ruthenium catalysed threading reaction and examine its products in somewhat more detail, it was first performed on small model peptides, which are relatively easy to analyze. We investigated if the coupling yielded only dimeric species or whether threading could also be observed, giving rise to the formation of larger oligomeric structures. Next the coupling reaction was extended to two self-assembled fibres, one based on  $\alpha$ -helices and coiled coil assembly, the other on a  $\beta$ -sheet assembly, to investigate the possibilities to use this coupling technique to create elastic self-assembled materials.

## Threading small peptides

The rather insoluble amino acid tyrosine (2.5 mM in water of neutral pH at RT) is the simplest molecule to test the ruthenium-catalysed crosslinking reaction on. After addition of ruthenium(II)trisbipyridine and ammonium persulfate (APS) and exposure to light, a precipitate formed, indicating the formation of even less soluble dimers and multimers. The formation of this insoluble material hampered the analysis of the products, but NMR and fluorescence spectroscopy both showed the disappearance of the starting material. Moreover, the progress of the reaction was corroborated by the appearance of a fluorescent peak around 410 nm, indicative for dityrosine. Therefore, dityrosine was at least slightly soluble and the precipitate may indicate larger oligomers.

In order to avoid the solubility problems associated with tyrosine, the more soluble peptide AKAY was employed. This peptide was designed to be water soluble, was synthetically easy accessible and still small enough to be analysed with NMR, HPLC and MALDI-TOF. Because of its easy sample preparation and assignment of the products, MALDI-TOF was used to monitor the reaction progress. The crosslinking of AKAY using ruthenium(II) as a catalyst was found to be very fast. Already in daylight part of the monomeric species was converted to dimers and multimers (black line in Figure 3a). After a few minutes illumination with a 60 W lamp the monomeric species had almost completely disappeared and up to hexamers were observed with MALDI (Figure 3a). However, assuming that in MALDI larger compounds are generally more difficult to measure because of less efficient ionisation, the formation of even larger species cannot be excluded. In Figure 3b the signal intensity (peak height in MALDI) for each oligomer is plotted in time. From this plot, the decrease of monomeric and increase of oligomeric species is clearly visible. As expected, the larger compounds reached their maximum intensity after longer illumination than the smaller oligomers.

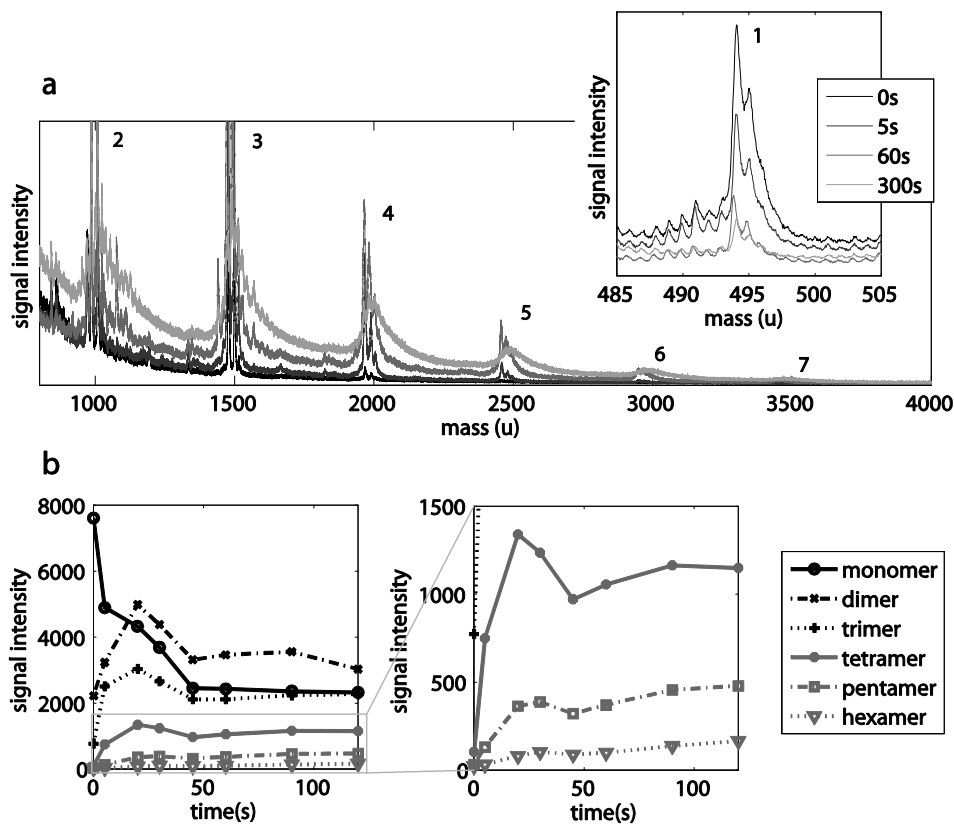


Figure 3. Crosslinking of AKAY monitored with MALDI-TOF a) Spectra at four time points in the reaction indicated with different greyscales. The insert shows the peak decrease of the monomer. The numbers at each peak show the numbers of peptide in the oligomer. Note that the x-axes of the plot and the insert do not overlap. b) A kinetic plot in which for each oligomer the intensity is plotted against time. The right plot is a zoom of the left plot, showing the lower intensity region.

In the aromatic region of the NMR spectrum (Figure 4) the peaks indicative of monomeric tyrosine decreased and a few smaller peaks appeared indicative for coupled product. Also in this experiment crosslinked species were already present in the samples which had only been exposed to daylight during sample preparation, indicating the high reaction speed. Typically, not only the aromatic peaks, but also other signals associated with tyrosine monomer reduced in size (peaks A and B, Figure 4). A detailed analysis was difficult due to the presence of multiple oligomers, and, since peaks A and B also reduced in size, probably also of other crosslinked species. Duroux-Richard *et al.* showed that crosslinking still proceeds if both protons *ortho* to the alcohol of the tyrosine were replaced by iodine,<sup>17</sup> which indicated that the ruthenium-catalysed threading reaction is not yet well understood.

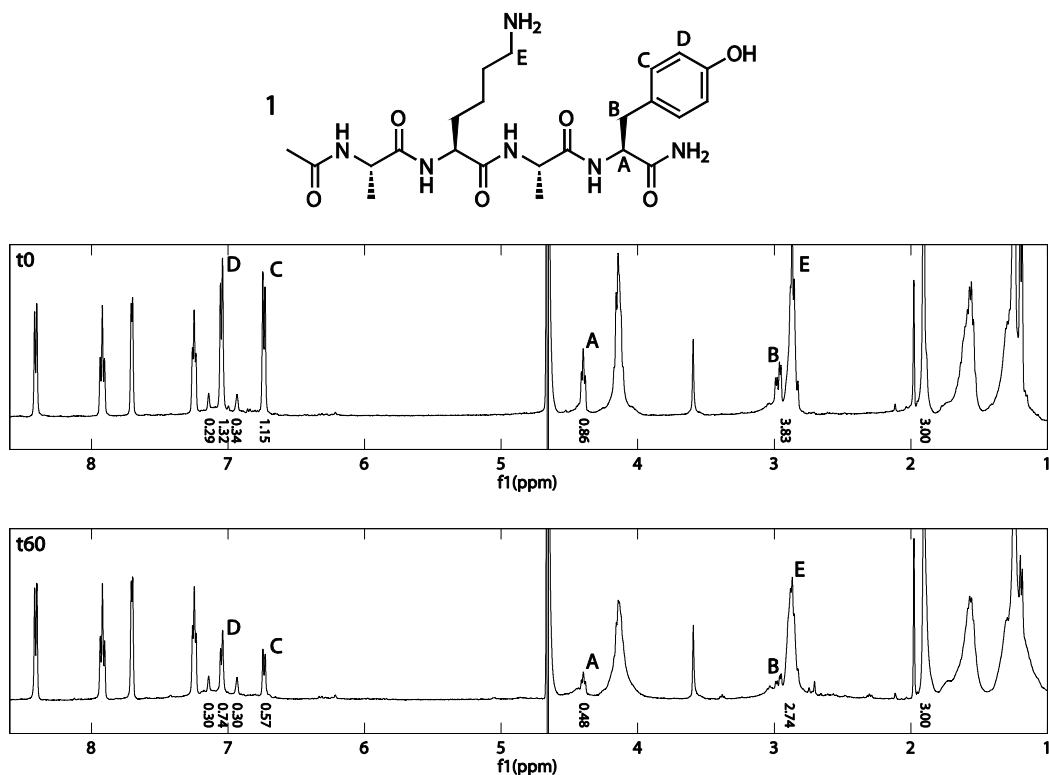


Figure 4.  $^1\text{H-NMR}$  of AKAY (1), at  $t=0$  and after 60 s illumination.

The high reaction speed was once more emphasized when the reaction was monitored with fluorescence spectroscopy (Figure 5). The monomeric tyrosine, excited at a wavelength of 264 nm, fluoresces around 300 and 600 nm, while the dimeric species fluoresces around 415 nm. The strongest dimer fluorescence was observed without any illumination (only daylight during sample preparation and illumination during the fluorescence experiment). Illumination resulted in a decrease of the emission at 415 nm, which we assumed could be due to further crosslinking. Conjugated polymers are known to absorb and fluoresce at higher wavelength at increasing conjugation length.<sup>21</sup> The fluorescence of the formed multimers would not be observed when excited with the same wavelength as the monomeric species, and these species could therefore not be detected in the spectrum.

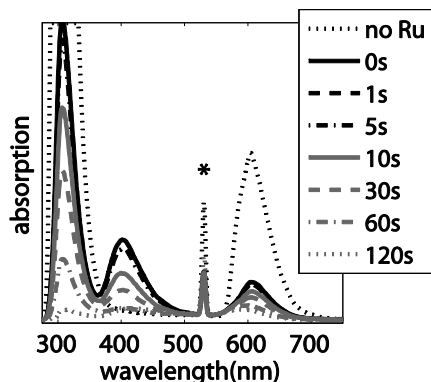


Figure 5. Fluorescence spectra during threading of the AKAY peptide. The asterisk at twice the excitation wavelength denotes an artefact.

To test whether also larger peptides could be threaded, the ruthenium catalysed reaction was extended to larger soluble peptides. The undecameric peptide AQTSSQYGAP was chosen because it is a repeat unit in the resilin protein of the african malaria mosquito,<sup>3, 22</sup> and crosslinking this oligopeptide may result in a mimic of that super-elastic protein. After addition of the ruthenium catalyst and ammonium persulfate the peptide solution was exposed to light. Oligomeric species up to heptamers were observed in subsequent analysis with MALDI. The relative ease of crosslinking this larger soluble peptide, also resulting in oligomers, shows in our opinion the versatility of the reaction.

### Threading self-assembled fibres

Next, the applicability of the cross-linking reaction was explored for self-assembling peptides. Two different peptide fibres were used: MW1, based on an  $\alpha$ -helix motif and a GAGAG derivative which assembles into  $\beta$ -sheets.

**MW1.** MW1<sup>23</sup> is a peptide consisting of 4 heptad repeats which folds into an  $\alpha$ -helix. Two of these 28-meric oligo-peptides assemble into a coiled-coil dimer. The assembly of MW1 (or magic wand peptide) is shown schematically in Figure 6. The design of the  $\alpha$ -helical peptides is such that the two strands do not pack parallel to each other, but overhang is created. This overhang functions as a 'sticky end' and induces the attachment of other dimers. The resulting fibres have a width corresponding to about 48 individual (i.e. dimeric-based) strands and exhibit a large aspect ratio. The exterior of the fibre is in continuous exchange with the building blocks in solution.



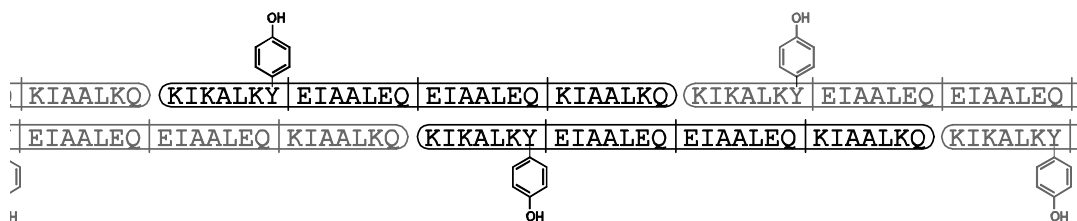


Figure 6. Assembly of MW1 into fibres. The side chains of the tyrosine are shown. One dimer is shown in black, the attaching dimers enabling fibre growth in grey.

Applying the crosslinking conditions yielded only a few dimers for the MW1 peptide (observed with MALDI, Figure 7), which is very limited threading compared with the formation of up to hexamers for the abovementioned AKAY. This may partly be caused by the fact that larger molecules are more difficult to detect in MALDI. Nevertheless, the main cause probably is the very limited accessibility of the tyrosines within the fibres. The majority of the peptides is buried in the interior of the fibres and therefore inaccessible for crosslinking. Moreover, the threading may be impaired due to the rigidity of the fibres. Flexible moieties may move towards each other to facilitate the threading reaction, but this mobility is hampered in large, rigid structures. The same limitations for crosslinking rigid systems have been described by Elvin *et al.*<sup>19</sup> Switching to a high-intensity light source (300 W) yielded a small amount of trimers in addition to the dimeric species observed when the threading reaction was initiated by a 60 W lamp. However, after initiation with the high intensity light source also some unassigned signals were observed which indicated oxidation of other amino acids. In line with the small amount of dimers present after crosslinking, no significant increase of fluorescence was observed at 415 nm. However, the tyrosine fluorescence (at about 315 nm) decreased considerably. Also HPLC showed a decrease of monomer intensity, but no clear increase of multimer peaks, while in literature for protein crosslinking a clear conversion from mono- to dityrosine was observed with HPLC.<sup>2, 19</sup>

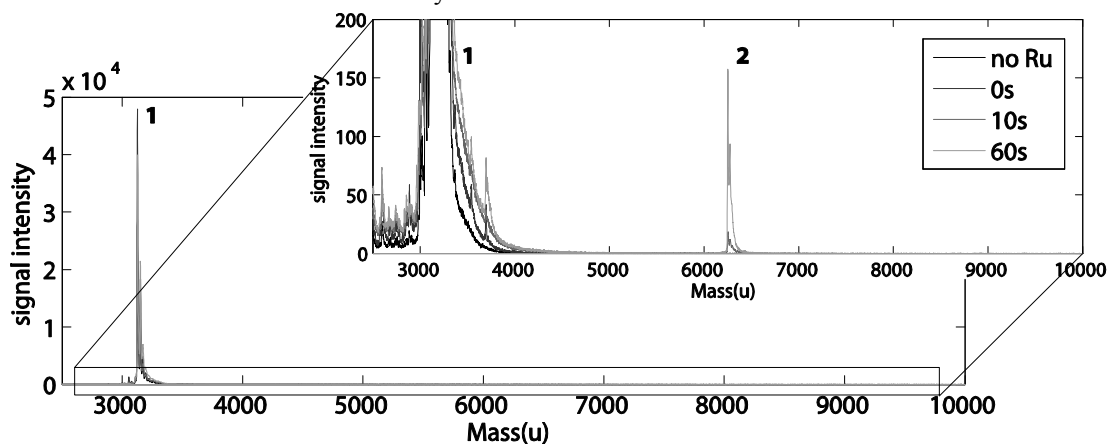


Figure 7: MALDI spectrum of a crosslinking reaction of peptide fibres of MW1. The numbers show the amount of monomers in the oligomer.

Unfortunately, neither gelling properties nor morphology as observed with transmission electron microscopy (TEM) had changed upon crosslinking the fibres. This was most likely due to the fast dynamics within the self-assembled fibres. The outer layers are in continuous exchange and therefore a singly crosslinked monomeric unit may detach from the fibre instead of increasing the stability or viscosity of the solution.

**GAGAE derivatives.** The five-amino acid peptide GAGAE mimicks the alternating glycine and alanine residues of the  $\beta$ -sheet regions which provide strength to silk-worm silk. Unmodified GAGAE is soluble, but when coupled to a hydrophobic tail (Figure 8) it self-assembles. The resulting fibres most likely have a structure with the hydrophobic tail in the interior and the glutamic acid residue solvent exposed. The morphology and polymerisation properties of this peptide coupled to pentacosadiynoic acid (peptide amphiphile (PA) **4**) have been described in chapter 6. Mixing of the GAGAE amphiphiles (PAs **2** and **4**) with GAGAEY peptides coupled to the same hydrophobic tail (PAs **3** and **5**) was expected to be homogeneous, most likely with the tyrosine residues solvent exposed. This proposed structure was supported by the possibility of initiating ATRP from similar fibres (chapter 7), consisting of PA **2**, mixed with a PA functionalised with an initiator moiety. Furthermore, preliminary results from solid state NMR experiments on palmitoyl-GAGAG indicate the same structure. A major advantage of these fibres is that the density of tyrosine can be tuned, unlike in fibres of MW1, in which the tyrosine was an inherent part of the building blocks. For the lower percentages of tyrosine, the tyrosine-tyrosine distance was expected to be too large to facilitate intramolecular threading, while also steric hindrance in the threading reaction was eliminated.

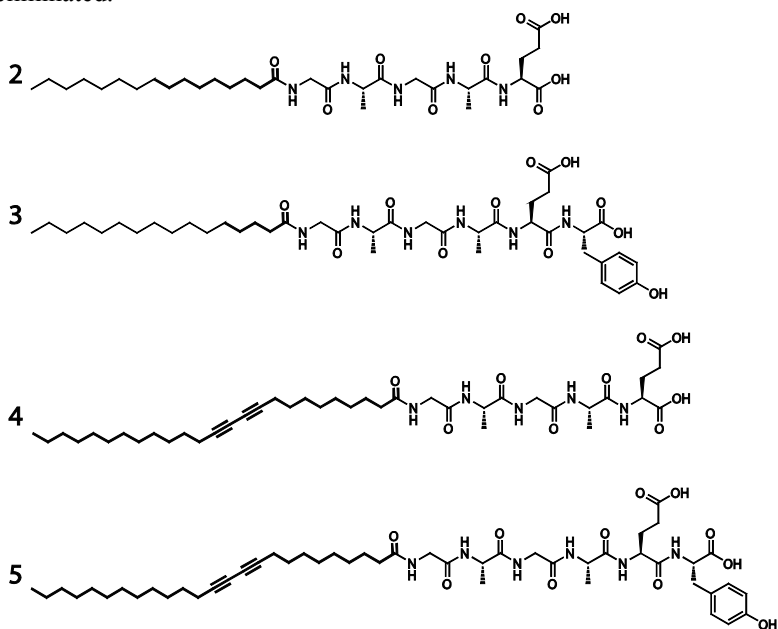


Figure 8. Structures of the silk- worm silk inspired structures.

The palmitoyl functionalized peptide fibres (a mixture of PAs **2** and **3**) yielded, like MW1, a dynamic assembly. The pentacosadiynoic containing peptide amphiphile fibres (consisting of **4** and **5**) were polymerized prior to crosslinking, yielding a covalently linked and thus very stable system (without monomer exchange). TEM measurements confirmed that both peptide mixtures assembled into fibres. Several percentages (0, 5, 20 and 100%) of the tyrosine-containing PAs (**3** and **5**) were mixed with **2** and **4** to investigate the tunability of the crosslinking reaction.

The crosslinking reaction was monitored using MALDI (Figure 9) for the palmitoyl functionalised peptides (the mixture of PA **2** and **3**). The monomer peak disappeared and up to tetramers were visible if the percentage of **3** was 20 or 100 %. However, no larger oligomers were observed upon increasing illumination time, probably because larger molecules are more difficult to detect in MALDI. For fibres prepared from 100 % **3** some precipitate/gel formation indicated the formation of larger oligomers without increase of the MALDI signal. Fluorescence spectroscopy yielded results similar to those of MW1. A decrease of the mono tyrosine signal (310 nm) was observed without increase of the dityrosine fluorescence at 410 nm. As discussed with the small peptides, this may be due to the shift to higher wavelength of both absorbance and fluorescence spectrum for the larger compounds. However, also insolubility of larger oligomers may play a role.

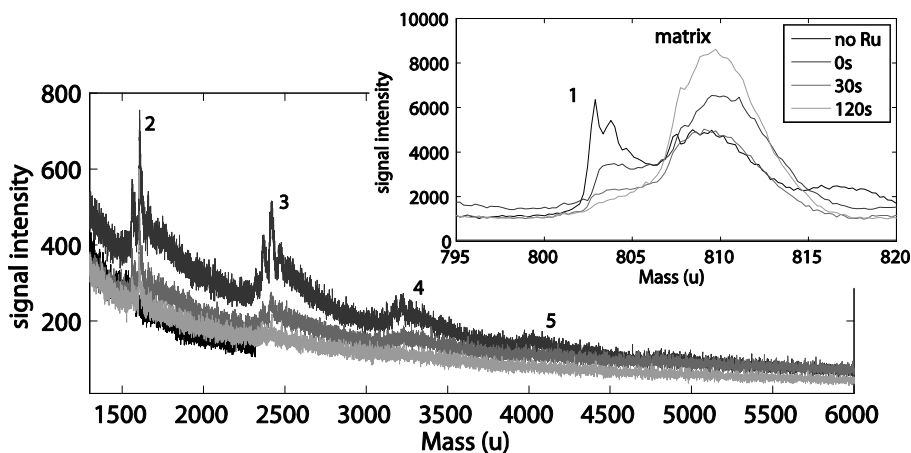


Figure 9: MALDI of a crosslinking reaction of **2** mixed with 20% **3**. The numbers show the amount of monomers in the oligomer.

The pentacosadiynoic acid functionalized PAs (**4** and **5**) yielded similar fibres as observed for mixtures of **2** and **3**. The diacetylene moiety allowed the polymerisation of the hydrophobic tails with light,<sup>24,25</sup> yielding a highly coloured species. Because of their size and insolubility, these polymers were very difficult to analyze. Threading of the polymerized fibres yielded a precipitate, suggesting that also for these fibres a reaction occurred. However, TEM analysis did not show a significant difference between the fibres after the threading conditions had been applied on samples with and without tyrosine. Moreover, it was unknown whether the threading was an inter- or intramolecular process. Especially for fibres containing higher percentages of the

tyrosine, the intramolecular reaction may play an important role. Because of the poor solubility of these fibres no other analyses were attempted.

## Conclusions

We have shown that threading of small peptides using ruthenium(II), APS and visible light resulted in formation of multimeric species. Oligomers obtained *via* crosslinking reactions were reported before with tyrosinases, but not for the ruthenium catalyzed threading. The analysis of the resulting oligomeric mixture was difficult and showed, as also described by Duroux-Richard *et al.*,<sup>17</sup> that the threading mechanism is not yet completely understood. Threading of dynamic self-assembled systems was possible, but because of exchange between fibre and solution, the gel properties of the material did not change as had been observed for crosslinking of large molecules.<sup>20</sup> Furthermore, it is unknown if the crosslinking proceeded within or between fibres. In fibres for which the assembly was locked *via* diacetylene polymerisation, the crosslinking caused gel formation and precipitation, and could therefore not be analysed. Again, precipitate formation indicated that a reaction had taken place, although it cannot be excluded that threading was predominantly an intramolecular process.

## Experimental section

**Synthesis of AKAY.** The name AKAY depicts a peptide (sequence AKAY) with an acylated N-terminus and an amidated C-terminus (Figure 11). Rink amide ChemMatrix™ resin was obtained from PCAS Biomatrix Inc. (St-Jean-sur-Richelieu, Canada), Fmoc-L-amino acids were obtained from AGTC bioproducts (Hessle, UK), 2-(1H-benzotriazol-1-yl)-1,1,3,3-tetramethyluroniumhexafluorophosphate (HBTU) was obtained from GL Biochem (Shanghai, China) and all other reagents were of peptide synthesis grade and obtained from Fisher. The peptide was synthesised on a 0.1 mmol scale on Rink amide resin using a Liberty™ microwave peptide synthesiser (CEMTM; Mathews, NC, U.S.A.). The peptide was assembled by systematically repeated steps of coupling and deprotection interspaced with washing (5 × 7 mL DMF). Coupling: Fmoc-amino acid (5 eq.), HATU (4.5 eq.), DIPEA (10 eq.), in DMF (5 mL) for 2 × 5 min, with 20 W microwave irradiation at 75 °C. Deprotection: 20% piperidine in NMP (1 × 30 sec, with 40 W irradiation at 38 °C; followed by 1 × 3 min, with 40W irradiation at 75 °C). Following linear assembly, the peptide was acetylated (acetic anhydride (3 eq.), DIPEA (4.5 eq.)) and then cleaved from the resin with simultaneous removal of side-chain protecting groups by treatment with a cleavage cocktail (2 mL) consisting of TFA (95 %), TIPS (2.5 %) and H<sub>2</sub>O (2.5 %) for 3 hours at room temperature. Suspended resin was removed by filtration and the peptide was precipitated in ice cold diethyl ether, centrifuged to give a solid pellet, which was subsequently dissolved in 1:1 MeCN/H<sub>2</sub>O and freeze-dried. The peptide was checked for purity with HPLC, and used without further purification. Analytical HPLC: AKAY eluted at 16.8 min (Figure 10).

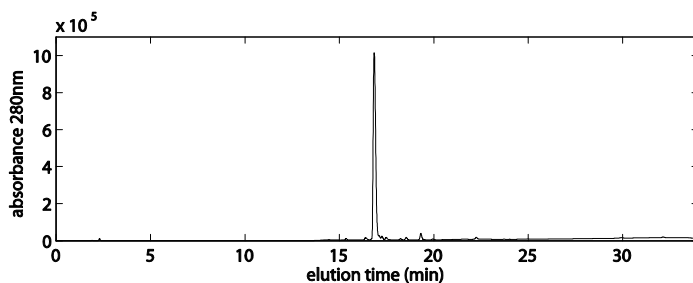


Figure 10. HPLC trace of AKAY after precipitation in ether.

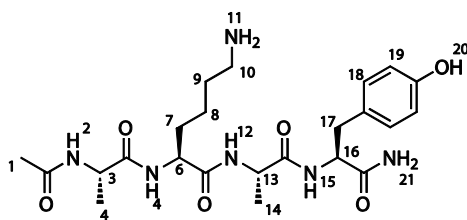


Figure 11. Structure of AKAY, with numbers corresponding to the NMR assignment below.

$^1\text{H-NMR}$  [DMSO- $d_6$ ] (see Figure 11):  $\delta$  1.17 (t, 6H, protons 4, 14), 1.2-1.7 (m, 6H, protons 7-9), 1.83 (s, 3H, protons 1), 2.7-2.9 (m, 4H, protons 10, 17), 4.1-4.3 (m, 4H, protons 3, 6, 13, 16), 6.62 (d, 2H, protons 19), 6.85 (d, 2H, protons 18), 7.05 (s, 1H, protons 21), 7.31 (s, 1H, protons 21), 7.64 (s, 2H, protons 11), 7.72 (d, 1H, proton 15), 7.92 (d, 1H, proton 12), 8.01 (d, 1H, proton 5), 8.09 (d, 1H, proton 2), 9.18 (s, 0.5H, proton 20, partly exchanged).

$^1\text{H-NMR}$  [D $_2$ O] (see Figure 11):  $\delta$  1.2- 1.4 (m, 8H, protons 4, 14, 8), 1.5-1.7 (m, 4H, protons 7, 9), 1.95 (s, 3H, protons 1), 2.91 (2H, t, protons 10), 2.95 (2H, ddd, protons 17), 4.1-4.3 (m, 3H, protons 3, 13, 16), 4.44 (t, 1H, proton 16), 7.85 (d, 2H, proton 18), 7.09 (d, 2H, proton 19).

**Synthesis of MW1.** The abbreviation MW1 (magic wand peptide 1) depicts a peptide with sequence KIKALKYEIAALEQEIAALEQKIAALKQ, with a free N- and C-terminus. Synthesis: The peptide was synthesized by standard Fmoc-based solid-phase peptide synthesis, similar to the synthesis of AKAY. We started from TentaGel Fmoc-Gln(Trt)PHB resin. After the last Fmoc deprotection, the peptide was cleaved from the resin. Peptides were purified by reverse-phase HPLC on a semipreparative Vydac C8 column (Grace Davison Discovery Sciences, Deerfield, IL), using a Jasco HPLC system (JASCO, Great Dunmow, Essex, U.K.). HPLC fractions were checked for the presence and purity of the required peptide by MALDI-TOF mass spectrometry and analytical HPLC. Peptide stocks were stored as freeze-dried powder and redissolved in deionized water just before use.

Analytical HPLC: MW1 eluted as a single peak at 23.8 min in a 20-60 % acetonitrile in water gradient.

MALDI-TOF: observed mass in negative reflection mode 3122.82 ( $[\text{M-H}]^- = 3122.83$ ).

**Synthesis of PA 2 to 5.** PA 2 to 5 depict peptide amphiphiles consisting of GAGAE and GAGA EY, with a free C-terminus and functionalized at the N-terminus with either palmitic acid (2 and 3) or pentacosadiynoic acid (4 and 5).

Synthesis of the palmitoyl peptide: The peptide was synthesized by standard Fmoc-based solid-phase peptide synthesis similar to the synthesis of AKAY, starting from 1 g (0.21 mmol) Tentagel resin. The palmitic acid coupling was performed in DCM. The peptide was cleaved from the resin by shaking it 2 h in a mixture of TFA:TIS:water (95:2.5:2.5) and purified by HPLC using a Jasco

HPLC system (JASCO, Great Dunmow, Essex, U.K.) with a gradient of 20 to 80% acetonitrile in water on a C<sub>18</sub> column. The purity was checked by NMR, analytical HPLC and MALDI-TOF. Analytical HPLC: **2** elutes at 17.44 min and **3** at 17.23 min, both with a 20-80 % acetonitrile in water gradient.

MALDI-TOF: observed masses in negative mode 640.44 for **2** ( $[M-H]^- = 640.40$ ) and 803.49 for **3** ( $[M-H]^- = 803.46$ ).

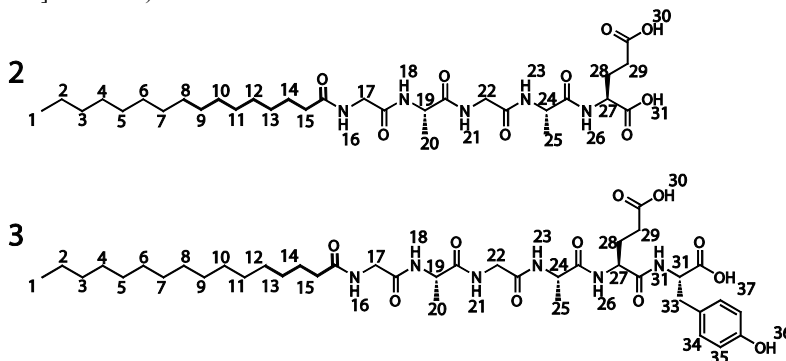


Figure 12. Structure of the silkworm silk inspired molecules. The numbers refer to the NMR assignment.

<sup>1</sup>H-NMR **2** [DMSO-d<sub>6</sub>] (see Figure 12):  $\delta$  0.85 (t, 3H, protons 1), 1.1-1.3 (m, 30H, protons 2-13, 20, 25), 1.46 (t, 2H, protons 14), 1.70-1.84 (m, 1H, proton 28), 1.91-2.03 (m, 1H, proton 28), 2.10 (t, 2H, protons 15), 2.28 (t, 2H, proton 29), 3.6-3.8 (m, 4H, protons 17, 22), 4.1-4.4 (m, 3H, protons 19, 24, 27), 7.88 (d, 1H, amide), 8.00 (t, 1H, amide), 8.11 (t, 2H, amide), 8.20 (t, 1H, amide), 12.23 (s, <1H, carbonyl), 12.52 (s, <1H, carbonyl)

<sup>1</sup>H-NMR **3** [DMSO-d<sub>6</sub>] (see Figure 12) :  $\delta$  0.85 (t, 3H, protons 1), 1.1-1.3 (m, 30H, protons 2-13, 20,25), 1.46 (t, 2H, protons 14), 1.64-1.78 (m, 1H, proton 28), 1.81-1.94 (m, 1H, proton 28), 2.10 (t, 2H, protons 15), 2.2-2.3 (m, 2H, protons 29), 2.7-3.0 (m, 2H, protons 39), 3.6-3.8 (m, 4H, protons 17, 22), 4.2-4.4 (m, 4H, protons 19, 24, 27, 32), 6.63 (d, 2H, protons 35), 6.99 (d, 2H, protons 34), 7.87 (d, 1H, amide), 7.93-8.03 (m, 3H, amide), 8.09 (d, 1H, amide), 8.21 (t, 1H, amide), 9.21 (s, <1H, proton 42), 12.10 (s, <1H, carbonyl), 12.63 (s, <1H, carbonyl).

Synthesis and purification of **4** has been described in chapter 6. The synthesis and purification of **5** was performed in the same way.

TLC: R<sub>f</sub> 0.09 (eluent: CHCl<sub>3</sub>:MeOH:H<sub>2</sub>O 65:25:4).

<sup>1</sup>H-NMR for **5** [DMSO-d<sub>6</sub>] :  $\delta$  0.85 (t, 3H), 1.1-1.3 (m, 32H), 1.4-1.5 (m, 6H), 1.7-1.8 (m, 1H), 1.8-1.9 (m, 1H), 2.0-2.2 (m, 4H), 2.26 (m, 3H), 2.75-2.85 (m, 1H), 2.89-2.97 (m, 1H), 3.6-3.8 (m, 4H), 3.89 (m, 1H), 4.00 (m, 1H), 4.1-4.3 (m, 2H), 6.54 (d, 2H), 6.89 (d, 2H), 7.34 (m, 1H), 7.86 (t, 1H), 8.03 (m, 1H), 8.40 (m, 1H), 8.58 (m, 1H), 8.81 (m, 1H).

MALDI-TOF: observed masses in negative mode 921.54 for **5** ( $[M-H]^- = 921.54$ ).

#### Fibre preparation.

**MWI**: From a 2 mM stock solution in water, of which the concentration was checked using the UV absorption of tyrosine, a 100  $\mu$ M solution was prepared in PBS buffer. This solution was heated to 90 °C for 10 min, cooled down with 1 °C/min and left at room temperature overnight.

**PAs 2-5**: from a 10 mM stock solution in TFE, solutions of 200  $\mu$ M, 500  $\mu$ M or 1 mM were prepared in water. The resulting solutions were heated to 50 °C for 30 min, put in an ultrasonic bath for 15 min, heated to 90 °C for 10 min, cooled down with 1 °C/min and left at room

temperature overnight. The amphiphile solutions were kept in the dark during the whole preparation process.

**Crosslinking protocol.** To a solution of fibres or small peptides in water or buffer, stock solutions of ruthenium trisbipyridine dichloride and ammonium persulfate (APS) were added in that order to yield concentrations of 20  $\mu\text{M}$  ruthenium(II) and 2 mM APS. The concentration of the peptides was between 100  $\mu\text{M}$  and 2 mM for tyrosine, 100  $\mu\text{M}$  for AKAY, between 200  $\mu\text{M}$  and 1 mM for peptide amphiphiles **2-5** and between 100  $\mu\text{M}$  and 2 mM for MW1. After the addition of all compounds, the sample was immediately illuminated in a weighing boat which was cooled using a coolpack. Either 60 W lamp with a lamp-sample distance of 10 cm or a 300 W projector lamp (a 100 V, 2.9 A/290 W Toshiba DLP projector) with a lamp-sample distance of 6 cm was used.

**Matrix assisted laser desorption ionisation – time of flight MALDI-TOF mass spectrometry.** Samples of the soluble peptides were prepared by mixing matrix and peptide solution. As a matrix, a saturated solution of alpha-cyano-4-hydroxycinnamic acid in a 1:1 solution of water:acetonitrile was used. One microliter of this solution was spotted on the MALDI plate (a 192 well plate from Applied Biosystems)

The fibres were treated with TFA after which 4x the volume acetonitrile was added. To this sample the matrix was added and the mixture was spotted on the MALDI plate.

The three soluble peptides and MW1 were measured in positive mode, PA **3** and PA **5** were better visible in negative mode due to the free acid groups within the structure and were consequently measured in negative mode.

The samples were measured using an applied Biosystems 4700 MALDI TOF/TOF with an Nd-Yag laser (200 Hz).

**Nuclear magnetic resonance (NMR) spectroscopy.** 15 mL of a 100  $\mu\text{M}$  solution AKAY, with 20  $\mu\text{M}$  Ru and 2 mM APS was illuminated for a specified time, freeze-dried and redissolved in 0.7 mL  $\text{D}_2\text{O}$  for NMR measurements. The measurements were performed on a Varian500 system instrument with a tunable triple resonance HC(X) probe. 128 scans were taken for the final spectrum.

**Fluorescence spectroscopy.** Fluorescence spectra were measured on a Jasco FP6500 fluorimeter, with an excitation wavelength of 264 nm and slit sizes of 3 for both excitation and emission.

**Transmission electron microscopy (TEM).** Samples were prepared by floating a carbon-coated TEM grid on a droplet of fibre solution. The grid was washed by floating it 2 times on a water droplet and the excess liquid was blotted away. MW1 fibres were subsequently stained by floating on a droplet of a 1% uranyl acetate solution, washed 2 times by floating on a water droplet and the excess liquid was blotted away. The samples were dried overnight prior to measurements on a JEOL JEM 1200 EX Mk 2, a standard tungsten filament TEM operated at 120KV up to magnifications of 1 million, fitted with MegaView III digital camera, using Soft Imaging Systems GmbH analySIS 3.0 image analysis software

## References

1. T. Weisfogh, *J. Exp. Biol.*, 1960, **37**, 889-&.
2. C. M. Elvin, A. G. Carr, M. G. Huson, J. M. Maxwell, R. D. Pearson, T. Vuocolo, N. E. Liyou, D. C. C. Wong, D. J. Merritt and N. E. Dixon, *Nature*, 2005, **437**, 999-1002.
3. K. M. Nairn, R. E. Lyons, R. J. Mulder, S. T. Mudie, D. J. Cookson, E. Lesieur, M. Kim, D. Lau, F. H. Scholes and C. M. Elvin, *Biophys. J.*, 2008, **95**, 3358-3365.

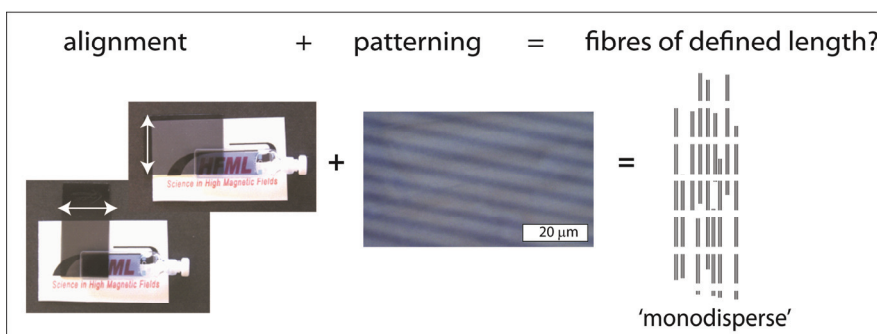
4. R. E. Lyons, E. Lesieur, M. Kim, D. C. C. Wong, M. G. Huson, K. M. Nairn, A. G. Brownlee, R. D. Pearson and C. M. Elvin, *Protein Eng. Des. Sel.*, 2007, **20**, 25-32.
5. A. M. Tamburro, S. Panariello, V. Santopietro, A. Bracalello, B. Bochicchio and A. Pepe, *ChemBioChem*, 2010, **11**, 83-93.
6. S. O. Andersen, *Annu. Rev. Entomol.*, 1979, **24**, 29-61.
7. S. O. Andersen, *Insect Biochem. Mol. Biol.*, 2010, **40**, 541-551.
8. G. C. Coles, *J. Insect Physiol.*, 1966, **12**, 679-&.
9. A. J. Gross and I. W. Sizer, *J. Biol. Chem.*, 1959, **234**, 1611-1614.
10. G. K. Qin, S. Lapidot, K. Numata, X. Hu, S. Meirovitch, M. Dekel, I. Podoler, O. Shoseyov and D. L. Kaplan, *Biomacromol.*, 2009, **10**, 3227-3234.
11. A. Bertazzo, C. V. L. Costa, G. Allegri, M. Schiavolin, D. Favretto and P. Traldi, *Rapid Commun. Mass Spectrom.*, 1999, **13**, 542-547.
12. S. O. Andersen, *Biochim. Biophys. Acta*, 1964, **93**, 213-&.
13. J. W. Heinecke, W. Li, G. A. Francis and J. A. Goldstein, *J. Clin. Invest.*, 1993, **91**, 2866-2872.
14. J. G. Jee, S. J. Park and H. J. Kim, *Rapid Commun. Mass Spectrom.*, 2000, **14**, 1563-1567.
15. M. L. Mattinen, R. Lantto, E. Selinheimo, K. Kruus and J. Buchert, *J. Biotechnol.*, 2008, **133**, 395-402.
16. D. A. Fancy and T. Kodadek, *Proc. Natl. Acad. Sci. U. S. A.*, 1999, **96**, 6020-6024.
17. I. Duroux-Richard, P. Vassault, G. Subra, J. F. Guichou, E. Richard, B. Mouillac, C. Barberis, J. Marie and J. C. Bonnafous, *Chem. Biol.*, 2005, **12**, 15-24.
18. D. A. Fancy, *Curr. Opin. Chem. Biol.*, 2000, **4**, 28-33.
19. C. M. Elvin, A. G. Brownlee, M. G. Huson, T. A. Tebb, M. Kim, R. E. Lyons, T. Vuocolo, N. E. Liyou, T. C. Hughes, J. A. M. Ramshaw and J. A. Werkmeister, *Biomaterials*, 2009, **30**, 2059-2065.
20. S. Rammensee, D. Huemmerich, K. D. Hermanson, T. Scheibel and A. R. Bausch, *Appl. Phys. A: Mater. Sci. Process.*, 2006, **82**, 261-264.
21. H. Du, R. C. A. Fuh, J. Z. Li, L. A. Corkan and J. S. Lindsey, *Photochem. Photobiol.*, 1998, **68**, 141-142.
22. R. E. Lyons, K. M. Nairn, M. G. Huson, M. Kim, G. Dumsday and C. M. Elvin, *Biomacromol.*, 2009, **10**, 3009-3014.
23. C. Gribbon, K. J. Channon, W. J. Zhang, E. F. Banwell, E. H. C. Bromley, J. B. Chaudhuri, R. O. C. Oreffo and D. N. Woolfson, *Biochem.*, 2008, **47**, 10365-10371.
24. G. Wegner, *Makromol. Chem.*, 1972, **154**, 35-48.
25. M. van den Heuvel, D. W. P. M. Löwik and J. C. M. van Hest, *Biomacromol.*, 2008, **9**, 2727-2734.





## Chapter 9

### Towards fibres of defined length.



A strategy was developed to construct peptide amphiphile based fibres of well-defined length. This approach consisted of two steps: alignment of polymerisable fibres, followed by selective polymerisation using lithography. The combination of alignment and lithography was anticipated to yield fibres of defined length. It was demonstrated that peptide amphiphile fibres could be aligned in solution in a magnetic field. Furthermore, lithographic patterning up to micrometer resolution was possible on dried samples. Since alignment was only possible in solution and patterning only on dried samples, we were not yet able to combine these methods to obtain fibres of defined length.

## Introduction

Peptide amphiphile (PA) fibres have gained much interest as molecular building blocks for a new generation of materials with a high degree of order on a nanoscopic level.<sup>1-3</sup> In our group we have extensively studied an eight-amino acid peptide moiety, GANPNAAG, derived from the CS protein of the malaria parasite *Plasmodium Falciparum*,<sup>4</sup> coupled to a hydrophobic tail. In an aqueous environment, the tail provides a driving force for assembly, which is directed by the hydrogen-bond forming peptide. The PAs self-assemble to yield fibres of which the stability can be tuned by changing the length of the hydrophobic tail.<sup>5</sup> We recently developed GANPNAAG-based diacetylene-functional PAs to make them polymerisable<sup>6-8</sup> (chapters 4 and 5). With a diacetylene moiety in the hydrophobic tail, the fibres were susceptible to the topochemical polymerisation reaction of diacetylenes,<sup>9</sup> indicating a well-defined packing of the diacetylenes within the fibre.<sup>7</sup> A similar well-defined packing of diacetylenes in self-assembled structures was shown by the groups of Stupp<sup>10</sup> and Tirrell.<sup>11</sup>

To be able to use the fibres of peptide amphiphiles as building blocks for larger assemblies, defined dimensions are a first prerequisite. One of the fibre dimensions which can be controlled well is width, since it is generally defined by the choice of the building blocks. The groups of Yamada<sup>12</sup> and Stupp<sup>13, 14</sup> for example developed fibres based on peptide amphiphiles of which the fibre width is twice the length of one building block. Other self-assembling peptide amphiphiles with a high level of dimensional control are peptide rings, as synthesized by Ghadiri *et al.*<sup>15, 16</sup> These cyclic peptides consist of alternating D- and L-amino acids, yielding stable, flat rings which stack into nanotubules. The width of the tubules was tuned by the number of amino acids in the ring. A similar tubular system was described by Valery *et al.*<sup>17</sup> In both cases the width of one tubule is well defined, but the tubules stick together into larger assemblies. This assembly of individual strands into bundles is commonly observed for many different systems, which makes the design of the fibre width more difficult. In some cases, however, control over this level of hierarchical assembly has been achieved. Stupp *et al.* developed a peptide amphiphile consisting of a palmitoyl tail, coupled to the peptide GV<sub>3</sub>A<sub>3</sub>E<sub>3</sub>, in which the nitrogen of the glycine was modified with a nitrobenzyl group. Fibres formed from this peptide amphiphile assembled into quadruple helical structures.<sup>18</sup> Illumination caused cleavage of the nitrobenzyl group, resulting in the disassembly of the quadruple helix into single fibres, which was accompanied by a change in width from 33 nm to 11 nm. Another example by Woolfson *et al.*,<sup>19-21</sup> is based on coiled coil structures. They designed peptides to fold into  $\alpha$ -helices which subsequently assembled into coiled coils. The coiled coils packed into fibrous superstructures, and the width of these fibres was tuned by the choice of solvent-exposed residues in the coiled coils. Also the group of Aggeli and Boden designed a fibrous system of defined width. Like the previously described system of Woolfson *et al.*, these fibres consisted entirely out of amino acids.<sup>22</sup> They designed one peptide *de novo* to assemble into  $\beta$ -sheets in aqueous solution, and another was based on a transmembrane motif of a protein. Both peptides formed tapes with a thickness

corresponding to the length of one  $\beta$ -strand. The width was determined by an interplay between the energy gain upon stacking and the energy loss of ‘untwisting’ of the helical fibres by which stacking was accompanied.<sup>23</sup>

Difficult as it is to design and tune the width of fibres, control of their length is even more challenging. A variety of approaches have been used to limit the length of self-assembled fibres. A specific distribution of fibre lengths can be obtained by choosing the right amphiphile concentration or by adding a molecule which prevents growth of the fibre.<sup>24, 25</sup> However, the length distribution of the fibres obtained with these methods is statistical in nature and hence still rather broad. Monodisperse fibres can be achieved by using a template for the assembly, exemplified by e.g. the tobacco mosaic virus (Figure 1a).<sup>26</sup> Inspired by that, several groups have designed scaffolds for molecules to assemble upon.<sup>27, 28</sup> E.g. Stupp *et al.*<sup>28</sup> designed a templated assembly, shown schematically in Figure 1. However, design or synthesis of such template molecules is not trivial and thus only shifts the problem.

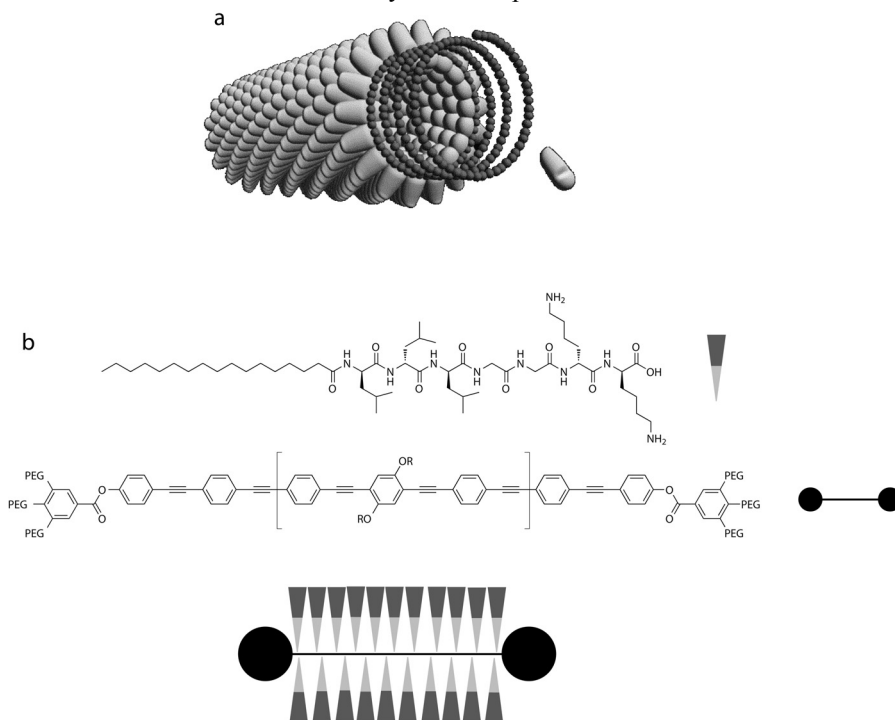


Figure 1. Two examples of templated fibres. a) The assembly of the tobacco mosaic virus. b) The assembly of peptide amphiphiles on an acetylene scaffold.

In this chapter, we describe a non-templated approach for the construction of well-defined fibres based on self-assembling peptides, which allows a facile variation of the length of the fibre. In this strategy, shown in Figure 2, aligned samples of peptide amphiphiles are ‘cut’ using spatially addressed stabilisation. Although this approach provides fibres that are not completely monodisperse, they will possess a much smaller length distribution than obtained when tuning fibre length with e.g. concentration. The

key components in this approach are peptide amphiphiles which can be stabilised, their spatial selective stabilisation and fibre alignment.

In chapters 4 and 5 we showed the design of a peptide amphiphile that assembles into fibres which can be stabilized by a UV-initiated polymerisation reaction (PA **1**, Figure 3). These fibres, therefore, fulfil the first of the requirements stated above. Spatial selectivity of the polymerisation could possibly be achieved by combining the topochemical polymerisation with lithography. With that technique only a well-defined portion of the fibres will be illuminated and, hence, polymerised. UV-lithography on diacetylenes has been extensively described in literature to create selectively polymerised surfaces.<sup>29-32</sup> The third requirement is fibre alignment, which we have shown before to be effective in a magnetic field.<sup>6</sup> In this chapter, the possibilities and limitations of lithography as a method for spatially addressed polymerisation of fibres from PA **1** are investigated. Furthermore, methods for alignment of these fibres are described and we looked into possibilities of combining these two methods to yield fibres of defined length.

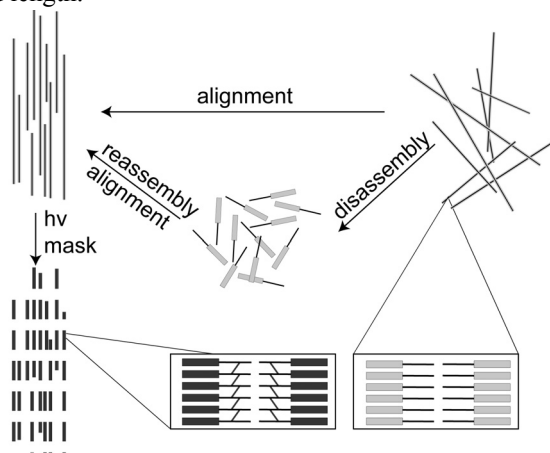


Figure 2. Our strategy towards fibres of defined length. Alignment, either directly or *via* disassembly (top), followed by patterning using lithography (left).

The peptide amphiphile used for these studies is compound **1** (Figure 3). It was synthesized, purified and assembled into fibres as described in chapter 4.

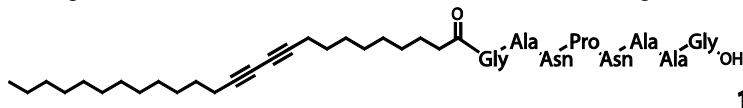


Figure 3. Structure of the fibre forming peptide amphiphile **1** used for the experiments described in this chapter.

## Spatially addressed polymerisation

In order to investigate the possibilities of spatially addressed polymerisation of these peptide amphiphile (PA) fibres using lithography, we started with randomly oriented samples in solution. If patterning with high resolution would be possible under

these circumstances, then it was expected to be relatively straightforward to repeat the procedure with aligned samples, since we recently developed a methodology to use high magnetic fields for aligning these fibres in solution.<sup>6</sup> In these experiments, a mask was placed on a cuvette filled with an aqueous solution containing fibres, and a photochemical polymerisation was carried out. To reduce loss of resolution because of a diverging light source, a laser was employed. Furthermore, gelled samples were used to minimize diffusion of any non-polymerised fibres into the exposed area of the sample. Although a pattern was visible, the resolution was poor (Figure 4), because of scattering from the walls of the sample cell, the sample thickness and the relative large mask-sample distance.

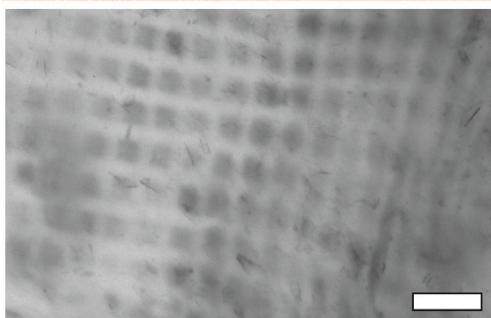


Figure 4. Patterning in a liquid, using a transmission electron microscopy (TEM) grid as a mask. The white bar represents 250  $\mu\text{m}$ .

In order to decrease the scattering, we moved to drop-casted, dried-in samples. With a chrome mask placed directly on the surface of the dried fibres a resolution of up to a few microns could be achieved (Figure 5). For these experiments, a Bluepoint UV lamp was used. Although this lamp did not provide a parallel light source, this did not affect the resolution of the pattern because of the small mask-sample distance. With fibres of PA **1**, hundreds of microns long, this resolution should be sufficient to get a relatively narrow length distribution if the patterning was performed on aligned samples. Besides this lithographic method, also polarization holography was, for the first time, successfully used as a means to selectively polymerise self-assembled architectures. Polarization holography employs the difference in polymerisation rate of fibres illuminated with light either parallel or perpendicular to the long axis. This allowed us not only to make polymeric patterns but also to introduce anisotropy in an otherwise isotropic sample, as will be described in chapter 10.<sup>33</sup>

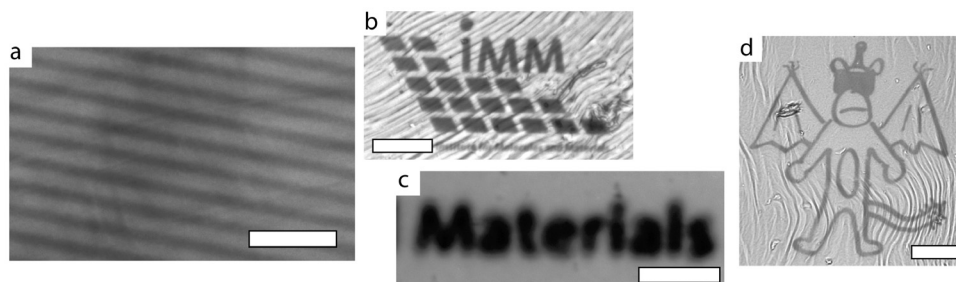


Figure 5. Patterning on dried samples using a chrome mask. White bars represent a) 20  $\mu\text{m}$ , b) 200  $\mu\text{m}$ , c) 50  $\mu\text{m}$  and d) 100  $\mu\text{m}$ .

Being able to selectively polymerise fibres of PA **1** with almost micrometer resolution, as a next step it was examined whether monomer could be removed from the surface while leaving the cross-linked material behind. To this purpose, the patterned sample was treated with dimethyl sulfoxide (DMSO) and dried, after which the surface was probed with atomic force microscopy (AFM). This revealed the polymeric parts of the surface to be higher than the monomeric parts (Figure 6), showing a faster desorption of the monomer. The difference in detachment rate, caused by a different solubility, enabled us to create patterns with a height up to 1.5 microns.

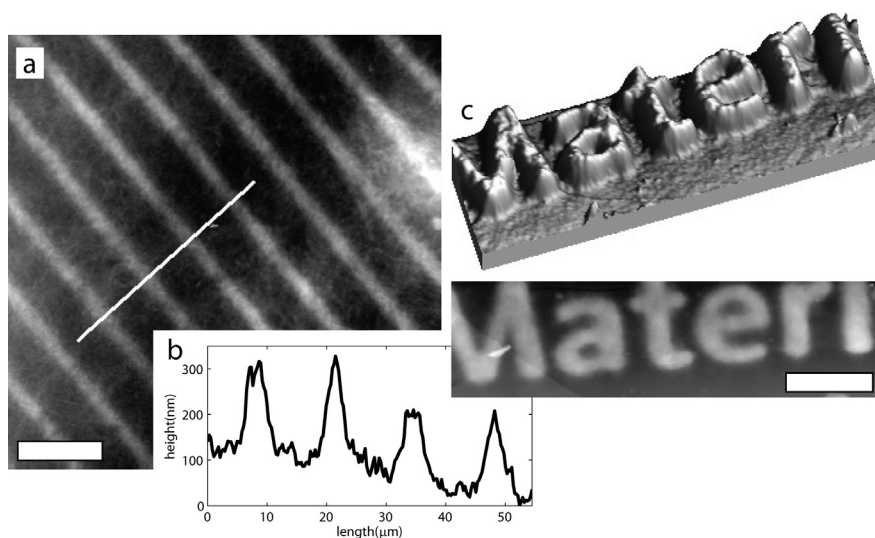


Figure 6. Removing monomeric peptide amphiphile from a patterned surface, imaging with AFM. a) and c) AFM picture, with b) height profile of a). The white bars represent 20  $\mu\text{m}$ .

## Alignment techniques

Having established UV lithography was only feasible on dried-in samples, the alignment of the fibres was investigated. In general alignment was performed in solution after which the fibres were dried to enable high-resolution lithography. To induce

alignment two methods were considered: alignment of preformed fibres, or alignment during the assembly process (Figure 1).

**Alignment of pre-formed fibres.** To align fibre-containing aqueous solutions, flow was used as a simple means of applying shear force. A convenient method is to make a droplet roll down a glass-slide under the influence of gravity. Angles ranging from approximately 15 to 50° were used, either with microscope slides or fused silica as substrate. The microscope slides were used as received, but the fused silica slides were etched prior to use in order to increase hydrophilicity. Unfortunately, with AFM no alignment was observed (Figure 7a). This may be caused by a too high concentration, at which the fibres might have been too entangled to be aligned with this method. However, this is unlikely since the result was found to be independent of concentration over a range from 0.2 to 5 mg/mL. As an alternative method a drop was spread using a coverslip. In this case a modest degree of alignment was observed (Figure 7b), which was unfortunately far from complete.

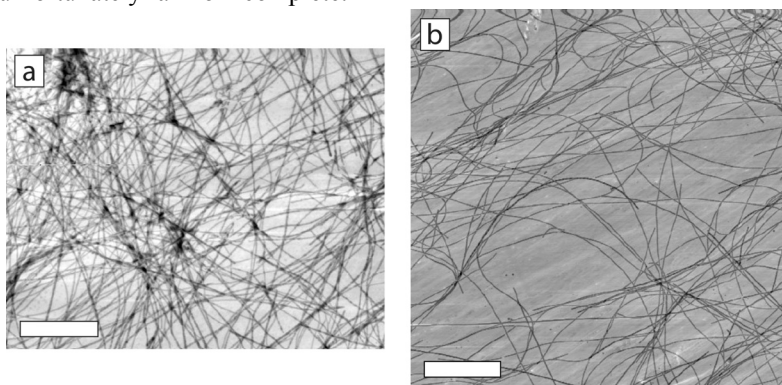


Figure 7. AFM of samples which are treated by a) rolling a droplet (1 mg/mL) down a glass plate, b) distributing a drop (0.2 mg/mL) over a fused silica plate using a coverslip. The white bars represent 2  $\mu\text{m}$ .

Because shear forces were expected to yield alignment and a modest degree was obtained by spreading a sample using a coverslip, methods yielding larger shear forces were considered. Two methods in which more force was applied to the sample were tested, i.e. spreading the sample with a K-bar hand coater<sup>34</sup> and spincoating.<sup>35</sup> A K-bar hand coater is used for applying thin films on surfaces, which is accompanied with larger and more defined shear forces than in the methods described above. With the hand coater solutions of several concentrations (0.2 to 5 mg/mL) were spread on an etched fused silica slide, subsequently dried and imaged with AFM (Figure 8). Unfortunately, the fibres were found to be damaged, while no alignment was observed. The damage was more severe at higher concentrations, probably because of increased entanglement. For spincoating again concentrations ranging from 0.2 to 5 mg/mL were used, at two spinning speeds (1100 and 2000 rpm). The centrifugal forces were expected to align the fibres in a radial fashion. Although for the patterning a parallel alignment was required, on a relatively small area distant from the centre of the spincoating, the lines of this radial pattern will practically be parallel. Unfortunately, AFM revealed the fibres to be damaged again by the spinning or possibly the drying process. The breakage



of fibres was more pronounced at higher concentrations, and at none of the concentrations alignment was observed.

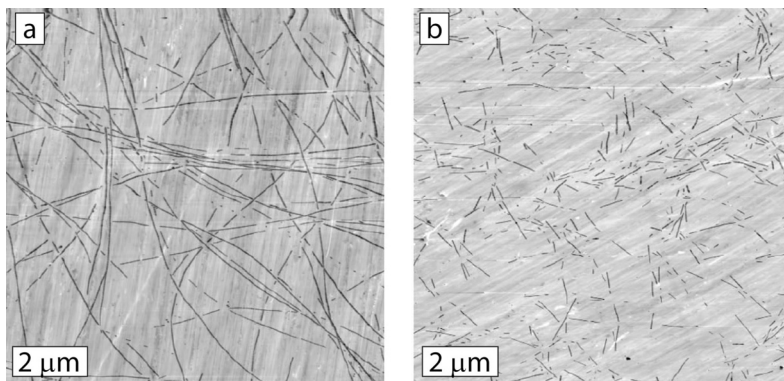


Figure 8. AFM of samples treated with a K-bar hand coater. Concentrations are a) 0.2 mg/mL and b) 5 mg/mL. The white bars represent 2  $\mu\text{m}$ .

Another method that was considered to apply shear force is sliding two slides of glass over each other, with a droplet of fibre-containing solution in between. Because of the large contact surface between the two plates, the applied force is much larger than using a coverslip (under an angle) to spread a drop over a glass slide as described above. To promote spreading of the droplets, the hydrophilicity of the glass plates was increased by etching.<sup>36</sup> Unfortunately, also in those cases, broken fibres were observed with AFM without any evidence of alignment.

With all abovementioned alignment methods, the surface was not homogeneously coated – on one spot on the sample the AFM measurements yielded other results than on another spot. Nevertheless, it was clear that in none of the cases macroscopic alignment was present. Therefore, it was concluded that shear forces are not suited to produce dried-in aligned samples. Although the fragility of the PA fibres was known (see chapter 3), the ease with which the fibres broke under influence of the relatively small forces that were applied was unexpected.

Electrospinning,<sup>37</sup> as a completely different alignment technique, was also considered for alignment of pre-formed PA **1** fibres. Unfortunately, the PA fibres turned out not to be suitable for this method. In electrospinning a high voltage is applied to a polymer solution. Charge carriers accumulate in a droplet until a jet forms which aligns the fibres.<sup>38</sup> Probably the fibres could not be charged easily enough for electrospinning to be successful, as no jet formation was observed.

**Alignment during fibre formation.** Aligning samples while fibres are forming requires much less force than aligning samples of pre-formed fibres, due to reduced entanglement and smaller size of the assemblies. For example alignment of PA **1** fibres in a magnetic field is easily achieved, but only possible during assembly.<sup>6</sup> Since with this alignment method the solution needs to be heated to 90 °C, it can only be used in a tightly closed cell. Unfortunately, to remove the aligned samples from the cell without disturbing the alignment proved difficult. Even after coating the inner surface of the cell with long alkyl chains using octadecyltrichlorosilane, in order to decrease the

interactions between surface and solution, the gel could not be removed from the cell without damaging it. Freezing the sample before removal from the cell could help to prevent the gel from being damaged. Unfortunately, freezing by itself also resulted in broken fibres (chapter 3). In a new cell from FutureChemistry (Figure 9a), the sample was sandwiched between an etched and thus hydrophilic glass plate and a hydrophobic Teflon cell (pretreated with heptane). To enable the heating to 90 °C, the cell was sealed using a rubber ring. It could be opened without any visible damage to the gel. However, after drying no alignment was observed with AFM and linear dichroism spectroscopy. This could have been caused by damage upon opening the cuvette, but also by drying effects. On the other hand, the fibres in the highly concentrated PA solutions (5 mg/mL to yield a strong gel) may not have disassembled completely upon heating to 90 °C and might therefore not have aligned in the first place.

Another way of preventing damage upon opening the cell is by using sample holders which are open to the air and allow the sample to dry within its cell. Of course in this case it should be avoided that the samples dry in before the fibres have formed and become aligned. Consequently, heating to 90 °C was not possible. In chapter 4 an alternative method for fibre formation was described, in which a concentrated solution of amphiphiles in trifluoroethanol (TFE) was injected in water. Birefringence measurements on a closed cuvette showed that mixing the TFE solution and water and immediately placing it in a magnetic field for 45 min yielded aligned samples. A disadvantage of this method was that the sample preparation was less controlled, because the mixing of the components took place outside the magnetic field, and fibres may start forming before the sample is placed in the magnetic field. Nevertheless, two methods of preparation using fibre formation from TFE were considered. In the first, the amphiphile-containing mixture was spotted onto transmission electron microscopy (TEM) grids, and in the second the mixed sample was placed in a cuvette with a detachable lid (Figure 9b). In both methods the drying was expected to compete with and possibly disturb the alignment process. Unfortunately, in both experiments, no alignment was observed. For the droplets on the TEM grids drying may have been too fast for the fibres to align, although also flow during drying may have played a role. A detailed analysis of these samples was hampered by the limitation of the TEM technique – concentrated samples or large droplets yielded a layer too dense to penetrate. Nevertheless, for the smaller drops it was clear that the fibre alignment was far from perfect (Figure 10). In the opened cell the volume was larger, so the fibres had more time to assemble and hopefully align before the sample had dried. Unfortunately, again no alignment was observed, this time probably because of flow induced by the drying process.

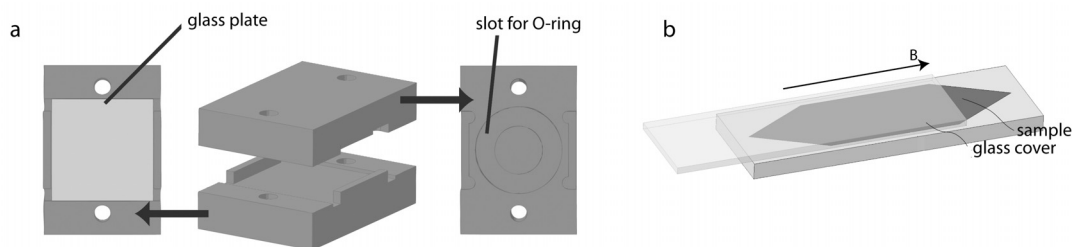


Figure 9. Two cuvettes used for alignment in a magnetic field. a) Designed by FutureChemistry. b) A cuvette with a detachable lid.

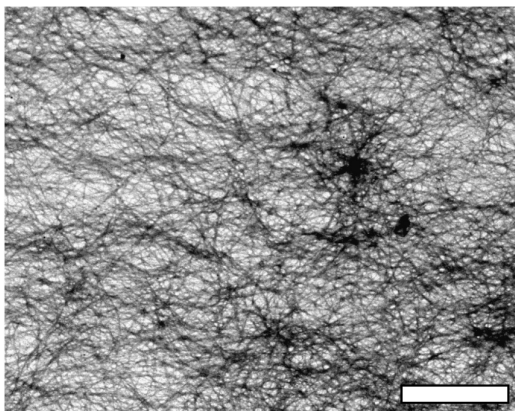


Figure 10. TEM picture of a droplet of fibre solution dried on a TEM grid in a magnetic field. The white bar represents 2  $\mu\text{m}$ .

The fibre solution showed both lyo- and thermotropic liquid crystalline behaviour and we tried to use this property to induce alignment. A simple but well-established method to align liquid crystals is by interaction with a pre-aligned surface.<sup>39</sup> The preparation of the alignment layer started with spincoating of a diluted polyimide precursor on a clean glassplate. Subsequently, polymerisation was initiated by heating. After polymerisation and drying, the glass plate was visually checked for inhomogeneities, and the polyimide alignment layer was completed by rubbing with a velvet cloth. A disadvantage of the use of the polyimide layer is its hydrophobicity. The hydrophilic exterior of the fibres may not attach to it. However, the use of a hydrophilic polymer not covalently attached to the surface was incompatible with the aqueous samples. Furthermore, when the fibres assembled in the presence of the rubbed surface, the first layer may consist of a monolayer PA **1** with its tails towards and the peptide part pointing away from the surface. This monolayer could then serve as an oriented hydrophilic layer for further assembly of the fibres. The alignment will probably only work if the assembly process takes place close to the surface. Therefore, a polyimide-coated glass plate was placed in a fibre-containing aqueous solution, heated to 90 °C and slowly cooled. A dilute solution was chosen, because in a concentrated solution the effect of fibres forming randomly in solution that attach randomly to the surface was

thought to be larger. The samples prepared in this way showed almost no fibres on the surface. Moreover, for the fibres that had attached, no alignment was observed, which may be due to the hydrophobicity of the polyimide layer.

In a final attempt to align fibres during assembly capillary flow was used.<sup>40, 41</sup> In this set-up the fibres were formed in a capillary under flow conditions. The first ~1.2 m (2 min) of a capillary with a diameter of 100  $\mu\text{m}$  was immersed in a water bath of 95 °C to ensure disassembly. The rest of the 15 m (~22 min) was used to allow the solution to cool and reassemble the fibres under flow. The liquid was deposited on a freshly etched fused silicon plate that moved away from the capillary at a constant speed. Unfortunately, also with this set-up no alignment was observed in AFM. One of the reasons for this may be the discrepancy between the velocity of the liquid in the capillary (about 65 cm/min) and the velocity with which the solution is deposited, between 1 and 5 cm/min. However, faster deposition speeds were hampered by the surface tension of the liquid, which prevented smaller lines of solution to be formed. For faster deposition speeds, the lines coalesced to droplets. Again, another factor disturbing alignment may have been the drying process.

## **Conclusions**

To obtain fibres of defined length, we perceived to align fibres and selectively stabilize them using lithography. For this approach three components were needed: fibres which could be stabilised, a means of spatially addressing the stabilisation and a method to align fibrous samples. We started with the diacetylene containing fibres described in chapters 4 and 5, which could be stabilised using a light-initiated polymerisation reaction and which fulfilled the first requirement. Lithography was investigated to spatially address the polymerisation reaction. In solution the resolution of the patterning was hampered by scattering, but on dried samples the patterning was successful and a resolution up to a few micron was realised. Alignment of the fibres was achieved by assembling fibres in a high magnetic field – either by cooling or by injecting a concentrated PA solution in TFE into water. However, obtaining aligned fibres which were dried proved difficult. A number of methods were investigated, both on pre-formed fibres as well as during fibre formation. These included several approaches in which shear force was applied, electrospinning, drying samples in a magnetic field and assembly under flow. However, none of these was successful, probably because of disturbance of alignment during the drying step and easy breakage of the fibres. Therefore, even though the two essential steps in our strategy – alignment and patterning – were accomplished, we could not combine the two techniques to produce fibres of defined length.

## **Acknowledgements**

We thank Peter Mulder for help with the lithography and mask design and FutureChemistry for designing the Teflon cell used for alignment in a magnetic field.

We thank Koos Wilke for use of his model trains for the capillary flow alignment, and Jeroen Gielen (HFML) for support with the experiments performed at the HFML.

## Experimental section

**Synthesis and characterization of PA 1 and its assemblies.** The synthesis and purification of PA 1 have been described in chapter 4. The assemblies formed by PA 1 in aqueous solution have been studied in the same chapter.

**Fibre preparation.** Unless stated otherwise, for the preparation of the fibres PA 1 was dispersed in milli-Q at the required concentration, followed by heating to 50 °C for 30 min, and 15 min sonication at that temperature. Subsequently, the samples were heated to 90 °C and allowed to cool overnight to room temperature.

**Spatially addressed polymerisation.** For lithography of the samples, an appropriate chrome mask, designed with CleWin (CleWin versie 2.90, WieWeb Software, Hengelo, the Netherlands), was placed on a dried fibre sample, with the chrome surface in contact with the sample. The set-up was placed on a soft surface and weights were placed on the mask to ensure maximum contact between the sample and the mask. The samples were illuminated for 15 min using a Bluepoint UV lamp, with a lamp-mask distance of 3 cm.

**Etching to make glass hydrophilic.** A fused silica slide was cleaned by sonication in acetone for 5 min. After this it was dried with argon, the slide was immersed in a freshly prepared 1:1 (v/v) mixture of HCl and methanol for 45 min. The cleaned slide was washed and sonicated with ultrapure water, washed and sonicated with methanol and dried with argon prior to use.

**Coating glass with polyimide.** Glass plates of 10x10 cm were cleaned by soaking in ~ 2 % detergent (Alconox) overnight, followed by 2x ultrasonic treatment with the detergent solution, 3x10 min ultrasonic treatment in milliQ and 1x10 min ultrasonic treatment in acetone. The plates were spincoated with freshly filtered imide monomer (PI2555, HD Microsystems), using 5 s at 500 rotations/min followed by 30 s at 3000 rotations/min. The plates were immediately placed in an oven at a temperature of 80 °C for 30 min, and at 180 °C for 1 h after which they were cooled down slowly overnight. Subsequently, the slides were visually checked for homogeneity, cut and rubbed with a velvet cloth to induce alignment.

**Atomic Force Microscopy (AFM).** The dried samples of the alignment experiments (see below) were visualized with AFM. The measurements were performed on a DI Dimension 3100 in tapping mode. The data were processed using the WSxM software package.<sup>42</sup>

**Transmission electron microscopy (TEM).** TEM samples were prepared by floating a carbon-coated copper grid on a peptide amphiphile solution of either 1.0 or 0.2 mg/mL for 10 min, followed by removal of residual water by blotting with a paper filter. The samples were visualized using a JEOL 1010 transmission electron microscope set on an accelerating voltage of 60 kV.

### Alignment in a magnetic field.

**Cooling in solution.** A 1 mg/mL PA 1 solution, loaded in a quartz optical cell (1 mm path length) was heated to 90 °C for at least 10 min inside a Bitter magnet and allowed to cool to room temperature in about 30 min in a 20 T magnetic field.

**Assembly from TFE in solution.** 270  $\mu$ L of deionized water was placed in a 1 mm pathlength quartz optical cell and 30  $\mu$ L of a 10 mg/mL solution of PA 1 in trifluoroethanol (TFE)

was added. The cell was shaken to mix and immediately placed in a 20 T magnetic field for 45 min.

**Drying from a solution with TFE.** A concentrated solution of 10 mM PA **1** in TFE was injected into milliQ to yield a 1 mg/mL solution. Of this mixture, 1 to 5 microliters were pipetted onto TEM grids, or a demountable cuvette was filled. The samples were immediately placed in a 20 T magnetic field for 45 min.

### Alignment of pre-formed fibres

**K-bar hand coater.** Solutions of PA **1** with concentrations between 0.2 and 5.0 mg/mL were deposited on a freshly etched fused silicon plate and spread homogeneously using a K-bar hand coater, designed to yield films of 12  $\mu\text{m}$  thickness.

**Spincoating.** Solutions of PA **1** with concentrations between 0.2 and 5.0 mg/mL were deposited on a freshly etched fused silicon plate, which was spinning at either 1100 or 2000 rotations/min.

**Gravity.** Solutions of PA **1** with concentrations between 0.2 and 5.0 mg/mL were deposited on a glass plate of 7.5 cm length which was placed under an angle between 15 and 50°. The droplet was allowed to roll down the glass and dry in air.

### Alignment during assembly.

**Using rubbed polyimide-coated glass plates.** The coated glass plates were placed in a fibre containing solution of 0.1 mg/mL, which was heated to 90 °C and slowly cooled. The plates were removed from the solution and allowed to dry.

**Capillary flow.** A concentration of 0.2 mg/mL amphiphile **1** was placed in a syringe and pushed through a capillary of 100  $\mu\text{m}$  inner diameter with 5  $\mu\text{l}/\text{min}$  (63.5 cm/min). The first ~1.2 m (2 min) of the capillary was submerged in a 95 °C waterbath, the rest of the capillary (~14 m, 22 min) was used to allow the solution to cool. The solution was deposited on a freshly etched fused silica slide. The velocity of deposition was between 1.3 and 5 cm/min. A constant velocity of deposition was realized by pulling the fused silica plate by another pump, while placed on a model train on a model track to minimize friction.

## References

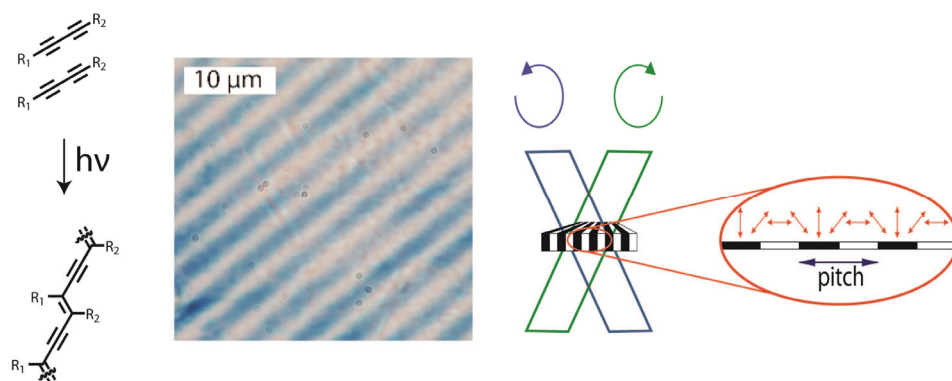
1. D. W. P. M. Löwik and J. C. M. van Hest, *Chem. Soc. Rev.*, 2004, **33**, 234-245.
2. J. D. Hartgerink, E. Beniash and S. I. Stupp, *Science*, 2001, **294**, 1684-1688.
3. G. A. Silva, C. Czeisler, K. L. Niece, E. Beniash, D. A. Harrington, J. A. Kessler and S. I. Stupp, *Science*, 2004, **303**, 1352-1355.
4. C. Cerami, U. Frevert, P. Sinnis, B. Takacs, P. Clavijo, M. J. Santos and V. Nussenzweig, *Cell*, 1992, **70**, 1021-1033.
5. D. W. P. M. Löwik, J. Garcia-Hartjes, J. T. Meijer and J. C. M. van Hest, *Langmuir*, 2005, **21**, 524-526.
6. D. W. P. M. Löwik, I. O. Shklyarevskiy, L. Ruizendaal, P. C. M. Christianen, J. C. Maan and J. C. M. van Hest, *Adv. Mater.*, 2007, **19**, 1191-1195.
7. M. van den Heuvel, D. W. P. M. Löwik and J. C. M. van Hest, *Biomacromol.*, 2008, **9**, 2727-2734.
8. M. van den Heuvel, D. W. P. M. Löwik and J. C. M. van Hest, *Biomacromol.*, 2010, **11**, 1676-1683.
9. G. Wegner, *Makromol. Chem.*, 1972, **154**, 35-48.
10. L. Hsu, G. L. Cvetanovich and S. I. Stupp, *J. Am. Chem. Soc.*, 2008, **130**, 3892-3899.
11. M. A. Biesalski, A. Knaebel, R. Tu and M. Tirrell, *Biomaterials*, 2006, **27**, 1259-1269.
12. N. Yamada, K. Ariga, M. Naito, K. Matsubara and E. Koyama, *J. Am. Chem. Soc.*, 1998, **120**, 12192-12199.
13. J. C. Stendahl, M. S. Rao, M. O. Guler and S. I. Stupp, *Adv. Funct. Mater.*, 2006, **16**, 499-508.

## Chapter 9

14. E. Beniash, J. D. Hartgerink, H. Storrer, J. C. Stendahl and S. I. Stupp, *Acta Biomater.*, 2005, **1**, 387-397.
15. J. D. Hartgerink, J. R. Granja, R. A. Milligan and M. R. Ghadiri, *J. Am. Chem. Soc.*, 1996, **118**, 43-50.
16. M. R. Ghadiri, J. R. Granja, R. A. Milligan, D. E. McRee and N. Khazanovich, *Nature*, 1993, **366**, 324-327.
17. C. Valery, M. Paternostre, B. Robert, T. Gulik-Krzywicki, T. Narayanan, J. C. Dedieu, G. Keller, M. L. Torres, R. Cherif-Cheikh, P. Calvo and F. Artzner, *Proc. Natl. Acad. Sci. U. S. A.*, 2003, **100**, 10258-10262.
18. T. Muraoka, H. Cui and S. I. Stupp, *J. Am. Chem. Soc.*, 2008, **130**, 2946-2947.
19. M. G. Ryadnov and D. N. Woolfson, *Nat. Mater.*, 2003, **2**, 329-332.
20. M. G. Ryadnov, A. Bella, S. Timson and D. N. Woolfson, *J. Am. Chem. Soc.*, 2009, **131**, 13240-13241.
21. C. Gribbon, K. J. Channon, W. J. Zhang, E. F. Banwell, E. H. C. Bromley, J. B. Chaudhuri, R. O. C. Oreffo and D. N. Woolfson, *Biochem.*, 2008, **47**, 10365-10371.
22. A. Aggeli, M. Bell, N. Boden, J. N. Keen, P. F. Knowles, T. C. B. McLeish, M. Pitkeathly and S. E. Radford, *Nature*, 1997, **386**, 259-262.
23. I. A. Nyrkova, A. N. Semenov, A. Aggeli and N. Boden, *Eur. Phys. J. B*, 2000, **17**, 481-497.
24. J. M. Lehn, *Polym. Int.*, 2002, **51**, 825-839.
25. L. Brunsveld, B. J. B. Folmer, E. W. Meijer and R. P. Sijbesma, *Chem. Rev.*, 2001, **101**, 4071-4097.
26. A. Klug, *Philos. Trans. R. Soc. London, B.*, 1999, **354**, 531-535.
27. P. G. A. Janssen, S. Jabbari-Farouji, M. Surin, X. Vila, J. C. Gielen, T. F. A. de Greef, M. R. J. Vos, P. H. H. Bomans, N. Sommerdijk, P. C. M. Christianen, P. Leclere, R. Lazzaroni, P. van der Schoot, E. W. Meijer and A. Schenning, *J. Am. Chem. Soc.*, 2009, **131**, 1222-1231.
28. S. R. Bull, L. C. Palmer, N. J. Fry, M. A. Greenfield, B. W. Messmore, T. J. Meade and S. I. Stupp, *J. Am. Chem. Soc.*, 2008, **130**, 2742-2743.
29. J. M. Kim, Y. B. Lee, D. H. Yang, J. S. Lee, G. S. Lee and D. J. Ahn, *J. Am. Chem. Soc.*, 2005, **127**, 17580-17581.
30. D. J. Ahn and J. M. Kim, *Acc. Chem. Res.*, 2008, **41**, 805-816.
31. K. Morigaki, T. Baumgart, A. Offenhausser and W. Knoll, *Angew. Chem., Int. Ed.*, 2001, **40**, 172-174.
32. K. Morigaki, T. Baumgart, U. Jonas, A. Offenhausser and W. Knoll, *Langmuir*, 2002, **18**, 4082-4089.
33. M. van den Heuvel, A. M. Prenen, J. C. Gielen, P. C. M. Christianen, D. J. Broer, D. W. P. M. Löwik and J. C. M. van Hest, *J. Am. Chem. Soc.*, 2009, **131**, 15014-15017.
34. L. A. Canalle, S. S. van Berkel, L. T. de Haan and J. C. M. van Hest, *Adv. Funct. Mater.*, 2009, **19**, 3464-3470.
35. M. C. LeMieux, M. Roberts, S. Barman, Y. W. Jin, J. M. Kim and Z. N. Bao, *Science*, 2008, **321**, 101-104.
36. T. Vong, J. ter Maat, T. A. van Beek, B. van Lagen, M. Giesbers, J. C. M. van Hest and H. Zuilhof, *Langmuir*, 2009, **25**, 13952-13958.
37. M. V. Kakade, S. Givens, K. Gardner, K. H. Lee, D. B. Chase and J. F. Rabolt, *J. Am. Chem. Soc.*, 2007, **129**, 2777-2782.
38. D. H. Reneker and I. Chun, *Nanotechnol.*, 1996, **7**, 216-223.
39. H. Sirringhaus, R. J. Wilson, R. H. Friend, M. Inbasekaran, W. Wu, E. P. Woo, M. Grell and D. D. C. Bradley, *Appl. Phys. Lett.*, 2000, **77**, 406-408.
40. R. Adachi, K. Yamaguchi, H. Yagi, K. Sakurai, H. Naiki and Y. Goto, *J. Biol. Chem.*, 2007, **282**, 8978-8983.
41. S. S. Rogers, P. Venema, L. M. C. Sagis, E. van der Linden and A. M. Donald, *Macromol.*, 2005, **38**, 2948-2958.
42. I. Horcas, R. Fernandez, J. M. Gomez-Rodriguez, J. Colchero, J. Gomez-Herrero and A. M. Baro, *Rev. Sci. Instrum.*, 2007, **78**, 0137051-0137058.

## Chapter 10

# Patterns of diacetylene-containing peptide amphiphiles using polarisation holography.



The polarisation dependence of diacetylene polymerisation was studied. For this purpose, peptide amphiphile fibres with a diacetylene moiety were employed which could only polymerise in the direction of the fibre. When non-aligned samples were illuminated with polarised light, only the fibres parallel to the polarisation direction of the light were polymerised. With magnetically aligned fibres, selective polymerisation resulting in patterned samples was accomplished using polarisation holography.

---

This work has been published in M. van den Heuvel, A. M. Prenen, J. C. Gielen, P. C. M. Christianen, D. J. Broer, D. Löwik and J. C. M. van Hest, *J. Am. Chem. Soc.*, 2009, **131**, 15014-15017.



## Introduction

The photochemical polymerisation of diacetylene-functionalized molecules has been studied for years. In particular the topochemical character of this polymerisation and the properties of the resulting polymer (for example its strong absorption in the visible spectrum), have intrigued many scientists. Although diacetylene-functional materials have to be highly structured, or even crystalline in order to allow polymerisation to take place, no examples are described in literature yet in which this level of organizational perfection is utilized to obtain control over the directionality of polymerisation. Peptide amphiphile fibres possessing a diacetylene functionality yield very defined assemblies, which may give the possibility of control over the polymerisation.

Peptide amphiphile (PA) fibres have gained much interest as molecular building blocks for a new generation of materials with a high degree of order on a nanoscopic level,<sup>1</sup> which can be applied as functional scaffolds in e.g. biomineralisation<sup>2</sup> or cell proliferation processes.<sup>3</sup> In our group we have extensively studied an eight-amino acid peptide moiety, GANPNAAG, derived from the CS protein of the malaria parasite *Plasmodium Falciparum*,<sup>4</sup> which, when coupled to a hydrophobic tail, yields a peptide amphiphile. The tail provides a driving force for assembly, which is directed by the hydrogen-bond forming peptide. The PAs self-assemble in water to yield fibres of which the stability can be tuned by changing the length of the hydrophobic tail.<sup>5</sup> In line with similar work performed by Stupp<sup>6</sup> and Tirrell<sup>7</sup> GANPNAAG-based diacetylene-functional PAs were recently developed to make them susceptible to polymerisation.<sup>8, 9</sup> When a diacetylene moiety was included in the hydrophobic tail (Figure 1), the fibres could be polymerised using the topochemical polymerisation reaction of diacetylenes,<sup>10</sup> indicating the well-defined packing of the diacetylenes within the fibre.<sup>9</sup> The PA fibres could also be aligned using a magnetic field and polymerised subsequently.<sup>8</sup> From the pronounced dichroic behaviour of the resulting polymer, the chromophoric centra of the polymeric backbone were shown to be aligned parallel to the magnetic field.

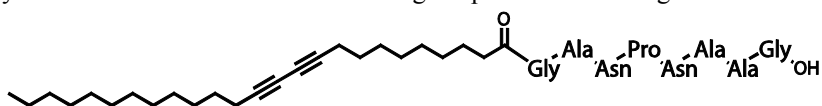


Figure 1. Structure of the PA employed in this chapter.

The combination of these properties – fibres with tunable stability, which can be aligned and polymerised, subsequently yielding aligned chromophoric centra – led us to hypothesize that also the polymerisation-initiating event, namely the absorption of light by the monomer, might be direction dependent. If so, polymerisation would be initiated faster for light which has the more strongly absorbed direction of polarisation, subsequently leading to a polarisation dependent rate of polymerisation. This may lead to the introduction of anisotropy in otherwise isotropic samples using only the polarisation of the light employed for the polymerisation process. Illumination would result in a dichroically coloured, partly polymerised sample, in which only fibres parallel to the polarisation direction are polymerised. When this concept of polarisation-

selective polymerisation would be applied on an aligned sample using polarisation holography, patterning by spatially confined polymerisation could be achieved, allowing maskless lithography of diacetylenes.

### **Introducing anisotropy.**

To investigate if polymerisation of a randomly oriented sample with polarised light would result in a dichroically coloured sample, non-aligned samples were polymerised with plane polarised 457 nm laser light. After polymerisation, anisotropy of the samples was investigated using linear dichroism spectroscopy (LD). In Figure 2a the expected polymerisation for horizontally and vertically polarised light and in Figure 2b the corresponding measured LD spectra are shown.

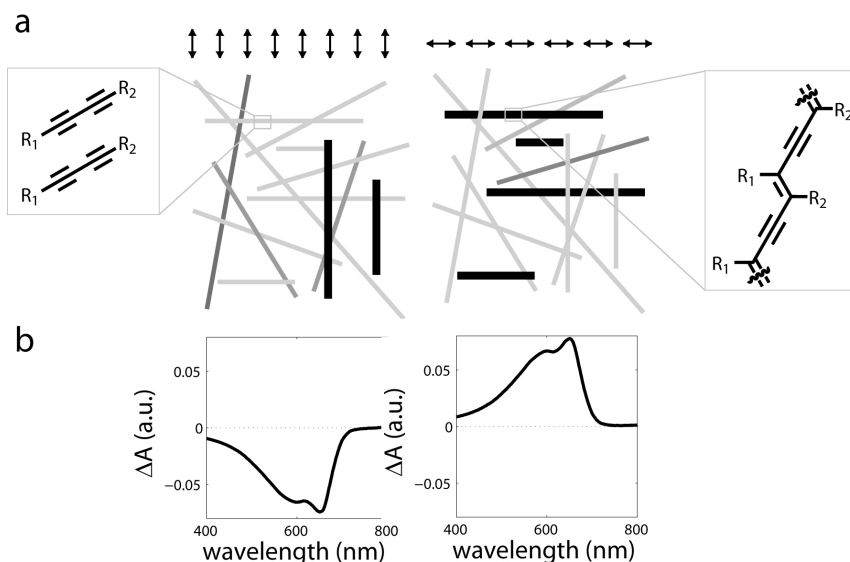


Figure 2. Illumination of a non-aligned sample with polarised light. a) Dependent on the polarisation direction of the light (the arrows) one or the other orientation of the fibres will polymerise. The darkness of the lines depicts their degree of polymerisation. A black line is fully polymerised, light grey non-polymerised. b) In agreement with this theory, vertically polymerised fibres yield indeed a negative linear dichroism (LD) signal (left). Horizontally polymerised fibres yield a positive LD signal (right).

Light parallel to the fibre was expected to be absorbed and thus induce polymerisation, where light perpendicular to the fibres yields no or negligible polymerisation, if the rate of polymerisation is indeed polarisation dependent. This would result in dichroic behaviour of the resulting, partly polymerised material. Figure 3 shows the observed linear dichroism signal at 650 nm of the polymerised sample plotted against the angle under which the sample was polymerised. A negative signal indicates, as shown in Figure 2b, a vertical orientation of the polymers while a positive signal shows a horizontal orientation. From this experiment, it can be concluded that indeed the fibres show pronounced dichroic behaviour resulting from the dependence of the

rate of polymerisation on the polarisation of the incident light. As a consequence, anisotropic properties are installed in an otherwise isotropic sample.

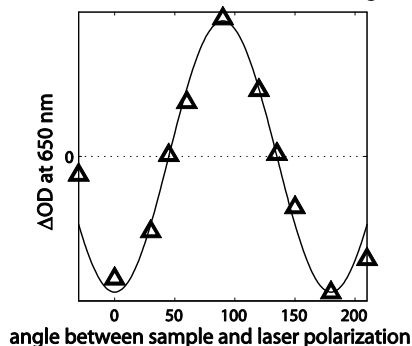


Figure 3. The angle dependence of the polymerisation process, monitored as the LD signal at 650 nm.

### Patterning using polarisation holography.

Because of the polarisation-dependent rate of polymerisation, we furthermore expected patterning of aligned PA fibres to be possible using polarisation holography. Of the different methods described to create micro to nanometer sized patterns in polymeric films, holography has as special feature that no template, mask or mechanical contact with the film is required. The pattern is induced by a periodical variation of the intensity of the incident light onto a sample. The difference in intensity causes a difference in response, which, in its turn, leads to pattern formation. Polarisation holography is a variation of this technique, in which not the intensity, but the polarisation direction of the light is modulated. This is accomplished by combining two circularly polarised laser beams with opposite handedness (Figure 4a).<sup>11</sup> At the interference plane a pattern of linearly polarised light is obtained.

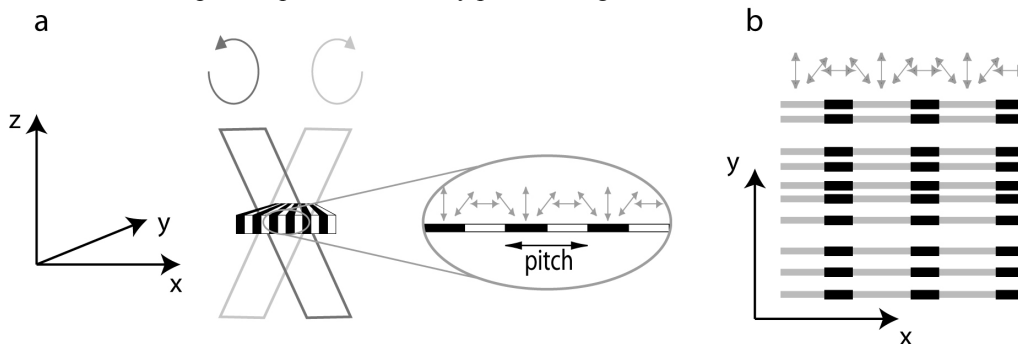


Figure 4. Setup and expected experimental results of polarisation holography a) Schematic representation of the polarisation holography setup. Two oppositely circularly polarised laser beams interfere to yield a linearly polarised pattern. b) If the polymerisation is polarisation dependent, polymerisation of an aligned sample is expected to only take place where the polarisation is parallel to the fibre orientation, yielding a pattern of polymer.

Polarisation holography has been used before to create patterns in polymeric films in several ways. In one approach a dichroic photo-initiator was employed, which dissociates preferentially with light of one polarisation, initiating the polymerisation at that specific spot.<sup>12</sup> In a second method polymers or linear photopolymerisable polymers were used which could reorient themselves towards the polarisation of the incident light,<sup>13-16</sup> creating a fully polymerised sample of which the orientation of the monomers followed the polarisation pattern. In all these methods, the orientational freedom of the monomers causes the pattern to form. To our knowledge, patterning a solid film with polarisation holography when the monomers do not have orientational freedom has not been reported before. This requires a unique set of characteristics of the material of which the film is composed, since the molecules have to be both pre-aligned and sensitive to the polarisation of the incident light, so that only one polarisation direction is able to initiate polymerisation. Because of the alignment capabilities of the PA fibres in combination with their unique susceptibility to the polarisation direction of the incident light (Figure 4b), these architectures represent an ideal candidate for patterning using polarisation holography. Although diacetylenes have been used for patterning before,<sup>17-20</sup> to our knowledge, this has never been accomplished with maskless lithographic patterning, employing the unique polarisation dependent selective polymerisation.

To test this patterning technique, we prepared aligned samples of the diacetylene-containing peptide amphiphilic fibres.<sup>8</sup> After drying, the samples were exposed to a pattern of linearly polarised light, using a polarisation holography set-up (Figure 4a). The result, depicted in Figure 5c, shows that patterning of diacetylene PAs using polarisation holography is not only possible, but even results in a very distinct pattern. The observed on-off behaviour could be caused by an intensity threshold below which no polymerisation takes place (see below).

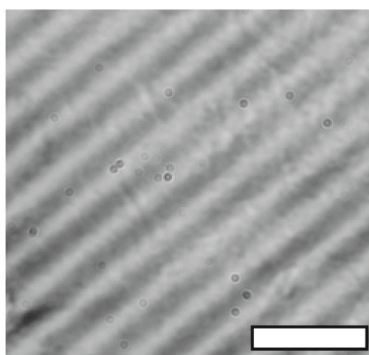


Figure 5. Pattern obtained with polarisation holography. The white bar represents 10  $\mu\text{m}$ .

In order to exclude patterning by intensity variation, it was verified that the intensities of the incident light did not deviate more than 1 % and their ellipticities were less than 10 %. Furthermore, two control experiments were performed, one on a lyophilysed and hence truly non-oriented sample and a second on the non-fibre forming 10,12-pentacosadiynoic acid dried in from a solution of chloroform. Both samples were spread on a glass plate and yielded a homogeneously coloured sample when

polymerised using polarisation holography, indicating that, indeed, intensity variations cannot be the cause of the observed patterns.

### Varying the pitch of the polarisation holography pattern.

Polarisation holography allows the pitch of the pattern to be easily varied by changing the angle between the incident circularly polarised beams. We used several pitches, varying from 1.5  $\mu\text{m}$  (Figure 6a) to 5.2  $\mu\text{m}$  (Figure 6b), which depend on the angle as follows

$$\Lambda = \frac{\lambda}{2 \sin \theta/2}$$

where  $\Lambda$  is the pitch,  $\lambda$  is the wavelength of the incident light and  $\theta$  is the angle between the two interfering beams. The observed pitches correlated closely to the calculated ones (Figure 6c), confirming that the polymerised lines are indeed caused by the pattern of polarised light. The measured pitch was on average 10 % higher than the calculated one. This may be caused by a deviation of the ideal 90° angle between the beams from the beam splitters in the set-up. The angle between the beams at the sample position will then also be slightly different from the calculated angle, causing a systematic error. Furthermore, the refractive index was neglected in the calculation of the pitch and may thus also cause a small deviation.

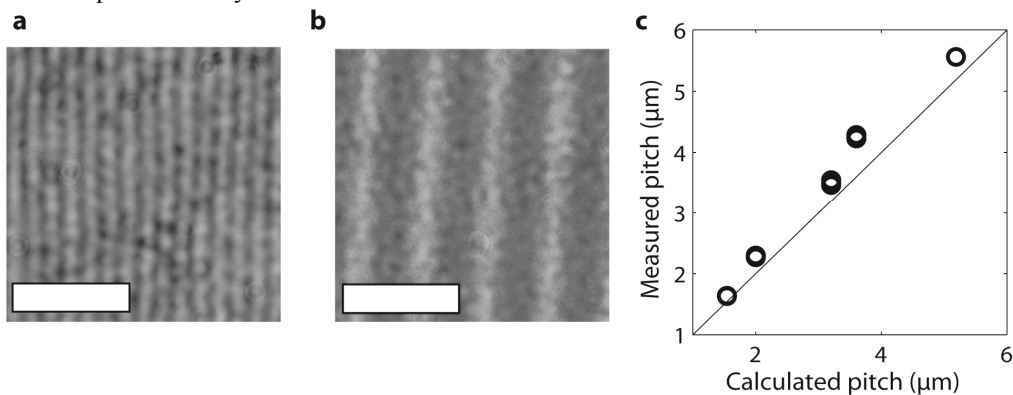


Figure 6. Varying the pitch of the polarisation holography setup results in a change in the observed pattern. a) pitch of 1.5  $\mu\text{m}$ , the b) pitch of 5.2  $\mu\text{m}$ , observed with optical microscopy. Both in a) and b) the white bar represents 10  $\mu\text{m}$ . c) The pitch of the polymer patterns of several samples compared with the calculated pitch.

### Presence of a threshold value for polymerisation

Since in polarisation holography the change between parallel and perpendicular light is gradual, which means that the component parallel to the fibres gradually decreases, a gradual transition between polymerised and non-polymerised parts of the sample was expected. That would result in a gradual colour change and not the sharp lines observed. The well-defined pattern observed (Figure 4c) could be caused by an

intensity threshold, causing an on/off switch for polymerisation. To investigate if such an intensity threshold was present, we performed polymerisation experiments at UV light intensities varying from 4 J/cm<sup>2</sup> to less than 30 mJ/cm<sup>2</sup>, corresponding to sample-lamp distances between 1.5 and 60 cm. The rate of polymerisation had a linear dependence with the intensity of the incident light for intensities smaller than 0.6 J/cm<sup>2</sup>, while at higher intensities the speed was lower than it would be following this relation (Figure 7). At the highest intensities (>25 mW/cm<sup>2</sup>) and longer illumination times (>15 min, resulting in >22.5 J/cm<sup>2</sup>) the position of the maximum absorbance peak shifted from 645 nm to 655 nm.

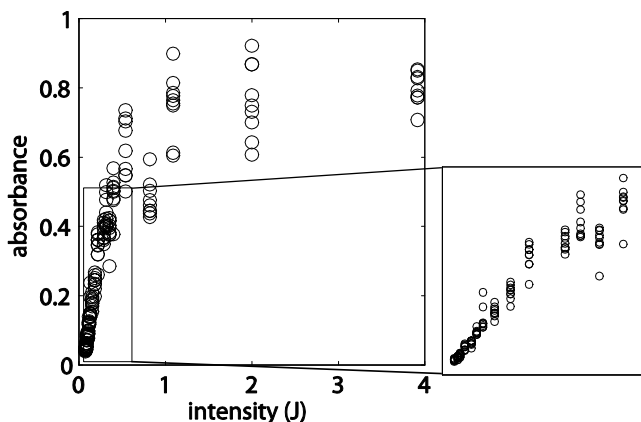


Figure 7. The absorbance of the formed polymer follows a linear relationship with the intensity of illumination for low intensity, which gets to a plateau for higher intensities

From these experiments it was concluded that a threshold value, if present, seems to be even lower than 30 mJ/cm<sup>2</sup>. The fact that no intensity threshold was measured could be due to the difference in conditions used for the experiments. First of all, the threshold measurements have been performed in solution, and the presence of a threshold may be influenced by the presence of oxygen. Moreover, the wavelength of the incident light may be very important for these measurements. The polarisation holography experiments were performed at 351 nm, the selective polymerisation of a non-aligned sample at 457 nm, while the threshold measurements were performed using lower wavelength UV light, down to 254 nm. The polymerisation is very sensitive towards the low-wavelength UV light, while 457 but also 351 nm are well outside the absorption band of the monomer. The intensity threshold was not investigated on dried samples using laser light of higher wavelengths because the analysis of the absorption of the sample is in that case highly dependent on the spot on the sample where the measurement takes place, yielding highly irreproducible results.

### **Domain formation in dried samples**

Remarkably, it was found that illumination using polarisation holography resulted in patterns even when samples were used which had not been aligned in a magnetic

field. Apparently, upon drying, some domain formation is taking place, resulting in local alignment, which is pronounced enough to yield visible differences between polymerisation with parallel or perpendicular polarised light. The formed domains were large enough for the pattern to form, but did not cover the whole sample, as confirmed with linear dichroism, with which a different orientation of the fibres at different positions on the sample was measured.

## Conclusions

In conclusion, we have shown that the rate of polymerisation in self-assembled, diacetylene containing PAs is dependent on the polarisation of the incident light. This allowed us to employ polarised light to polymerise a randomly oriented sample to yield a dichroic coloured sample, thus introducing anisotropy in an isotropic sample using only polarisation of light. Furthermore, with an aligned sample and spatially addressed polarised light, polymerisation takes place only at positions where the polarisation of the incident light is parallel to the fibre orientation, yielding a pattern of polymer. The pitch of this pattern can easily be varied by changing the angle at which the two incident beams are combined. The possibility of using polarised light in the polymerisation and hence stabilisation of PA fibres opens opportunities to a further level of control within nano-architectures. For example, if the pattern, applied with polarisation holography, is positioned perpendicular to the alignment direction of the fibres, the length of the fibres can be controlled, as is currently investigated in our group.

## Acknowledgements

We want to thank An Prenen, Dick Broer and Blanca Serrano for help with the polarisation holography set-up and useful discussions.

## Experimental section

**General.** UV/Vis spectra were recorded on a VARIAN Cary 50 Conc spectrometer. CD and LD spectra were recorded on a Jasco J-810 spectropolarimeter equipped with a Jasco PTC-423S/L Peltier type temperature control system. TEM images were obtained with a JEOL- JEM-1010 equipped with a CCD camera.

**Synthesis.** The GANPNAAG peptide amphiphiles were prepared by an earlier reported procedure,<sup>5</sup> described in chapter 2. The characterization of the PA is described in chapter 4.

**Preparation of the fibre samples.** The amphiphiles were dissolved in milliQ, heated to 50 °C for 30 min, followed by 15 min sonication at that temperature. Subsequently, the samples were heated to 90 °C and allowed to cool to room temperature. After this annealing the solutions were allowed to dry on a glass substrate prior to the patterning procedure.

**Sample illumination.** For the polarisation holography a 351 nm SpectraPhysics Beamlok 2085 Argon ion laser with a power varying between 100 and 500 mW was used to illuminate the samples for time intervals between 1 and 10 min. The polymerisation of non-aligned samples

employing plane polarised light was performed with a 200 mW, 457 nm laser. LD measurements were performed on a JASCO J-810 spectropolarimeter. For the measurements to determine an intensity threshold a Bluepoint UV lamp was employed and UV-Vis spectra were recorded on a Varian Cary-50 spectrometer.

## References

1. D. W. P. M. Löwik and J. C. M. van Hest, *Chem. Soc. Rev.*, 2004, **33**, 234-245.
2. J. D. Hartgerink, E. Beniash and S. I. Stupp, *Science*, 2001, **294**, 1684-1688.
3. G. A. Silva, C. Czeisler, K. L. Niece, E. Beniash, D. A. Harrington, J. A. Kessler and S. I. Stupp, *Science*, 2004, **303**, 1352-1355.
4. C. Cerami, U. Frevert, P. Sinnis, B. Takacs, P. Clavijo, M. J. Santos and V. Nussenzweig, *Cell*, 1992, **70**, 1021-1033.
5. D. W. P. M. Löwik, J. Garcia-Hartjes, J. T. Meijer and J. C. M. van Hest, *Langmuir*, 2005, **21**, 524-526.
6. L. Hsu, G. L. Cvetanovich and S. I. Stupp, *J. Am. Chem. Soc.*, 2008, **130**, 3892-3899.
7. M. A. Biesalski, A. Knaebel, R. Tu and M. Tirrell, *Biomaterials*, 2006, **27**, 1259-1269.
8. D. W. P. M. Löwik, I. O. Shklyarevskiy, L. Ruijzendaal, P. C. M. Christianen, J. C. Maan and J. C. M. van Hest, *Adv. Mater.*, 2007, **19**, 1191-1195.
9. M. van den Heuvel, D. W. P. M. Löwik and J. C. M. van Hest, *Biomacromol.*, 2008, **9**, 2727-2734.
10. G. Wegner, *Makromol. Chem.*, 1972, **154**, 35-48.
11. M. Attia and J. M. C. Jonathan, *Opt. Commun.*, 1983, **47**, 85-90.
12. B. Serrano-Ramón, C. Kjellander, S. Zakerhamide, C. W. M. Bastiaansen and D. J. Broer, *Proc. SPIE-Int. Soc. Opt. Eng.*, 2008, **6911**, 691109/691101-691109/691113.
13. J. L. Zhou, J. J. Yang, Y. Ke, J. Shen, Q. J. Zhang and K. Y. Wang, *Opt. Mater.*, 2008, **30**, 1787-1795.
14. X. Pan, C. S. Wang, C. Y. Wang and X. Q. Zhang, *Appl. Opt.*, 2008, **47**, 93-98.
15. C. Provenzano, P. Pagliusi and G. Cipparrone, *Opt. Express*, 2007, **15**, 5872-5878.
16. G. P. Crawford, J. N. Eakin, M. D. Radcliffe, A. Callan-Jones and R. A. Pelcovits, *J. Appl. Phys.*, 2005, **98**.
17. D. J. Ahn and J. M. Kim, *Acc. Chem. Res.*, 2008, **41**, 805-816.
18. J. M. Kim, Y. B. Lee, D. H. Yang, J. S. Lee, G. S. Lee and D. J. Ahn, *J. Am. Chem. Soc.*, 2005, **127**, 17580-17581.
19. J. M. Kim, Y. B. Lee, S. K. Chae and D. J. Ahn, *Adv. Funct. Mater.*, 2006, **16**, 2103-2109.
20. A. Mata, L. Hsu, R. Capito, C. Aparicio, K. Henrikson and S. I. Stupp, *Soft Matter*, 2009, **5**, 1228-1236.





# Summary

The research in this thesis has two main components: fibres of peptide amphiphiles (PAs) and polydiacetylenes (PDAs). The peptide amphiphiles we work with consist of peptides coupled to an alkyl tail. These compounds assemble into fibres in aqueous solutions. Similar assemblies have been used as hydrogels for cell culturing, as MRI contrasting agent and to direct neurite growth. Polydiacetylenes, the other important component in this thesis, are the product of a light-initiated polymerisation. This reaction is topochemical, which means that it can only take place if the components have a highly defined orientation with respect to each other.

In chapter 2 the structure of a specific peptide amphiphile is investigated, consisting of the peptide GANPNAAG coupled to palmitic acid. The assembly of fibres in water is driven by the hydrophobic forces between the alkyl tails, while the hydrogen bonds in the peptide part provide directionality. The morphology of the fibres is studied by electron microscopy, and the internal fibre structure by X-ray diffraction and solid state NMR.

Chapter 3 describes the dynamic properties of the same PA assemblies. The disassembly with heating and reassembly with cooling as well as the concentration at which fibres start to assemble are important parameters for the fibre behaviour, investigated in this chapter. Furthermore, damage because of the growth of ice crystals and behaviour of the fibres in elongational flow are studied. How easily do the fibres align and when will they break? An important technique in this chapter is rheo-optics, which is used to determine both alignment and fibre length in a flow field.

In chapter 4 a diacetylene functionality is introduced into the alkyl chain of the amphiphile. Because of the high ordering of the alkyl chains when assembled into fibres, the diacetylenes can react under influence of light to yield polydiacetylenes. These polymers have a highly conjugated backbone which absorbs visible light, yielding blue fibres. The properties of the fibres before and after polymerisation are studied. Two amphiphiles with the same peptide and similar alkyl chains, in which the only difference was the length of the chain, are compared. Unpolymerised fibres with the shorter alkyl chain melt at lower temperature and do not form readily on cooling. The colour of the fibre consisting of amphiphiles with a longer alkyl chain is blue after polymerisation, while the shorter chain yields a red polymer. Heating results in a red and orange compound, respectively. The difference between the two amphiphiles is large for the seemingly small variation in structure.

In chapter 5 we study the influence of the position of the diacetylene group in the alkyl chain on the assembly, polymerisation and polymer properties of the diacetylene-containing fibres. Three compounds are prepared, with the same peptide GANPNAAG as used in chapters 2-4, coupled to an alkyl chain in which only the position of the diacetylene group differs. The colour of the three fibres (after polymerisation) is

different. A diacetylene group close to the peptide yields a purple polymer, the diacetylene in the middle of the alkyl chain polymerises to a blue polymer, while at the end of the alkyl chain the resulting polymer is pink. The colour is indicative for the packing of the polydiacetylene backbone, and therefore we conclude that the polymer packing is best if the backbone is located in the middle of the alkyl chain. Mixing of the amphiphiles has an influence on the colour after polymerisation, surprisingly enough even when the amphiphiles are mixed after polymerisation.

In chapter 6 the peptide sequence is varied while the diacetylene containing alkyl chain is kept constant. In this chapter the influence of charges and sterical hindrance on fibre formation and colour is investigated using pH variations. The peptide design is inspired on the  $\beta$ -sheet regions of silkworm silk, of which we use the pentameric motif GAGAG. The first and last glycine in the sequence is replaced by lysine or glutamic acid, yielding the possibility to study charge and sterical hindrance separately. From this study we conclude that the colour of the fibres (after polymerisation of the diacetylene) is connected to the morphology as studied with electron microscopy. This result is surprising as the colour is determined on a molecular level, while microscopy yields macroscopic data.

In chapter 7 the amphiphile fibre with the highest pH sensitivity from chapter 6 is used as a macro-initiator for a polymerisation reaction. A series of monomers, ranging from hydrophobic to hydrophilic was employed. The hydrophobic polymers attached to the fibres yield a colour change from blue to pink, while the hydrophilic monomers result in a purple fibre.

Chapter 8 describes a reaction for the ruthenium catalysed and light-initiated crosslinking of tyrosines. In literature, this reaction is used for coupling of proteins, resulting in dimers. We study the reaction with small, soluble peptides and observe the formation of much larger oligomers. Therefore, the term ‘threading’ seems more appropriate than ‘crosslinking’. With mass spectrometry oligomers up to six units are observed. The reaction is extended to the fibres described in chapters 6 and 7, to which a tyrosine is coupled to enable the threading reaction. The reaction on these self-assembled systems is much slower and yields oligomers of only two or three monomeric units.

Chapters 9 and 10 look into possible applications of the fibres. In chapter 9 we aim for fibres of defined length. By covering part of the sample with a lithography mask, only the rest of the sample is illuminated and polymerised. A patterning resolution of a few micron is achieved, which should be enough to yield a relatively small length distribution if applied on aligned samples. Therefore, several methods for fibres alignment are investigated. In solution the fibres can be aligned by assembly in a high magnetic field. Unfortunately, alignment on dry samples remains a challenge, while the high resolution lithography is only possible on dried samples. Therefore, even though the two essential steps in our strategy – alignment and patterning – are accomplished, we could not combine the two techniques to produce fibres of defined length.

Chapter 10 also deals with selective polymerisation, but uses the intrinsic polymerisation properties of the PDA fibres instead of lithography. The fibre polymerisation is much faster if the light is polarised parallel to the fibres than when it is

### *Summary*

oriented perpendicular. Therefore, only fibres parallel to the light polymerise in a randomly oriented sample which is illuminated with polarised light. This yields an anisotropic surface which functions as a polariser. On the other hand, using a pattern of linearly polarised light on a (locally) aligned surface yields selective polymerisation with the same pattern as the incident light.



# Samenvatting

Het onderzoek in dit proefschrift heeft twee belangrijke componenten: vezels van peptide amfifielen (PAs) en polydiacetylenen (PDAs). In het inleidende hoofdstuk (hoofdstuk 1) worden deze twee belangrijke componenten van dit proefschrift geïntroduceerd. De peptide amfifielen bestaan uit peptides gekoppeld aan een alkylstaart. Deze verbindingen vormen vezels in waterige oplossing. Soortgelijke vezels zijn gebruikt om hydrogelen te maken om cellen op te groeien, maar ook als MRI contraststof en om de groei van neuriten te helpen. Polydiacetylenen, de andere component in dit proefschrift, zijn het product van een bijzondere polymerisatie, die geïnitieerd wordt door licht. Deze polymerisatiereactie is topochemisch, wat betekent dat zij alleen plaatsvindt als de componenten een goed gedefinieerde ordening ten opzichte van elkaar hebben.

In hoofdstuk 2 wordt gekeken naar de structuur van een specifiek peptide amfifiel, bestaande uit het peptide GANPNAAG, gekoppeld aan palmitinezuur. De vorming van vezels in water wordt gedreven door de hydrofobe interacties tussen de vetzuurstaarten terwijl de waterstofbrug vormende peptides zorgen voor de nette stapeling. De morfologie van de vezels is bestudeerd met electronmicroscopie en de onderlinge orientatie van de moleculen met röntgendiffractie en vaste stof NMR.

Hoofdstuk 3 behandelt de dynamische eigenschappen van hetzelfde PA. Het uit elkaar vallen met verhitten en hervormen met koelen en de concentratie waarbij de vezels beginnen te vormen zijn belangrijke parameters die het gedrag van de vezels bepalen en die in dit hoofdstuk worden bestudeerd. Ook worden beschadigingen die optreden door ijsvorming bij bevriezing en het gedrag in een stromingsveld onderzocht – hoe makkelijk lijnen de vezels uit en wanneer breken ze? Een belangrijke techniek in dit hoofdstuk is reo-optica, waarmee alignment maar ook vezellengte bepaald kan worden als een stromingsveld wordt aangelegd.

In hoofdstuk 4 wordt een diacetyleen functionaliteit in de vetzuurstaart van het amfifiel geïntroduceerd. Doordat de alkylstaarten in een bijna kristallijn rooster zijn geordend, kunnen de diacetyleengroepen polymeriseren onder invloed van licht. Dit levert sterk geconjugeerde polymeren op, die licht absorberen in het zichtbare gebied en dus gekleurd zijn. De eigenschappen van de vezels voor en na polymerisatie zijn bestudeerd. Daarvoor zijn PAs met twee verschillende vetzuurstaarten vergeleken waarbij de diacetyleen op dezelfde plek zit, maar in een van de twee verbindingen twee koolstofatomen korter is. Ongepolymeriseerde vezels van de amfifielen met kortere staart smelten bij lagere temperatuur en vormen moeilijker bij afkoelen. Na polymerisatie is het amfifiel met de lange staart blauw en die met de korte staart rood, terwijl verhitten een rode respectievelijk oranje stof oplevert. De verschillen tussen de twee amfifielen zijn groot voor het kleine lengteverschil in de staart.

In hoofdstuk 5 bestuderen we de invloed van de positie van de diacetylene groep in de vetzuurstaart. Drie stoffen zijn gemaakt, met hetzelfde peptide GANPNAAG dat ook in hoofdstuk 2 tot 4 is gebruikt, en met een vetzuurstaart van dezelfde lengte waarin alleen de positie van de ingebouwde diacetylene groep verandert. De vorming van de vezels, het polymerisatiegedrag, de eigenschappen van de polymeren en het menggedrag van de vezels is onderzocht. De kleur van de vezels is afhankelijk van de diacetyleenpositie in de staart. De diacetyleen dichtbij het peptide zorgt voor paarse vezels. Vezels met de polydiacetyleen ruggegraat ver van het peptide worden roze, en met de ruggegraat in het midden van de alkylstaart worden blauwe vezels gevormd. Een blauwere kleur geeft een betere ordening van de polymere ruggegraat aan. Een diacetyleen in het midden van de alkylstaart levert dus de beste ordening van de polydiacetyleen. Het mengen van de drie amfifielen verandert de kleur, zelfs als ze eerst gepolymeriseerd en pas daarna gemengd worden.

In hoofdstuk 6 stappen we over op andere peptides, maar laten we de vetzuurstaart – met diacetyleen – gelijk. In dit hoofdstuk wordt de invloed van ladingen en sterische hindering op het vormen van de vezels en hun gedrag bestudeerd. Daarvoor gaan we uit van GAGAG, een peptide geïnspireerd op de  $\beta$ -sheet vormende stukken van zijdwormzijde. Het eerste of laatste aminozuur is vervangen door ofwel lysine ofwel glutaminezuur, zodat door middel van variaties in de pH lading en sterische hindering gescheiden bestudeerd kunnen worden. Uit deze studie volgt dat de kleur van de vezel (na de diacetyleen polymerisatie) informatie bevat over de morfologie van de vezel (bepaald met elektronenmicroscopie). Dit is bijzonder omdat de kleur op moleculair niveau wordt bepaald, terwijl met microscopie alleen veel grotere kenmerken gezien kunnen worden.

In hoofdstuk 7 gebruiken we de vezel uit hoofdstuk 6 dat het meest gevoelig is voor kleurverandering als de pH veranderd wordt. Vezels van dit PA kunnen als initiator van een polymerisatiereactie dienen. De reactie is uitgevoerd met een reeks monomeren, variërend van hydrofoob tot hydrofiel. Wanneer een hydrofoob polymeer aan de vezels groeit verandert de blauwe vezelkleur naar roze, terwijl met een hydrofiel monomeer de vezels paars worden.

Hoofdstuk 8 gaat over een reactie waarmee tyrosines gekoppeld kunnen worden, gekatalyseerd door ruthenium ionen, en geïnitieerd met licht. Deze reactie is in eerder onderzoek gebruikt om eiwitten aan elkaar te plakken, waarbij alleen dimeren werden gevormd. Wij hebben de reactie uitgetoetst met kleine oplosbare peptides, waarmee veel grotere oligomeren gevormd worden. De reactie lijkt zo meer op rijgen dan op koppelen. Met massaspectrometrie zijn kettingen te zien die tot zes eenheden bevatten. Daarna is de reactie uitgetoetst op de vezels die in hoofdstuk 6 en 7 zijn beschreven, waar een tyrosine aan vast is gezet om de rijgreactie mogelijk te maken. Deze reactie is veel langzamer en leverde veel kleinere kettingen op (met slechts twee of drie moleculen).

Hoofdstuk 9 en 10 gaan over de toepassingen van de vezels. In hoofdstuk 9 proberen we vezels op maat te knippen. Door met een masker een gedeelte van een monster af te dekken wordt alleen de rest van het monster belicht en dus gepolymeriseerd. Daarmee kan een resolutie van een paar micrometer gehaald worden,

wat genoeg moet zijn om een relatief kleine lengteverdeling van polymeren te krijgen als deze techniek op uitgelijnde samples wordt toegepast. Daarom zijn verschillende methodes om de vezels uit te lijnen onderzocht. In oplossing kunnen de vezels uitgelijnd worden door ze te laten vormen tijdens afkoelen in een magneetveld. Helaas blijkt het veel moeilijker te zijn om uitgelijnde samples in droge vorm te krijgen, terwijl de vereiste resolutie met de lithografie juist alleen gehaald wordt als de samples zijn ingedroogd. Dus hoewel de beide belangrijke onderdelen van het op maat maken van vezels – uitlijnen en selectief polymeriseren – werken, kunnen we ze op dit moment nog niet combineren.

Hoofdstuk 10 gaat ook over selectief polymeriseren, maar maakt gebruik van de unieke eigenschappen van de diacetyleen polymerisatie. De polymerisatie reactie gaat namelijk veel sneller met licht parallel aan de vezels dan met licht dat er loodrecht opstaat. Met willekeurig georiënteerde vezels en gepolariseerd licht wordt dan ook alleen het gedeelte van het monster gepolymeriseerd dat parallel aan het licht ligt. Daarmee wordt een anisotroop oppervlak verkregen, dat functioneert als een polarisator. Aan de andere kant kunnen we ook een (lokaal) uitgelijnd monster beschijnen met een patroon van gepolariseerd licht. Het selectief gepolymeriseerde oppervlak dat dan ontstaat laat hetzelfde patroon zien als het invallende licht.





# Dankwoord

En dan ben ik nu echt toe aan het laatste en misschien wel moeilijkste stuk van mijn proefschrift, de pagina's die iedereen leest – het dankwoord. Want er zijn nogal wat mensen die ik moet en wil bedanken. En dan denk ik niet alleen aan het wetenschappelijke deel, maar ook aan de high teas, de maaltijden, het volleybal, en af en toe het broodnodige luisterende oor. Omdat dit boekje echter een wetenschappelijk verhaal is, zal ik me proberen te beperken tot alle bedankjes op wetenschappelijk vlak.

Zo heb ik voor de structuurbeplanning en dynamische eigenschappen van de vezels (hoofdstuk 2 en 3) stad en land afgereisd op zoek naar nieuwe technieken om op mijn vezels los te laten. Daarvoor wil ik Peter Frederik uit Maastricht bedanken (cryo-TEM), Remco Fokink uit Wageningen (DLS), Loes Kroon-Batenburg uit Utrecht (X-ray) en Kristina Kvashnina en Wim Bras van het ESRF in Grenoble (SAXS en WAXS). Verder zijn de reo-optica metingen uitgevoerd met hulp van Erik van der Linden, Paul Venema en Harry Baptist en heb ik metingen in Delft gedaan met Aurelie Brizard.

Ook aan het thuisfront heb ik de nodige hulp gekregen. Voor de massametingen werd ik bijgestaan door Peter van Galen, overigens ook een geduldig man als het op herrie in de vroege ochtend aankomt. Hij was niet de enige die positief tegen klarinetstudie aankeek, maar wel de enige die ook moest werken in hetzelfde kantoor waar ik 's ochtends oefende. Andreas Brinkmann, Ernst van Eck en Jorge Garibay waren onmisbaar voor het vaste stof NMR gedeelte, Ad Swolfs heeft geholpen bij de hoge temperatuur NMR en Arnold Nijhuis, Martin Feiters en Mark Damen maakten van de vermoeiende uren in Grenoble toch een klein feestje. Wat hadden ze daar in de kantine lekkere chocoladetoetjes! Al kwamen Mark en ik daar niet echt aan toe dank zij onze voorraad snoepgoed... Verder bouwde ik voort op het werk van een masterstudent (en jaargenote) Loes Ruizendaal, die al een hoop had geprobeerd om de structuur van de vezels te bepalen.

Soms heb je collega's nodig waar je chemische verbindingen gaat lenen voor een synthese die maar niet wil lukken. Als je geluk hebt helpen die collega's je dan aan het gouden idee voor een alternatieve syntheseroute (hoofdstuk 5) – dankjewel Dennis Waalboer! Behalve collega's zijn ook studenten een belangrijke factor in het slagen van een promotie, en ik heb twee geweldige studenten gehad. Nicole van Gijzel heeft een groot gedeelte van het werk voor hoofdstuk 6 verricht. Ik ben nog steeds onder de indruk dat ze je ziet/'hoort'/begrijpt als je tegen haar rug praat (Nicole is doof). Aan Nearchos Spithas heb ik hoofdstuk 7 te danken. Gelukkig wist hij meer van onder Schlenk condities werken dan ik. In de begeleiding van deze stage waren René Brinkhuis en Vincent Lemieux van groot belang. Dankzij hen kon ik rustig een paar maanden naar het buitenland zonder me zorgen te hoeven maken om Nearchos' vorderingen.

## *Dankwoord*

En die paar maanden buitenland (hoofdstuk 8) waren geweldig! What a welcoming and lovable group in Bristol. I never expected that the idea of a postdoc abroad would appeal to me, but you made it seem very attractive! Thanks to the whole Woolfson group, but mostly Zahra Mahmoud and Dek Woolfson – I'll remember the Dutch and Hindi lessons...

Aligning en patterning (hoofdstuk 9) was de polydiacetyleen-blauwe draad door mijn hele onderzoek heen. Daarbij heb ik gebruik gemaakt van de creativiteit van de halve afdeling. De uiteindelijke opstelling om vezels te drogen en te alignen was dan ook de mooiste van mijn promotietijd. Met modeltreintjes, elastiekjes, een kokend waterbad en meters capillair – dank aan Koos Wilke en Tu Ha Vong. Ook heb ik samen met Jeroen Gielen heel wat uren bij de magneet in het HFML doorgebracht. We hebben daar ook veelvuldig de brandslang 'getest' – een makkelijke en snelle koelmethode! Voor de lithografie heb ik veel hulp gehad van Peter Mulder, terwijl Jing Zhang me met de polyimide coatings geholpen heeft.

Voor mij blijft hoofdstuk 10 het mooiste hoofdstuk – ik kan nooit meer zeggen dat je niets aan Lunteren hebt, aangezien ik daar met Blanca Serrano kennismakte. Zij introduceerde me in de wereld van de polarisatieholografie. An Prenen en Dick Broer hebben enorm bijgedragen aan dit werk, wat ik in Eindhoven heb uitgevoerd.

Wat niet specifiek bij een hoofdstuk hoort is natuurlijk de hulp die ik van Jan van Hest en Dennis Löwik gehad heb. Die waren er altijd met nieuwe ideeën, enthousiasme en motivatie als dat nodig was. Hans Adams is niet weg te denken in elk onderzoek waarin peptides een rol spelen. Toen ik met mijn onderzoek begon, hoorde Joris Meijer bovendien ongeveer bij het meubilair van de afdeling – hij wist alles en stond altijd klaar om te helpen. Na enige tijd durfde ik bijna niets meer te vragen omdat hij alles erbij neer gooide om EERST te helpen... Ook onze secretaresses Jacky Versteeg en Desiree van der Wey en logistiek man Peter van Dijk stonden altijd klaar om te helpen, al kon je er ook binnenlopen om gewoon even gezellig bij te praten. Ik heb de afgelopen vier jaar ook heel wat uurtjes in het algemeen instrumentarium doorgebracht, waarbij ik vooral TEM en lichtmicroscopie heb gemeten, maar een enkele keer ook SEM en confocal. Daarvoor wil ik Liesbeth Pierson en Geert-Jan Janssen hartelijk danken. Verder heb ik me ook met veel plezier bemoeid met de stages van Jeroen Heldens, Paula van der Aa en Anniek Bruins. Hun onderzoek staat niet in dit proefschrift – officieel waren ze ook niet 'mijn' studenten – maar het was zeker de moeite waard en hopelijk hebben zij er net zoveel van geleerd en er net zoveel plezier aan gehad als ik.

En daarmee komt niet alleen een eind aan dit dankwoord, maar ook aan een geweldige promotietijd. Ik zou er zo weer aan beginnen!

## List of publications

M. van den Heuvel, D. W. P. M. Löwik, P. Venema, H. Baptist, E. van der Linden and J. C. M. van Hest.

*Mechanics and thermodynamics of peptide amphiphile fibres.*

In preparation.

M. van den Heuvel, N. van Gijzel, D. W. P. M. Löwik and J. C. M. van Hest.

*The influence of amino acid sequence on morphology and colour of polydiacetylene-containing peptide amphiphile fibres.*

In preparation.

M. van den Heuvel, L. Kroon-Batenburg, A. Brinkmann, Jorge Garibay, L. Ruizendaal, D. W. P. M. Löwik and J. C. M. van Hest.

*Structure elucidation of palmitoyl-GANPNAAG fibres.*

In preparation.

M. van den Heuvel, D. W. P. M. Löwik and J. C. M. van Hest.

*Effect of the diacetylene position on the chromatic properties of polydiacetylenes from self-assembled peptide amphiphiles.*

Biomacromol., 2010, **11**, 1676-1683.

M. van den Heuvel, A. M. Prenen, J. C. Gielen, P. C. M. Christianen, D. J. Broer, D. W. P. M. Löwik and J. C. M. van Hest.

*Patterns of diacetylene-containing peptide amphiphiles using polarization holography.*

J. Am. Chem. Soc., 2009, **131**, 15014-15017.

M. van den Heuvel, D. W. P. M. Löwik and J. C. M. van Hest.

*Self-assembly and polymerization of diacetylene-containing peptide amphiphiles in aqueous solution.*

Biomacromol., 2008, **9**, 2727-2734.

M. Damen, J. Aarbiou, S. F. M. van Dongen, R. M. Buijs-Offerman, P. P. Spijkers, M. van den Heuvel, K. Kvashnina, R. J. M. Nolte, B. J. Scholte and M. C. Feiters.

*Delivery of DNA and siRNA by novel gemini-like amphiphilic peptides.*

J. Controlled Release, 2010, **145**, 33-39.

D. Löwik, E. H. P. Leunissen, M. van den Heuvel, M. B. Hansen and J. C. M. van Hest.

*Stimulus responsive peptide based materials.*

Chem. Soc. Rev., 2010, **39**, 3394-3412.

## Curriculum Vitae

Maaïke van den Heuvel werd op 25 juni 1983 geboren in Almelo. Na het cum laude behalen van haar VWO diploma aan het Isendoorn College te Warnsveld, begon ze in 2001 aan haar studie Scheikunde aan de Radboud Universiteit Nijmegen. In 2006 sloot ze deze studie cum laude af. In haar hoofdvakstage deed ze onderzoek naar het modelleren van menggedrag van vetten om zo een fasesdiagram te kunnen berekenen. Haar bijvakstage doorliep ze bij (toenmalig) Organon op het gebied van host-guest chemie. Daarna begon ze aan haar promotieonderzoek, dat in dit proefschrift beschreven is.



Dit onderzoek is uitgevoerd onder leiding van prof. dr. ir. Jan C. M. van Hest en dr. Dennis W. P. M. Löwik in de vakgroep bio-organische chemie aan de Radboud Universiteit Nijmegen. Momenteel is Maaïke werkzaam als onderzoeker bij de afdeling functional ingredients van TNO in Zeist.